Light Harvesting *via* Energy Transfer in the Dye Solar Cell

Inaugural-Dissertation
zur Erlangung der Doktorwürde
der Fakultät für Chemie und Pharmazie und Geowissenschaften
der Albert-Ludwigs-Universität Freiburg im Breisgau

vorgelegt von

Conrad Siegers
aus Aachen

Freiburg im Breisgau 2007

Für Gabi, Andor und Finn

Vorsitzender des Promotionsausschusses:	Prof. Dr. G. E. Schulz
Leiter der Arbeit:	Prof. Dr. R. Haag
Referent:	Prof. Dr. R. Mülhaupt
Korreferent:	Prof. Dr. R. Haag
Tag der Bekanntgabe des Prüfungsergebnisses:	09.11.2007

Die experimentellen Untersuchungen zu dieser Arbeit wurden im Rahmen des vom Bundesministerium für Bildung und Forschung (BMBF) geförderten Netzwerkprojekts „Farbstoffsolarzellen“ (01SF0304) in der Zeit von März 2003 bis Juni 2007 am Freiburger Materialforschungszentrum und am Institut für Makromolekulare Chemie der Albert-Ludwigs-Universität Freiburg im Arbeitskreis von Prof. Dr. R. Mülhaupt, in enger Zusammenarbeit mit der Gruppe von Herrn Prof. Dr. J. Luther am Fraunhofer Institut für Solare Energiesysteme, durchgeführt.

Ich danke Herrn Prof. Dr. Mülhaupt und Herrn Prof. Dr. Haag (Freie Universität, Berlin) außerordentlich für die Aufnahme in ihre jeweiligen Arbeitsgruppen, die interessante Themenstellung, die exzellenten Arbeitsbedingungen, ihr Interesse, ihre Unterstützung und ihre Diskussionsbereitschaft in allen Phasen der Arbeit. Besonderer Dank gilt Herrn Prof. Dr. Rainer Haag außerdem für die zahlreichen Einladungen zu Seminarvorträgen in seine Arbeitsgruppe und nicht zuletzt für die Übernahme des Korreferats.

Danksagung

Die vorliegende Arbeit wurde in diesem Umfang nur durch intensive, interdisziplinäre Zusammenarbeit ermöglicht. Ich möchte allen danken, die durch ihre Unterstützung zum Gelingen dieser Arbeit beigetragen haben.

Mein besonderer Dank gilt Herrn Dr. Bela Olah für die großartige präparative und organisatorische Unterstützung im Labor.

Mein besonderer Dank gilt weiterhin Herrn Prof. Dr. Joachim Luther und den Mitarbeitern seiner Gruppe, im Einzelnen Dr. Andreas Hinsch, Dr. Rainer Kern, Dr. Uli Würfel und nicht zuletzt Herrn Simon Hemming, Frau Melanie Schumann und Frau Carmen Vetter für den Bau von Photoelektroden und Masterplates sowie die exzellente Einweisung ins „Dye-Solar-Cell-Business."

Herrn Jochen Hohl-Ebinger danke ich für die EQE-Messungen und ausgiebigen Diskussionen über Solarzelltechnologie. Herrn Dr. Boris Zimmermann danke ich für die fruchtbaren Diskussionen über Energietransfer und die exzellente Einweisung in alle möglichen Techniken zur Charakterisierung von Fluoreszenz und respektive Datenanalyse. In diesem Zusammenhang danke ich Prof. Dr. Peter Gräber für die Möglichkeit, in seinem Labor messen zu können.

Den Mitarbeiterpraktikanten Thomas Richter, Felicitas Brömmel und Christoph Fik danke ich für ihre äußerst engagierte Mitarbeit. Lisa Boch, Felix Kalchschmidt und Anja Koppert bin ich ebenso für die Synthesen, die sie durchgeführt haben, sehr dankbar.

Frau Heidemarie Weinhart danke ich für die Bereitstellung von linearem Polyglycerin. Herrn Dr. Harald Hahn und Herrn Prof. Dr. Heinrich Lang danke ich für die Bereitstellung von Carbosilan-Dendrimeren. Herrn Dr. Holger Türk und Herrn Bernhard Siegel danke ich für die Bereitstellung von hyperverzweigtem Polyglycerin. Herrn Shanjie Xu danke ich für die Bereitstellung einer Probe Polyglycerin-Azid.

Mein Dank gilt Herrn Prof. Dr. Michael Grätzel und seiner Gruppe für die Diskussionen im Rahmen eines Workshops im November 2003. Insbesondere danke ich Herrn Dr. Mohammed K. Nazeeruddin für die Einweisung in die säulenchromatographische Trennung von carboxylierten Ru-Polypyridin-Komplexen.

Herrn Alfred Hasenhindl und Herrn Dr. Michael Kowalski danke ich für die Aufnahme der NMR-Spektren. Weiterhin sei Herrn Christoph Warth und Herrn Dr. Jürgen Wörth für die Messung von Massenspektren, und Ernst Hickl für die Durchführung von Elementaranalysen gedankt. Dr. Ralf Thomann danke ich für die Aufnahme von TEM-Bildern.

Ich bedanke mich bei Herrn Alexander Rossel, Herrn Bernd Machuta und Herrn Karl-Heinz Weiß für die zügige Erledigung von Anfertigungen.

Herrn Thomas Richter, Herrn Andreas Fuchs, Herrn Birger Zimmermann und Frau Korinna Dormann und insbesondere Frau Dr. Pam Winchester danke ich für die Durchsicht der Arbeit.

Ich bedanke mich bei den Mitarbeitern der FMF-Verwaltung Frau Dr. Stefanie Meisen, Frau Nicola Weis, Frau Stefanie Kuhl und Herrn Kurt Ruf für die immer währende Unterstützung in allen Verwaltungsfragen.

Herrn Prof. Dr. Georges Hadziioanou, Herrn Dr. Cyril Brochon und Frau Madalina Badila danke ich für ihre Diskussionsbereitschaft und Kooperation bezüglich des TiO_2-Projekts. In diesem Zusammenhang danke ich auch Herrn Reinhard Bieber für die Diskussionsbereitschaft zur Partikelmodifizierung.

Frau Anke Drewitz und Herrn Prof. Dr. Dieter Fassler möchte ich für die Zusammenarbeit im Rahmen des BMBF-Netzwerks „Farbstoffsolarzellen“ danken.

Herrn Markus Zistler, Herrn Philip Wachter und Herrn PD Dr. Heiner Gores danke ich für CV-Messungen. Herrn Oliver Ehlert danke ich für die Einweisung in das Photolumineszenz-Spektrometer. Herrn Roland Bienert und Frau Verena Rombach danke ich für die Unterstützung bei Anisiotropie-Messungen.

Herrn Prof. Dr. Alexander Blumen danke ich für sein Interesse und seine Diskussionsbereitschaft im Bezug auf Energiemigration in Farbstoff-funktionalisierten, hyperverzweigten Polymeren.

Meinen Labor- und Bürokollegen, Frau Christine Beierlein, Herrn Dr. Nico Bruns, Herrn Stephan Dech, Herrn Christoph Fik, Herrn Andreas Fuchs, Herrn Dirk Heiser, Herrn Hon Ho, Frau Anja Koppert, Herrn Dr. Michael Krämer, Herrn Dr. Bela Olah, Herrn Axel Pfahler, Herrn Sebastian Roller, Herrn Gil Scheuermann, Herrn Jan Tobis und Herrn Dr. André Warnecke danke ich für ihre große Hilfsbereitschaft und die angenehme Arbeitsatmosphäre.

Den noch nicht genannten Kollegen der Gruppe von Prof. Dr. Joachim Luther, Herrn Dr. Ronald Sastrawan, Herrn Henning Brand, Herrn Birger Zimmermann, Herrn Dr. Moritz Riede, Herrn Dr. Markus Glatthaar, Herrn Dr. Michael Niggemann, Frau Dr. Anneke Georg, Herrn Dr. Andreas Gombert und Herrn Dr. Kristian Sylvester danke ich für die gute Zusammenarbeit und Diskussionsbereitschaft.

Mein Dank gilt auch den weiteren, noch nicht genannten Mitarbeitern der Gruppen von Prof. Dr. Rainer Haag und Prof. Dr. Rolf Mülhaupt.

Dem Bundesministerium für Bildung und Forschung danke ich für die finanzielle Unterstützung im Rahmen des Netzwerkprojekts „Farbstoffsolarzellen“ (Antrag 01SF0304).

Last but not least danke ich meiner Frau Gabrielle Siegers und meinen Söhnen Andor und Finn. Gabi für ihre Unterstützung, vor allem in den letzten Monaten und Wochen der Arbeit sowie Andor und Finn für ihre Beharrlichkeit, wenn es darum ging, ihren Vater daran zu erinnern, dass es auch noch etwas anderes als Energietransfer, Farbstoffsolarzellen und Ruthenium-Komplexe gibt!

Ergebnisse der vorliegenden Arbeit wurden in folgenden Publikationen, Postern und Vorträgen öffentlich gemacht:

Veröffentlichungen:

C. Siegers, J. Hohl-Ebinger, B. Zimmermann, U. Würfel, R. Mülhaupt, A. Hinsch, R. Haag, *ChemPhysChem* **2007**, Advanced Online Publication.
"A Dyadic Sensitizer for Dye Solar Cells with High Energy-Transfer Efficiency in the Device"

A. Gombert, S. Hemming, A. Hinsch, M.-J. Hloucal, J. Luther, M. Peters, R. Sastrawan, M. Schumann, C. Siegers, W. Veurman, E. Weber, U. Würfel, *FMF Jahresbericht* **2006**.
„Farbstoffsolarzellen"

C. Siegers, J. Hohl-Ebinger, U. Würfel, M. Zistler, A. Hinsch, R. Haag, in Vorbereitung.
"A Photoelectrochemical Pulley: FRET-mediated Electron Injection from a Low-lying Excited State in the Dye Solar Cell"

Vorträge:

C. Siegers, U. Würfel, A. Hinsch, R. Haag, European Materials Research Society Spring Meeting, Mai **2007,** Strasbourg, Frankreich
"Efficiency Enhancement of the Dye Solar Cell via Resonant Energy Transfer"

C. Siegers, R. Haag, BMBF-Netzwerkprojekt Abschlusstreffen, März **2007**, Freiburg, Deutschland
"Energy Transfer in Mono- and Polymeric Donor Acceptor Sensitizers: Current enhancement in the Dye Solar Cells"

A. Hinsch, H. Bönnemann, A. Drewitz, F. Einsele, D. Fassler, D. Gerhard, H. Gores, S. Himmler, G. Kheshliavilli, D. Koch, G. Nasmudinova, U. Opara-Kras, M. Peters, P. Putira, U. Rau, R. Sastrawan, T. Schauer, S. Sensfuß, C. Siegers, K. Skupien, J. Walter, P. Wasserscheid, U. Würfel, M. Zistler, 21st European Photovoltaic Solar Energy Conference and Exhibition, September **2006**, Dresden, Deutschland
"Developments for Dye Solar Modules: Results from an Integrated Approach"

C. Siegers, SFB 428 Doktorandenseminar, Juni **2006**, Waldau, Deutschland
"Synthesis and Characterization of Energy-Donor-Acceptor Systems in the Dye Solar Cell"

C. Siegers, SFB 428, Dezember **2005,** Freiburg, Deutschland
"Synthesis of Polymers Functionalized with Fluorescent Dyes"

C. Siegers, G. Hadziioannou, R. Mülhaupt, 13. FMF-Kolloquium **2004**, Titisee, Deutschland
„Maßgeschneiderte TiO_2-Partikel für die Anwendung in elektronischem Papier"

C. Siegers, SFB 428 Doktorandenseminar, Juni **2004**, Waldau, Deutschland
"Light-harvesting via Fluorescent Resonance Energy Transfer in the Dye-sensitized Solar Cell"

Poster:

Conrad Siegers, Felicitas Brömmel, Thomas Richter, Sebastian Roller, Rainer Haag, Fourth International Dendrimer Symposium (IDS-4), Juni **2005**, Mount Pleasant, MI, Vereinigte Staaten von Amerika
"Branched Systems for Increased Light-Harvesting via Fluorescent Resonant Energy Transfer in the Dye-Sensitized Solar Cell"

Table of Contents

I Abbreviations

#	entry
A	acceptor
A	absorbance
A	see nomenclature
A'	acceptor-precursor
AM1.5G	standarized global solar emission spectrum at 48° incident angle (corresponds to the solar emission on a clear spring day in middle Europe at noon)[1]
a.u.	arbitrary units
acac	acetylacetonato
acacH	acetyl acetone
α_{Allyl}	degree of functionalization with allyl groups
α_{Donor}	degree of functionalization with aminonaphthalimide units (energy donor)
α_{FG}	degree of functionalization with functional group FG
α_{N3}	degree of functionalization with azide groups
α_{OMs}	degree of functionalization with mesyl groups
α_{OPr}	degree of functionalization with propyl groups
α_{Ru}	degree of functionalization with $[Ru(dcbpy)_2acac]^+$
allyl-acac	oct-7-en-2,4-dione anion
allyl-acacH	oct-7-en-2,4-dione
Allyl-PG	allylated PG
A-PG-N_3	acceptor functionalized polyglycerol azide (see also nomenclature)
aq.	aqueous
$\mathbf{A_{thick}}$	see nomenclature
$\mathbf{A_{thick,allyl}}$	see nomenclature
bpy	2,2'-bipyridine
calc.	calculated
CP MAS NMR	cross polarization magic angle spinning NMR
d	day
D	donor
d	thickness
δ	chemical shift

D-Allyl-PG	donor-functionalized allylated polyglycerol
D-A-PG	donor acceptor-modified polyglycerol derivatives
D-A-PG-N_3	donor acceptor-modified polyglycerol derivatives
dcbpy	4,4'-dicarboxy-2,2'-bipyridine
DCM	dichloromethane
di-Me-dcbpy	4,4'-dicarboxy-2,2'-bipyridine dimethyl ester
DMF	N,N-dimethyl formamide
$\Delta m\ m_0^{-1}$	mass loss
DMSO	dimethyl sulfoxide
Δn	refractive index difference
DSC	dye solar cell
$\mathbf{D_{thick}}$	see nomenclature
e.g.	for example
EE	ethyl acetate
en	ethylene diamine
eq.	equation
EQE	external quantum efficiency
EQE_{Acceptor}	EQE mediated *via* acceptor absorption
EQE_{exp}	experimental *EQE*
EQE_{RET}	EQE mediated *via* resonant energy transfer
EQE_{sim}	simulated *EQE*
eqs.	equations
ETE	energy transfer efficiency
EtOH	ethanol
ϕ_{inj}	injection efficiency
ϕ	anisotropy decay time
Φ	fluorescence quantum yield
Φ	photon flux
h	hour
η	global power conversion efficiency
*h*PG	hyperbranched polyglycerol
i.e.	
IPCE	incident photon to current efficiency (same as EQE)

IR	infra red
IV	current-voltage
j_{sc}	short circuit current
$\lambda_{abs,\ max}$	wavelength of maximum absorption
λ	wavelength
$\lambda_{em,\ max}$	wavelength of maximum emission
LHE	light harvesting efficiency
LHE_A	light harvesting efficiency mediated by acceptor absorption
*l*PG	linear polyglycerol
MA	methyl acrylate
MAA	metacrylic acid
MeOH	methanol
MMA	methyl metacrylate
MMAA	methyl metacrylic acid
n.d.	not determined
n.p.	not present
N_{FG}	number of functional groups FG
N^H	number of protons accounting for an NMR signal
N3	$[Ru(dcbpy)_2(NCS)_2]$
N719	$[Ru(dcbpy)_2(NCS)_2]$-di-tetrabutylammonium salt
N719	see nomenclature
N719+D	see nomenclature
NMP	N-methyl pyrrolidone
NMR	nuclear magnetic resonance
PA	see nomenclature
PDA	see nomenclature
PG-N_3	polyglycerol azide
PG-OMs	polyglycerol mesylate
PHMS	poly-dimethyl-co-hydromethy-siloxane
ppm	parts per million
propargyl-acac	oct-7-in-2,4-dione anion
Pt-cat.	Platinum-1,1,3,3-tetramethyl-1,3-divinyldisiloxane in Xylene (2.1%)
py-d_5	deuterated pyridine

r	fluorescence anisotropy
R_0	Förster radius
RT	room temperature
τ	fluorescence lifetime
t	time
T	transmission
TBA-OH	tetrabutylammonium hydroxide
TEM	transmission electron microscopy
TEOS	tetraethoxysilane
TGA	thermogravimetric analysis
THF	tetrahydrofurane
THF-d_8	deuterated tetrahydrofurane
TLC	thin layer chromatography
TPS	trimethylsilylpropanesulfonic acid [$Me_3Si(CD_2)_3SO_3D$, NMR-standard for D_2O]
UF	ultrafiltration
UV-Vis	ultraviolet and visible
$x_{Acceptor}$	fraction of light absorbed by the acceptor
x_{Donor}	fraction of light absorbed by the donor
z_{DA}	donor acceptor ratio

II Nomenclature

II.I Glossary

acceptor unit	[Ru(dcbpy)$_2$acac]Cl and its derivatives or a residue comprising this complex
donor unit	alkylated 4-aminonaphthalimide derivatives or a residue comprising this aromatic system
fluorol unit	donor unit

II.II Aminonaphthalimides

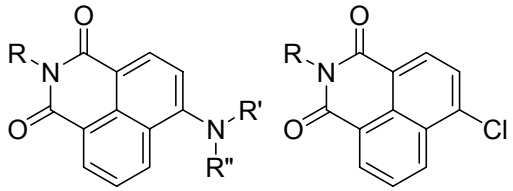

R = R′ = Bu; R" = H Fluorol 7GA, commercial laser dye

Aminonaphthalimides were named by attaching the names of R, R′, and R" in front of "fluorol." If there was a chloride atom in the 4 position, "chloro" was attached. R" = H is omitted. The following residues were abbreviated

R' = $(CH_2)_3SiMe_2(CH_2)_2SiMe_2H$: "hydrosilyl"

R' = $(CH_2)_3SiMe_2(CH_2)_2SiMe_2(CH_2)_4CO\text{-}CH_2CO\text{-}CH_3$: "acacH"

II.III Polymers

PG-OMs$_{\alpha OMs}$	polyglycerol mesylate with a degree of functionalization of α_{OMs}
PG-N$_{3,\ aN3}$	polyglycerol azide with a degree of functionalization of α_{N3}
D$_{\alpha Donor}$-Allyl-PG	allylalted polyglycerol with a degree of donor funct. of α_{Donor}
A$_{\alpha Ru}$-PG-N$_{3,\ \alpha N3}$	acceptor functionalized polyglycerol azide with α_{N3}. The degree of functionalization with acceptor groups is α_{Ru} with respect to PG-units.
D$_{zDA}$-A$_{\alpha Ru}$-PG-N$_{3,\ \alpha N3}$	donor acceptor functionalized PG. The PG azide had an initial degree of functionalization of α_{N3}, the degree of functionalization with acceptor groups is α_{Ru} and the donor acceptor ratio on the polymer is z_{DA}.

II.IV Dye Solar Cells

Throughout the thesis the device names below are formatted in boldface. Unless stated otherwise, the photoelectrode thickness was 3.7 µm. The index "thick" indicates an electrode thickness of 8 µm.

A	Cell stained with $[Ru(dcbpy)_2acac]Cl$
$\mathbf{A_{Allyl,\ thick}}$	Cell stained with $[Ru(dcbpy)_2$allyl-acac$]Cl$ and an photoelectrode thickness of 8 µm
$\mathbf{A_{thick}}$	Cell stained with $[Ru(dcbpy)_2acac]Cl$ and an photoelectrode thickness of 8 µm.
$\mathbf{D_{thick}}$	Cell stained with 4-carboxybutyl butyl fluorol and a photoelectrode thickness of 8 µm
N179	Cell stained with N719
N179+D	Cell stained with a mixture of N719 and 4-carboxybutyl butyl fluorol
PA	Cell stained with $A_{29\%}$-PG-$N_{3,\ 40\%}$
$\mathbf{PDA_{0.8}}$	Cell stained with $D_{0.8}$-$A_{5\%}$-PG-$N_{3,\ 30\%}$
$\mathbf{PDA_{1}}$	Cell stained with D_{1}-$A_{(20\%)}$-PG-$N_{3,\ 30\%}$
$\mathbf{PDA_{4}}$	Cell stained with $D_{3.7}$-$A_{8\%}$-PG-$N_{3,\ 60\%}$
$\mathbf{PDA_{5}}$	Cell stained with D_{5}-$A_{(10\%)}$-PG-$N_{3,\ 100\%}$
$\mathbf{PDA_{7}}$	Cell stained with D_{7}-$A_{(10\%)}$-PG-$N_{3,\ 85\%}$
$\mathbf{PDA_{8.6}}$	Cell stained with D_{9}-$A_{3\%}$-PG-$N_{3,\ 30\%}$

1 Introduction

One of today's major challenges is the energy management for a globally increasing population and prosperity. Awareness of the limitations posed by finite natural resources, notably the fossil fuels, is spreading partially because of rising energy costs. There are two major, viable strategies for reconciling the right of populations from second and third world countries to catch up on quality of life with the need to contain the consequences resulting from an increasing inavailability of energy: (i) energy production based on renewable resources and (ii) a more efficient energy use of today's applications and life-style. These challenges have led to an increased motivation for sponsorship and promotion of research and developments in alternative technologies for energy conversion and saving. The topic of this thesis is in part in response to the need for the new technological developments in order to help solving the ecological and energy related problems facing the the world right now.

In particular, the dye solar cell (DSC) has the potential to be produced at low-cost and with a low energy input. In this work the concept of applying energy transfer as a means to increase dye solar cell efficiency, as suggested for the first time by Amadelli *et al.* in 1990,[2] has been evaluated here in greater detail. As a result, its potential in future dye or alternative hybrid solar cell applications has been highlighted.

1.1 Dye Solar Cell

In the past few years the interest in alternative photovoltaic technologies, especially with respect to reducing production cost and new properties (e.g., flexibility), has encouraged extensive research efforts in the fields of organic and supramolecular photovoltaic devices. One major field of research deals with the dye sensitized solar cell (DSC, Grätzel-cell),[3] which features potentially low production costs due to the fact that the materials used in the assembly of this device are commodities, e.g., TCO and TiO_2. The state of the art for the overall efficiency in DSCs is 10% for individual cells.[4] This efficiency, which is comparable to that of amorphous silicon solar cells, was reached by the optimization of the individual components and materials used for its assembly. In the following three chapters the setup and principle of the DSC is described, as well as the electrical characteristics and spectral properties.

1.1.1 Setup and Principle of the Dye Solar Cell

Figure 1a presents the setup and individual components of a DSC schematically.

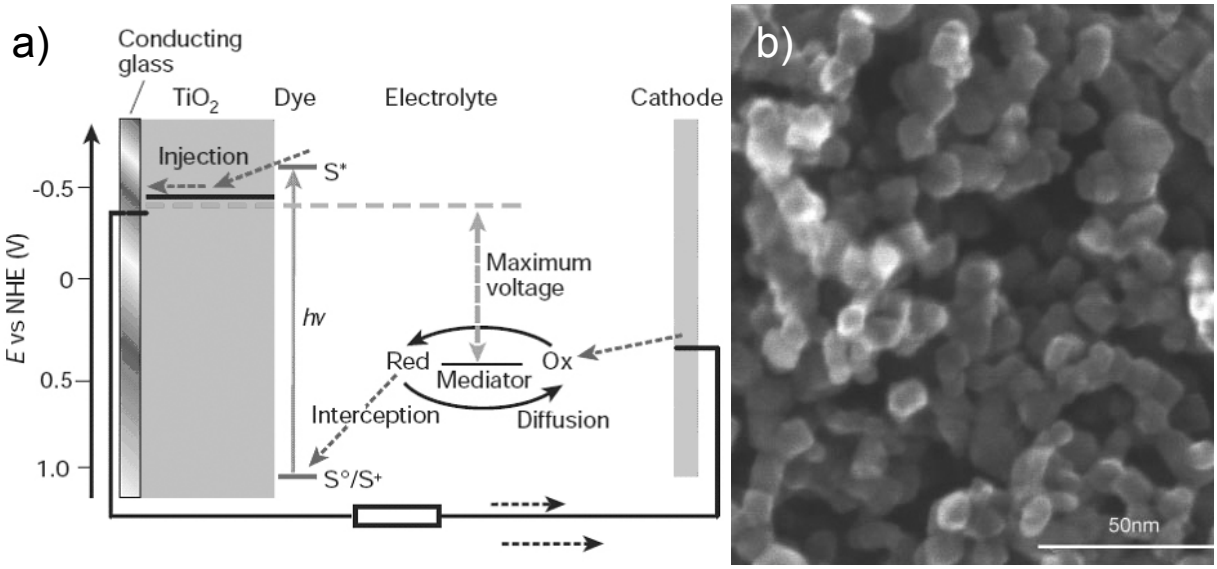

Figure 1. a) Schematic setup of the DSC. The spatial arrangement of the cell's components is indicated in combination with their energy levels (*y*-axis of the scheme). The dashed arrows indicate the way of the electrons through the device. b) Scanning electron micrograph of the surface of a mesoporous TiO_2 film (anatase) used as support for the dye and thus as front electrode within a DSC.[4]

They include the front electrode, which comprises (i) the transparent conducting substrate (TCO) for (ii) the nanoporous TiO_2-layer (Figure 1b) which carries in turn (iii) the redox-active dye. The back electrode (cathode) is functionalized with a catalytic layer and may be designed transparently as well. The electrodes are connected by an electrolyte containing a redox couple (mediator). The latter consists typically of an I^-/I_3^--system. The device operation consists in the sequence of processes shown in equations (1.1) to (1.4).

$$S + h\nu \longrightarrow S^* \tag{1.1}$$

$$S^* + \mathrm{TiO_2} \longrightarrow S^+ + \mathrm{TiO_2}(e^-) \tag{1.2}$$

$$S^+ + \frac{3}{2}\mathrm{I}^- \longrightarrow S + \frac{1}{2}\mathrm{I}_3^- \tag{1.3}$$

$$\frac{1}{2}\mathrm{I}_3^- + e^- \longrightarrow \frac{3}{2}\mathrm{I}_3^- \tag{1.4}$$

Initially a photon is absorbed ($h\nu$) effectuating the dye being transferred from its ground (S^0) into its excited state [S^*, eq. (1.1)]. Then electron injection into the TiO_2 takes place [Injection, eq. (1.2)] leaving the dye in its oxidized state (S^+, a hole is produced on the dye). The electron diffuses through the nanoporous TiO_2 to the front electrode and the hole is transferred from the dye to the electrolyte [Interception, eq. (1.3)]. Finally the holes diffuse to

the back electrode. The processes shown in eqs. (1.1) – (1.3) provide efficient charge separation and lead to a photovoltage under illumination.[5] On connecting a load to the contacts (front and back electrode of the device) electrical power may be extracted from the device; a photocurrent flows from the front electrode through the load to the back electrode. The electrons that flowed through the external circuit then recombine at the back electrode with the holes [I_3^-, eq. (1.4)] and thus regenerate the system into the state it was in prior to light absorption. Ideally, there is no net change in the chemical constitution of the cell's components, thus the DSC is also termed as regenerative electrochemical photovoltaic cell. The processes described so far all contribute to the conversion of light to energy, however, not every photon absorbed by the device necessarily leads to the generation of an electron to be collected at the front electrode. The following factors may play a role in decreasing the device's performance: (i) absorption of light not followed by electron injection [e.g., absorption by the electrolyte or absorption of a dye molecule not connected electronically to the TiO_2 semiconductor, eq. (1.5)]

$$S + h\nu \longrightarrow S^* \longrightarrow S + \text{heat} \tag{1.5}$$

and (ii) recombination of electrons that have been injected into the conduction band of TiO_2 with the holes in the electrolyte [e.g., triiodide, eq. (1.6)].

$$\frac{1}{2} I_3^- + TiO_2(e^-) \longrightarrow \frac{3}{2} I_3^- + TiO_2 \tag{1.6}$$

1.1.2 Electrical Characteristics of a Photovoltaic Device

The characteristics of a photovoltaic device are generally determined *via* the measurement of a current voltage curve (IV-curve) under illumination. During this measurement the current that is extracted from the illuminated device is determined as a function of a bias voltage that is applied to the device (Figure 2). This measurement allows extracting of the following electrical characteristics for a specific illumination: (i) the open circuit voltage U_{oc}, (ii) the short circuit current density j_{sc} and (iii) the fill factor *FF*. The open circuit voltage U_{oc} in the device is caused by the difference in the electron concentration in the conduction band under illumination ($n_{CB}^{illuminated}$) and in the dark (n_{CB}^{dark}).

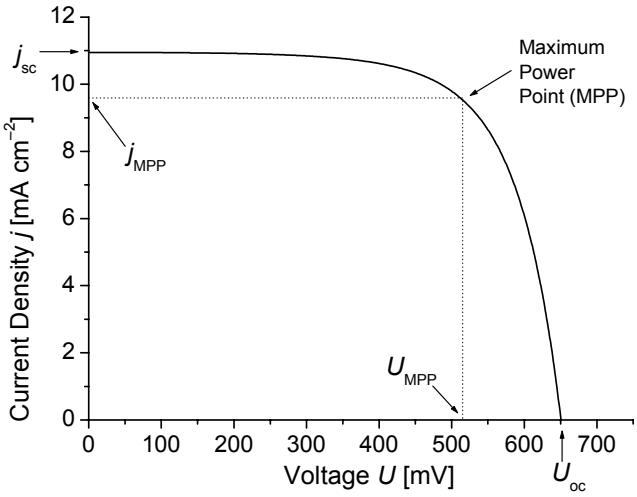

Figure 2. Typical IV-curve for a DSC under illumination. The current density j is plotted as a function of the bias voltage U.

The dependence of the latter two values and U_{oc} is described by eq. (1.7).[1, 6, 7]

$$U_{oc} = \frac{kT}{e} \ln \frac{n_{CB}^{illuminated}}{n_{CB}^{dark}} \tag{1.7}$$

j_{sc} is largely dependent on the solar cell's spectral properties and is thus described in the next section. The fill factor is defined as the fraction between the maximal extractable power of the device ($= j_{MPP} \cdot U_{MPP}$) and the product of j_{sc} and U_{oc} [eq. (1.8)].

$$FF = \frac{j_{MMP} U_{MMP}}{j_{sc} U_{oc}} \tag{1.8}$$

The latter measurement allows the determination of the global efficiency η_{global} of a solar cell, which is defined in eq. (1.9) as the ratio between the maximum power extractable from the device and the incident power $P_{inc.}$ (ca. 1000 W m^{-2} for full sunlight).

$$\eta = \frac{j_{sc} \cdot U_{oc} \cdot FF}{P_{inc}} \tag{1.9}$$

1.1.3 Spectral Characteristics of a Photovoltaic Device

The amount of light that is absorbed by the cell is referred to as the light-harvesting efficiency *LHE* which depends on the surface concentration Γ and the extinction coefficient ε of the dye in the cell.[1] This wavelength-dependant function may be calculated according to eq. (1.10) if the cell is transparent.[1]

$$LHE(\lambda) = 1 - 10^{-\Gamma \varepsilon(\lambda)} \tag{1.10}$$

Furthermore, the ratio between the number of incident photons and collected electrons is referred to as external quantum efficiency *EQE*. $EQE(\lambda)$ for devices stained with one sensitizer is proportional to $LHE(\lambda)$ [eq. (1.11)]. The proportionality factors are the injection (ϕ_{inj}) and collection (η_{coll}) efficiencies. Since these efficiencies were not determined separately in this work they will be summarized as k in the following [eq. (1.12)].[8]

$$EQE(\lambda) = \phi_{inj}\eta_{coll}LHE(\lambda) \tag{1.11}$$

$$\phi_{inj}\eta_{coll} = k \tag{1.12}$$

The short circuit current density j_{sc} is a function of the spectral properties of both the solar cell, as characterized by the $EQE(\lambda)$, and the light source, as described by its photon flux $\Phi(\lambda)$ [eq. (1.13)].

$$j_{sc} = \frac{F}{N_A}\int_{300\text{ nm}}^{800\text{ nm}} EQE(\lambda)\cdot\Phi(\lambda)\mathrm{d}\lambda \tag{1.13}$$

F = Faraday constat
N_A = Avogadro constant

1.1.4 Sensitizers

Research towards novel sensitizers is one of the most active areas in basic DSC research. A variety of sensitizers that has been evaluated in the DSC is presented in Scheme 1. Initial success was achieved especially with carboxylated Ru polypyridyl complexes. Today's standard sensitizer is $[Ru(dcbpy)_2(NCS)_2]$ ("N3", **1**) or rather its bis-tetrabutylammonium salt termed "N719" (**2**). This sensitizer is commercially available and was the first one to give devices with $\eta > 10\%$.[1, 9] The latter dye collects photons up to 750 nm, however, a considerable fraction of the solar emission is in the near IR. In order to harvest this part of the sunlight efforts were undertaken to find dyes which absorb further into the near IR region of the solar emission spectrum. Such dyes are the terpyridine based Ru-complex termed "Black Dye."[10] With respect to the application of the devices a good efficiency is only one condition. Equally if not more important is their stability. The motivation for the development of amphiphilic sensitizers like the dyes "Z907" (**3**) and "K19" (**4**) were their superior long-term stability ("K19" reveals a more efficient light harvesting in the near IR due to the more extended π-system on one bpy-ligand).[11, 12]

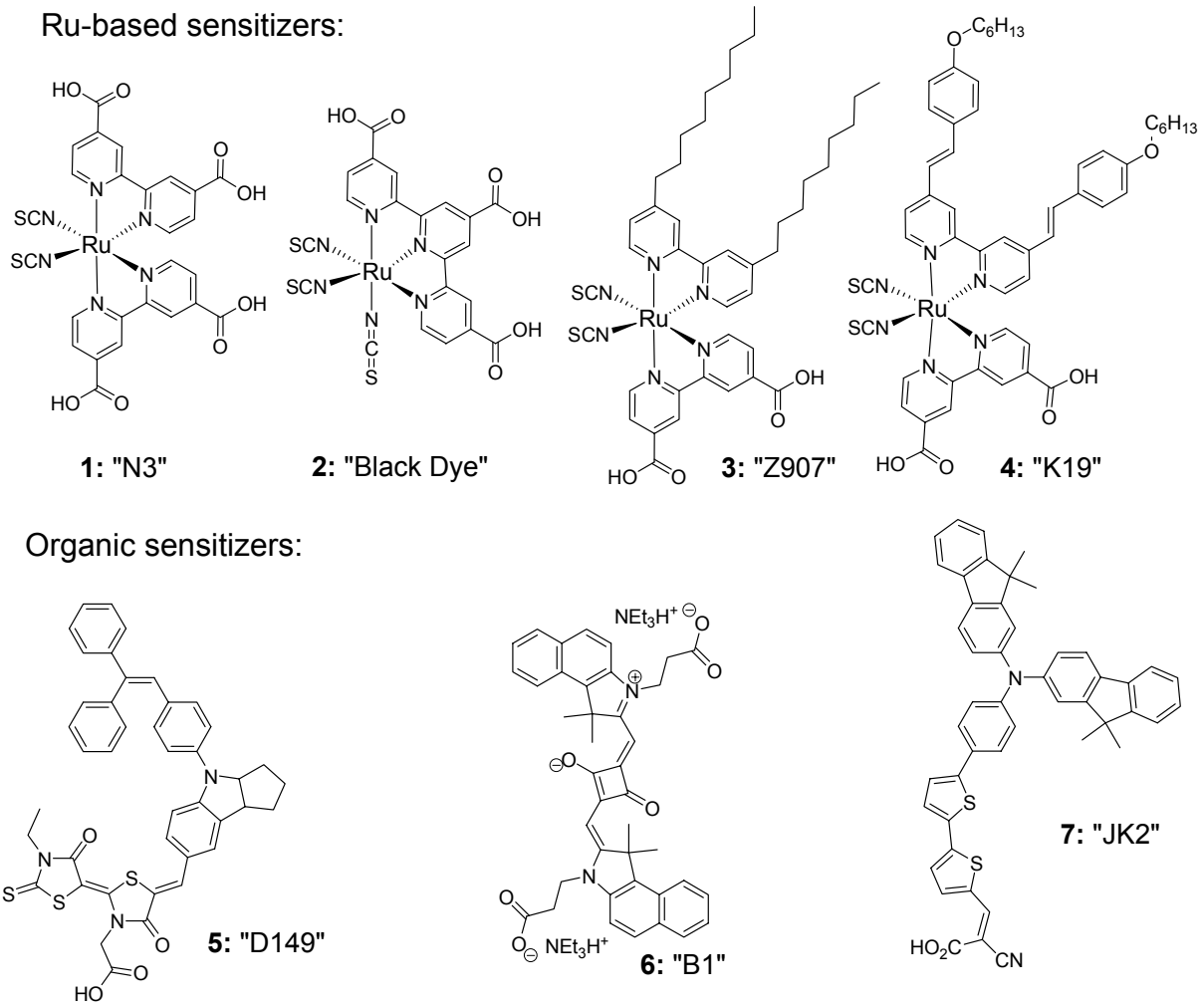

Scheme 1. Selection of sensitizers based on Ru-complexes and purely organic dyes that have been described in the literature.

Furthermore, there is a large interest in developing new purely organic dyes, which are suitable as sensitizers for the DSC.[13-21] This interest can be partially rationalized by the fact that the extinction coefficient of some classes of organic dyes (e.g., perylene- and xanthene-based dyes) are about one magnitude larger than that of the presently used Ru-based dyes (e.g., N719[9]). The use of dyes with high extinction coefficients ($\varepsilon > 50 \cdot 10^3$ M^{-1} cm^{-1}) imply that the optimal surface density for the operation of a DSC could be lower than for conventional DSCs based on Ru-complexes ($\varepsilon = 10 - 15 \cdot 10^3$ M^{-1} cm^{-1}).[9] Thus, one should be able to design the nanoporous electrode functionalized with a strongly absorbing dye so that it has a lower thickness than with the present standard electrode (< 10 μm) but an equal ability to absorb light. In general, a reduced electrode thickness would also result in a reduced rate of electron recombination with the electrolyte. In turn the open circuit voltage U_{oc} increases due to a higher electron concentration in the conduction band of the TiO_2, which further results in a higher overall efficiency [assuming a constant j_{sc} and FF, see also eq. (1.7)]. The above-mentioned organic dyes do not yield devices with good photoelectrochemical properties, e.g.,

Rhodamine 6G yields very low photocurrents due to major recombination of the electrons injected into the semiconductor with the oxidized dye,[22] and DSCs with perylene sensitizers have not reached efficiencies comparable to devices based on Ru-complexes *inter alia* due to a low open circuit voltage due to recombination.[19, 20] By the variation and optimization of the photoelectrochemical properties it was possible to find a variety of purely organic sensitizers giving good efficiencies in DSCs;[14, 15, 18, 21, 23, 24] however, producing a molecule which combines photophysical and electrochemical features so that its performance as sensitizer is excellent is a challenging task. Very recently an efficiency comparable to devices stained with "N719" was reached with the purely organic sensitizer "D149" **5**,[25] and the organic squaraine derivative "B1" **6**[26] absorbs predominantly in the red and near IR. The development of sensitizers has initially been an empirical field. Only recently the rational design of sensitizers has led to new, promising structures like the dye "JK2" **7** which presents a large aromatic system with electron donating and accepting substituents.[27] In conclusion present topics in DSC research include the development of a sensitizer that absorbs over the whole spectral range, notably in the near IR, and also possesses an excellent photo- and electrochemical stability.

1.2 Förster Energy Transfer

Energy transfer is a process, which has attracted extensive research interest in the past, due to its large implications in biology and in the past decade also for analytical purposes and in supramolecular chemistry. There are different mechanisms of energy transfer, one of which, the resonant energy transfer [(F)RET, long-range-, fluorescent-resonant- or Förster-energy transfer],[28, 29] will be briefly considered here. According to the Förster-theory,[30, 31] this type of energy transfer proceeds exclusively through dipolar interactions over distances of 1 nm – 10 nm. The rate of energy transfer k_{ET} between the energy donor and acceptor is rationalized by the equations (1.14) through (1.16) and depends largely on the photophysical properties and orientation of those moieties. This set of properties is summarized in the Förster-radius R_0 [eq. (1.14)], which describes the distance at which the energy transfer efficiency (*ETE*) is 50%. R_0 is dependant on the spectral overlap integral J, the fluorescence quantum yield of the energy donor Φ_D, the orientation factor κ^2, which is assumed to be 2/3 for flexibly linked chromophores and finally the refractive index of the surrounding media n. J describes the spectral overlap of donor emission with acceptor absorption. In eq. (1.15) F_D describes the fluorescence intensity of the donor normalized to unity and ε_A is the extinction coefficient of

the energy acceptor, both of which are dependent on the wavelength λ. Furthermore, k_{ET} depends on the interchromophoric distance r and the donor lifetime in absence of the acceptor τ_D (see eq. (1.16))

$$R_0^{\,6} = \frac{9000(\ln 10)}{128\pi^5} \cdot \frac{\kappa^2 \Phi_D J}{N n^4} \tag{1.14}$$

$$J = \int_0^\infty F_D(\lambda)\varepsilon_A(\lambda)\lambda^4 \mathrm{d}\lambda \tag{1.15}$$

$$k_{ET}(r) = \frac{1}{\tau_D}\left(\frac{R_0}{r}\right)^6 \tag{1.16}$$

Due to its distance dependence, RET is widely used to elucidate distances in chromophore-labeled biomolecules.[28] From the equations (1.14) to (1.16) it becomes apparent which conditions favor a high k_{ET} and thus a high *ETE*, namely, (i) a good overlap of the emission spectrum of the donor with acceptor absorption, (ii) an energy donor with a large value for Φ_D, (iii) a small interchromophoric distance r, and (iv) a molecular orientation allowing suitable dipole-dipole-interactions ($\kappa^2 \geq ⅔$). Energy transfer from one or more energy donors to an energy acceptor is also commonly referred to as the antenna effect.

1.3 Natural Light Harvesting Complexes and Synthetic Analogues

The process of light harvesting is the basis for most life on earth. By capturing light energy plants are able to convert water and carbon dioxide into dioxygen and matter with a higher energy content which then serve as energy suppliers for other species. Thus the process of natural light to energy conversion is of tremendous importance for life. Figure 3 is a schematic representation of the structure of the photosynthetic unit of purple bacteria.[32] It reveals a central reaction center encircled by light-harvesting complexes termed LH1 and LH2. The LH1 complex is composed of a ring-shaped assembly of chlorophyll and carotenoid moieties embedded in a protein matrix that surrounds the RC. A similar ring-shaped assembly, arranged further away from the RC, makes up the LH2 complex.

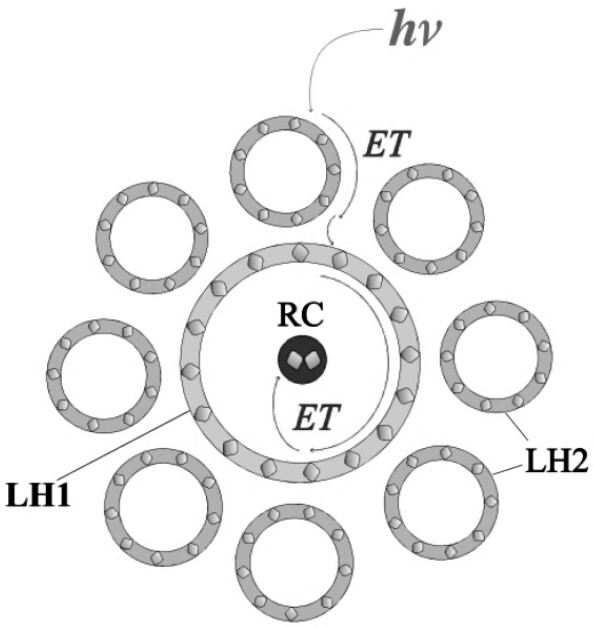

Figure 3. Schematic representation of bacterial light-harvesting complexes (LH1 and LH2) showing the different protein-embedded light-absorbing porphyrins (presented as the rhombi) arranged in circles around the reaction center (RC). The path of the excitonic energy is indicated by arrows.[29] The hopping of excitonic energy between identical chromophores (i.e., between rhombi within one circle) is referred to as energy migration, while energy transfer is defined as the energy hopping between different chromophores (typically from a chromophore with a high HOMO-LUMO-gap to a chromophore with a lower one).

These chlorophyll-containing assemblies enhance the light absorbing area: Photons that strike the relatively large surface area that the LH complexes cover are absorbed more efficiently and their energy is transferred to the RC *via* several hundred chlorophylls within the extensive LH system with unit efficiency.[29, 32] A considerable amount of work has been carried out towards the synthesis and characterization of artificial light-harvesting systems based on dendrimers.[29, 33-37] In such systems the excitonic energy resulting from light absorption of chromophores located in the periphery is efficiently funneled to one central chromophore. The latter behavior was termed antenna effect.[29] It was argued that these types of compounds are good platforms for the simulation of natural light-harvesting systems due to the well-defined and spherical structure. One example of a multichromophoric molecule simulating highly efficient energy transfer from several peripheral to one central chromophoric unit is shown in Scheme 2.[38] The chromophoric units composing the dendrimer **8** shown in Scheme 2 are typically highly luminescent if prevalent in diluted solution. Within **8**, the fluorescence of the chromophores within the periphery is quenched while the emission intensity of the central chromophore is increased. The latter results were consistent with nearly quantitative cascade energy transfer from the coumarines *via* the naphthalimides to the perylene core.[38] It turned out, however, that the defined structure from

dendrimers is not necessary for efficient energy transfer. Statistical copolymers decorated with suitable chromophoric units on the polymeric chain were also shown to effectuate near-quantitative excitonic energy transfer. One example is polymer **9** shown in Scheme 3, where the energy acceptor is a Ru-complex.[39-41]

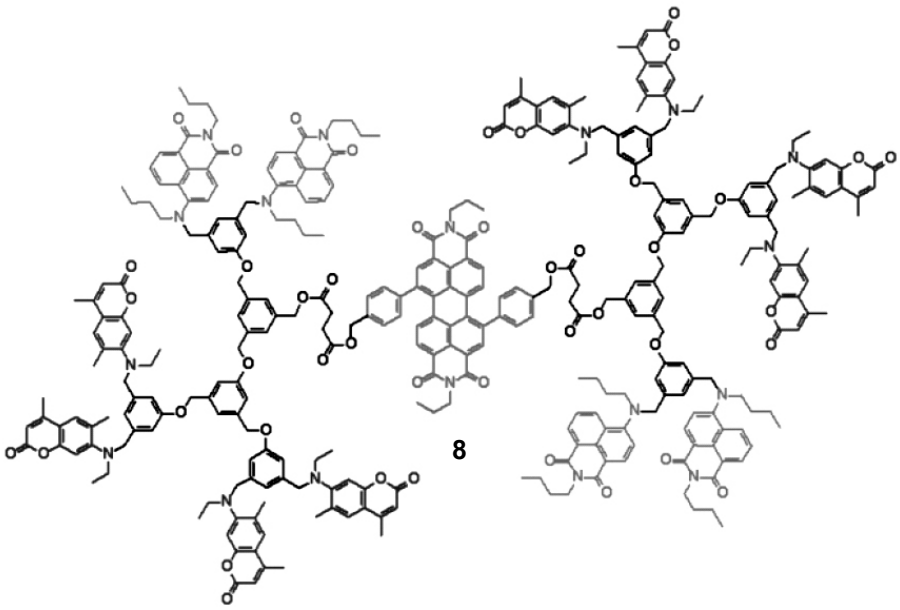

Scheme 2. Fréchet-type dendrimer carrying 8 coumarin and 4 aminonaphthalimide moieties that are arranged around one central perylene core.

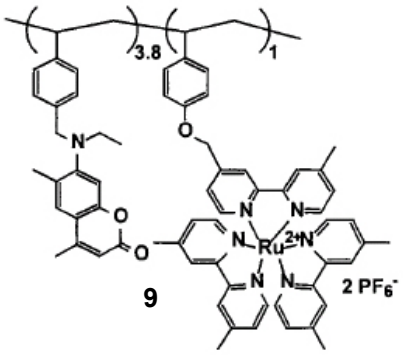

Scheme 3. Polymer comprising coumarin and $[Ru(bpy)_3](PF_6)_2$-units effecting energy transfer from the coumarin to the Ru complex.

The conclusion from the above-mentioned examples is that resonant energy transfer is a very robust tool: As long as the conditions for efficient resonant energy transfer, namely, a high fluorescent quantum yield of the donor, freely rotating chromophores, a high spectral overlap integral, and interchromophoric distances that are well below the Förster-radius are met, efficient energy transfer will take place.

1.4 The Antenna-Effect in the Dye Solar Cell

As it was shown above, the antenna effect is a crucial strategy for making an effective use of light for energy conversion in light-harvesting natural systems.[32] Furthermore, it has also been explored in synthetic, supramolecular systems.[29, 42-44] In case of the artificial systems presented above the event following the energy transfer was the emission of a photon. Rather than using the antenna effect before an energy conversion event, it only led to an enhancement of the Stokes shift. The utilization of the antenna effect within a DSC, however, would mimic the energy transfer – energy conversion – cascade from natural light-harvesting systems. Using such a cascade in the DSC has been proposed[42, 45] and its feasibility was proven by experimental work. Some multichromophoric sensitizers are shown in Scheme 4.

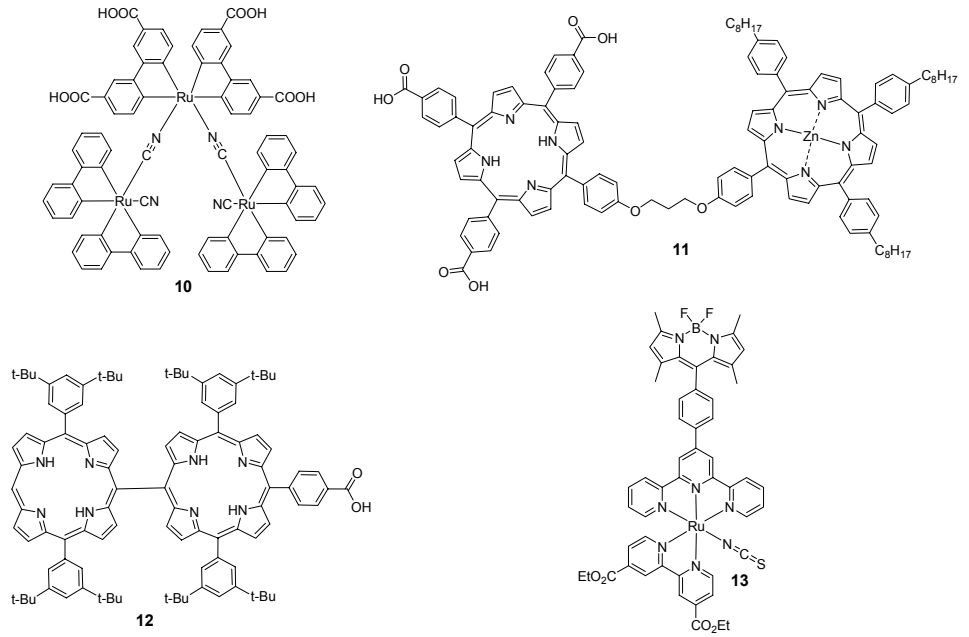

Scheme 4. Structures of some multichromophoric sensitizers described in the literature.

Within the trinuclear Ru complex **10** the energy donor and acceptor species both present metal complexes.[2, 46] Different modifications of porphyrins (e.g., **11** and **12**) have also been used as sensitizers.[47-49] The $EQE(\lambda)$ of devices stained with these sensitizers clearly sustained the fact that the chromophoric unit that is not in direct contact with the semiconductor also contributes to the photocurrent. The above-mentioned sensitizers, though, do not emanate from compounds known to give highly efficient dye solar cells. Odobel and Zabri[43] described the synthesis of compound **13**, which presents a dyad comprising an organic energy donor and a Ru-complex that is very similar to sensitizers known to give highly efficient devices, however, the performance of this dye in the DSC was not investigated.

2 Objective

One alternative strategy to make effective use of light for energy conversion, which is primarily applied in light-harvesting natural systems,[32] but which has also been used in synthetic, supramolecular systems, is the antenna effect.[29, 42-44] The rationale for the present thesis is that it should be possible to enhance DSC performance using energy transfer systems (Figure 4). This rationale offers the advantage of a simple, independent optimization of photophysical and electrochemical features of the sensitizing system by choosing different units for the light-harvesting and the electron-injection. It was already shown that energy transfer can be followed by electron injection for a fluoresceine-antracene dyad adsorbed on TiO_2. However, in this work, the absorption of the antenna was exclusively in the UV, which is not practical for DSC applications.[50] Furthermore, using this effect in the DSC has already been proposed by others and its feasibility was proven by experimental work dealing with either metal complexes as energy donor and acceptor chromophores,[2, 42, 45, 46] or different modifycations of porphyrins.[47-49] These publications, however, do not emanate from sensitizers known to give a high performance in the DSC (e.g., $[Ru(dcbpy)_2(NCS)_2]$[9]). The concept of this work was to test the work hypothesis that *combining the advantages of organic dyes, like a high extinction coefficient with the advantages of highly efficient Ru-sensitizers, namely the ability to efficiently inject electrons into the TiO_2-conduction band, will lead to an increase in DSC performance*. The increase in performance would be the result of the absorption – energy transfer – electron injection cascade shown in Figure 4: The organic dye enhances light absorption and serves as energy donor, a Ru-complex is the energy acceptor and subsequently transfers excitation into electronic energy. The energy is transferred from the energy donor to the acceptor by resonant energy transfer.

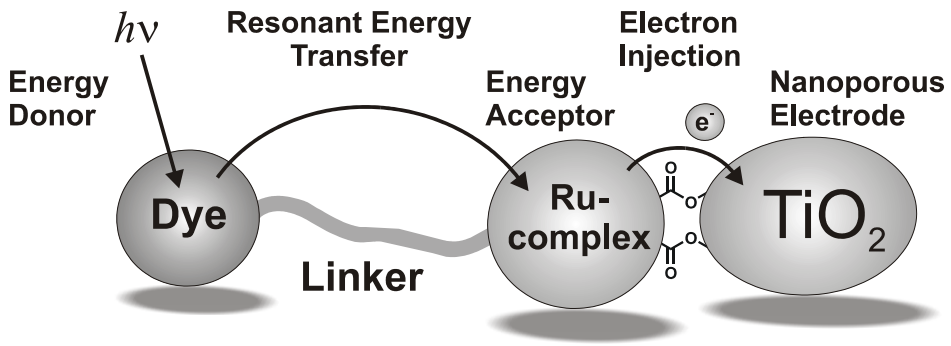

Figure 4. Mechanism of the enhancement of light-harvesting *via* resonant energy transfer.

The second work hypothesis was inspired by the way natural systems (e.g., the light harvesting complexes I and II) manage to capture light efficiently for light-to-chemical energy conversion: It should be tested whether it is possible to use *the energy transfer from multiple energy donors to one acceptor*, thus whether the above-mentioned concept also works for artificial energy transfer systems having energy donor acceptor ratios larger than one, *for an increase in DSC performance*.

The following approach was to be followed for the testing of the hypotheses:

(i) Identification of suitable chromophores

(ii) Synthesis of model chromophores and functional chromophores allowing covalent attachment to a linker

(iii) Covalent attachment of donor and acceptor chromophores to suitable small and polymeric substrates

(iv) Photophysical characterization of donor-modified polymers towards their energy transfer behavior

(v) Photophysical characterization of model donor acceptor-compounds

(vi) Evaluation of donor acceptor systems in the DSC

The choice of chromophores and synthesis of compounds is discussed in chapter 3. Results from the photophysical characterization of donor polymers are presented in chapter 4. The detailed photophysical characterization of the synthesized compounds within the solar cell is portrayed in chapter 5.

3 Synthesis of Donor Acceptor Systems for the Dye Solar Cell

In order to test the work hypotheses considering energy transfer in the DSC, a variety of compounds with different characteristics was necessary for photophysical studies in solution as well as sensitizers in the DSC. These compounds comprised (i) small model chromophores and donor acceptor dyads with a defined donor acceptor-ratio (1:1), (ii) polymers functionalized exclusively with donor or acceptor chromophores, and (iii) polymers functionalized with both kinds of chromophores. Isolating compounds that carry the dissimilar chromophoric units on a common linker was not trivial. The successful synthetic strategies that lead to the isolation of such compound are described in the following.

3.1 Choice of Chromophores

The chromophoric units that were employed here comprised the ruthenium polypyridine complex [Ru(dcbpy)$_2$acac]Cl **14** as energy acceptor and the alkylated aminonaphthalimide Fluorol 7GA **15** as energy donor (Scheme 5). In the following two sections the reasons for the choice of this set of chromophores is presented.

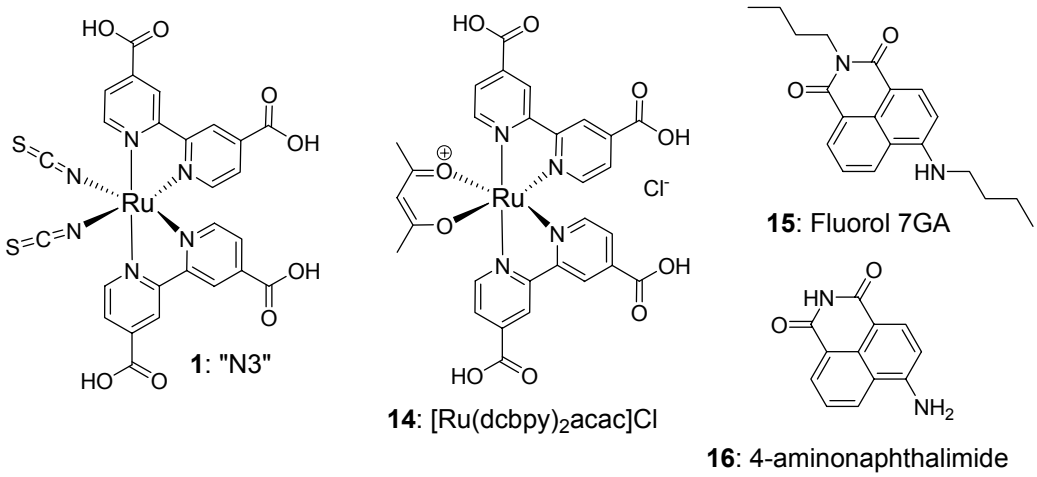

Scheme 5. Structure of the most common dye used in the DSC ("N3," **1**), and of the chromophores [Ru(dcbpy)$_2$acac]Cl (**14**) and Fluorol 7GA (**15)**, along with its parent compound 4-aminonaphthalimide (**16**), that were used in this work as energy acceptor and donor, respectively.

3.1.1 Energy Acceptor

Today's most common dye used in the DSC, [Ru(dcbpy)$_2$(NCS)$_2$] "N3" (**1),** was developed by Nazeeruddin *et al.* (Scheme 5).[9] This molecule does not offer a facile means of covalent attachment of a linker group without affecting its photophysical properties. Takahashi *et*

al.[51] and Sugihara *et al.*[52] showed that complexes, in which the two thiocyanato ligands have been replaced by a 1,3-diketonato moiety, e.g., [Ru(dcbpy)$_2$acac]Cl **14,** Scheme 5, have very similar efficiencies to N3, if employed as sensitizers in the DSC. The latter was proven by the similarity in *EQE*(λ)-data shown in Figure 5 and solar cell characteristics. [51]

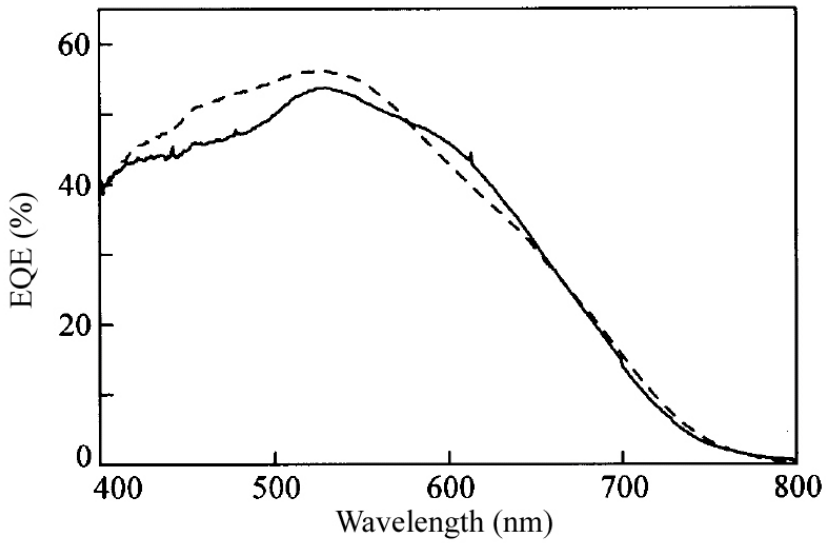

Figure 5. *EQE*(λ)of DSCs sensitized with [Ru(dcbpy)$_2$(NCS)$_2$] (**1,** dash) and [Ru(dcbpy)$_2$acac]Cl (**14**, solid).

The assumption that modification at the terminal positions of the acetylacetonato-ligand would not drastically alter the photophysical and photoelectrochemical properties of the parent complex led to the choice of [Ru(dcbpy)$_2$acac]$^+$ as energy acceptor for resonant energy transfer within the DSC. This complex offers (i) efficient electron injection into the nanoporous electrode and (ii) a means of chemical modification *via* the introduction of functional groups on the terminal Me-group of the acac-ligand.[53]

3.1.2 Energy Donor

The energy donor will serve as an additional absorber within the DSC. Combining a donor and acceptor chromophore should be a means to tune the DSC absorbance towards the solar emission spectrum. The energy of the light absorbed by the donor should furthermore be transferred to the energy acceptor, thus the rate for energy transfer should be high. Taking into account the conditions for optimal RET presented in Section 1.2, the energy donor should possess (i) a complementary absorption to the energy acceptor, (ii) a high quantum yield, (iii) an emission spectrum which overlaps with the acceptor absorption, i.e., large overlap integral, (iv) a facile means of chemical modification considering the introduction of a linking unit,

and (v) (photo)chemical stability. The parent compound 4-amino-1,8-naphthalimide **16**[54-57] was chosen as a suitable chromophoric system since it fulfills all of the above-mentioned criteria. 4-butylamino-N-butyl-1,8-naphthalimide (Fluorol 7GA) **15** is a commercial product, which has found an application as a laser dye. Fluorol 7GA derivatives have been used for energy transfer studies in the past.[38] It absorbs in a wavelength regime, where $[Ru(dcbpy)_2acac]^+$ does not strongly absorb and has a high quantum yield even in polar solvents (Figure 6). The emission spectrum matches well with the low-wavelength absorption of $[Ru(dcbpy)_2acac]^+$ (Figure 6) and the extinction coefficient of these chromophores is comparable. The Förster-radius of the Fluorol 7GA/$[Ru(dcbpy)_2acac]$Cl-chromophore pair is $R_0 = 4.6 \pm 0.1$ nm in EtOH.

Table 1. Summary of spectral properties of parent chromophores in ethanol.

Chromophore	$\lambda_{abs,\,max}$ [nm]	ε [M^{-1} cm^{-1}]	$\lambda_{em,\,max}$ [nm]	Φ [%]
Fluorol 7GA (**15**)[54]	440	16000	536	81
$[Ru(dcbpy)_2acac]$Cl (**14**)[51]	544	13500		

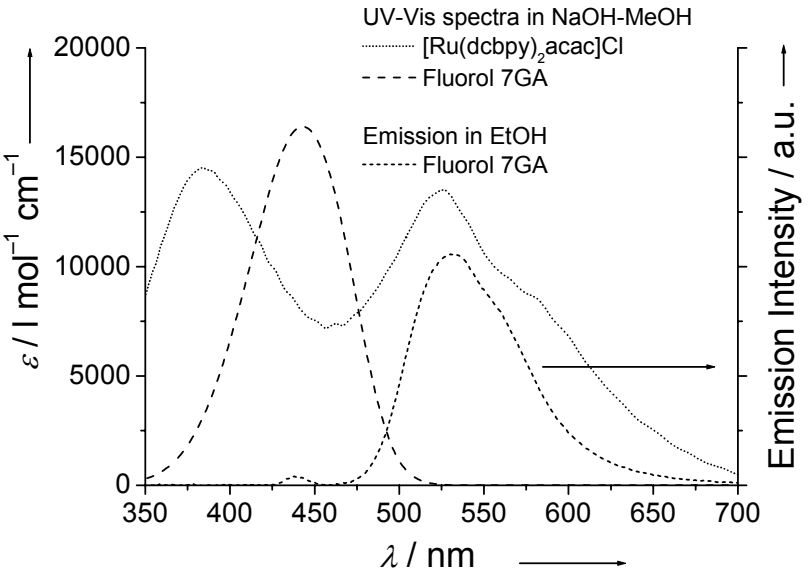

Figure 6. Juxtaposition of the absorption and emission spectra of the energy donor Fluorol 7GA (**15**) and the absorption spectrum of the energy acceptor $[Ru(dcbpy)_2acac]$Cl (**14**). There is a good overlap between the Fluorol emission and Ru-absorption.

3.2 Experimental Design

In order to test the hypothesis that photons absorbed by a fluorescent dye close to an electron injecting Ru-complex in the DSC will result in additional current generation, the following experimental approach was chosen: (i) development of a synthetic strategy allowing the facile covalent attachment of Fluorol 7GA (**15**) to [Ru(dcbpy)$_2$acac]Cl (**14**); (ii) photophysical characterization of the model compounds in solution including absorption and emission spectra and excited state lifetime measurements in solution and (iii) evaluation of these systems within the DSC by determination of the external quantum efficiency (EQE) and the overall efficiency under different types of illumination. Previous energy transfer studies using chromophore decorated Fréchet-type dendrimers showed that energy transfer in these systems is highly efficient.[29, 36] However, less perfect structures, i.e., statistical copolymers also reveal high energy transfer efficiencies.[41] Thus in addition to bifunctional linkers leading to defined donor acceptor compounds with a 1:1 donor acceptor ratio, the support of the respective chromophores to multifunctional linkers was followed as a strategy to acquire donor acceptor systems with donor acceptor ratios larger than unity.

3.2.1 Retrosynthetic Considerations

Scheme 6 summarizes retrosynthetic considerations towards the synthesis of donor acceptor compounds **17** suitable for an application in the DSC.

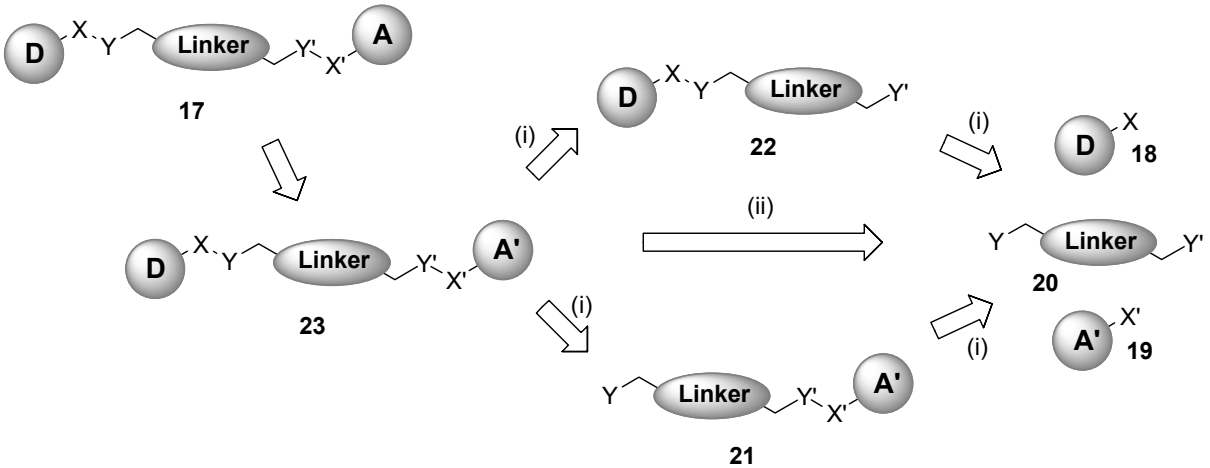

Scheme 6. Retrosynthesis of donor acceptor systems. The synthesis of such systems is led back to the functional chromophores and linker. Two different synthetic strategies are presented: (i) sequential addition of donor and acceptor chromophores to the linker (or vice versa) and (ii) simultaneous support of donor and acceptor chromophores.

This scheme traces donor acceptor systems **17** back to respective functional donors (**18,** D-X), acceptors (A-X′) or acceptor precursors (**19,** A′-X′) and linkers **20**. The donor acceptor systems could be synthesized *via* the acceptor or donor functionalized linker **21** and **22**, respectively [strategy (i)], or *via* the simultaneous support of donor and acceptor units to **20** [strategy (ii)]. Since there might be restrictions posed by the solubility of the desired acceptor moiety in most common solvents, chemical transformations leading to the support of [Ru(dcbpy)$_2$acac]Cl derivatives could result in the necessity of acceptor precursors (A′) for the supporting reaction. The latter will finally be transferred to the acceptor for use in the DSC (conversion from **23** to **17** in Scheme 6).

3.2.2 Different Synthetic Strategies

A variety of synthetic strategies was evaluated for the synthesis of molecular systems comprising Fluorol 7GA and [Ru(dcbpy)$_2$acac]Cl derivatives covalently bound to a mono- and polymeric linking unit. Table 2 presents an overview of the functional groups that were chosen for the evaluation of linking chemistry. The functionalities X, X′, Y and Y′ refer to Scheme 6. A more detailed description of the linking units used is given prior to the sections describing the respective synthetic results.

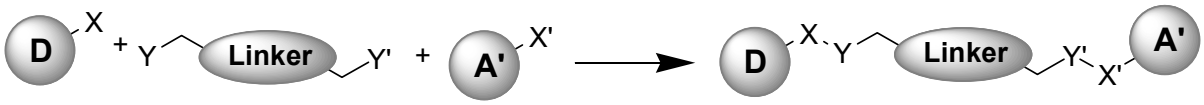

Table 2. Summary of strategies which were evaluated towards the synthesis of donor acceptor systems. These strategies were based on the support of respective donor and acceptor chromophores on di- and multifunctional linking units (see Scheme 6 for the significance of X, X', Y and Y').

Entry	Functional groups X, X′, Y and Y′ on D-X	Y-Linker-Y'	A'-X'	Reaction Type	Results in Section
1	-CH=CH$_2$	-SiMe$_2$-H	-CH=CH$_2$	hydrosilylation	3.4.1
2	-SiMe$_2$-H	CH=CH$_2$	none	hydrosilylation	3.4.2
3	-C≡CH	-CH$_2$-N$_3$	-C≡CH	cycloaddition	3.6
4	cycl. aromatic anhydride	H$_2$N-(CH$_2$)$_4$-N$_3$	-C≡CH	imide-formation + cycloaddition	3.3 and 3.6

The motivation for referring to hydrosilylation reactions as a means to support functional units was inspired by work from Finkelmann *et al.* who applied this reaction successfully to the synthesis of liquid crystalline poly- and elastomers from olefin-functionalized entities (e.g., mesogens and crosslinkers) and polyhydrosiloxanes.[58-61] The motivation for the use of the 1,3-dipolar cycloaddition between azides and terminal alkynes (Huisgen-reaction, Click-Chemistry) was its tolerance towards a large variety of solvents and functional groups, which turned out to be crucial for this work.[62-65] In the following the syntheses carried out according to Scheme 6 and Table 2 will be presented. These results are classified as follows: Initially Section 3.3 presents the synthesis of linker-modified Fluorol 7GA derivatives. Then the reactions towards linking the donor chromophore to acceptor precursors *via* hydrosilylation is discussed (Section 3.4). The synthesis of functional $[Ru(dcbpy)_2acac]Cl$ derivatives (some of which are employed as substrates in Section 3.4) is presented in section 3.5. Finally the linking of alkyne functionalized chromophores to azides is presented in Section 3.6.

3.3 Functionalization of 4-Aminonaphthalimides with Linker Units

The 4-amino-1,8-naphtalimide derivative Fluorol 7GA (**15**) that served as parent chromophore does not allow immobilization to suitable linkers. Thus the synthesis of functional Fluorol 7GA derivatives was necessary. Their synthesis proceeds in two steps from commercial 4-chloro-1,8-naphtalic anhydride (**24**) (Scheme 7).[54-57]

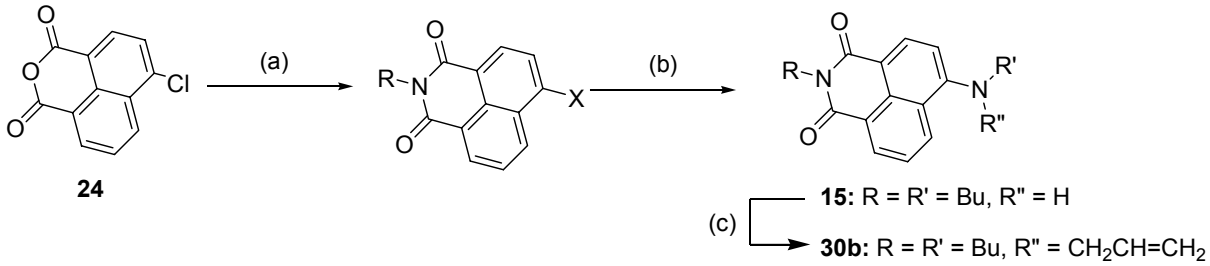

Scheme 7. Synthesis of functional aminonaphthalimides from commercial 4-chloro-1,8-naphthalic anhydride and from commercial Fluorol 7GA **15**. (a) R-NH_2 in EtOH (X = Cl) or R-NH_2 in imidazole (R = 2,6-diisopropylpheny l, X = $C_3H_3N_2$). (b) R'-NH_2 in NMP (R" = H). (c) **15** to **30b**: Allyl bromide and NaH in DMF. The imide formation reactions carried out according to this scheme are summarized in Table 3 (Section 3.3.1). The aromatic nucleophilic substitutions performed are associated in Table 4 (Section 3.3.2).

Generally, the first step in the synthesis of aminonaphthalimides consists in the imide formation of a 1,8-naphthalic anhydride carrying a functional group, e.g., Cl, or NO_2 in the 4-position with an amine. The second step involves the displacement of the functional group in the 4-position by another amine *via* an aromatic nucleophilic substitution. The latter reaction

proceeds only in polar aprotic solvents. Thus by running the above-mentioned reactions it is possible to selectively functionalize the anhydride in EtOH and subsequently the aromatic ring in NMP with different amines.[54, 55, 57, 66]

An alternative route to functionalize aminonaphthalimides carrying a hydrogen atom on the aromatic amine nitrogen is the abstraction of the proton with NaH in DMF, which leads to a dark purple anion, and alkylation with an alkyl bromide (conditions c in Scheme 7).[38]
In this work the following amines were used for their introduction into the naphthalimide system: butyl amine, allyl amine, propargyl amine, 4-azidobutylamine, 5-aminovaleric acid and 2,6-diisopropy aniline. Butyl amine served as a dummy. Allyl amine was introduced in order to acquire a derivative which could be further subjected to hydrosilylation reactions. Propargyl amine and 4-azidobutyl amines were the basis for fluorol derivatives suitable for 1,3-dipolar cycloadditions. The synthesis of a carboxylated Fluorol 7GA derivative required for NMR experiments in aqueous solution and as sensitizer in the DSC started from 5-aminovaleric acid. 2,6-Diisopropy aniline was frequently used as a substrate to introduce bulky substituents sandwiching a more extended aromatic system. Therefore this amine was also used here in order to evaluate the synthesis of fluorol derivatives which possibly do not show concentration quenching.[67] The compounds synthesized here are designated using the following nomenclature scheme: R-R′-R"-fluorol. R is the name of the substituent on the imide nitrogen, R′ and R" are the names of the substituents on the amine nitrogen or the 4-position of the aromatic ring. R" = H is omitted. For example the imide formation of **24** with butyl amine leads to butyl-chloro-fluorol; the $S_{N, Ar}$ reaction with allyl amine leads to butyl allyl fluorol.

3.3.1 Imide Formation with Halogenonaphthalic Anhydrides

The imide formation of the chloronaphthalimide **24** is a very straight forward reaction (Scheme 7, first reaction step). The individual products that resulted from the latter reaction are presented in Table 3. Runs 1 – 4 were carried out by dissolving the chloronaphthalic anhydride in refluxing EtOH and addition of the amine.[55] The work-up consisted solely in the removal of the solvent and drying. If amines with a hydrophobic residue were used, product formation was quasi instantaneous (entries 1 and 2). If the functional amines H_2N-$(CH_2)_4$-COOH and H_2N-$(CH_2)_4$-N_3 were used, the conversion did not proceed to completion (entries 3 and 4). Reacting the anhydride with 2,6-diisopropyl aniline under the above-mentioned conditions did not lead to product formation. In analogy to the imide formation

with perylene tetracarboxylic acid anhydride, this imide formation succeeded using molten imidazole as solvent.[67-69] The NMR spectra of the products showed aromatic impurities which were already present in the starting material. The crude products were used in the next reaction step, the nucleophilic aromatic substitution, without further purification. In conclusion the conversion of halogenonaphthalic anhydrides with primary amines led to a series of functional halogenonaphthalimides suitable for their further conversion into Fluorol 7GA derivatives with linker units.

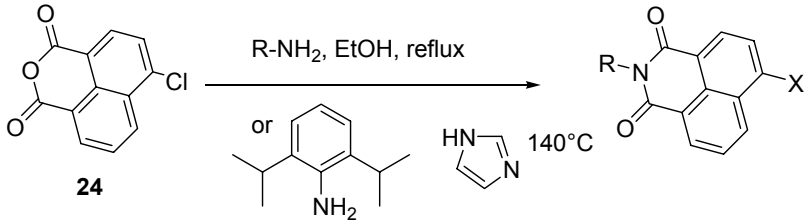

Table 3. (Pseudo-)halogenonaphthalimides synthesized in this work. The reactions were carried out by dissolving 4-chloro-1,8-naphthalimide in refluxing ethanol and addition of an excess of the corresponding amine (except for entry 5: conversion with 2,6-diisopropylaniline in molten imidazole).

Entry	Product	R =	X =	Solvent	Yield
1	butyl chloro fluorol **25**	$-(CH_2)_3CH_3$	-Cl	EtOH	80%
2	propargyl chloro fluorol **26**	$-CH_2-C\equiv CH$	-Cl	EtOH	71%
3	4-carboxybutyl chloro fluorol **27**	$-(CH_2)_4-COOH$	-Cl	EtOH	56%[a)]
4	4-azidobutyl chloro fluorol **28**	$-(CH_2)_4-N_3$	-Cl	EtOH	34%[a)]
5	2,6-diisopropylphenyl imidazolo fluorol **29**[b)]	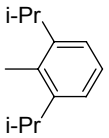		Imidazole	72%

a) These reactions did not proceed to completion. The reaction product consisted of a mixture of starting material and title compound, which was employed for the next synthetic step without further purification. Instead of the yield, the conversion was calculated from a ^{1}H-NMR of the crude product.
b) This reaction was carried out at 140°C. Under these conditions the chloride atom on the aromatic ring was substituted by an imidazole group.

3.3.2 Functional Fluorol Derivatives

The 4-halogeno-1,8-naphthalimides from Table 3 were further reacted with amines to yield the respective 4-aminonaphthalimide derivatives (Scheme 7, conditions b, Table 4 except for run 2). The reactions were carried out by dissolving the respective halogenonaphthalimide and the butyl or allyl amine in NMP and stirring at 60 – 80°C for 1 to 3 days. Under these conditions both chloride atoms and the imidazole group in **29** were substituted. During the

reaction an intense yellow color appears. The work-up consisted in the removal of the solvent by condensation under high vacuum and column chromatography on silica gel using isohexane ethyl acetate mixtures and/or recrystallization from EtOH.

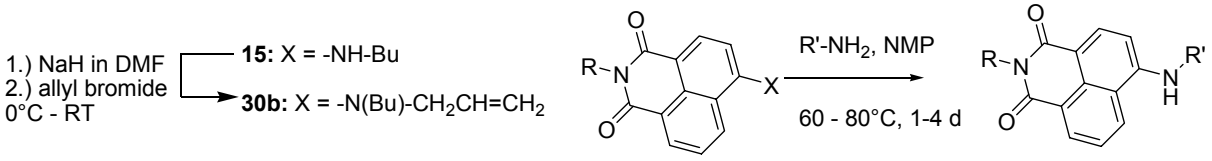

Table 4. Aminonaphthalimide derivatives synthesized in this work. The reactions were carried out by stirring the halogenonaphthalimides with 3 – 5 equivalents of amine at 40 – 80 °C for 1 – 4 days (except for Entry 2: This compound was synthesized via the allylation of the parent compound Fluorol 7GA 15 with allyl bromide and NaH in DMF). The products were isolated by column chromatography on silica gel.

Entry	Product Name	Structure	X =[a)]	R′ =	Yield
1	butyl allyl fluorol **30a**	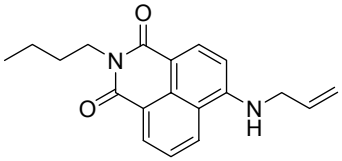	-Cl	Allyl	92%
2	dibutyl allyl fluorol **30b**	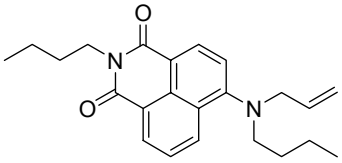	-NH-Bu	n.a.	80%
3	propargyl butyl fluorol **31**[b)]	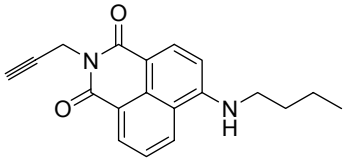	-Cl	Bu	85%
4	4-carboxybutyl butyl fluorol **32**	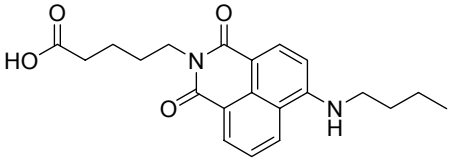	-Cl	Bu	10%[c)]
5	4-azidobutyl butly fluorol **33**	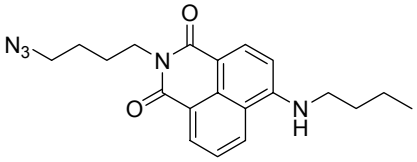	-Cl	Bu	90%
6	2,6-diisopropyl-phenyl allyl fluorol **34**[d)]	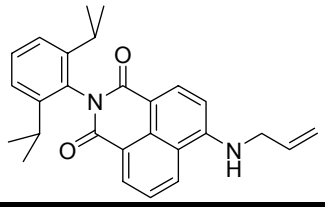		Allyl	60%

a) Aromatic substituent in starting material (see Scheme 7). b) This product was purified by recrystallization from ethanol. c) Unoptimized yield. d) The product was only characterized by ^{1}H NMR.

A slightly faster approach to the synthesis of an olefin functionalized fluorol derivative was realized by the substitution of the amine hydrogen on Fluorol 7GA by the allyl group. The

latter conversion was achieved using NaH and allyl bromide in DMF [Scheme 7, conditions (c), Table 4, entry 2]. This reaction, however, brings about a significant change in the photophysical properties of the aminonaphthalimide moiety: The fluorescence quantum yields of aminonaphtalimides carrying 2 alkyl substituents on the amine nitrogen is close to zero in polar organic solvents[54, 55] and the absorption maximum in EtOH is blue-shifted by about 10 nm. The latter is possibly a result of peri-interactions impairing the interaction of the amine-nitrogen's lone-pair with the aromatic system. The compounds were consistent with their ^{1}H and ^{13}C NMR, mass spectrometry and/or elemental analysis data. The ^{1}H NMR spectra of compounds **30a** and **30b** are shown in Figure 7a and Figure 8a. The reactions described in this chapter lead to a variety of fluorol derivatives that are suitable for different immobilization strategies. While no attempts were undertaken to proceed with compound **34,** further conversions of compounds **30a**, **30b**, **31** and **33** are described in the following chapters. Furthermore **32** will serve as an important model compound in ^{1}H NMR and photophysical studies within the DSC.

3.4 Hydrosilylations with Olefin Functionalized Chromophores

The hydrosilylation with Si-H-bearing linkers was an important strategy for linking the olefin-bearing donor and acceptor chromophore or chromophore precursors to each other. Furthermore, this reaction was employed to immobilize the donor chromophore to allylated polyglycerol (Allyl-PG). In the next sections the reactions carried out towards the Pt-mediated addition of hydrosilanes to olefins will be presented.

3.4.1 Addition of Si-H Moieties to Donor Chromophores and Acceptor Precursors

Scheme 8 summarizes the hydrosilylation reactions carried out in this work and their respective substrates. $[Ru(dcbpy)_2acac]Cl$-derivatives used as energy acceptor chromophores in this work are completely insoluble in unpolar organic solvents, which renders hydrosilylation reactions with this type of compounds impossible. Thus the methylated species $[Ru(di\text{-}Me\text{-}dcbpy)_2allyl\text{-}acac]^{+}$ derivatives **35a** and **35b** as well as allyl-acacH **36** were used as acceptor precursors in hydrosilylations (the synthesis of the latter 2 compounds is described in sections 3.5.2.3 and , respectively). In contrast to the energy acceptor, the olefin functionalized donor chromophores **30a** and **30b** are suitable for hydrosilylation reactions. The rational for using **30b** in addition to **30a** was founded on the fact that **30b** was available within one reaction step from the commercially available Fluorol 7GA **15**.

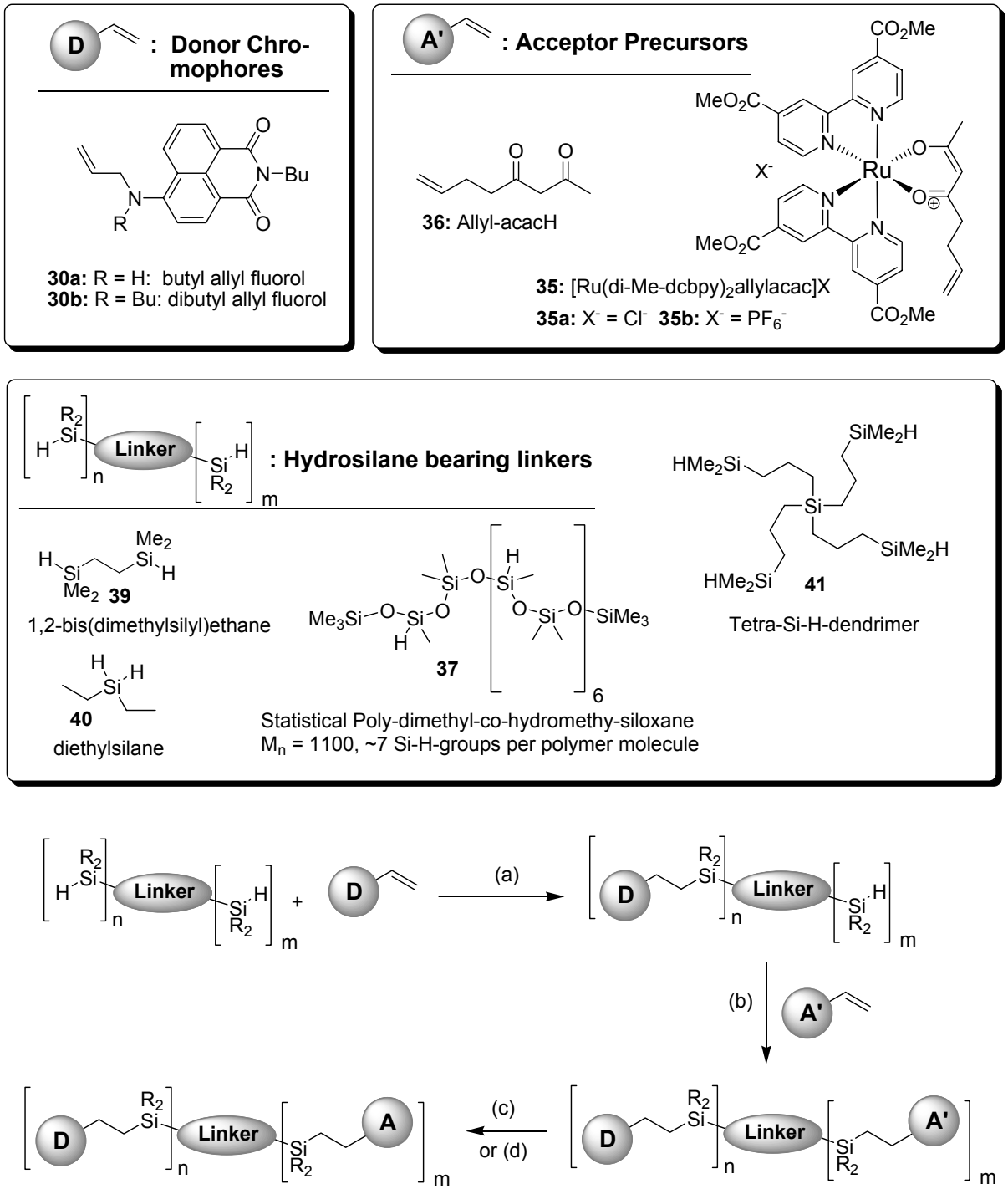

Scheme 8. General synthetic scheme describing the synthesis of donor acceptor systems *via* the addition of Si-H-bearing linkers to the olefin functionalized donor chromophore and/or olefin functionalized acceptor precursor. The types of olefin-functionalized donor chromophores, acceptor precursors and Si-H-bearing linkers that were used in this work are shown in the boxes. Platinum-1,1,3,3-tetramethyl-1,3-divinyldisiloxane (Pt-cat.) was employed as hydrosilylation catalyst. (a) toluene or DCM, Pt-cat, (b) toluene or DCM, Pt-cat, (c) NaOH, H_2O, (d) [Ru(di-Me-dcbpy)$_2$Cl$_2$], solvent, base (This reaction is described in detail in Section 3.5.2).

Initial experiments towards the syntheses shown in Scheme 8 were carried out with the Si-H-bearing polymer poly-dimethyl-co-hydromethy-siloxane **37** (PHMS). One example of these preliminary experiments is shown in Scheme 9. It was shown that it is possible to link the

donor chromophores **30a** and **30b** and acceptor precursors **35a** and **36** to Si-H moieties yielding the polymer **38**. However, the conversion of Si-H to the respective Si-CH_2CH_2-R group was not necessarily quantitative, although IR-spectroscopy data proved that Si-H had completely reacted. In conclusion, these experiments showed that despite the hydrosilylation with the olefin-bearing chromophores and precursors proceeding in the desired manner, it does not proceed free of side reactions.

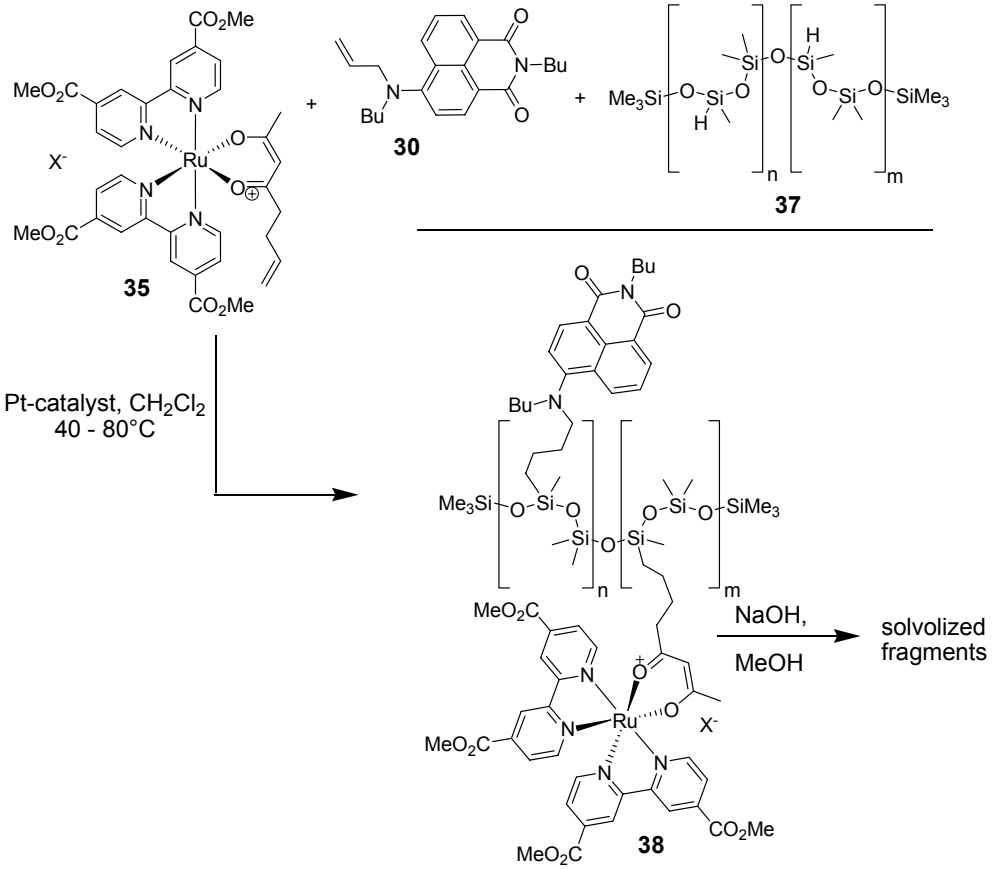

Scheme 9. Hydrosilylation comprising the functional olefins **30** and **35** as well as the Si-H bearing polysiloxane **37**.

Polysiloxanes are not suitable as a linking unit, especially because the Si-H moieties are partially converted into a different functional group, whose identity was not further investigated, and because of the instability of the siloxane polymer towards the reaction conditions prevailing during conversion of the acceptor precursor (A') to the acceptor (A, second step in Scheme 9, third step in Scheme 8).

On the other hand, hydrosilylation reactions with carbosilanes **39**, **40** and **41** lead to compounds that do not comprise hydrolytically sensitive Si-O-bonds. Although side reactions leading to the decomposition of the Si-H-groups cannot be ruled out, the resulting side products may be removed by appropriate purification steps. The rationale for the choice of this set of hydrocarbosilanes as linkers was (i) variation in the resulting donor acceptor distance

by employing two different difunctional silanes **39** and **40**, respectively, and (ii) variation in the donor acceptor ratio by using the tetra-Si-H-dendrimer **41**.

Reactions with aminonaphthalimides carrying a hydrogen atom on the amine nitrogen were conducted in DCM under reflux, the other hydrosilylations proceeded in toluene at 40 – 60°C. Platinum-1,1,3,3-tetramethyl-1,3-divinyldisiloxane (Pt-cat.) was employed as hydrosilylation catalyst. The initial step of the hydrosilylation sequences served to couple the donor chromophores **30** to the difunctional Si-H-linkers **39** and **40** resulting in the Si-H-bearing donor units **42** and **43** (Table 5, entries 1 – 3, Scheme 8, step a). In these reactions an excess of disilane was used in order to minimize dimer formation. The acceptor precursors **35** and **36** were subsequently coupled *via* a second hydrosilylation step to the reaction products **42a** and **42b** (Table 5, entries 4 – 6, Scheme 8, step b). The products butyl acacH fluorol (**44a**) and dibutyl acacH fluorol (**44b**) as well as the tetramethylester of **45** emerged from these reactions. Furthermore the decoration of **41** was performed with 4 units of allyl-acacH (**36**, Table 5, entry 7). In this run an excess of olefin was employed. The transformation of the acceptor precursor to the acceptor moiety suitable for its application as sensitizer in the DSC is the third step of the sequence in Scheme 8. Depending on the nature of acceptor precursor, this step consists in the hydrolysis of the tetramethyl ester of **45** in aq. NaOH if the precursor was a $[Ru(di\text{-}Me\text{-}dcbpy)_2allyl\text{-}acac]^+$ derivative, and the complex formation between $[Ru(dcbpy)_2Cl_2]$ and the functional acac-derivative if allyl-acacH was used in the hydrosilylation. The latter reaction is discussed in detail in Section 3.5.2.2. In case of runs 1 and 2 yielding the products butyl hydrosilyl (**42a**) and dibutyl hydrosilyl fluorol (**42b)** the hydrosilylation reaction proceeded smoothly in relatively good yields (77 and 61%). These products were isolated *via* column chromatography on silica gel. Run 3 led to a complex product mixture. By isolating the side products formed during the latter reaction it was shown that butyl propyl fluorol emerged from the hydrogenation of the double bond in a yield larger than 15%. The results from runs 1 – 3 are consistent with bulkier substituents on the silane leading to enhanced formation of side products, e.g., the reduction of the olefin. The products of runs 1 and 2 were subjected to further hydrolsilylation reactions (Runs 4 – 6) which led in all cases to the desired compounds **44a**, **44b** and **45** which present donor chromophores covalently linked to the acceptor precursors. Run 4 proves that the hydrosilylation principally proceeds smoothly with the β-diketonato derivative allyl-acacH (**36**, 92%). In run 5 the low yield (34%) was due to problems with the column chromatography. The yield of **45** in run 6 was calculated over 2 steps (hydrosilylation and cleavage of the methyl ester).

Table 5. Reactions carried out towards the addition of multifunctional or aminonaphthalimide-functionalized Si-H moieties to functional olefins. Reactions in DCM were stirred under reflux; reactions in toluene were stirred at 40 – 60 °C. The reaction control was carried out *via* TLC in isohexane ethyl acetate mixtures.

Entry	Product		Substrates		Reaction parameters			
	Structure	Name	Olefin	Silane	Ratio[a]	Solvent[b]	Purif.	Yield
1	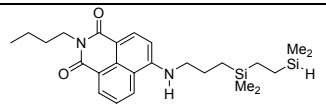	butyl hydrosilyl fluorol **42a**	butyl allyl fluorol **30a**	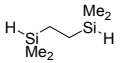	3.0	DCM	chrom. on silica gel	77%
2	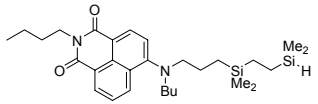	dibutyl hydrosilyl fluorol **42b**	dibutyl allyl fluorol **30b**	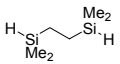	5.0	toluene	chrom. on silica gel	61%
3	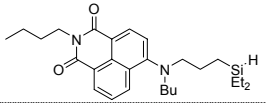	butyl-(diethylsilyl) propyl-fluorol **43**	butyl allyl fluorol **30a**		7.3	DCM	chrom. on silica gel	27%
4	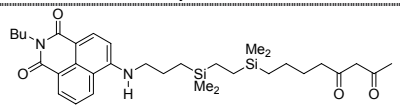	butyl acacH fluorol **44a**	oct-7-en-2,4-dione **36**	butyl hydrosilyl fluorol **42a**	0.8	DCM	chrom. on silica gel	92%
5	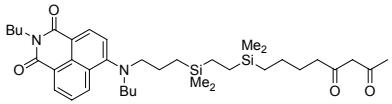	dibutyl acacH fluorol **44b**	oct-7-en-2,4-dione **36**	dibutyl hydrosilyl fluorol **42b**	1.1	toluene	chrom. on silica gel	34%
6	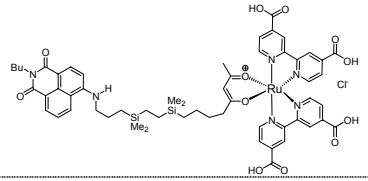	donor acceptor dyad **45**	[Ru(di-Me-dcbpy)$_2$allyl-acac]PF_6 **35b**	butyl hydrosilyl fluorol **42a**	1.1	DCM	chrom. on Sephadex LH20[c]	19%[d]
7	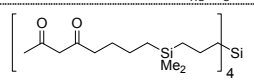	tetra acacH dendrimer **46**	oct-7-en-2,4-dione **36**	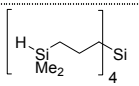	0.2	toluene	chrom. on silica gel	25%

a) Silane-olefin ratio in the reaction mixture. b) Reactions in DCM were stirred under reflux, reactions in toluene were stirred at 40 – 60°C. c) The tetramethylester employed in this run hydrolyses upon NaOH-addition prior the column chromatography step in water. c) This compound was only characterized by ^{1}H NMR. d) Yield over 2 steps.

^{1}H NMR and IR data from the crude reaction mixture showed that no Si-H-groups were present with the conversion of the olefin **35** being incomplete. These facts are consistent with the Si-H groups undergoing a side reaction. Hypothetical side reactions are the reduction of the ester group on the di-Me-dcbpy ligand or the formation of SiF_4 or SiF_6^{2-} resulting from a ligand exchange between the phosphorous center of the PF_6^--counterion and the carbosilane. The addition of aq. NaOH to the latter hydrosilylation's crude product led to quantitative cleavage of the tetramethyl ester and formation of the tetrasodium salt within seconds. The latter was purified *via* column chromatography over Sephadex LH20 with water as eluent. Product **45** was isolated by precipitation upon acidification in a 19% overall yield.

Run 7 shows that it was also possible to couple multiple acceptor precursors to the tetra-Si-H-dendrimer **41** resulting in the tetra acacH dendrimer **46**. Further experiments, which are not mentioned in Table 5, consisted of the reaction of silane **43** with the olefins [Ru(di-Me-dcbpy)$_2$allyl-acac]PF_6 **35b** and allyl-acacH **36**. In the former case no conversion was detectable *via* ^{1}H NMR. The latter led to a complex product mixture; the isolation of the desired reaction product failed. In order to synthesize a molecule comprising three donor and one acceptor units tetrasilane **41** was reacted with 3 eq. of **30a**. The isolation of the respective dendrimer carrying 3 fluorol and 1 Si-H unit from the mixture of dendrimers decorated with 0 – 4 chromophoric groups formed under these conditions was not successful.

Representative ^{1}H NMR spectra from the products of runs 1, 2, 4, and 5 are shown in Figure 7 and Figure 8 in combination with the spectra of the respective olefinic substrate. The ^{1}H NMR spectra clearly show the type of functional group present on the fluorol moiety. On reacting the olefin group in **30a** and **b** (see spectra a) with the difunctional hydrosilane **39** the typical olefin signals between δ = 6.2 – 5.2 ppm disappear, new signals around δ = 0.7 – 0.2 ppm and 3.8 ppm indicate the presence of Si-CH_2 and Si-H groups in the molecule (spectra b). The coupling of **42a** and **b** to allyl-acacH is confirmed by the additional Si-CH_2 signal and the respective change in integration ratio for δ = 0.7 – 0.2 ppm. The keto enol tautomerism prevalent in β-diketonates is also observed in ^{1}H NMR data from the compounds **44a** and **b** (Figure 7 and Figure 8c). The latter spectra show that the hydrogen atoms on the 28-, 26- and 24-carbon atoms reveal significantly different chemical shifts depending on the constitution of the β-diketonate moiety.

In conclusion, the experimental work described in the section above lead to the development of a methodology for the covalent attachment of the fluorol moiety attached to an acceptor precursor *via* a linker that is stable under a wide variety of conditions. Notably the sequential addition of butyl allyl fluorol **30a** and the acceptor precursors **36** and **35** were

key reactions towards the synthesis of the donor acceptor dyad **45**, a bichromophoric compound that was evaluated as energy transfer sensitizer in the DSC. The conversion of compounds **44a** and **b** are described in section 3.5.2.2.

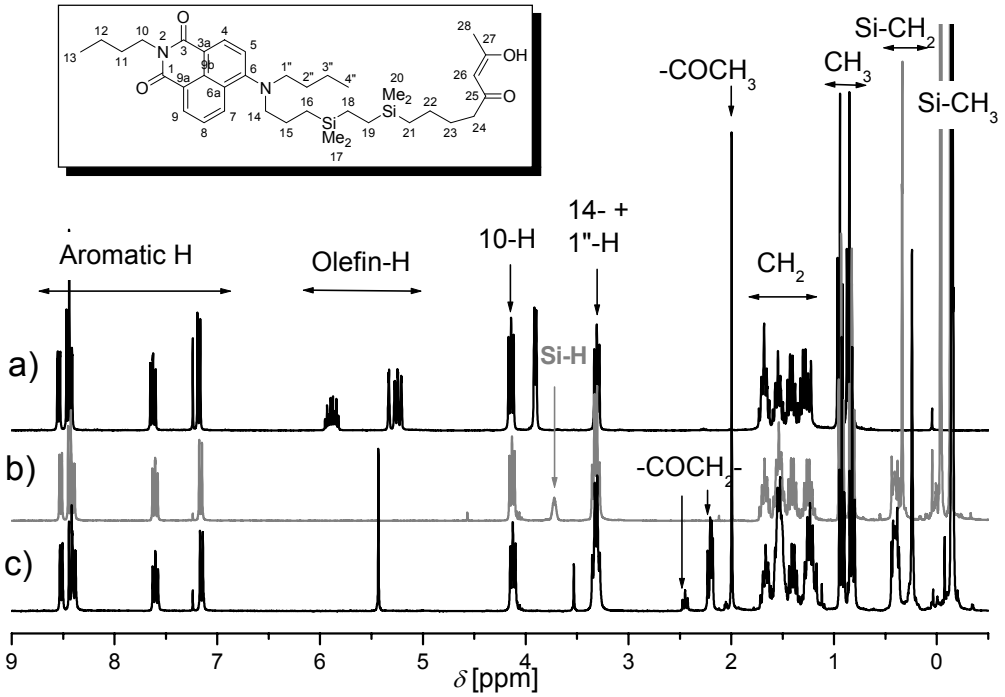

Figure 7. ^{1}H NMR spectra (300 MHz, $CDCl_3$) of a) the olefin-bering energy donor **30b** and products b) **42b** and c) **44b** emerging from the hydrosilylation sequence.

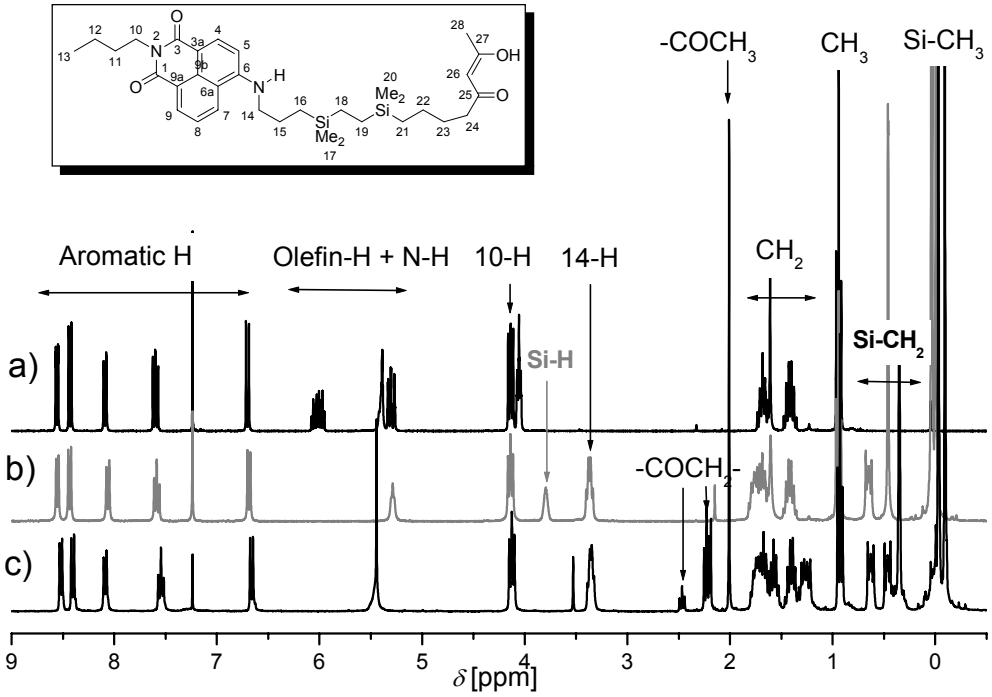

Figure 8. ^{1}H NMR spectra (300 MHz, $CDCl_3$) of a) the olefin-bering energy donor **30a** and products b) **42a** and c) **44a** emerging from the hydrosilylation sequence.

3.4.2 Addition of Si-H bearing Fluorol Derivatives to Allyl-PG

A series of donor-modified polymers was synthesized by the Pt-catalyzed addition of Si-H-bearing energy donor **42a** to allylated polyglycerol **47** (Allyl-PG) with a degree of polymerization of 67 (M_n = 5000 g mol^{-1}) in refluxing DCM (Scheme 10) yielding the donor functionalized polyglycerol derivatives **48**. These polymers will be referred to as $D_{\alpha D}$-Allyl-PG (α_D corresponds to the degree of loading in %). More details towards **47** will be given in Section 3.6. The loading of the Allyl-PG with the energy donor was adjusted by the reaction stoichiometry. This series was synthesized in order to study whether it is possible to use polymeric Fluorol 7GA derivatives to effectuate energy migration (energy hopping between identical chromophoric units) prior to energy transfer from the donor to the acceptor, thus extending thereby the light harvesting distance, if a suitable Ru-acceptor was present. The detailed photophysical characterization of these polymeric energy donor compounds is presented in Chapter 4 of this work.

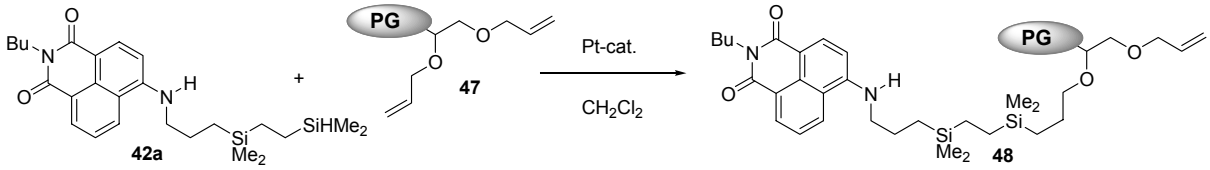

Scheme 10. Synthesis of D-Allyl-PG via the addition of a Si-H-bearing fluorol derivative (**42a**) to allylated polyglycerol (**47**).

Four derivatives with different loadings were synthesized. The loadings were chosen such that polyglycerols (i) with a near quantitative conversion of allyl to chromophoric groups (run 1 leading to **48a**), (ii) with a considerable loading of chromophores (run 2 leading to **48b**) and (iii) with a low loading of chromophores (down to loadings corresponding to less than one chromophoric unit per polymer molecule, runs 3 and 4 leading to **48c** and **48d**) would result. The experimental parameters and results are summarized in Table 6. The details considering the calculation of α_{FG} from ^{1}H NMR data are given in the Appendix (9.1.1). The polymeric substrate Allyl-PG used for these reactions did not carry remaining OH-groups, as determined by IR-spectroscopy. An α_{Allyl} value of 100% would be expected. The fact that this value is larger than 100% is thus due to the experimental error in the method used for the determination of α_{FG}. The data presented in Table 6 clearly demonstrates that the loading with donor chromophore may be tuned *via* the stoichiometry. In runs 2 – 4 $\alpha_{Donor, calc.}$ and α_{Donor} agree within the experimental error.

Table 6. Reactions carried out towards the addition of butyl hydrosilyl fluorol **42a** to Allyl-PG **47**.

#	Product	$\alpha_{Donor, calc.}$ [a]	α_{Donor} [b]	N_{Donor} [c]	α_{Allyl} [d]	α_{OPr} [e]	$\Sigma\alpha$	Work-up	Yield
0	Allyl-PG **47**	-	-	-	106%	0%	106%	-	
1	$D_{63\%}$-Allyl-PG **48a**	92%	63%	42	17%	35%	115%	Precipitation in MeOH[f]	90%
2	$D_{25\%}$-Allyl-PG **48b**	25%	24%	16	71%	13%	109%	UF in acetone	75%
3	$D_{3\%}$-Allyl-PG **48c**	4.5%	3%	2	98%	3%	104%	dialysis in $CHCl_3$	51%
4	$D_{0.3\%}$-Allyl-PG **48d**	0.75%	0.3%	> 1	103%	2%	106%	dialysis in $CHCl_3$	45%

a) $\alpha_{Donor, calc.}$: degree of loading that should result according to the reaction stoichiometry. b) α_{Donor}: degree of loading with the donor moiety as determined from the products ^{1}H NMR spectrum. c) N_{Donor}: average number of chromophoric units per polymer molecule. d) α_{Allyl}: degree of loading with remaining allyl group. e) α_{OPr}: degree of loading with O-$CH_2CH_2CH_3$, possibly resulting from the reduction of the double bond, a plausible side reaction of the hydrosilylation. The details considering the calculation of α_{FG} from ^{1}H NMR data are given in the appendix. f) From a solution of toluene:acetone (3:1).

The significant deviation between those values observed in run 1 might be due to the hydrosilylation being impaired by steric hindrance which might occur after a certain degree of functionalization has been reached. The increase in α_{Donor} also effectuates a decrease in α_{Allyl}. In case of run 1 this decrease in α_{Allyl} (17% in stead of 37%) is significantly more pronounced than expected for α_{Donor} = 63%. This behavior could be explained by side-reactions leading to the chemical modification of the allyl group; e.g., the hydrogenation of the allyl group would result in an *n*-propyl group. In order to estimate the conversion from the latter side reaction the parameter α_{OPr} was calculated from the intensity of the signal centered at around 0.9 ppm (see appendix for details). It indicates the degree of loading with *n*-propyl groups. For runs 2 – 4 α_{OPr} is low, however, α_{OPr} = 35% for run 1 points to the fact that olefin reduction might be a significant side reaction if the hydrosilylation proceeds slower due to sterical limitations. The latter observation is in consistence with the results obtained during the synthesis of compound **43**, however, ^{13}C NMR data does not give clear evidence for this side reaction.

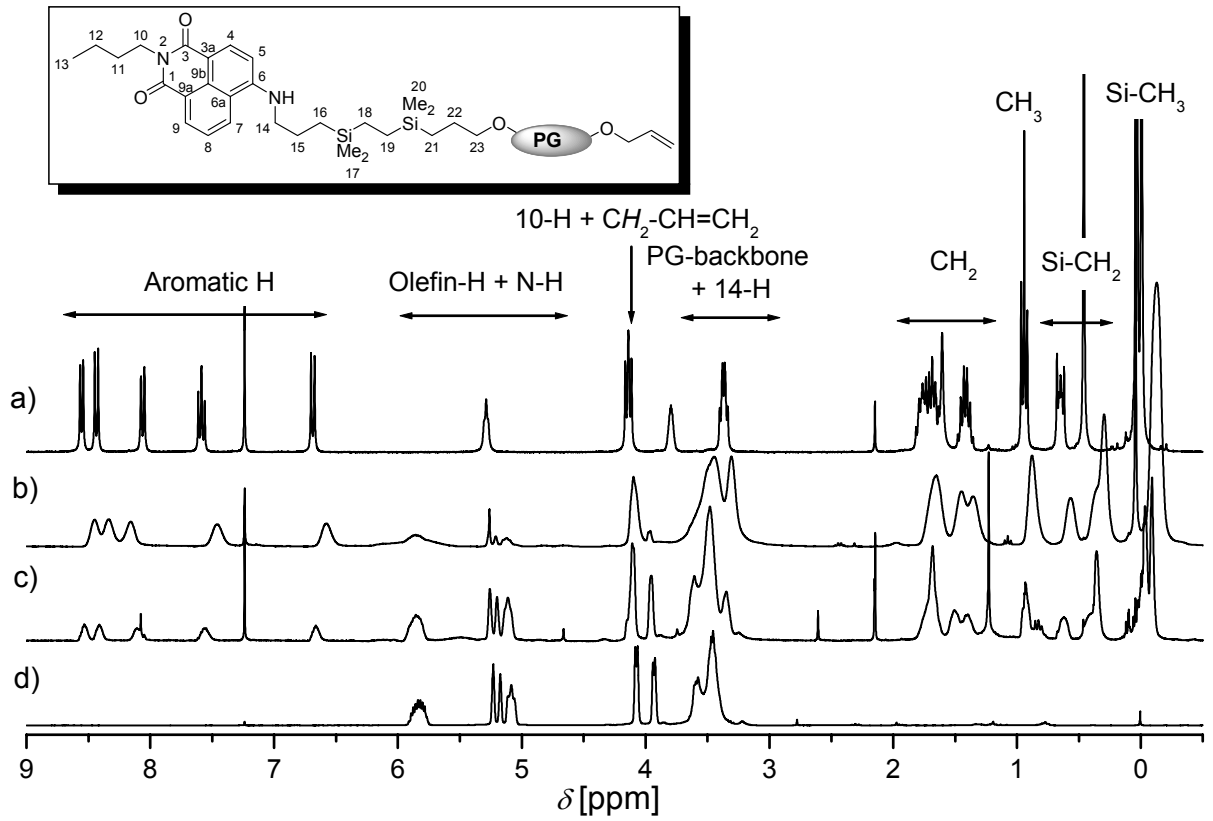

Figure 9. ^{1}H NMR spectra (300 MHz, $CDCl_3$) of a) butyl hydrosilyl fluorol (**42a**), b) $D_{63\%}$-Allyl-PG (**48a**), c) $D_{24\%}$-Allyl-PG (**48b**), and d) Allyl-PG (**47**).

Selected ^{1}H NMR spectra of D-Allyl-PGs are shown in Figure 9b and c in combination with the spectra of the reaction's starting materials (Figure 9a and d). This figure clearly shows that the characteristic chemical shifts of both substrates are present in the product spectrum. The support to the polymeric substrate is proven by the following facts: (i) the significant line broadening with respect to the monomeric donor upon its immobilization (ii) the decrease in intensity of the signals from the $CH_2CH{=}CH_2$ protons (around 5.3 and 5.9 ppm), and (iii) the increasing signal intensity between $\delta = 0.7 - 0.1$ ppm (the signals corresponding to Si-CH_2-protons). In the ^{13}C NMR spectra of the D-Allyl-PG derivatives, signals at $\delta = 10.5$, 24.0 and 24.5 ppm are characteristic for the 21- and 22-C atoms on the newly formed Si-$CH_2CH_2CH_2O$-linker.

In conclusion, the reactions summarized in Table 6 lead to a series of polymers with a varying degree of loading with donor chromophore (α_{Donor}). The magnitude for α_{Donor} covered values corresponding to more than one fluorol unit per 2 monomer units to less than one fluorol unit per polymer molecule. The detailed photophysical characterization of this series' compounds are presented in Chapter 4.

3.5 Functional [Ru(dcbpy)$_2$acac]Cl Derivatives

The ruthenium complexes for energy transfer studies in the DSC were exclusively derivatives of [Ru(dcbpy)$_2$acac]Cl (**14**). The synthesis of the latter compound described in the literature proceeds from $RuCl_3 \cdot x\,H_2O$ ($x \sim 3$) and 4,4'-dicarboxy-2,2'-bipyridine (dcbpy, **49)** *via* [Ru(dcbpy)$_2$Cl$_2$][9] (**50)** to **14** (Scheme 11).[51] For the last reaction step 2,4-pentadione (acacH, **51**) was used as chelating ligand. In this work functional Ru-complexes were synthesized by using α-substituted acacH derivatives for complex formation with [Ru(dcbpy)$_2$Cl$_2$] derivatives. In the following the synthesis of the ligands and their further conversion to Ru-complexes is described (Scheme 11).

3.5.1 Synthesis of Ligands

dcbpy was synthesized in a 2-step procedure from 4-picoline (**52**) *via* 4,4'-dimethyl-2,2'-bipyridine **53**[70] to 4,4'-dicarboxy-2,2'-bipyridine **49** according to the literature.[71, 72] Raney-nickel was used as a catalyst for the dimerization of 4-picoline. The oxidation of the latter to dcbpy was carried out using $KMnO_4$ in aqueous H_2SO_4 (4M) or CrO_3 in conc. H_2SO_4. The product was isolated with either condition by taking up the raw product into a basic aqueous solution. Under these conditions an insoluble metal hydroxide formed which was separated *via* filtration. dcbpy was finally isolated by precipitation upon acidification of the basic aqueous solution. The yields were 40% with $KMnO_4$ and 75% with CrO_3. Although the ^{1}H NMR spectrum was consistent with literature data the elemental analysis of the thus synthesized dcbpy did not fit the calculated values. This fact is consistent with the product containing crystal water and/or not being fully neutralized (with, some sodium ions remaining in the product). 4,4'-dicarboxy-2,2'-bipyridine dimethyl ester (di-Me-dcbpy, **54**) was synthesized in a heterogeneous reaction by refluxing dcbpy in MeOH with H_2SO_4 for 7 days.[72] Extraction and recrystallization gave an analytically pure product according to ^{1}H NMR, ^{13}C NMR spectroscopy and elemental analysis.

The introduction of alkyl groups selectively into the terminal Me-group in 2,4-pentadione has been described in the literature *via* the monoalkylation of the dianion.[53] The latter is formed with NaH and *n*-BuLi in THF and reacts readily with alkyl halogenides to give the product substituted at the terminal position.

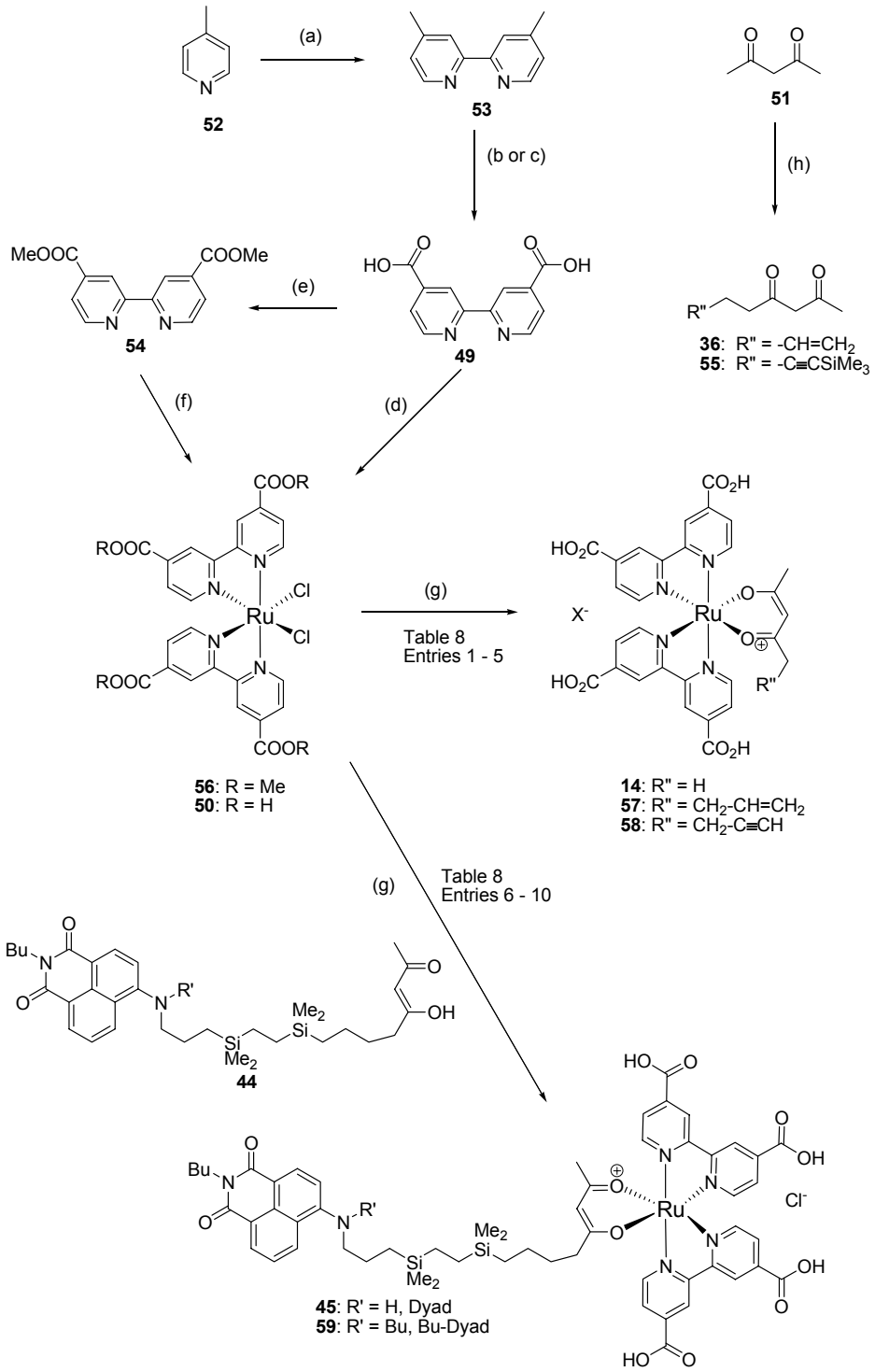

Scheme 11. Synthesis of functional $[Ru(dcbpy)_2acac]^+$ derivatives from commercially available compounds and acacH bearing fluorol derivatives **44**. (a) Raney-Ni, reflux; (b) KMnO4, H_2SO_4 (4M), H_2O, then Na_2CO_3 and precipitation *via* addition of HCl, then post-oxidation in 6M HNO_3, 40%; (c) CrO_3 in conc. H_2SO_4, 2h, then Na_2CO_3 and precipitation *via* addition of HCl, 75%; (d) DMF, 3 h, reflux (see also Table 7); (e) H_2SO_4, MeOH, reflux, 89% based on recovered starting material; (f) **54** to **56**: $RuCl_3 \cdot x\,H_2O$ ($x \sim 3$), EtOH, reflux, 12 h, > 97% (see also Table 7); (g) solvent, base, acacH derivatives, details are described in Table 8; (h) 1.) NaH, THF, 0 °C, 2.) *n*-BuLi, –20 °C, 3.) R"-CH_2-Br; **51** to **36**: purification *via* distillation, 42%; **51** to **55**: purification *via* column chromatography on silica gel, 78%.

In this work allyl bromide and 3-trimethylsilylpropargyl bromide were used to react with the above-mentioned dianion to give oct-7-en-2,4-dione (**36**, allyl-acacH) and 8-trimethylsilyl-oct-7-yne-2,4-dione (**55**, TMS-propargyl-acacH) in a 42% and 78% yield, respectively. **36** was isolated *via* distillation at reduced pressure, the low yield is due to the decomposition of the product to a higher molecular weight compound. **55** was isolated *via* column chromatography.

3.5.2 Synthesis of Complexes

The synthesis of $[Ru(dcbpy)_2acac]Cl$ derivatives was a challenging part of this work. It consisted in (i) the synthesis of a precursor comprising two chloro ligands on the ruthenium center and (ii) the exchange of the chloride ligands with acacH derivatives (Scheme 11). Furthermore, considerable effort was put into the synthesis of $[Ru(di\text{-}Me\text{-}dbpy)_2allyl\text{-}acac]^+$ (tetraesters of $[Ru(dcbpy)_2allyl\text{-}acac]^+$) since preliminary results showed that these complexes may be coupled to Si-H moieties *via* hydrosilylation (see Section 3.4.1).

3.5.2.1 $[Ru(dcbpy)_2Cl_2]$ and $[Ru(di\text{-}Me\text{-}dcbpy)_2Cl_2]$

Although initial attempts at reproducing literature procedures were successful, the yields of isolated compounds were very low. Different strategies applied for the synthesis of $[Ru(dcbpy)_2Cl_2]$ derivatives are summarized in Table 7). It was difficult to synthesize $[Ru(dcbpy)_2Cl_2]$ **50** from $RuCl_3 \cdot x\ H_2O$ and dcbpy according to literature procedures[9] for the following factors: (i) The exact 2:1 stoichiometry of the reactants required for this reaction could not be precisely adjusted due to the high hygroscopy of $RuCl_3$ and the undefined salt and water content of dcbpy. (ii) Evaluation of the purity of **50** *via* ^1H NMR spectroscopy in D_2O/NaOD was difficult due to the partial exchange of Cl-ligands for OH^- leading to complex mixtures of $[Ru(dcbpy)_2XY]$ derivatives (Table 7, entry 1). Converting the crude product **50** by refluxing in MeOH in presence of a catalytic amount of H_2SO_4 led to the tetramethylester **56**, a compound that is soluble in organic solvents and well characterizable by ^1H NMR. **56** synthesized by this method still contained a range of impurities. Furthermore, column chromatography led to the decomposition of the **56** (Table 7, entry 2). The method of choice for the synthesis of precursors for the formation of $[Ru(dcbpy)_2acac]$ derivatives turned out to be the preparation of $[Ru(di\text{-}Me\text{-}dcbpy)_2Cl_2]$ **56** from $RuCl_3 \cdot x\ H_2O$ ($x \sim 3$) and di-Me-dcbpy **54** in EtOH (Table 7, entry 3).[73]

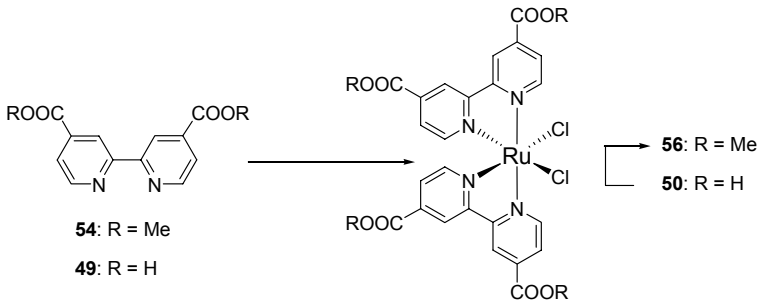

Table 7. Synthesis of Ru dichloro precursors according to different reaction conditions.

#	Product	Substrates	Conditions	Result
1	$[Ru(dcbpy)_2Cl_2]$ **50**	$RuCl_3 \cdot x\ H_2O$ ($x \sim 3$) dcbpy **49**	DMF, reflux, 3 h	difficult to monitor and characterize
2	$[Ru(di\text{-}Me\text{-}dcbpy)_2Cl_2]$ **56**	$[Ru(dcbpy)_2Cl_2]$ **50** MeOH	MeOH, H_2SO_4	decomposition of product upon column chromatography[a)]
3	$[Ru(di\text{-}Me\text{-}dcbpy)_2Cl_2]$ **56**	$RuCl_3 \cdot x\ H_2O$ ($x \sim 3$) di-Me-dcbpy **54**	EtOH	> 97%, crude product (analytically pure!)

a) It was probably during drying at 40 C in presence of silica gel that lead to the decomposition.

Although the latter strategy requires an additional step (the esterification of dcbpy), the extra effort pays off since this complex formation proceeds smoothly to $[Ru(di\text{-}Me\text{-}dcbpy)_2Cl_2]$ (**56**) by refluxing the starting materials in EtOH overnight in yields greater than 97%.[73] Considering the further reaction of $[Ru(dcbpy)_2Cl_2]$ derivatives to acac-complexes it was found that it was not of importance whether **50** or the respective tetraester **56** was used as substrate: It was observed that the COOMe-groups on the ligand bound to a Ru(II) center hydrolyze quasi instantaneously if exposed to alkaline water (see below).

3.5.2.2 [Ru(dcbpy)$_2$acac]Cl derivatives

Reactions carried out towards the synthesis of Ru acac complexes with carboxylic acid groups according to (g) in Scheme 11 are summarized in Table 8. This set of reactions allowed the complex formation between the dichloro precursors **50** and **56** and acacH (**51**) and its functional α-substituted derivatives **36**, **55**, **44a** and **44b** yielding the linker-functionalized complexes $[Ru(dcbpy)_2$allyl-acac]Cl (**57)** and $[Ru(dcbpy)_2$propargyl-acac]Cl (**58)** as well as the bichromophoric complexes **45** and **59** which will be termed donor acceptor dyad (**45)** and butyl dyad (**59)** in the following.

The reaction conditions for the formation of $[Ru(dcbpy)_2acac]Cl$ from $[Ru(dcbpy)_2Cl_2]$ described in the literature consist in refluxing the substrates in DMF:H_2O (2:1) with ligand **51** and Na_2CO_3.

Table 8. Reactions carried out towards the complex formation of $[Ru(dcbpy)_2Cl_2]$ derivatives with functional acetylacetone derivatives. The number in parentheses corresponds to the equivalents of reagent added. The reactions were carried out under nitrogen atmosphere. Oxygen was excluded from the reaction mixture by bubbling nitrogen through the reaction mixtures prior to heating.

#	Product	Run	Ligand	R[a)]	Base	Solvent	Temp. reaction time	Slow addition of[b)]	Purification[c)]	Yield
1	$[Ru(dcbpy)_2acac]Cl$ **14**	CS 145	acacH (1.5)	H	Na_2CO_3 (10)	DMF:H_2O 2:1	reflux 2 h	-	water, 1.4; then KOH/MeOH, 0.9	11%
2	$[Ru(dcbpy)_2$allyl-acac$]Cl$ **57**	CS 100	allyl-acacH (1.1)	Me	Na_2CO_3 (10)	DMF:H_2O 2:1	reflux 1 h	-	water, 3.3	36%
3	$[Ru(dcbpy)_2$allyl-acac$]Cl$ **57**	CS 160	allyl-acacH (2.1)	Me	KO*t*Bu (2.7)	MeOH	reflux 4 h	base in MeOH	water, 2.8	40%
4	$[Ru(dcbpy)_2$allyl-acac$]Cl$ **57**	CS 198	allyl-acacH (1.5)	H	Na_2CO_3 (10)	DMF:H_2O 2:1	60 – 100 °C 2.5 h	ligand in DMF	water (2x), 2.9; then MeOH:H_2O 3:1 with NaOH, 3.0	66%
5	$[Ru(dcbpy)_2$propargyl-acac$]Cl$ **58**	LB 19	TMS-propargyl-acacH (1.5)	Me	KO*t*Bu (2)	MeOH, abs.	reflux 4.5 h	base in MeOH	water, 2.0	55%
6	Donor acceptor-Dyad[d)] **45**	CS 171	butyl acacH fluorol (0.9)	Me	KO*t*Bu (1.2)	MeOH:DMF 5:1	reflux 4 h	ligand in DMF	water, 2.0; then MeOH with NaOH, 2.4	17%
7	Donor acceptor-Dyad **45**	LB 50	butyl acacH fluorol (0.9)	Me	TBAOH (10)	DMF:H_2O 2:1	60°C 3 h	base in solvent mixture	water, 2.5	8%
8	Donor acceptor-Dyad **45**	LB 30	butyl acacH fluorol (0.9)	Me	Na_2CO_3 (10)	DMF:H_2O 2:1	60-80 °C 7.5 h	ligand in DMF	water, 2.0	n.d.
9	Donor acceptor-Dyad **45**	LB 89	butyl acacH fluorol (0.9)	Me	KO*t*Bu (3)	MeOH	reflux 6 h	base in MeOH	water, 2.5[e)]	32%
10	Butyl-Dyad **59**	TR 25	dibutyl acacH fluorol (0.75)	H	Na_2CO_3 (10)	DMF:H_2O 2:1	reflux 4 h	-	water, 2.4	5%

a) Substituent on the carboxy group of the ruthenium precursor. b) In some cases one reagent was added dropwise to the reaction mixture, which one is indicated in this column. c) the solvents used for the individual chromatography steps and the pH the solution was titrated to with aq. HCl. are given in this column. d) In this run, yellow side products that would not elute from Sephadex LH20 with water were isolated and further purified *via* chromatography on silica gel. e) The crude product was purified *via* extracting impurities soluble in the organic media into CH_2Cl_2 prior to the column chromatography on Sephadex LH20.

The reproduction of the literature synthesis was tedious due to low yields and the formation of side products (Entries 1, 2, and 10). One reason for the low yields of this reaction is the decomposition of the acetylacetone unit during the reaction. In run CS 171 (Table 8, Entry 6) the side products of the reaction were isolated and further purified *via* column chromatography on siliga gel. One compound was identified *via* ^{1}H NMR and MS to be compound **60**, which results from a retro-claisen condensation.

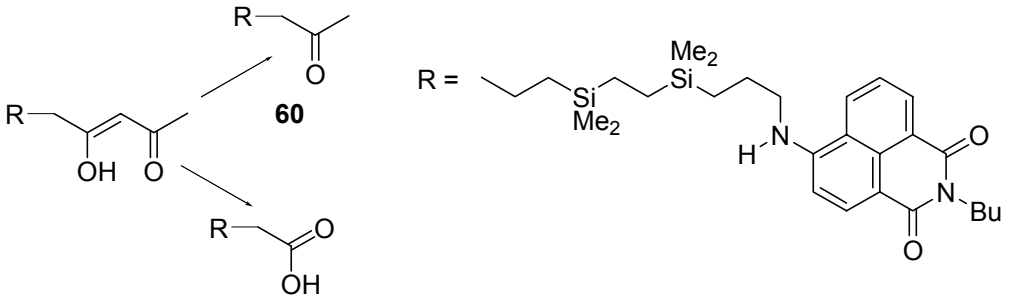

Scheme 12. Side reactions leading to a decomposition of the functional acacH-ligands. By the isolation of the side products of run CS 171 (Table 8, entry 6) it was shown that compound **60** was formed.

Strategies to improve the reaction yields included the choice of different solvents, bases, and temperatures and the dropwise addition of one reagent. The best yield was achieved in this series of reactions with DMF:H_2O (2:1) and dropwise addition of allyl-acacH (Table 8, entry 4) despite several chromatography steps. Adding a solution of KO*t*Bu to the refluxing reaction mixture containing the Ru precursor and functional acacH ligand also lead to higher yields than the ones achieved using literature conditions (Table 8, entries 3, 5, 6, and 9). Lowering the reaction temperature was the crucial factor for attaining better yields. Avoiding the presence of the entire amount of base and functional acacH derivative in the reaction mixture by dropwise addition of one or the other might also have contributed to the improvement of the yield. Using TBAOH as base did not afford an improvement (Table 8, entry 7) in the reaction's outcome. The products were all isolated from the reaction mixture in the same manner. After the evaporation of the solvent the crude product was taken up in water (if it was not entirely soluble, some NaOH was added), loaded onto a Sephadex LH20 column, and eluted with water. The side products eluted first; the title compound last. The individual fractions containing the title compound were identified *via* their UV-Vis spectrum. The fractions containing the title compound were acidified with diluted HCl. Precipitation of $[Ru(dcbpy)_2acac]^+$ derivatives was observed below a pH of 3.5. The precipitate was best isolated by centrifugation and freeze-drying. If one chromatography step did not lead to a satisfactory purity, a second one using alkaline MeOH or MeOH-water mixtures was performed.

In conclusion, by the syntheses presented in Scheme 11, several functional $[Ru(dcbpy)_2acac]^+$ derivatives were made. By lowering the reaction temperature and variation of solvents an increase in yields was achieved. Most importantly the complex formation between butyl acacH fluorol **44a** and $[Ru(dcbpy)_2Cl_2]$ derivatives **50** and **56** led to dyad **45**. Through this pathway the access to **45** in sufficient amounts for spectroscopic and photophysical was achieved. **45** lives up to the requirements posed for monomolecular donor acceptor sensitizers in the objective.

3.5.2.3 [Ru(di-Me-dcbpy)$_2$allyl-acac]X

Table 9 shows strategies carried out towards the synthesis of the $[Ru(di\text{-}Me\text{-}dcbpy)_2allyl\text{-}acac]^+$ cation which was used as an intermediate to donor acceptor systems as described in Section 3.4.1.

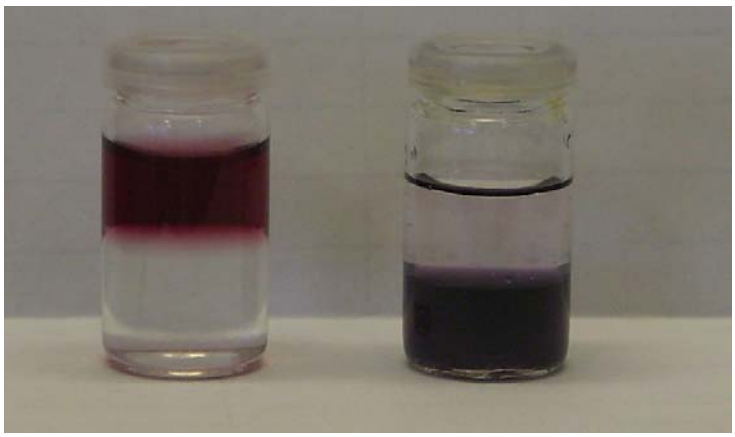

Figure 10. Photography of viles containing water (top) and CH_2Cl_2 (bottom). The left one contains $[Ru(dcbpy)_2allyl\text{-}acac]Cl$ **57** (the water phase is dark red), the right one $[Ru(di\text{-}Me\text{-}dcbpy)_2allyl\text{-}acac]PF_6$ **35b** (the organic phase is black).

Substituting the acidic hydrogens in **50** by methyl groups leads from a very polar material that is only soluble in alkaline water and polar organic solvents to a compound that is soluble in organic media (e.g., CH_2Cl_2), thus rendering it suitable for hydrosilylation reactions (Figure 10). Three different strategies towards the synthesis of $[Ru(dcbpy)_2allyl\text{-}acac]^+$ derivatives were evaluated: (i) esterification of $[Ru(dcbpy)_2ally\text{-}acac]Cl$ **57** using $MeOH/H_2SO_4$, (ii) complex formation between $[Ru(di\text{-}Me\text{-}dcbpy)_2Cl_2]$ **56** and allyl-acacH **36** in analogy to the experiment from entry 4 in Table 8, and (iii) methylation of the tetra-sodium salt of $[Ru(dcbpy)_2ally\text{-}acac]Cl$ **57** with CH_3I in DMSO.

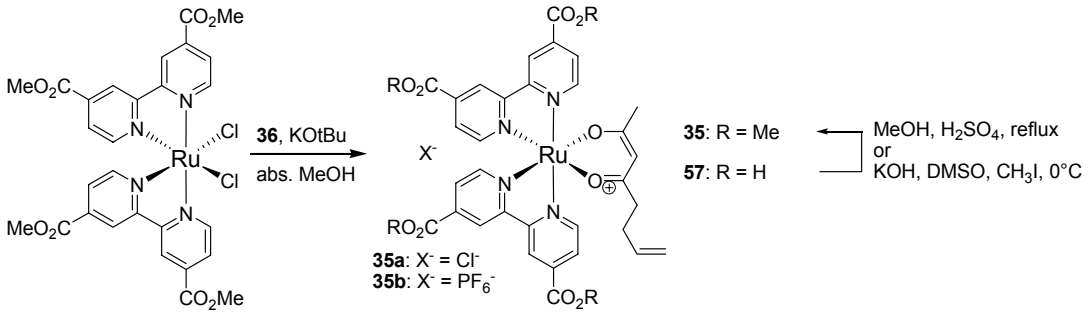

Table 9. Reactions carried out towards the synthesis of [Ru(di-Me-dcbpy)$_2$allyl-acac]$^+$ derivatives.

#	Substrate	Run	Counterion	Cond.	Work-up	Result
1	[Ru(dcbpy)allyl-acac]Cl **57**	CS 102	X^-	MeOH, cat. H_2SO_4, reflux	extraction in CH_2Cl_2 with $NaHCO_3$, column with CH_2Cl_2:MeOH (10:1)	~15%, formation of [Ru(di-Me-dcbpy)$_2$Cl$_2$] was observed[a)]
2	[Ru(di-Me-dcbpy)$_2$Cl$_2$] **56**	AK 120	X^-	allyl-acacH, MeOH, KO*t*Bu, reflux	column with CH_2Cl_2:MeOH (10:1)	~13%, formation of numerous side products[a)]
3	[Ru(dcbpy)allyl-acac]Cl **57**	CS 176	PF_6^-	CH_3I, NaOH, DMSO, 0 °C – RT	extraction in CH_2Cl_2 with cold NH_4Cl, HNO_3 and NaCl[b)]	76%
4	[Ru(dcbpy)allyl-acac]Cl **57**	CS 196	PF_6^-	CH_3I, NaOH, DMSO, 0 °C – RT	extraction in CH_2Cl_2 with cold HCl, extraction with $NaHCO_3$[c)]	33%

a) Product still contains a considerable amount of impurities. b) The residue in the organic phase was either dried or precipitated with NH_4PF_6. c) Furthermore, elution over Sepahdex LH20 with H_2O:Acetone 2:1, then with added NaCl, precipitation after column with NH_4PF_6.

All three strategies lead to compounds containing the [Ru(di-Me-dcbpy)$_2$allyl-acac]$^+$ cation. It was possible to form [Ru(di-Me-dcbpy)$_2$allyl-acac]$^+$ *via* the esterification reaction in MeOH (Table 9, Entry 1), however, the decomposition of the substrate by the formation of [Ru(di-Me-dcbpy)$_2$Cl$_2$] was one major side reaction under these reaction conditions. Furthermore, the substitution of the chloro ligands in [Ru(di-Me-dcbpy)$_2$Cl$_2$] by allyl-acac$^-$ in KO*t*Bu and MeOH (Table 9, Entry 2, in analogy to the reaction from Table 8, Entry 3) also leads to [Ru(di-Me-dcbpy)$_2$allyl-acac]$^+$. The formation of the latter species was monitored by the color of a solution resulting from adding one drop of the reaction mixture into CH_2Cl_2: A deep green color is characteristic for [Ru(di-Me-dcbpy)$_2$Cl$_2$], while the presence [Ru(di-Me-dcbpy)$_2$allyl-acac]$^+$ is indicated by a deep purple – black color. Since the reactions described so far did not smoothly lead to [Ru(di-Me-dcbpy)$_2$allyl-acac]$^+$, the reaction mixtures were worked-up *via* extraction with alkaline water and brine and subsequent column chromato-

graphy on silica gel using CH_2Cl_2-MeOH mixtures as eluent. The chromatography was difficult due to smearing of the product over the column.[74] During these purification steps, partial hydrolysis of the methyl ester was observed. The difficulties described above were the reasons for the low yields in these runs. However, [Ru(di-Me-dcbpy)$_2$allyl-acac]$^+X^-$ isolated according to these procedures reacted smoothly in hydrosilylation reactions. The identity of the counter ion was not further analyzed. It might be Cl^- but there is also the possibility that it was exchanged during the purification. On the other hand, the methylation of the tetrasodium derivative of [Ru(di-Me-dcbpy)$_2$allyl-acac]Cl with CH_3I in DMSO smoothly led to [Ru(di-Me-dcbpy)$_2$allyl-acac]$^+$ which was isolated from the reaction mixture by the addition of acidic water and the extraction into CH_2Cl_2. In order to obtain high yields *the contact of* [Ru(di-Me-dcbpy)$_2$allyl-acac]$^+$ *with basic water had to be absolutely avoided*. Thereforme it was crucial to make sure that the amount of acid added in order to quench the reaction mixture overcompensated the base that was initially present. It was shown *via* ^{1}H NMR spectroscopy on samples of the crude product that no isomerization or chemical transformation on the Ru-center took place. The crude product was water soluble and [Ru(di-Me-dcbpy)$_2$allyl-acac]PF_6 **35b** precipitated on addition of NH_4PF_6 to the aqueous solution. Alternatively, aqueous solutions containing [Ru(di-Me-dcbpy)$_2$allyl-acac]$^+$ were further purified over Sephadex LH20 in water (or acetone-water mixtures if the loading of the column was high) using an NaCl gradient. No hydrolysis of the methyl ester in neutral H_2O was observed. Using [Ru(di-Me-dcbpy)$_2$allyl-acac]PF_6 **35b** as a source for [Ru(di-Me-dcbpy)$_2$allyl-acac]$^+$ in hydrosilylation reactions led to conversions that were not as smooth as conversions relying on [Ru(di-Me-dcbpy)$_2$allyl-acac]X **35a**. The latter might be due to remaining crystal water in **35b** or interference of PF_6^- with silicon compounds.

In conclusion, the reaction conditions from Entries 1 and 2 in Table 9 lead to [Ru(di-Me-dcbpy)$_2$allyl-acac]$^+$-derivatives in poor yields due to side reactions on the Ru center and resulting difficulties with the work-up and purification. The latter side reactions do not take place if [Ru(dcbpy)$_2$allyl-acac]Cl is converted to [Ru(di-Me-dcbpy)$_2$allyl-acac]$^+$ *via* the methylation of the carboxylates. The isolation of [Ru(di-Me-dcbpy)$_2$allyl-acac]$^+$ as PF_6^- salts by chromatographic separation over Sephadex LH20 in water or water-acetone mixtures was possible. These results suggest that [Ru(di-Me-dcbpy)$_2$allyl-acac]$^+$ derivatives could alternatively be synthesized by the conversion of **56** with allyl-acacH in an organic solvent, e.g., pyridine, and isolation of the product from the reaction mixture *via* quenching in acidic water, column chromatography over Sephadex LH20 in neutral or slightly acidic water,[75] and finally by extracting the complex into the organic phase or precipitation with PF_6^-.

3.5.3 Characterization of Ru Complexes

3.5.3.1 ^{1}H NMR of [Ru(dcbpy)$_2$acac]Cl and its Functional Derivatives

The measurement of NMR spectra of the Ru polypyridine complexes presented in this work was carried out in alkaline D_2O or CD_3OD. Deuterated sodium hydroxide served as base. Figure 11 shows ^{1}H NMR spectra of [Ru(dcbpy)$_2$acac]Cl **14** and its linker-functionalized derivatives **58** and **57**.

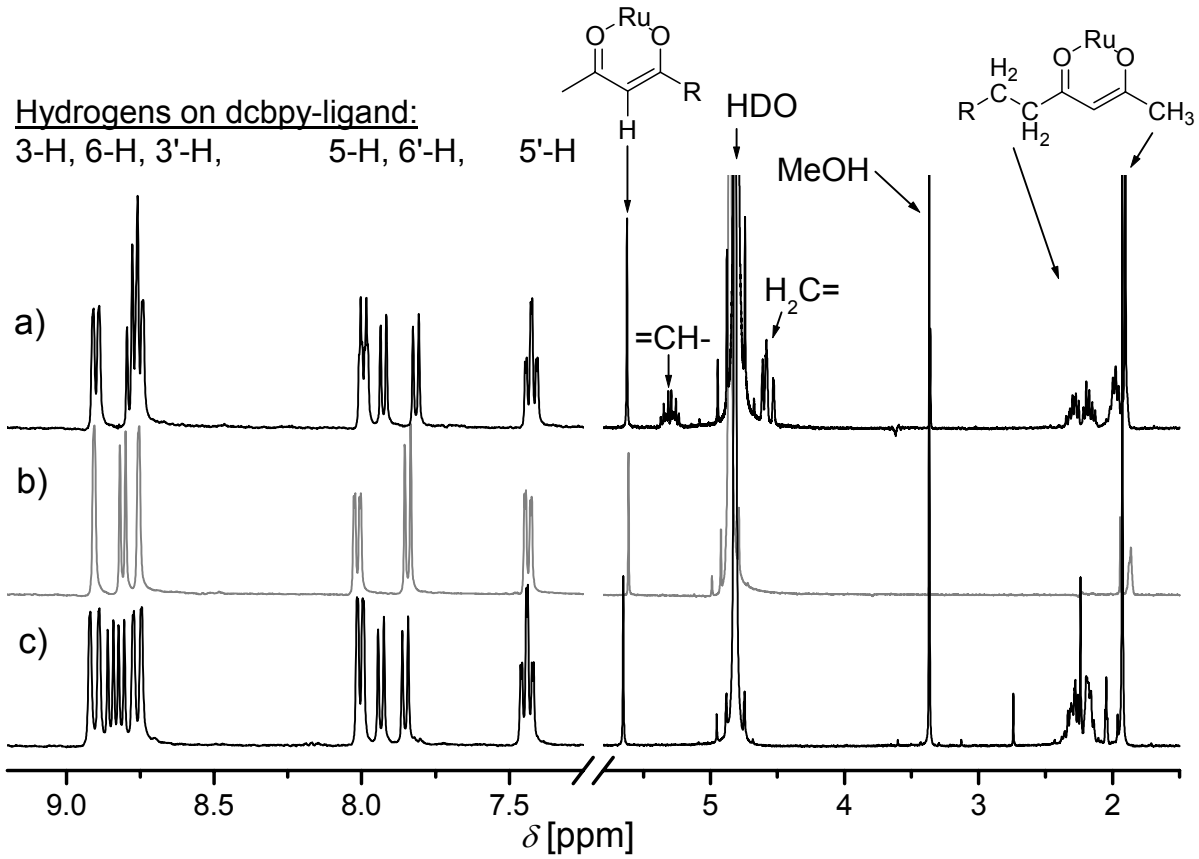

Figure 11. ^{1}H NMR spectra (300 MHz, D_2O/NaOD) of a) [Ru(dcbpy)$_2$allyl-acac]Cl (**57**), b) [Ru(dcbpy)$_2$acac]Cl (**14**) and c) [Ru(dcbpy)$_2$propargyl-acac]Cl (**58**). The spectra do not have signals within the break.

Spectrum b in Figure 11 shows 6 signals between 9.0 and 7.4 ppm. This is consistent with the symmetry of this type of enantiomeric Ru complex. Introducing *one* functional group into the α-position of the acac-ligand reduces the symmetry; these compounds may be composed of two different diastereomers. The respective hydrogens on either dcbpy ligand resonate at slightly different chemical shifts with the result that the ^{1}H NMR spectra of [Ru(dcbpy)$_2$allyl-acac]Cl and [Ru(dcbpy)$_2$propargyl-acac]Cl show 12 aromatic signals, some of which are overlapping. A detailed assignment of the different signals to the type of diastereomer was not performed. The introduction of the allyl group leads to characteristic olefinic signals

around 5.3 and 4.6 ppm. Methylene groups between the coordinating CO-unit and the functional group resonate around 2.40 and 1.95 ppm, the terminal CH_3 group around 1.9 ppm. The signal intensity of hydrogens in α-position to the coordinating carbonyl groups is lower than predicted from the structure. Furthermore, the signal for the alkyne proton is missing. The latter two facts are consistent with H-D-exchange in the basic environment.

3.5.3.2 ^{13}C NMR of [Ru(dcbpy)$_2$acac]Cl and its Functional Derivatives

Figure 12 and Figure 13 show ^{13}C NMR spectra of [Ru(dcbpy)$_2$acac]Cl **14** and its linker-functionalized derivatives **58** and **57**. The terminal CH_3 unit resonates at around 30 ppm, the α-CH_2 unit at around 43 ppm. The fact that the signal at 30 ppm is not present in spectrum b is probably due to H-D-exchange. The introduction of the allyl (propargyl) group leads to characteristic olefin (alkyne) signals at 139 (87) and 117 (73) ppm and one signal at 34 (19) ppm for the additional methylene group. The latter chemical shifts are typical for the respective functional units (notably in case of the propargyl group). Thus, the chemical shifts of the alkyne moiety prove unambiguously that the trimethylsilyl group from **55** was cleaved during the complex formation. In order to measure a ^{13}C NMR spectrum of [Ru(dcbpy)$_2$propargyl-acac]Cl revealing the signal at 73 ppm, the sample had to be prepared in non-deuterated water with traces of deuterated methanol as standard. If the sample was prepared exclusively in deuterated solvents, H-D-exchange at the terminal alkyne-C led to a ^{13}C NMR spectrum without the latter signal. Spectrum b in Figure 13 shows 9 signals between 164 and 124 ppm. In analogy to results from ^{1}H NMR this is consistent with the symmetry of this type of enantiomeric Ru complex assuming that the 3 and 3' carbon atoms resonate at the same chemical shift (125 ppm). The transformation from enantio- into diastereomers *via* the introduction of one functional group into the α-position of the acac-ligand is also obvious from the ^{13}C NMR spectrum of [Ru(dcbpy)$_2$allyl-acac]Cl and [Ru(dcbpy)$_2$propargyl-acac]Cl. For most of the signals that were present in the spectrum of [Ru(dcbpy)$_2$acac]Cl two signals with a slightly different chemical shift appear (Figure 13).

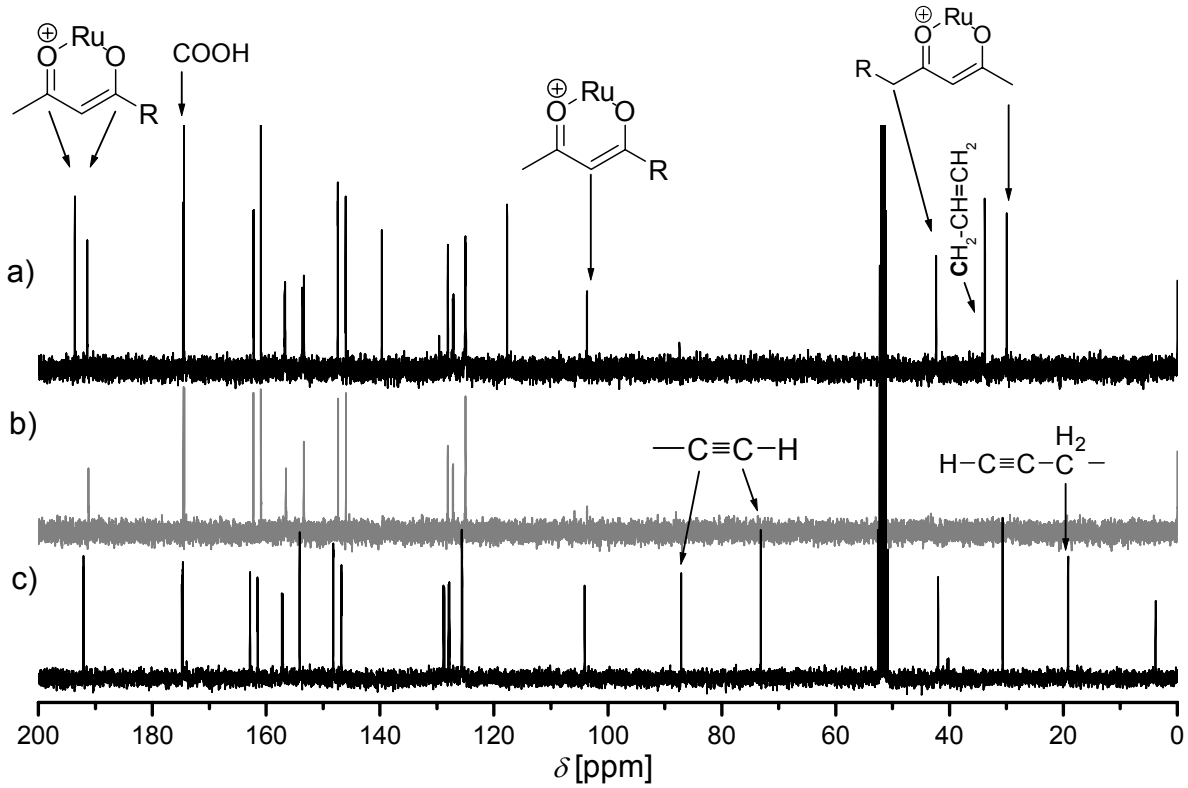

Figure 12. ^{13}C NMR spectra (75 MHz) of a) [Ru(dcbpy)$_2$allyl-acac]Cl (**57**) in D_2O/NaOD, b) [Ru(dcbpy)$_2$acac]Cl (**14**) in D_2O/NaOD, and c) [Ru(dcbpy)$_2$propargyl-acac]Cl (**58**) in H_2O/NaOH with some CD_3OD.

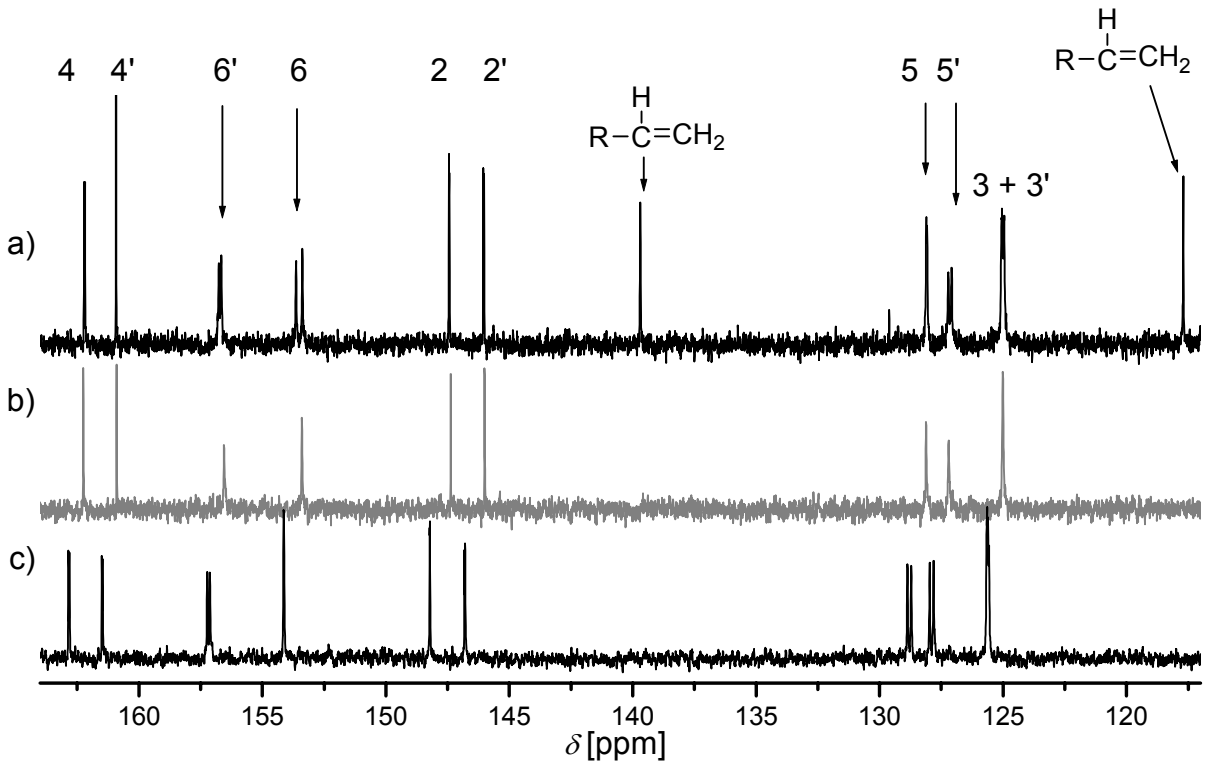

Figure 13. Cutout of ^{13}C NMR spectra (75 MHz, D_2O/NaOD) of from Figure 12. a) [Ru(dcbpy)$_2$allyl-acac]Cl (**57**) in D_2O/NaOD, b) [Ru(dcbpy)$_2$acac]Cl (**14**) in D_2O/NaOD, and c) [Ru(dcbpy)$_2$propargyl-acac]Cl (**58**) in H_2O/NaOH with some CD_3OD. The numbering of the C-atoms on the dcbpy ligands is in analogy to the numbering of **45** as presented in Scheme 13.

3.5.3.3 ^{1}H NMR of Donor Acceptor Dyads

The NMR solvent of choice for the characterization of the dyads was deuterated alkaline methanol. Measurements in alkaline D_2O did not lead to clearly resolved signals supposedly due to the aggregation of the highly amphiphilic structure **45** if prevalent as tetrasodium salt in water. Figure 14 summarizes ^{1}H NMR spectra allowing the confirmation of the structure of the donor acceptor dyad: spectrum a) belongs to butyl acacH fluorol **44a**, b) to the donor acceptor dyad **45** and c) to [Ru(dcbpy)$_2$acac]Cl **14** in CD_3OD.

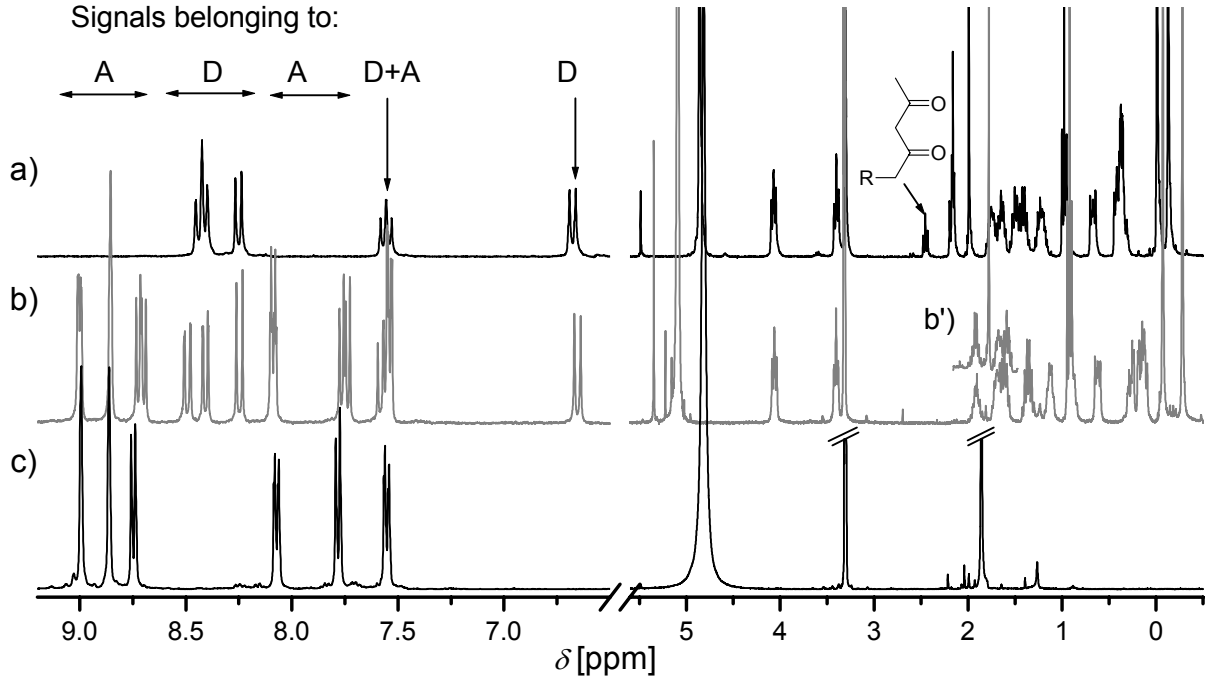

Figure 14. ^{1}H NMR spectra (300 MHz) of a) butyl acacH fluorol (**44a**), b) donor acceptor dyad (**45**), and c) [Ru(dcbpy)$_2$acacH]Cl (**14**) in MeOD. Some NaOD in D_2O was added to the NMR sample for spectra b) and c). The spectra do not show signals within the break between δ = 6.5 – 5.6 ppm. The section of the ^{1}H NMR spectrum shown between spectra a) and b) and δ = 2.0 – 1.5 ppm (b') is from dyad **45** in a mixture of alkaline MeOH/MeOD (5:1).

The spectrum in Figure 14b clearly shows that the signals of the butyl acacH fluorol unit are also present in the dyad with exception of the triplett at 2.45 ppm. The latter signal is characteristic for the keto form of **44a**. Thus its disappearance on reaction **44a** with [Ru(dcbpy)$_2$Cl$_2$] confirms the complex formation. Furthermore, the ^{1}H NMR spectrum of **45** also comprises aromatic signals that are characteristic for the [Ru(dcbpy)$_2$acac]$^+$-unit (see spectrum c). The integral ratio of the signals belonging to one hydrogen atom from the donor and acceptor group, respectively, is 1. All of the above-mentioned characteristics confirm the successful complex formation between **44a** and **56**. In analogy to observations made during measurements with [Ru(dcbpy)$_2$acac]Cl derivatives (see 3.5.3.1) the signals of the α-CH_3 and –CH_2-groups at δ = 1.82 and 1.89 ppm, respectively, are underrepresented if

MeOD/NaOD/D_2O is used as NMR solvent system. The analogous measurement of a spectrum in a mixture of CD_3OD and CH_3OH leads to an enhanced signal intensity due to the suppression of H-D-exchange (see spectrum b' in Figure 14). In analogy to the spectrum of dyad **45,** the ^1H NMR spectrum of butyl-dyad (**59**) contains the signals of donor and acceptor units, however, the donor acceptor chromophore ratio in the sample isolated from the reaction with dibutyl acacH fluorol **44b** was only 0.8:1 and thus contained impurities, which were likely decomposition products formed during the isolation of the material after the fractionation *via* chromatography in water.

3.5.3.4 ^{13}C NMR of Donor Acceptor Dyad

Figure 15 shows ^{13}C NMR spectra of butyl-acacH -fluorol **44a** and the donor acceptor dyad **45** in MeOD and [Ru(dcbpy)$_2$acacH]Cl **14** in D_2O. Scheme 13 shows the atom numbering applied for the assignment of NMR signals.

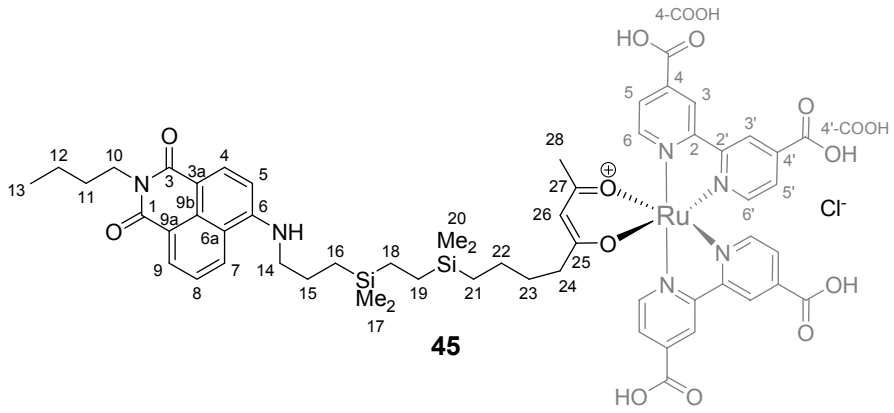

Scheme 13. Structure of donor acceptor dyad **45** and atom numbering used for the assignment of NMR signals. Although not chemically equivalent to the upper dcbpy ligand, the atoms of the lower ligand are numbered identically. The atom number of signals originating from the dcbpy ligands are followed by "-bpy" in the NMR assignment in Figure 15.

In analogy to the results of ^1H NMR data from **45** the ^{13}C NMR spectrum is also largely a sum of the signals of the individual functional units butyl acacH fluorol **44a** and [Ru(dcbpy)$_2$acac]Cl **14**. In analogy to the results of ^{13}C NMR spectra of the functionalized Ru complexes **58** and **57**, the introduction of one substituent at the terminal Me-groups on the acac-moiety leads to two signals with slightly different chemical shifts for each position on the dcbpy ligand. The assignment of the spectra was based on a DEPT-spectrum of **44a** and CH-COSY measurements with **45**.

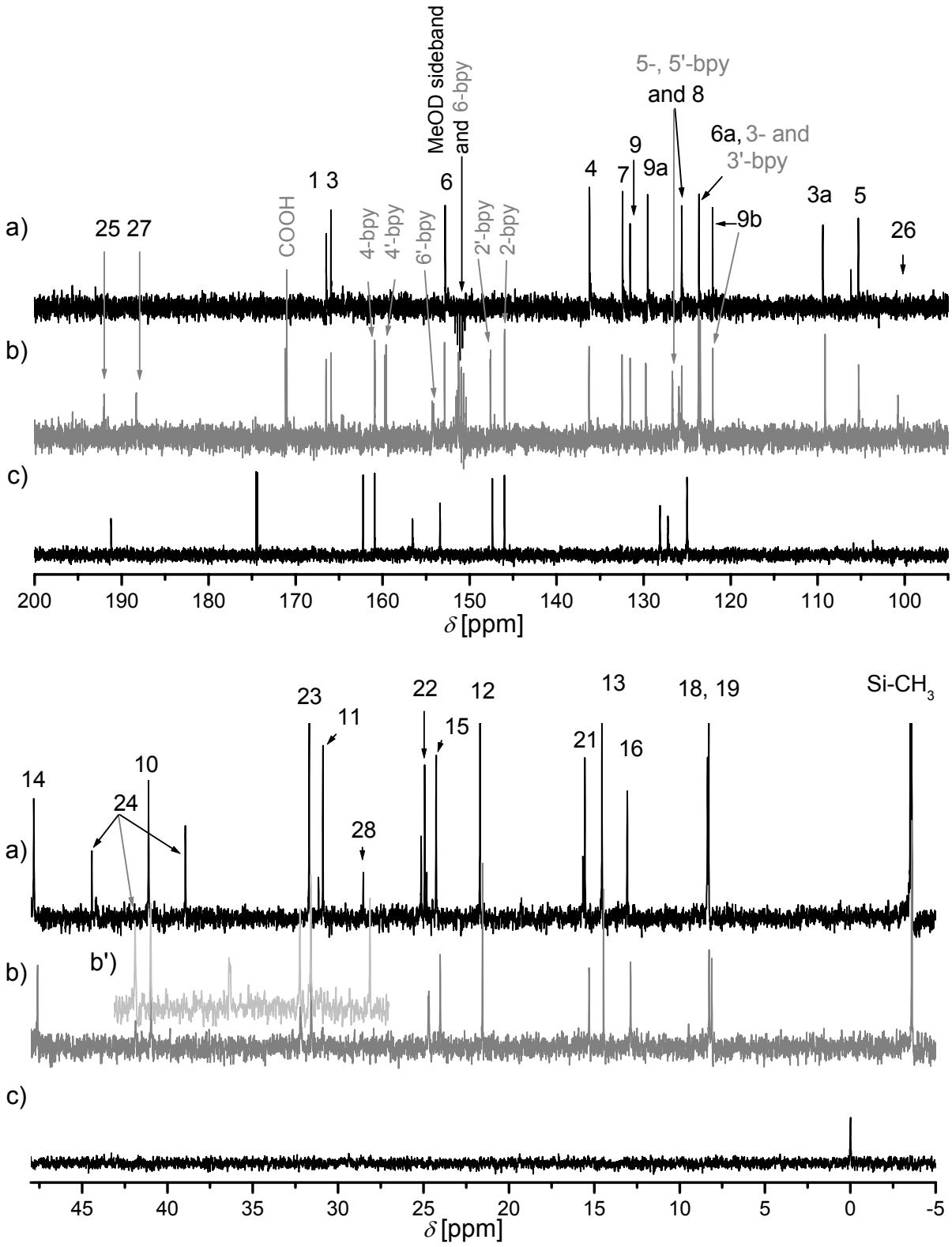

Figure 15. ^{13}C NMR spectra of a) acacH-butyl-fluorol (**44a**) in MeOD, b) the donor acceptor dyad (**45**) in MeOD, and c) [Ru(dcbpy)$_2$acacH]Cl (**14**) in D_2O. Some NaOD in D_2O was added to the NMR sample for spectra b) and c). Top: δ = 200 – 95 ppm. Bottom: δ = 47 – -5 ppm. The signals within the break between δ = 95 – 48 ppm are exclusively from MeOD. The section of the ^{13}C NMR spectrum shown between spectra a) and b) and δ = 43 – 27 ppm (b') is from the dyad in a mixture of alkaline MeOH/MeOD (5:1).

The H-D-exchange on the α-positions of the acac-ligand described before had also implications on the ^{13}C NMR spectrum: Signals of the 24 and 28 carbon atoms are very weak or not present if the spectrum is recorded in alkaline MeOD. The same measurement in a MeOH/MeOD mixture leads to intense signals at 42 and 28 ppm (see spectrum b' in Figure 15).

3.5.3.5 Elemental Analysis and Mass Spectrometry

Table 10 shows the results of elemental analysis and mass spectrometry data of [Ru(dcbpy)$_2$acac] derivatives. The deviations between the calculated and experimental C, H and N content are below 0.3%. Different amounts of crystal water were taken into account. These results confirm the structure of the Ru complexes. Furthermore, the most intensive peak of the mass spectra corresponds to the calculated exact mass for the cationic complex. The mass spectra typically revealed another peak exceeding the mass of the cationic complex with 22 to 23 units. This points to incomplete neutralization of the carboxy groups during the precipitation from alkaline aqueous solution, which could lead to sodium ions bound to the carboxylates.

Table 10. Results of elemental analysis and mass spectrometry of functional Ru complexes. The calculated values are shown in parantheses.

Compound	C	H	N	M_r
[Ru(dcbpy)$_2$acac]Cl	n.d.	n.d.	n.d.	689.0
[Ru(dcbpy)$_2$allyl-acac]Cl · 4 H_2O	46.02 (45.97)	4.00 (4.22)	6.86 (6.70)	729.1
[Ru(dcbpy)$_2$propargyl-acac]Cl · H_2O	49.38 (49.27)	3.48 (3.49)	7.06 (7.18)	727.0
donor acceptor-dyad · H_2O	55.27 (55.35)	5.61 (5.46)	6.53 (6.79)	1183.2
butyl-dyad	n.d.	n.d.	n.d.	1239.4

3.5.3.6 UV-Vis spectra of Functional [Ru(dcbpy)$_2$acac] Derivatives

Figure 16 shows normalized, electronic spectra of Ru compounds **58**, **57**, **14**, **45** and **59** as well as the spectrum of **15** in alkaline EtOH. Absorption maxima are summarized in Table 11. [Ru(dcbpy)$_2$acac]Cl and its linker modified derivatives show close to identical spectra. The spectra of **45** and **59** are also identical to [Ru(dcbpy)$_2$acac]Cl for λ > 510 nm, however

the absorption at 390 > λ > 510 nm is significantly and somewhat larger for **45** and **59**, respectively. These observations agree with the following facts: (i) The introduction of a substituent into the terminal position of the acac-ligand does not alter the absorption properties significantly, (ii) the significantly higher absorption of **45** and **59** as supposed to **58** in the range 390 > λ > 510 nm is in consistence with light absorption by the donor moiety, and (iii) the latter effect is weaker than expected for butyl-dyad.

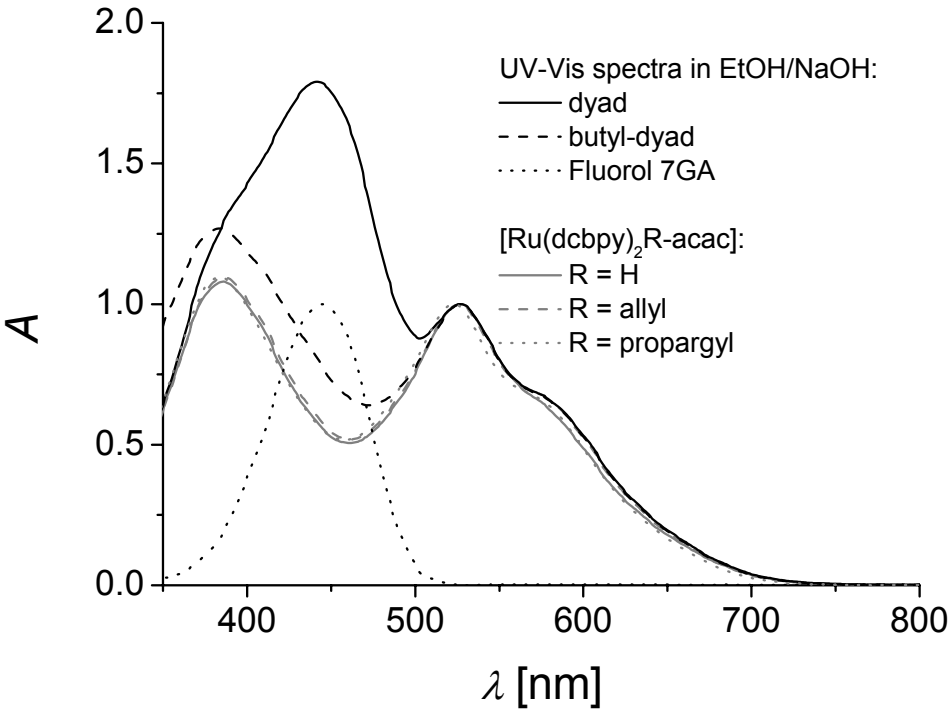

Figure 16. UV-Vis spectra of [Ru(dcbpy)$_2$acac]Cl **14** and its linker functionalized derivatives **57** and **58** in alkaline EtOH (gray lines). Furthermore the spectra of dyad **45**, butyl-dyad **59** and Fluorol 7GA **15** are displayed. The spectra were normalized to 1 at their reddest absorption maximum.

Table 11. Absorption maxima of [Ru(dcbpy)$_2$acac]$^+$ derivatives and Fluorol 7GA in alkaline EtOH.

Compound	$\lambda_{max,\,1}$ [nm]	$\lambda_{max,\,2}$ [nm]	$\lambda_{max,\,3}$ [nm]
[Ru(dcbpy)$_2$acac]Cl	310	385	527
[Ru(dcbpy)$_2$allyl-acac]Cl	310	385	527
[Ru(dcbpy)$_2$propargyl-acac]Cl	309	384	523
dyad	310	442	527
butyl-dyad	310	382 (422[a)])	527
Fluorol 7GA	-	445	-

a) maximum in neutral EtOH.

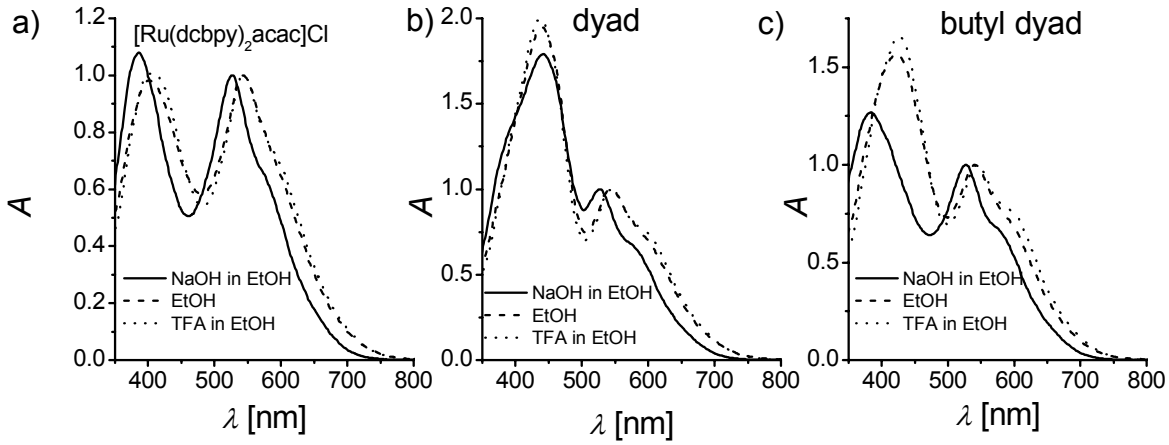

Figure 17. 3 Sets of UV-Vis spectra illustrating the pH dependence of the electronic specra of a) $[Ru(dcbpy)_2acac]Cl$ (**14**), b) dyad **45**, and c) butyl-dyad (**59**).

Figure 17 shows UV-Vis spectra of **58**, **45** and **59** in alkaline, neutral, and acidic EtOH. All the spectra in Figure 17 show a dependence of the absorption spectrum on the pH of the solvent. The addition of TFA does not alter the spectral properties significantly (the shoulder at 630 nm becomes somewhat more pronounced). The addition of base, on the other hand, effects a significant hypsochromic shift of the spectrum from the $[Ru(dcbpy)_2acac]^+$ moiety of about 20 nm in all cases. The absorption maximum at 445 nm from **45** decreases somewhat with increasing pH (Figure 17b). In addition, the absorption at 422 nm of **59** in EtOH is significantly reduced by the addition of base (Figure 17c). The absorption of the aminonaphthalimide moiety does not reveal a pH dependence in EtOH (not shown). The observations mentioned above are consistent with (i) an increase in the electronic energy of the ligand-centered LUMO in $[Ru(dcbpy)_2acac]^+$ due to additional electron density generated *via* deprotonation of the carboxy groups, (ii) bleaching of the donor moiety in **59** by the addition of base (Figure 17c), and (iii) the slight decrease of the absorption maximum at 445 nm in Figure 17b being effectuated by the shift of the acceptor absorption. The latter conclusion, the additivity of the absorption spectra of the donor and acceptor unit is further underlined by the results presented in Figure 18. It shows the extinction coefficient $\varepsilon(\lambda)$ of dyad **45** in combination with corresponding spectra of the parent chromophores in alkaline MeOH. Furthermore, Figure 18 shows a curve, which was calculated according to eq. (3.1).

$$\varepsilon_{Dyad} = 0.99 \cdot \varepsilon_{Donor} + 0.96 \cdot \varepsilon_{Acceptor} \quad (3.1)$$

$$\varepsilon_{Dyad} = \varepsilon_{Donor} + \varepsilon_{Acceptor} \quad (3.2)$$

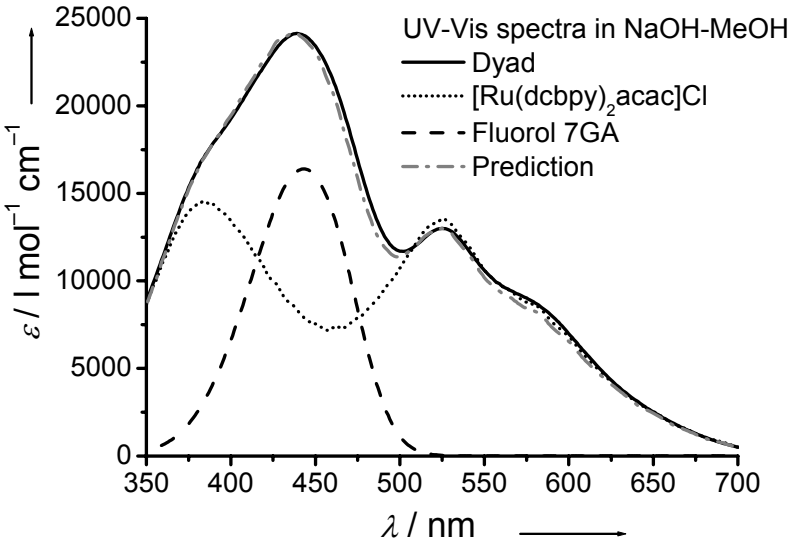

Figure 18. UV-Vis spectra of the donor acceptor dyad **45** (solid), the energy acceptor [Ru(dcbpy)$_2$acac]Cl **14** (dot) and the energy donor Fluorol 7GA **15** (dash) in NaOH/MeOH. Furthermore, a theoretical spectrum calculated according to $\varepsilon_{Dyad} = 0.99 \cdot \varepsilon_{Donor} + 0.96 \cdot \varepsilon_{Acceptor}$ is shown (light gray, dash-dot).

This curve is in very good agreement with the experimental spectrum of the dyad. The very moderate derivations of the simplest prediction [eq. (3.2)] show that there are no significant interactions between the electronic ground states of the individual chromophoric units within dyad **45**. The above-mentioned deviations are in consistence with minor alterations in the chemical environment of the chromophores effectuated by the introduction of the linker.

In conclusion, the characterization of the Ru-compounds synthesized in this work *via* UV-Vis spectroscopy in EtOH and MeOH at different pH showed a pronounced dependence of the absorption of the acceptor unit for pH > 7. The donor unit in **59** was bleached by the addition of base. The pH did not have any influence on the donor unit of **45**. Thus, the presence of at least one hydrogen atom on the aromatic amine nitrogen is crucial for the stability of the 4-aminonaphtalimide unit. Donor and acceptor absorption were shown to be additive.

3.5.3.7 Luminescence

The emission behavior of the dyad **45** was characterized by the emission spectra of solutions of both, the dyad and an optically matched mixture comprising the chromophores Fluorol 7GA and [Ru(dcbpy)$_2$allyl-acacH]Cl in EtOH. In order to exclude artifacts resulting from the luminescence of unbound aminonaphthalimides units, the sample of **45** used for luminescence studies was purified one additional time and separated from the eluent *via* freeze drying instead of precipitation.[76] The emission spectra of both solutions showed a maximum at 532 nm. This value is within the typical range for alkylated 4-aminonaphthalimides.[54]

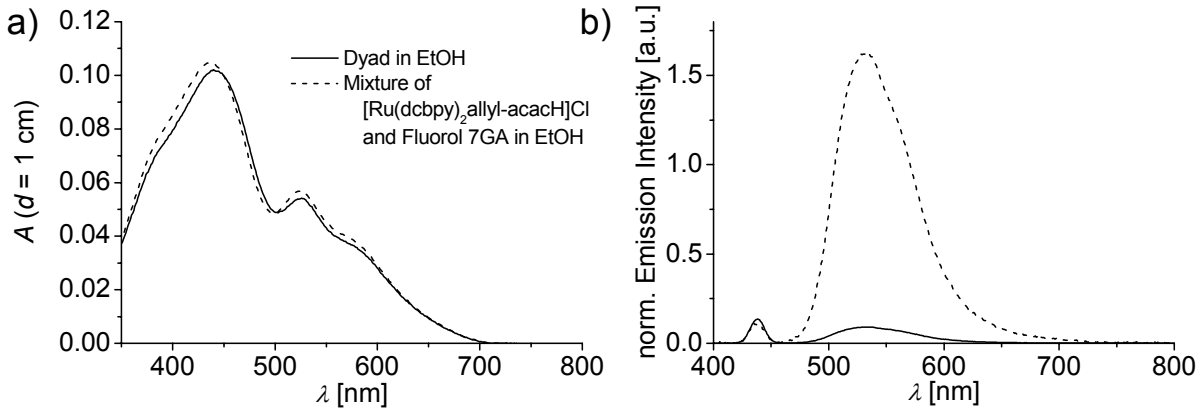

Figure 19. Results of experiments towards the emission behavior of the donor acceptor dyad. a) UV-Vis and b) emission spectra ($\lambda_{exc.}$ = 440 nm) of the donor acceptor dyad (solid) and an optically matched solution containing [Ru(dcbpy)$_2$allyl-acacH] and Fluorol 7GA (dashed).

The emission intensity of the solutions is decreased by 94% by the covalent link between the chromophores. This strong decrease in donor emission intensity is an indication towards a high energy transfer efficiency to the energy acceptor. The characteristic donor absorption maximum is present at a wavelength between 439 (MeOH) and 450 nm (TiO_2/electrolyte), depending on the solvent. Linking the Fluorol unit covalently to the ruthenium center brought about a drastic reduction in fluorescence intensity. This behavior is typical for efficient resonant energy transfer.[28] However, due to the poor luminescent properties of the energy acceptor, it was not possible to prove that donor quenching also leads to acceptor excitation. As a consequence, the measurement of an excitation spectrum based on the acceptor luminescence was not an option for the determination of the energy transfer efficiency.

3.5.4 Conclusion: Functional Ru Complexes and Aminonaphthalimides

In conclusion several functional chromophores were made by the syntheses described so far. These chromophores comprised the linker modified naphthalimides (notably **31**) and Ru complexes (notably **58**) for different immobilization strategies. The successful one is described in the next chapter. Furthermore, the work described so far also led to the energy transfer sensitizers **45** and the model chromophores **32** (as donor) as well as **57** and **14** (as acceptor models) to be evaluated in the dye solar cell (see Chapter 5).

3.6 Clicking Alkyne Functionalized Chromophores to (Poly)azides

Since recently, an overwhelmingly number of publications keep describing the 1,3-dipolar cycloaddition of azides to alkynes,[63] also termed "Click Chemistry,"[62] as a versatile method for the covalent attachment of a wide variety of different molecular units. The attractions of this reaction are the mild reaction conditions and the compatibility with a wide range of functional groups. It has been used to functionalize materials with chromophores before.[65] In this work, the click reaction was also employed to link the alkyne functionalized donor and acceptor chromophores **31** and **58** to a polymeric azide which was the key step towards the synthesis of polymers carrying the donor and acceptor moiety. Two different methodologies consisting of the sequential and the simultaneous addition of the acceptor and donor units were evaluated (Scheme 14). The experimental work described in the following section aimed at the variation of the following molecular parameters: (i) the polymeric architecture, (ii) the donor acceptor ratio, and (iii) the donor acceptor distance.

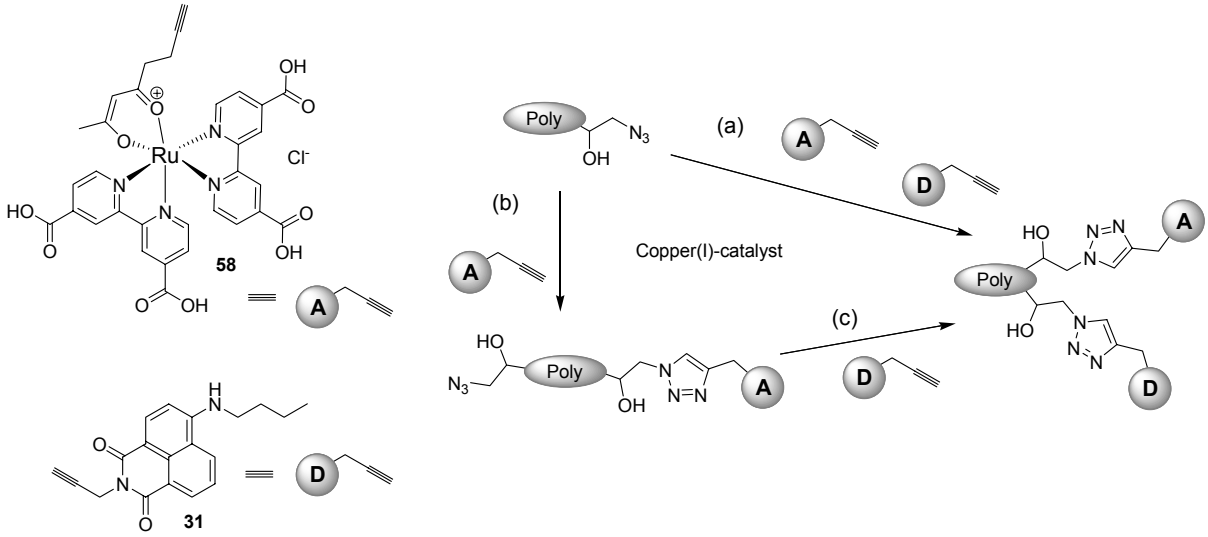

Scheme 14. Synthesis of donor acceptor functionalized polymers *via* the 1,3-dipolar cycloaddition of a polymeric azide to the alkyne functionalized chromophores. Reaction step (a) presents the simultaneous addition of donor and acceptor chromophores; the sequence encompassing steps (b) and (c) is the sequential addition to the polymeric azide.

The motivation for the variation of these parameters was the subsequent evaluation of their influence onto the energy transfer efficiency of D-A-systems within a dye solar cell. The synthesized compounds will be designated using the following abbreviation scheme: $D_{z_{DA}}$-$A_{\alpha_{Ru}}$-Polymer-$FG_{\alpha_{FG}}$. $D_{z_{DA}}$ indicates the presence of the donor with the donor acceptor ratio of z_{DA} and $A_{\alpha_{Ru}}$ specifies the presence of the acceptor with its respective degree of functionalization α_{Ru}. The degree of functionalization α_{FG} used here is defined as the ratio

between the number of functional groups (N_{FG}) and the number of monomeric units (N_M) per polymer molecule [eq. (3.3)].

$$\alpha_{FG} = N_{FG} \cdot N_M^{-1}. \quad (3.3)$$

"Polymer" indicates the type of polymer used and "- $FG_{\alpha_{FG}}$ " indicates that the polymer carries another species of functional groups with a degree of functionalization of α_{FG}. If the respective polymer has not been functionalized with the donor or acceptor $D_{\alpha_{Donor}}$ or $A_{\alpha_{Ru}}$ will be omitted.

3.6.1 Synthesis of Polyglycerol Azide

In order to study the above-mentioned structure-property relationships, the polymer used as a support should fulfill the following requirements: (i) it should be available in different architectures; (ii) it should allow the facile chemical modification to a respective polymeric azide, and (iii) it should be soluble or swellable under the conditions applied for the chemical reactions and in the acetonitrile-based electrolyte of the DSC. Polyglycerol (PG, **61**) is a polymer that was considered to meet these requirements (Scheme 15).

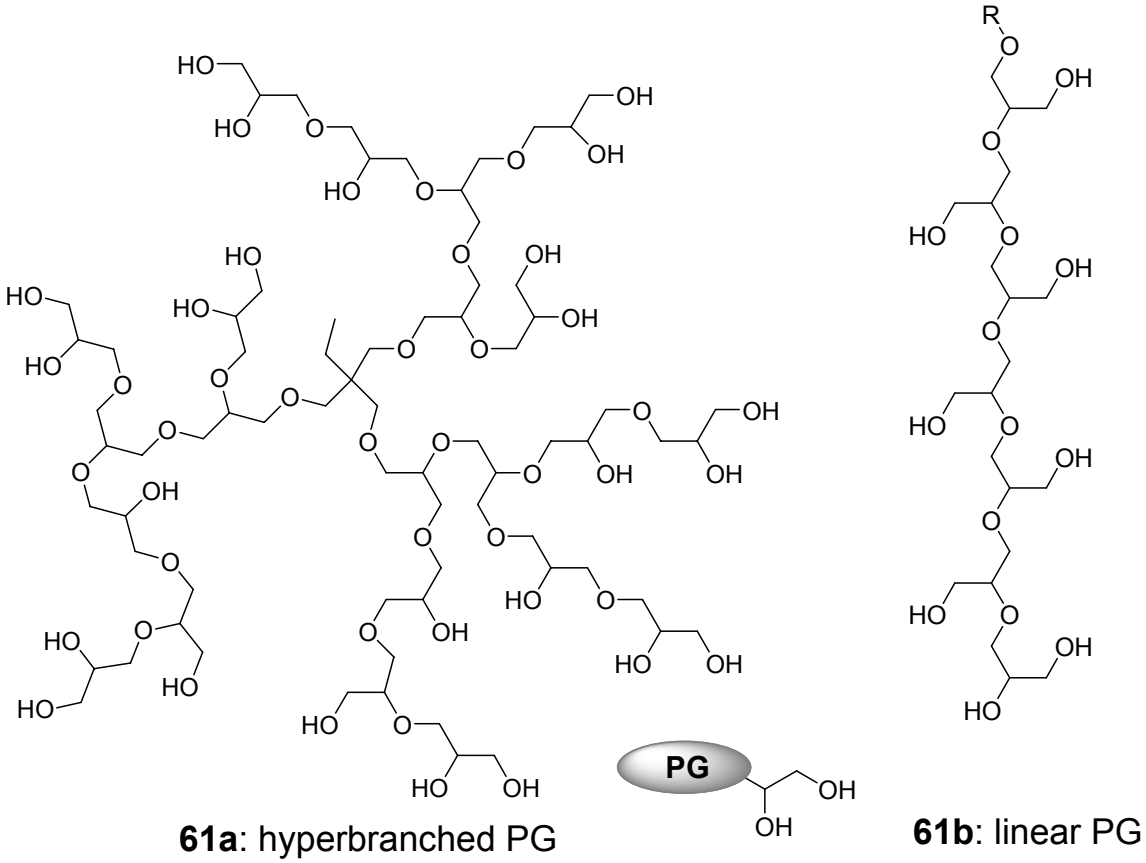

Scheme 15. Structures of the different types of polyglycerol used for the synthesis of polyglyerol azides in this work.

PG is available through the anionic ring-opening polymerization of glycidol or its derivatives. The polymerization of glycidol leads to a hyperbranched polymer (**61a**).[77-79] On the other hand, the polymerization of protected glycerol derivatives, e.g., ethoxyethyl glycidyl ether, leads to linear polyglycerol derivatives which may be deprotected to yield linear PG (**61b**).[80] An alkoxide moiety initiates the polymerization reaction. Two different polyglycerols were used in this work: (i) hyperbranched polyglycerol[81] with M_n = 5000 g mol^{-1} (n = 67, *h*PG) and (ii) linear polyglycerol with M_n = 1700 g mol^{-1} (n = 20, *l*PG).[82] Both polymers were available from previous studies. The rational for using these polymers for the support of the donor and acceptor chromophores was (i) their stability towards a range of reaction conditions especially, hydrolytic stability under basic conditions, (ii) their solubility in water and organic solvents, which is to some extent dependant on the nature of the polymer's functionalization, (iii) the possibility of establishing structure-property relationships considering the molecular architecture (hyperbranched vs. linear), and (iv) the facile substitution of OH groups by azide groups *via* a two step sequence, which was first described by Roller *et al*.[83] The latter sequence yielding polyglycerol azides (**62**, PG-N_3) is shown in Scheme 16 and consisted in (i) the mesylation of polyglycerol using methanesulfonyl chloride in absolute pyridine and (ii) subsequent nucleophilic substitution of the resulting mesylated PG (**63**, PG-OMs) with sodium azide in DMF.[83] Polymers with two different architectures (linear vs. hyperbranched) were used for the synthesis and the degree of functionalization with azide was varied for the hyperbranched polymer.

Table 12 gives an overview about the different PG-N_3 derivatives that were synthesized. For the synthesis of **63a - f** the polymer was dissolved in pyridine and methanesulfonyl chloride was added dropwise at 0°C. In most cases, the resulting PG-OMs was worked up exclusively by addition of ice and evaporation of the solvents. In some cases PG-OMs was purified *via* dialysis. The reaction products were characterized by ^{1}H NMR and ^{13}C NMR spectroscopy. The methyl group of the OMs moiety leads to signals between 3.15 and 3.25 ppm and 36.6 and 38.4 ppm in the ^{1}H and ^{13}C NMR spectra, respectively. The degree of loading with OMs (α_{OMs}) was calculated from ^{1}H NMR data by relating the intensity of the CH_3 resonance to the intensity of the PG backbone (see Appendix for details). From Table 12 it becomes obvious that the desired loading as controlled by the reaction stoichiometry is mostly experimentally achieved.

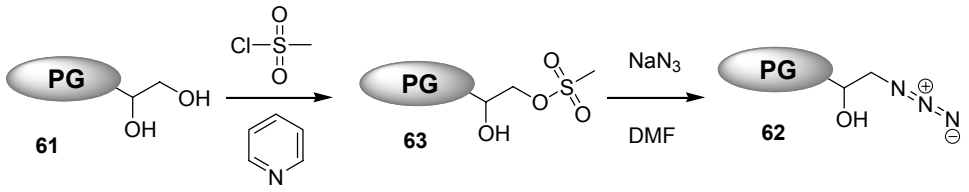

Scheme 16. Synthesis of polyglycerol azides **62** from polyglycerol (**63**) *via* the mesylation of OH-groups and the nucleophilic substitution of the resulting mesyl groups in **63** with azide.

Table 12. Reactions carried out towards the synthesis of polyglycerol azides (**62**) *via* the sequence shown in Scheme 16. The polyglycerol used was either hyperbranched with M_n = 5000 g mol^{-1} (*h*PG) or linear with M_n = 1700 g mol^{-1} (*l*PG).

Entry	Product (intermediate)	Sub-strate	$\alpha_{OMs} = \alpha_{N_3}$ [a]		Purification		Yield[b]	Charge
			theor.	exp.	of **63**	of **62**		
1	PG-$N_{3,\ 10\%}$ **62a** (**63a**)	*h*PG	10%	15%	-	dialysis in MeOH	60%	BO 567
2	PG-$N_{3,\ 30\%}$ **62b** (**63b**)	*h*PG	30%	31%	-	dialysis in MeOH	29%	BO 556
3	PG-$N_{3,\ 40\%}$ **62c** (**63c**)	*h*PG	40%	40%	dialysis in acetone/H_2O	dialysis in MeOH	33%	BO 542
4	PG-$N_{3,\ 60\%}$ **62d** (**63d**)	*h*PG	60%	59%	dialysis in acetone/H_2O	dialysis in MeOH	38%	BO 540
5	PG-$N_{3,\ 100\%}$ **62e** (**63e**)	*h*PG	100%	98%	-	Extraction into CH_2Cl_2	20%[c]	BO 573
6	*l*PG-$N_{3,\ 83\%}$ **62f** (**63f**)	*l*PG	100%	83%	-	Extraction into CH_2Cl_2	36%	BO 582

a) It was assumed that the loading of α_{N3} equals α_{OMs} as determined by ^{1}H NMR. b) Isolated yield over two steps. c) In this run, the conversion from OMs to azide was initially 92%, stirring the reaction product further with NaN_3 in DMF led to a complete conversion but low yield.

The mesylated PGs **63a** – **f** were further reacted with NaN_3 in DMF at 60°C for 3 days. Evaporation of the solvent and dialysis of the crude product afforded the polyglycerol azides **62a** – **f** (PG-$N_{3,\ 10\%}$ – *l*PG-$N_{3,\ 100\%}$, see Table 12). The products were characterized by ^{1}H NMR and ^{13}C NMR spectroscopy. After dialysis or extraction, the ^{13}C NMR spectrum of the reaction products did not show the characteristic signal for the CH_3 group of the OMs-moiety. The respective signal in the ^{1}H NMR spectra of the products had a marginal intensity. Signals at 53.7 – 50.9 ppm and 60.5 – 61.2 ppm in the ^{13}C NMR spectrum indicate the presence of primary[84] and secondary[83] azide groups, respectively. In the following work it was assumed that the loading of azide was equal to the loading with mesylate (α_{N3} =

α_{OMs}) as determined from the ^{1}H NMR spectra of the compounds **63a** – **f**. The thus prepared PG-N_3 derivatives were used as polymeric supports for alkyne functionalized chromophores.

3.6.2 Clicking: Preliminary Experiments

Preliminary experiments showed that the choice of solvent is crucial for the synthesis of donor acceptor systems. For example the simultaneous addition of the donor and acceptor chromophores to PG-$N_{3,\,40\%}$ in a THF-water mixture led to donor functionalized PG-N_3, which precipitated from the reaction mixture and acceptor functionalized PG-N_3, which stayed in solution. From this result it was concluded that it is absolutely crucial that the solvent system is able to dissolve (i) the hydrophilic acceptor substrate, (ii) the hydrophobic donor chromophore **31**, and (iii) the resulting donor acceptor polymers during the entire course of the reaction.

3.6.3 Simultaneous Addition of Donor and Acceptor Chromophores to PG-N_3

The simultaneous addition of both chromophores to PG-N_3 leads to donor acceptor polymers within one reaction step (Scheme 17). The reactions were conducted so that the acceptor chromophore **58** was added to the polymer first and the alkyne functionalized donor **31** 3 – 12 hours later. Two different reaction conditions leading to donor acceptor functionalized polymers were successful. Reactions carried out according towards these strategies are summarized in Table 13.

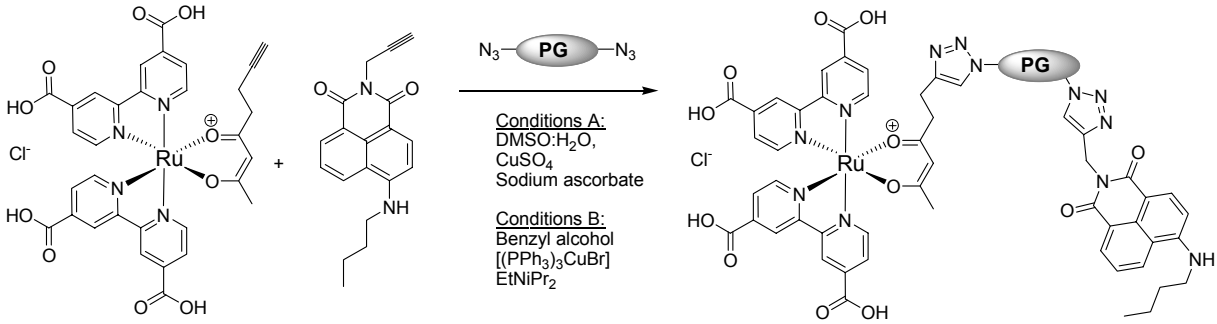

Scheme 17. Simultaneous addition of donor and acceptor chromophores **31** and **58** to polyglycerol azide **62** the number of equivalents refers to azide groups. a) PG-$N_{3,\,40\%}$ (**62c**), [Ru(dcbpy)$_2$propargyl-acac]Cl (**58)** (0.5 eq.), $CuSO_4$ (0.25 eq.), sodium ascorbate (2 eq.) in DMSO:water 1:1, after 3 h addition of propargyl butyl fluorol (**31**) in DMSO (the final DMSO water ratio was 2:1), stirring for 7 d in the dark, then work-up *via* extraction, precipitation, chromatography, precipitation and freeze-drying, resulting z_{DA} = 1 acc. to UV-Vis measurements, 47%. b) PG-$N_{3,\,100\%}$ (**62e**) or *l*PG-$N_{3,\,85\%}$ (**62f**), **58** (0.1 eq.), [$(PPh_3)_3$CuBr] (0.1 eq.), Et*N*iPr_2 50 °C (1 eq.), in benzyl alcohol, 12 h; then addition of **31** (0.4 eq.) and [$(PPh_3)_3$CuBr] (0.1 eq.), 50 °C, 4d, purification *via* column chromatography on Sephadex LH20 in THF:aq. TBA-OH (3:1). The yields were 67% and 54%, respectively.

Reacting the substrates **31**, **58,** and PG-$N_{3,\ 40\%}$ (**62c**) in DMSO:water (2:1) with $CuSO_4$ (0.25 eq.) and sodium ascorbate (2 eq.) in the dark over the course of one week and work-up by extraction, precipitation, column chromatography, and finally precipitation and freeze drying led to the desired polymer (Table 13, Entry 1).

Table 13. Reactions carried out towards the synthesis of D-A-PG-N_3 derivatives from different PG-$N_{3,\ \alpha N3}$-derivatives propargyl butyl fluorol and [Ru(dcbpy)$_2$propargyl-acac]Cl.

Entry	Product.[a] (run)	Conditions[b]	Stoichiometry			Results			
			α_{Ru}	α_{Donor}	z_{DA}	α_{Ru}[c]	α_{Donor}[c]	z_{DA}[d]	Yield[e]
1	D_1-$A_{(20\%)}$-PG-$N_{3,\ 40\%}$ **64**	A	20%	20%	1	29% (20%)	15% (20%)	1	47%
2	D_5-$A_{(10\%)}$-PG-$N_{3,\ 100\%}$ **65a**	B	10%	40%	4	20%	65%	5	67%
3	D_7-$A_{(10\%)}$-*l*PG-$N_{3,\ 85\%}$ **65b**	B	10%	40%	4	18%	>100%	7	54%

a) The substrate used for the supporting reaction becomes obvious from the last third of the product name. b) See conditions stated in Scheme 17. c) Calculated from ^{1}H NMR spectra in THF-d_8:D_2O:py-d_5 (in case of **65**, TBA-OH had to be added). The experimentally determined values are discussed in detail in Section 3.6.5.2 as of page 71). The values in parentheses is the loading determined from combining IR and UV-Vis results. d) Determined *via* UV-Vis spectroscopy. e) The yield calculated here assumed the donor acceptor ratio and conversions according to the reaction stoichiometry.

Figure 20 shows a photography of the chromatography column during the separation of the crude product of the latter reaction. The functionalized polymer forms a band that is clearly separated from the starting materials remaining in the crude product. The product revealed a donor acceptor ratio of $z_{DA} = 1$ according to UV-Vis measurements in good agreement with the value expected according to the reaction stoichiometry.

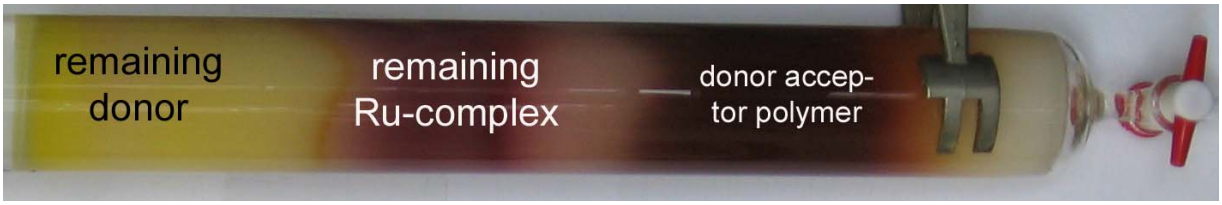

Figure 20. Photography of the chromatography column filled with Sephadex LH20 and water during the separation of D_1-$A_{20\%}$-PG-$N_{3,\ 40\%}$ (**64**). The individual bands are labeled. Unsupported donor remains at the start of the column if water is used as eluent and the polymeric species clearly elutes first (right band, brown). The intermediate band is purple and thus assigned to unsupported [Ru(dcbpy)$_2$propargyl-acac]Cl.

As the IR spectrum of the product did not show an azide band, it was assumed that the conversion of azide groups was close to quantitative. From a combination of results from IR and UV-Vis measurements the loading of this polymer with donor and acceptor units of

$\alpha_{Donor} = \alpha_{Ru} = 20\%$ is inferred assuming that no decomposition of azide took place. This is in clear contrast to results from ^{1}H NMR (Table 13) leading to a donor acceptor ratio of $z_{DA} = 0.5$. Since the measurement of UV-Vis spectra was considered very reliable, this disagreement points to the fact that ^{1}H NMR measurements do not reflect the actual donor acceptor ratio. The latter fact is discussed in more detail in Section 3.6.5.2. However, D-A-PG-N_3 derivatives are compounds with highly different monomeric units considering their polarity. Thus, although D_1-$A_{20\%}$-PG-$N_{3,\,40\%}$ forms a homogeneous solution in D_2O/NaOD or THF-d_8:D_2O:py-d_5, the formation of aggregates or the precipitation of unpolar domains within a polymer molecule leads to major difficulties for the determination of α_{FG} from ^{1}H NMR spectra. In conclusion, the synthesis of **64** led to the following results which were important with regard to the synthesis of the series of D-A-PG-N_3 derivatives described in the next two sections: According to conditions (a) in Scheme 17 (i) good conversions and (ii) a good control over z_{DA} *via* the stoichiometry were achieved; (iii) comparing z_{DA} determined by two different methods revealed that the information from ^{1}H NMR data is rather qualitative; (iv) the purification methods applied to Ru polypyridine complexes is also applicable to D-A-PG-N_3 derivatives. In order to allow for a more precise determination of α_{Ru} additional D-A-PG-N_3 derivatives were synthesized by the two-step route shown in Scheme 14. It consists of the sequential addition of **58** to polyglycerol azides **62**, purification and characterization of the resulting A-PG-N_3 derivatives **66**, and subsequent addition of **31**. This method offers a more reliable value for α_{Ru}.

Anticipating the results of sections 3.6.4 and 3.6.5 the control over α_{Ru} and α_{Donor} that was achieved in the synthesis of **64** was not necessarily reproducible. In most other runs in DMF/water or DMSO/water mixtures aiming at the addition of the alkyne functionalized chromophores the conversions and control over α_{FG} were only fair or poor. This was ascribed to the fact that although the substrates are dissolved in these mixtures, they still formed aggregates impeding the reaction. This was the motivation for conducting one final experiment relying on only one solvent. According to conditions (b) in Scheme 17 the addition of **58** and **31** to PG-$N_{3,\,100\%}$ and *l*PG-$N_{3,\,85\%}$ was carried out in the absence of water using benzyl alcohol as solvent. The rational for using an aromatic alcohol was its ability to interact with the polar moieties as well as the aromatic moieties of the reaction partners. It turned out that the combination of benzyl alcohol and *i*Pr_2NEt is an excellent solvent system for the substrates as well as the resulting D-A-PG-N_3 derivatives. In contrast to the other D-A-PG-N_3 derivatives described in this work the polymers **65** were not soluble in basic water.[85] Instead a 3:1 mixture of THF and aqueous TBA-OH (0.12 M) was used as solvent

and THF:water (3:1) was used as eluent over Sephadex LH20. After precipitation, considerable amounts of an aromatic impurity were still left in the product. Even an additional column chromatography step did not lead to a complete elimination of the impurity from polymers **65** (see signals around δ = 7.6 ppm in ^{1}H NMR spectra in Figure 29 on page 73).

65a and **65b** had a rather peculiar solubility behavior. The measurement of satisfactory ^{1}H NMR spectra was only possible in THF-d_8:D_2O:TBA-OH mixtures. Although ^{1}H NMR is not a reliable method for the precise determination of the loading, there are pronounced signals of both acceptor and donor moieties in the ^{1}H NMR spectra. In combination with the relatively good agreement between experimental and theoretical z_{DA} and the poor solubility of the products a high conversion and good control of z_{DA} may be inferred. Although these conditions require more optimization with respect to the amount of catalyst employed and the work-up procedure benzyl alcohol, DIPEA and [Cu(PPh$_3$)$_3$Br] might be the solvent/catalyst system of choice for the addition of the alkyne functionalized chromophores to polyglycerol azides. No further experiments were carried out according to these conditions due to time limitations. The detailed characterization of the D-A-PG-N_3 derivatives **64** and **65** described here will be presented as of section 3.6.5.1.

3.6.4 Addition of Alkyne-functionalized Energy Acceptor to PG-Azides

Supporting of [Ru(dcbpy)$_2$propargyl-acac]Cl **58** to polyglycerol azides was carried out using aqueous $CuSO_4$ (typically 0.05 eq. based on alkyne groups) and sodium ascorbate (typically 0.35 eq. based on alkyne groups) as catalyst system according to step (b) in Scheme 14.[65] Table 14 shows the reaction scheme and summarizes the reactions that were carried out leading to A-PG-N_3 derivatives **66**. DMF-water mixtures were used as solvents for this reaction. The DMF-water ratio was chosen so that the reaction mixture was homogeneous. Generally, the DMF content required to get a homogeneous solution of PG-$N_{3,\,\alpha N3}$ increased with its increasing azide functionalization (α_{N3}). The optimal pH for the reaction was not determined, but it was reasoned that the solubility of Cu^{2+} would be very limited under strong basic conditions. Therefore, the pH of the solution containing the Ru-complex was adjusted to 6 – 7 after its dissolution in alkaline water. The reactions were stirred at room temperature in the dark for several days (up to two weeks). Their purification consisted generally in column chromatography on Sephadex LH20 using water as eluent. In most cases the latter elution led to two clearly separated fractions.

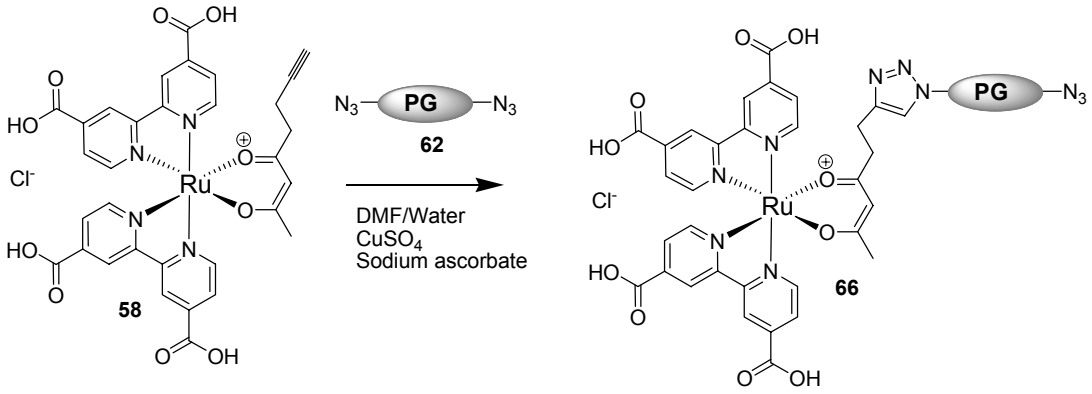

Table 14. Reactions carried out towards the synthesis of A-PG-N_3 derivatives from different PG-N_3, α_{N3}-derivatives and [Ru(dcbpy)$_2$propargyl-acac]Cl.

#	Product[a] (Run)	Reaction parameters[b]			Results			
		Solvent[c] DMF:H_2O	t [d][d]	α_{Ru} calc.[e]	α_{Ru} exp.[f]	Yield[g]	Con-vers.[h]	IR-int.[i]
1	$A_{1.5\%}$-PG-$N_{3,\ 10\%}$ **66a** (CS 233e)	1:2	14	4%	1.5%	n.d.	38%	s
2	$A_{3\%}$-PG-$N_{3,\ 30\%}$ **66b** (CS 233c)	1:9	6	8%	3%	n.d.	40%	s
3	$A_{5\%}$-PG-$N_{3,\ 30\%}$ **66c** (CS 233b)	1:9	6	10%	5%	n.d.	50%	s
4	$A_{10\%}$-PG-$N_{3,\ 30\%}$ **66d** (CS 233f)	1:5	14	12%	10%	n.d.	83%	s
5	$A_{11\%}$-PG-$N_{3,\ 30\%}$ **66e** (CS 233a)	1:9	6	15%	11%	n.d.	73%	s
6	$A_{29\%}$-PG-$N_{3,\ 40\%}$ **66f** (FK 76)	0:1	1.5	40%	29%	67%	73%	w
7	$A_{8\%}$-PG-$N_{3,\ 60\%}$ **66g** (CS 227-2)	3:1	1.5	10%	8%	57%	83%	s
8	$A_{0\%}$-*l*PG-$N_{3,\ 85\%}$ **66h** (CS 233d)	33:1	6	6%	-	-	0%	-
9	$A_{19\%}$-PG-$N_{3,\ 100\%}$ **66i** (CS 233h)	9:1	14	40%	19%	49%	48%	s

a) The substrate used for the supporting reaction becomes obvious from the last two thirds of the product name. b) $CuSO_4$ (typically 0.05 eq. based on alkyne groups) and sodium ascorbate (typically 0.35 eq. based on alkyne groups) was used as catalytic system. The pH of the reaction mixture was adjusted to 6 – 7 with aq. HCl. c) DMF:water ratio used as solvent. d) Reaction time in days. e) Degree of loading with Ru-complex according to the stoichiometry of the reaction mixture, and f) experimentally determined after isolation of product *via* ^{1}H NMR. g) The yield was only calculated if it was possible to isolate the polymer *via* precipitation upon acidification. h) The conversion was calculated according to $\alpha_{Ru,\ exp.} \cdot \alpha_{Ru,\ calc.}^{-1}$. i) Intensity of the azide-band of the product's IR spectrum (w = weak, s = strong).

The first one contained the acceptor functionalized polymer (A-PG), the second one contained unreacted **58**, which could be reisolated *via* precipitation upon addition of HCl. From the series of A-PGs synthesized in this work the isolation of the A-PGs from their aqueous solutions was possible by titration to a pH of 2 – 2.5 with HCl if $\alpha_{N3} \geq 30\%$ and $\alpha_{Ru} \geq 29\%$ (Table 14, entries 6 – 9). If the respective degrees of functionalization were lower, the precipitation upon acidification into water, methanol, or acetone was incomplete. A considerable amount of Ru compound remained in the supernatant. In these cases (Table 14, entries 1 – 5) the compounds were isolated by (azeotropic) removal of the solvent and freeze drying. The thus isolated products likely contained inorganic salts that formed during the pH-adjustment. Hence the yields were calculated only after the addition of the donor chromophore over two steps (see Section 3.6.5). The factors leading to a high conversion in this reaction remain unclear from the results shown in Table 14. There is no correlation between the conversion and the parameters reaction time, solvent composition, and the type of PG-N_3 used. The poor conversion in case of PG-$N_{3,\ 100\%}$ and *l*PG-$N_{3,\ 83\%}$ is probably due to the large difference in polarity of the two different substrates: The deprotonated Ru-complex is highly hydrophilic; the latter two PG-derivatives, on the other hand, are rather hydrophobic.

3.6.4.1 ^{1}H NMR Spectra of A-PG-N_3

Figure 21 shows the ^{1}H NMR spectra of $A_{29\%}$PG-$N_{3,\ 40\%}$, $A_{10\%}$PG-$N_{3,\ 30\%}$ and [Ru(dcbpy)$_2$acac]Cl in D_2O/NaOD. Furthermore, [Ru(dcbpy)$_2$acac]Cl in MeOD is also shown. The signal for the hydrogen atom remaining on the triazole ring resonates typically at 7.6 – 7.8 ppm.[84, 86] This signal was not clearly resolved due to overlap with the signals from the dcbpy ligands. However, the following facts support the successful immobilization of the Ru-complex to the PG-N_3 without chemical alteration on the [Ru(dcbpy)$_2$acac]$^+$-moiety: (i) The characteristic chemical shifts of the aromatic hydrogen atoms are close to identical in the monomeric and polymeric Ru complexes for the spectra measured in D_2O with exception of the signal assigned to the 6-bpy-H; (ii) the significant peak broadening with respect to the ^{1}H NMR spectrum of **14,** which is prevalent in the spectra of all A-PG-N_3 derivatives, supports the fact that A-PG-N_3 derivatives are actually polymeric species; (iii) the new signal at around 4.2 ppm is typical for triazole-N-CH_2-groups;[84] and (iv) there is a significant shift of the signal assigned to the 6-bpy-H in D_2O from around 8.80 (see Figure 21 spectrum d) to 8.65 ppm (see Figure 21 spectra a + b) brought about by the supporting reaction. Such a shift is also observed in [Ru(dcbpy)$_2$acac]Cl for this signal on changing the NMR solvent from the polar solvent D_2O to less polar MeOD (see Figure 21 spectra c and d).

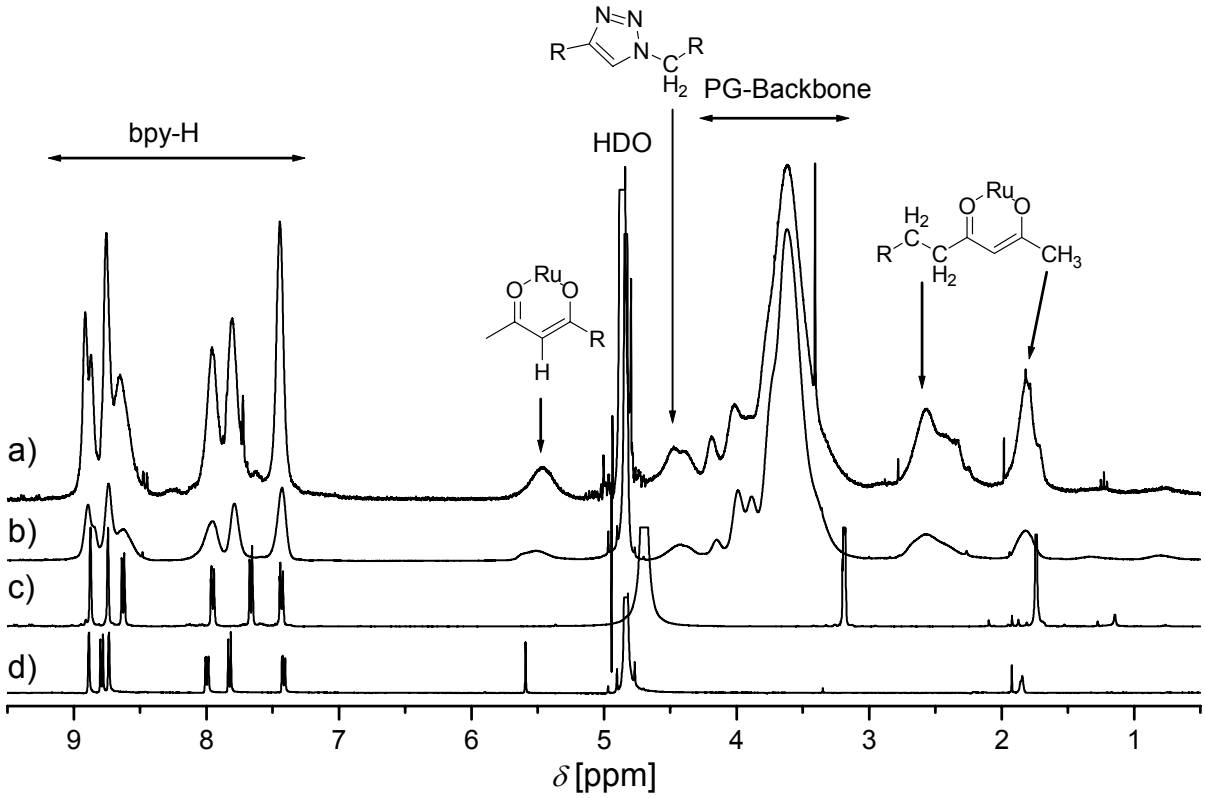

Figure 21. ^{1}H NMR spectra of a) $A_{29\%}PG\text{-}N_{3,\ 40\%}$ in D_2O, b) $A_{10\%}PG\text{-}N_{3,\ 30\%}$ in D_2O and $[Ru(dcbpy)_2acac]Cl$ in c) MeOD and d) D_2O.

Thus, the fact that the Ru-complexes are exposed to a less polar environment by the addition to the polymer backbone is also evident for the chemical shift of the 6-bpy-H in D_2O.

3.6.4.2 ^{13}C NMR Spectra of A-PG-N_3

Typical ^{13}C NMR spectra of the $[Ru(dcbpy)_2acac]$-derivatives prior (gray) and after (black) immobilization onto PG-N_3 are shown in Figure 22. In analogy to the results from ^{1}H NMR experiments the carbon atoms from the dcpby ligand resonate at identical chemical shifts whether linked to the polymer or not. This fact underlines once again the absence of chemical alteration on the $[Ru(dcbpy)_2acac]^{+}$-moiety. Furthermore, two new signals appear at 123 and 145 ppm. These chemical shifts are typical for 1,4-disubstituted 1,2,3-triazoles.[84, 87][88] In order to determine the chemical shift of the hydrogen atom on the triazole ring a HSQC measurement was carried out with $A_{29\%}$-PG-$N_{3,\ 40\%}$ **66f** (Figure 23). This measurement showed that the signal at δ = 123 ppm (black dotted line) does not correlate with any signal within the ^{1}H NMR spectrum. This fact would be consistent with an H-D exchange or a very broad peak leading to no significant C-H-correlation signal of the respective hydrogen atom.

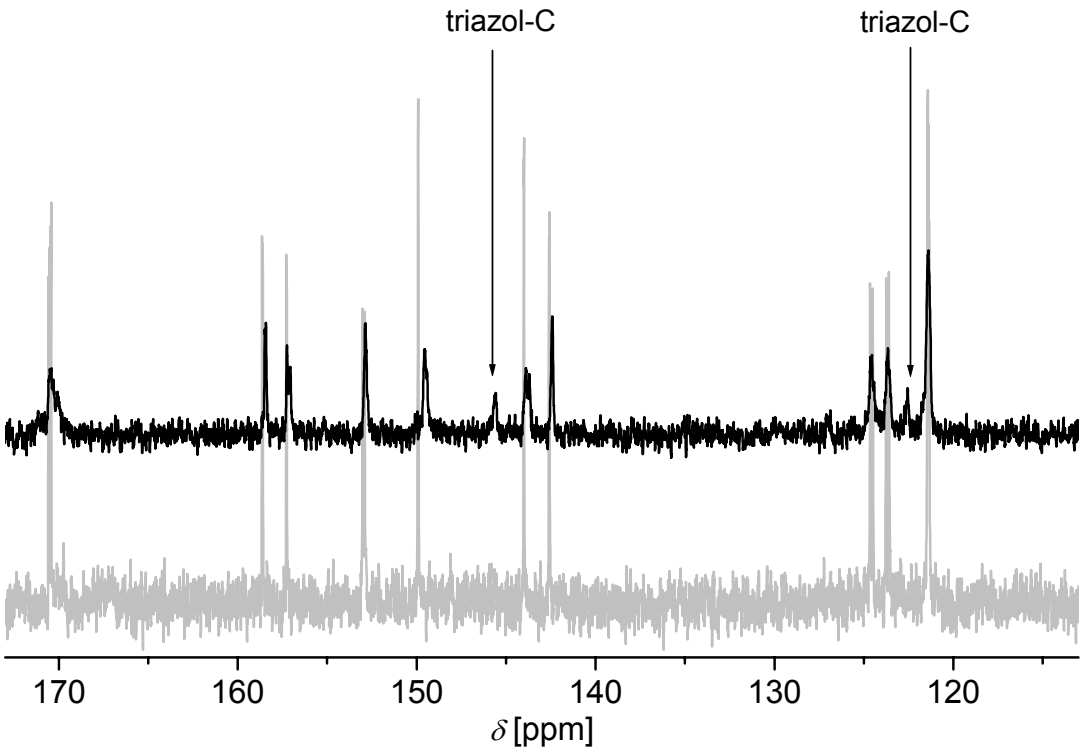

Figure 22. ^{13}C NMR spectra (75 MHz) of $A_{10\%}PG\text{-}N_{3,\ 30\%}$ (black, top) and [Ru(dcbpy)$_2$propargyl-acac]Cl (gray, bottom) measured in D_2O.

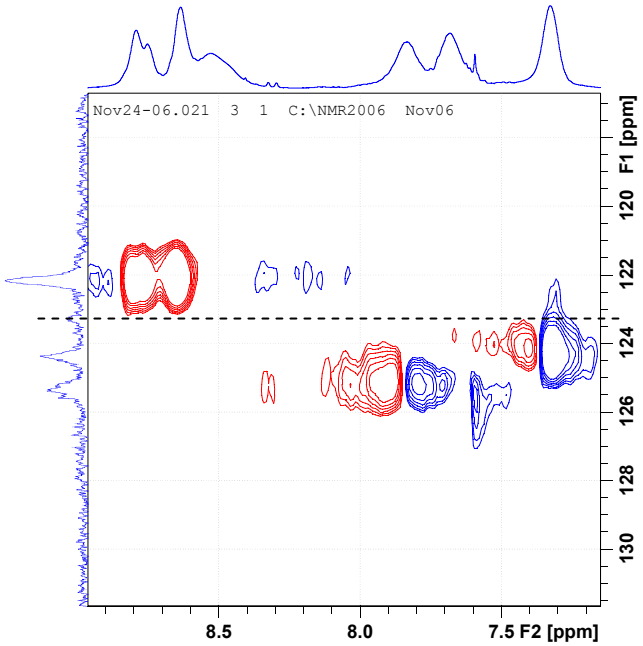

Figure 23. 2D-NMR spectrum of $A_{29\%}$-$PG\text{-}N_{3,\ 40\%}$ **66f**. The black dotted line indicates the position of the 5-C atom from the triazole ring.

3.6.4.3 UV-Vis Spectra

Figure 24 shows UV-Vis spectra of [Ru(dcbpy)$_2$propargyl-acac]Cl (dashed) and A$_{29\%}$-PG-N$_{3,\,40\%}$. The longest wavelength absorption maxima for **14** and **66f** are 515 and 519 nm, respectively. The shape of the spectrum is nearly identical. Thus, the only change in absorption properties upon the addition of the azide to the alkyne is a slight red-shift. This result confirms once again the presence of the [Ru(dcbpy)$_2$acac]$^+$-moiety on the polymer.

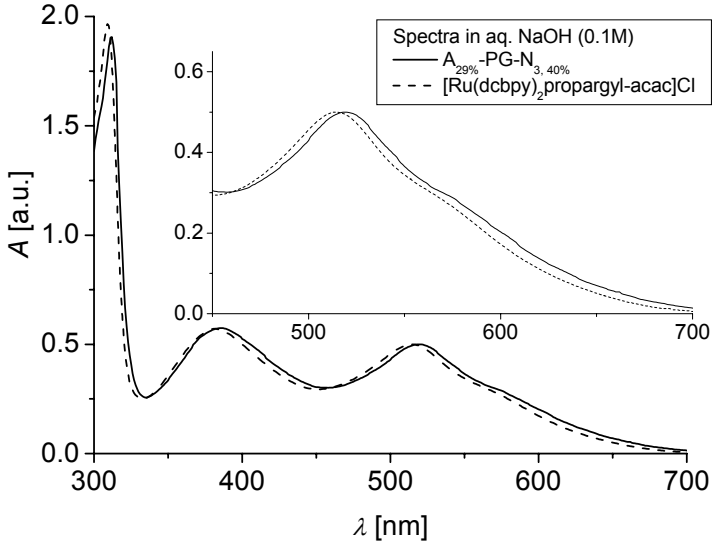

Figure 24. UV-Vis spectra of [Ru(dcbpy)$_2$propargyl-acac]Cl (dashed) and A$_{29\%}$-PG-N$_{3,\,40\%}$ (solid) in aq. NaOH (0.1 M).

3.6.4.4 IR Spectra

The last column in Table 14 summarizes results from the IR spectra of the A-PG-N$_3$ derivatives. The fact that the azide band at around 2100 cm^{-1} is weak in case of A$_{29\%}$-PG-N$_{3,\,40\%}$ underlines the fact that the conversion was high in this run. In the other isolated products a strong azide band was prevalent in the respective IR spectrum. This demonstrates that azide groups remain after the cycloaddition reaction and isolation thus offering the possibility to further derivatize these polymers by addition of the alkyne-functionalized energy donor moiety.

3.6.5 Addition of the Energy Donor to A-PG-N$_3$

All products that were isolated from the runs presented in Table 14 were subjected to the cycloaddition with the donor chromophore resulting in donor acceptor polymers D-A-PG-N$_3$ (**67**). Supporting of propargyl butyl fluorol **31** to A-PG-N$_3$ was carried out using aqueous CuSO$_4$ and sodium ascorbate as catalyst system [according to Table 15 as well as Scheme 14,

conditions (c)][65] as well as DMSO-water mixtures as solvent.[89] The DMSO-water ratio was adjusted for every run individually.

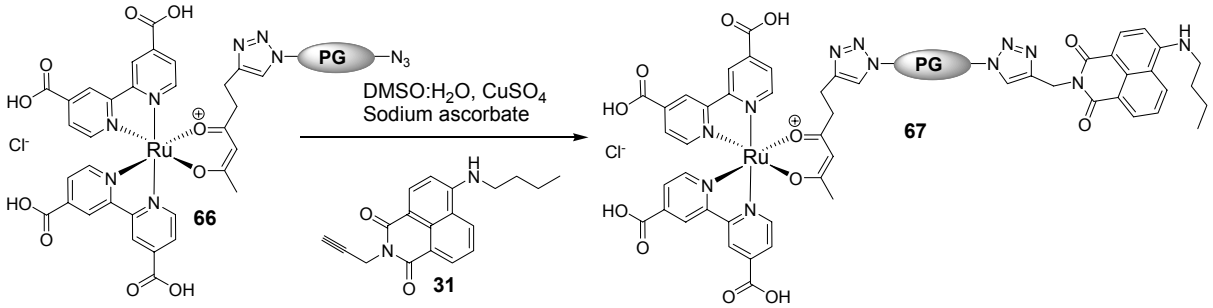

Table 15. Reactions carried out towards the synthesis of D-A-PG-N_3 derivatives from different A-PG-$N_{3,\ \alpha,N3}$-derivatives and propargyl-butyl-fluorol.

#	Product[a, b] (Run)	Conditions				Results				
		Sol.[c]	pH	t[d] [d]	z_{DA} calc.	z_{DA} exp.[e]	α_{Donor}[f]	Yield[g]	Conv.	IR-int.[h]
1	D_0-$A_{1.5\%}$-PG-$N_{3,\ 10\%}$ **67a** (CS 233-2e)	4:1	> 9[i]	32	1.5	0	0%	n.d.[k]	0%	n.d.
2	$D_{8.6}$-$A_{3\%}$-PG-$N_{3,\ 30\%}$ **67b** (CS 233-2c)	3:2	> 9[i]	7	9[j]	8.6	26%	30%	96%	w
3	$D_{0.8}$-$A_{5\%}$-PG-$N_{3,\ 30\%}$[l] **67c** (CS 233-2b)	3:1	5.5	7	5[j]	0.80	3.2%	34%	16%	w
4	$D_{0.3}$-$A_{10\%}$-PG-$N_{3,\ 30\%}$ **67d** (CS 233-2f)	4:1	> 9 [i]	35	1.5	0.30	3%	n.d.[k]	20%	n.d.
5	$D_{0.5}$-$A_{11\%}$-PG-$N_{3,\ 30\%}$ **67e** (CS 233-2a)	3:1	7.3	7	1.7[j]	0.54	5%	33%	31%	n.p.
7	$D_{3.7}$-$A_{8\%}$-PG-$N_{3,\ 60\%}$ **67g** (CS 227-2 F1)	5:1	6.8	7	5.25	3.7	30%	69%	70%	n.d.
8	$D_{0.8}$-$A_{19\%}$-PG-$N_{3,\ 100\%}$ **67i** (CS 233h)	4:1	> 9 [i]	21	1.5	0.76	14%	44%	50%	s

a) The substrate used for the supporting reaction becomes obvious by omitting the D_{zDA}- part of the product name. b) $CuSO_4$ (typically 0.05 eq. based on alkyne groups) and sodium ascorbate (typically 0.35 eq. based on alkyne groups) was used as catalytic system. c) The solvent used for the reaction was a mixture of DMSO and water. The DMSO:water ratio is given in this column. d) Reaction time in days. e) donor acceptor ratio as determined from UV-Vis spectroscopy. f) Calculated according to $z_{DA} \cdot \alpha_{Acceptor}$. g) Isolated yield over two steps. h) Intensity of the azide band in the product's IR spectrum. i) In these runs, adjusting the pH with HCl was omitted. The basic solution of the A-PG-N_3 derivatives was used for the reaction. j) In these runs an excess of propargyl-butyl-fluorol was added to the reaction mixture, the value for z_{DA} was thus calculated by $z_{DA} = (\alpha_{N3} - \alpha_{Acceptor}) \cdot \alpha_{Acceptor}^{-1}$. k) In these cases the polymer did not precipitate upon acidification, it was isolated *via* evaporation of the solvents. The products contained considerable amounts of salts. l) This product was eluted with MeOH and subsequently with acetone:H_2O (3:1).

The A-PG-N_3 derivatives **66** were dissolved in basic water ($NaHCO_3$); in some cases the pH of the resulting aqueous solution was adjusted to a pH between 5.5 and 7.3 using aq. HCl. Table 15 summarizes the reactions that were carried out accordingly. The work-up of these polymers generally consisted in addition of HCl, upon which the precipitation of the crude product occurred. The purification consisted in column chromatography on Sephadex LH20 with water as eluent and freeze drying of the precipitate that formed on acidification. The products were characterized *via* ^{1}H NMR spectroscopy in D_2O and a mixture of THF-d_8:D_2O:pyridine-d_5, IR spectroscopy, and UV-Vis spectroscopy. In some products the copper content was determined by atomic absorption spectroscopy. The reactions carried out according to Table 15 show in most cases a poor agreement between z_{DA} adjusted *via* the reaction stoichiometry (z_{DA} calc.) and the experimental value determined *via* UV-Vis spectroscopy (z_{DA} exp.). Satisfactory conversions were only achieved in entries 2 and 7. The pH of the reaction mixture does not influence the outcome significantly within the range that was studied here. This becomes obvious from a comparison of entries 2 and 7. The reasons for low conversions in the other runs thus remain unclear. Most likely, insolubility of the substrate or shielding of the azide groups by the hydrophilic Ru-complexes were the causes for the poor conversions. The former hypothesis was underlined by UV-Vis experiments conducted with samples of the reaction mixture from runs 2, 3, and 5 (Figure 25). The samples of the reaction mixture in DMSO were clear solutions (as revealed by the high transparency of their UV-Vis spectra between 750 and 900 nm, Figure 25, black curves). It turned out, however that the donor acceptor ratio within the sample of runs 5 and 3 is dependant on whether the sample was filtered through a 0.22µ syringe filter or not. After filtration, the donor acceptor ratio in the filtrate is a lot higher than before. This is consistent with the Ru-functionalized polymer forming aggregates impeding the reaction. If no aggregates are formed (as in case of run 2, where the filtration does not alter the UV-Vis spectrum) the conversion is quantitative. An optically transparent reaction mixture is thus not a sufficient criterion for efficient solubilization of the reaction partners. Furthermore, the decomposition of azide groups on the polymer backbone might also explain low conversions: In **67e** (Entry 5) there is no azide band remaining in the product, although the sum of α_{Ru} and α_{Donor} is below α_{N3}. In contrast to the synthesis of **64** (Section 3.6.3) the sequential addition of acceptor and then donor chromophores to polyglycerol azides did not generally yield good control over α_{Ru} and z_{DA}.

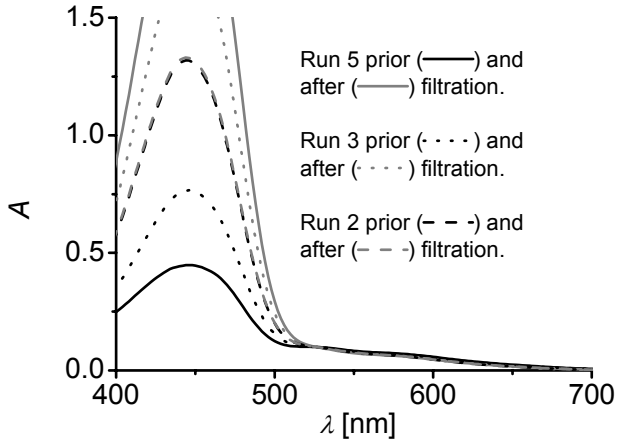

Figure 25. Normalized UV-Vis spectra of reaction mixtures of runs 2, 3, and 5 from Table 15. Spectra of samples from the respective reaction mixtures were measured prior (black) and after (gray) filtration of the sample through a 0.22µ syringe filter.

In conclusion, despite the formation of a homogeneous solution of the reaction partners the click addition of propargyl-butyl-fluorol to A-PG-N_3 derivatives proceeded in two out of eight runs to satisfactory conversions. The products $D_{0.8}$-$A_{5\%}$-PG-$N_{3,\ 30\%}$ **67c,** $D_{3.7}$-$A_{8\%}$-PG-$N_{3,\ 60\%}$ **67g** and $D_{8.6}$-$A_{3\%}$-PG-$N_{3,\ 30\%}$ **67b** obtained according to Table 15 were considered as polymeric donor acceptor sensitizers for testing in the DSC. Their UV and NMR spectra are presented in the next sections in combination with the ones of **64** and **65** synthesized according to Table 13.

3.6.5.1 UV-Vis spectra of D-A-PG-N_3 Derivatives

As it was shown in previous sections, the characteristic absorption properties of the chromophoric units do not drastically change by the alterations on their linker groups. As a result, the absorption spectra of donor and acceptor (Figure 26a) will behave additively and the donor acceptor ratio is reflected in the relative intensities of the donor and acceptor absorption. UV-Vis spectra were measured in order to determine z_{DA}. If possible, alkaline water was used as solvent (see Figure 26b). Polymers **65** were not water soluble. Alternatively, a mixture of THF:aq. TBA-OH (0.12 M, 3:1) was used as solvent for these polymers. These spectra are shown in Figure 26b and Figure 27. They are all similar with respect to their absorption maxima and their shape for $\lambda > 525$ nm, however, the ratio of maximal donor and acceptor absorption was highly dependant on the polymer composition, namely, z_{DA}. Determining z_{DA} from UV-Vis data was performed by comparing the product's experimental spectra [$A_{exp.}(\lambda)$] to a simulated spectrum [$A_{calc.}(\lambda, z_{D\text{-}A})$] calculated according to eq. (3.4).

$$A_{calc} = \varepsilon_{Acceptor} + z_{DA} \cdot \varepsilon_{Donor} \tag{3.4}$$

z_{DA} was chosen so that $A_{exp.}(\lambda)$ and $A_{calc.}(\lambda, z_{D\text{-}A})$ agree. The thus determined value for $z_{D\text{-}A}$ for the individual products of the runs is presented in Table 13 and Table 15. Furthermore, they are compared to z_{DA} acquired from ^{1}H NMR data in Table 17. Figure 28 underlines z_{DA} within polymer **64** impressively. This compound has an absorption behavior that is close to identical to **45**, a compound where the precise 1:1 ratio was proven by both ^{1}H NMR and UV-Vis spectroscopy.

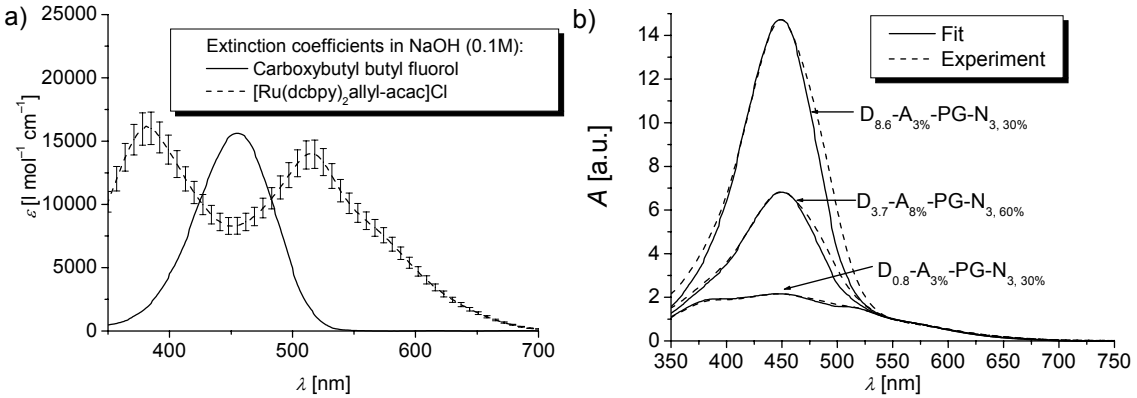

Figure 26. UV-Vis spectra of a) the water soluble parent chromophores **14** and **32** and b) D-A-PGs **67b**, **67g**, and **67c** in aqueous NaOH (0.1 M). The simulated spectra were calculated using eq. (3.4) and the data from a) as well as z_{DA} = 8.6, 3.7 and 0.8 for **67b**, **67g** and **67c**, respectively.

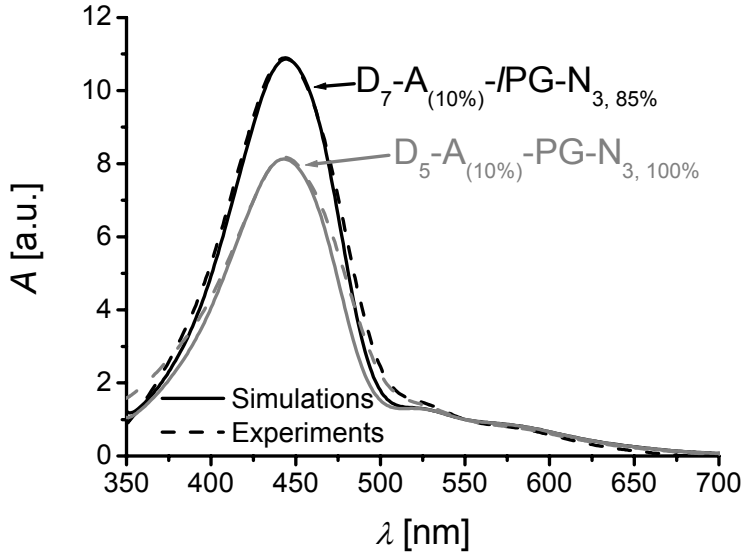

Figure 27. UV-Vis spectra of D-A-PGs **65a** and **65b** in THF:aq. TBA-OH (0.12 M, 3:1). The following values were assumed for the simulation: $\varepsilon_{max,\,Donor}$ = 16000 l mol^{-1} cm^{-1}, $\varepsilon_{max,\,Acceptor}$ = 13500 l mol^{-1} cm^{-1} and z_{DA} = 5.0 and 7.0 for **65a** and **65b**, respectively.

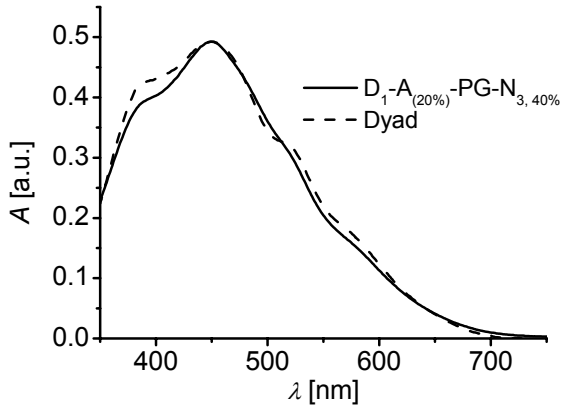

Figure 28. UV-Vis spectra of dyad **45** and D_1-$A_{(20\%)}$-PG-$N_{3,\ 40\%}$ (**64**) in aqueous NaOH (0.1 M).

3.6.5.2 ^{1}H NMR Spectra of D-A-PG-N_3

In order to acquire a NMR spectrum comprising signals of both the donor and acceptor moieties, the samples have to be dissolved in a solvent that can dissolve both units with a concentration which allows a satisfactory signal-to-noise ratio. Since the donor and acceptor have completely different solution properties, the characterization of polymers comprising the donor and acceptor moieties was challenging. Although it was possible to prepare a clear solution of D-A polymers with remaining OH groups in alkaline water, the ^{1}H NMR spectrum of such solutions only revealed signals of the acceptor moiety, the polymer backbone, and the butyl group of the donor moiety. The latter were significantly less intense than expected from the donor acceptor ratio and no signals of the aromatic protons from the donor group were detectable.[90] Better NMR spectra were measured in a mixture of THF-d_8:D_2O in presence of a base. For the polymers **64** and **67** py-d_5 was sufficient. In case of **65** py-d_5 and NaOD did not to lead solutions of the polymer with a concentration high enough to perform ^{1}H NMR measurements. Addition of NaOD and NMe_4OH to the THF water mixture led to phase separation of the solvent system. Thus NBu_4OH, which was not available in its deuterated form, had to be added to the NMR samples in order to prepare a homogeneous solution. This gave rise to intense signals from HDO at δ = 4.24 ppm and from NBu_4^+ at δ = 3.20, 1.61, 1.35, and 0.90 ppm making it impossible to evaluate the resulting spectra around these signals.

A selection of ^{1}H NMR spectra from donor acceptor modified PGs recorded in deuterated THF water mixtures is shown in Figure 29 and Figure 30. Furthermore, the spectra of the compounds [Ru(dcbpy)$_2$allyl-acac]Cl (**57**) and Fluorol 7GA (**15**) is shown in a mixture of the deuterated solvents THF-d_8, D_2O and py-d_5 and the spectrum of 4-carboxybutyl butyl fluorol **32** in alkaline D_2O is also presented. Figure 30 shows the spectra of D-A-PGs with a considerable amount of remaining OH-groups in the backbone ($\alpha_{N3} \leq 60\%$) and Figure 29 the

spectra of D-A-PGs featuring $\alpha_{N3} \geq 85\%$. The assignments that were made to the signals are compiled in Table 16. The following signals in the aromatic region of the spectrum are assigned by comparing the spectra of the polymers (Figure 29a and b as well as Figure 30a – c) with the spectra from the model compounds (remaining spectra in Figure 29 and Figure 30): (i) The 3-, 3'- and 6-bpy-Hs on the acceptor moiety and (ii) the aromatic 8- and 5-Hs on the donor moiety. The 3-bpy-H, 3'-bpy-H and 6-bpy-H in $[Ru(dcbpy)_2allyl\text{-}acac]Cl$ appear at 9.06, 8.90 and 8.75 ppm, respectively. The corresponding signal in the polymers appears with a slight upfield shift between 8.99 – 8.92, 8.84 – 8.79 and 8.71 – 8.65 ppm, respectively. For the latter spectral range it cannot be ruled out that the aromatic proton's resonances of the donor unit contribute to the signal. A comparison of the ^{1}H NMR spectra of 4-carboxybutyl butyl fluorol (**32**) in alkaline D_2O (Figure 29d) and Fluorol 7GA (**15**) in THF-d_8:D_2O:py-d_5 (9:3:1), (Figure 29e) reveals a pronounced solvent dependence of ^{1}H NMR resonances within this type of aromatic system. In Figure 29e, the signals at 7.61 and 6.71 ppm are assigned to the 8-H and 5-H of the donor moiety, respectively. The aromatic signals of 4-carboxybutyl butyl fluorol (**32**) in an organic solvent appear at identical chemical shifts than those of Fluorol 7GA, however, in alkaline water, the aromatic resonances exhibit a pronounced upfield shift. The signals at 7.01 and 6.05 in the spectrum shown in Figure 29d were assigned to the 8- and 5-H. The above-mentioned considerations are relevant for the assignment of the distinct broad signals of the polymers around 7.16 and 6.15 ppm. Since these chemical shifts are in between the ones for the 8-H and 5-H in organic solvents and D_2O, respectively, these resonances were assigned to the aromatic protons of the donor group in the 8- and 5-positions. *The upfield shift of these resonances clearly proves the change in chemical environment brought about by the binding to the acceptor-functionalized polyglycerol support.* The signals in the range 8.3 – 7.4 ppm are poorly resolved and were thus assigned to the remaining aromatic protons including the triazole-H. Furthermore, the methylene unit on the imide nitrogen resonates at $\delta = 5.2$ ppm in the polymer as supposed to 4.9 ppm in **31**. The linking $(CH_2)_2$-unit between the ruthenium complex and the triazole resonates between 2.7 and 2.3 ppm in analogy to **66**. The terminal butyl group on the donor unit leads to a shoulder at around 3.0 ppm as well as broad signals at 1.4, 1.2 and 0.7 ppm. In case of polymers **65a** and **65b**, where TBA-OH had to be added to the NMR sample the resonances of TBA^+ dominate the spectra between 4.0 and 0.5 ppm.

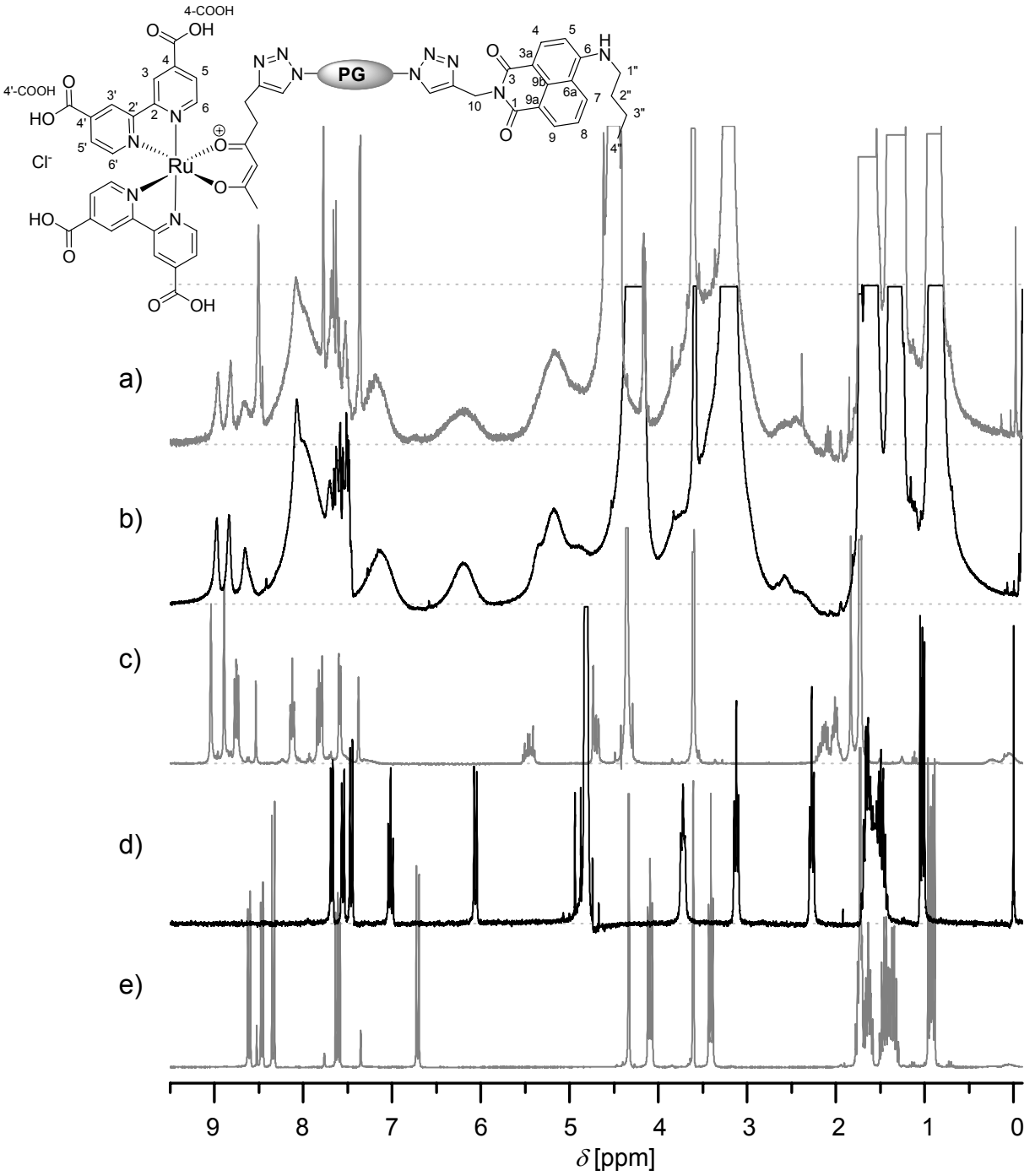

Figure 29. ^{1}H NMR spectra (300 MHz) of polyglycerols functionalized with the donor and acceptor chromophores and small model compounds. a) D_7-$A_{(10\%)}$-*l*PG-$N_{3,\ 85\%}$ (**65b**) in THF-d_8:D_2O:py-d_5 (12:4:1) with TBA-OH; b) D_5-$A_{(10\%)}$-PG-$N_{3,\ 100\%}$ (**65a**) in THF-d_8:D_2O (3:1) with TBA-OH; c) [Ru(dcbpy)$_2$allyl-acac]Cl (**57**) in THF-d_8:D_2O:py-d_5 (9:3:1); d) 4-Carboxybutyl butyl fluorol (**32**) (ca. 7 mM) in alkaline D_2O; e) Fluorol 7GA (**15**) in THF-d_8:D_2O:py-d_5 (9:3:1).

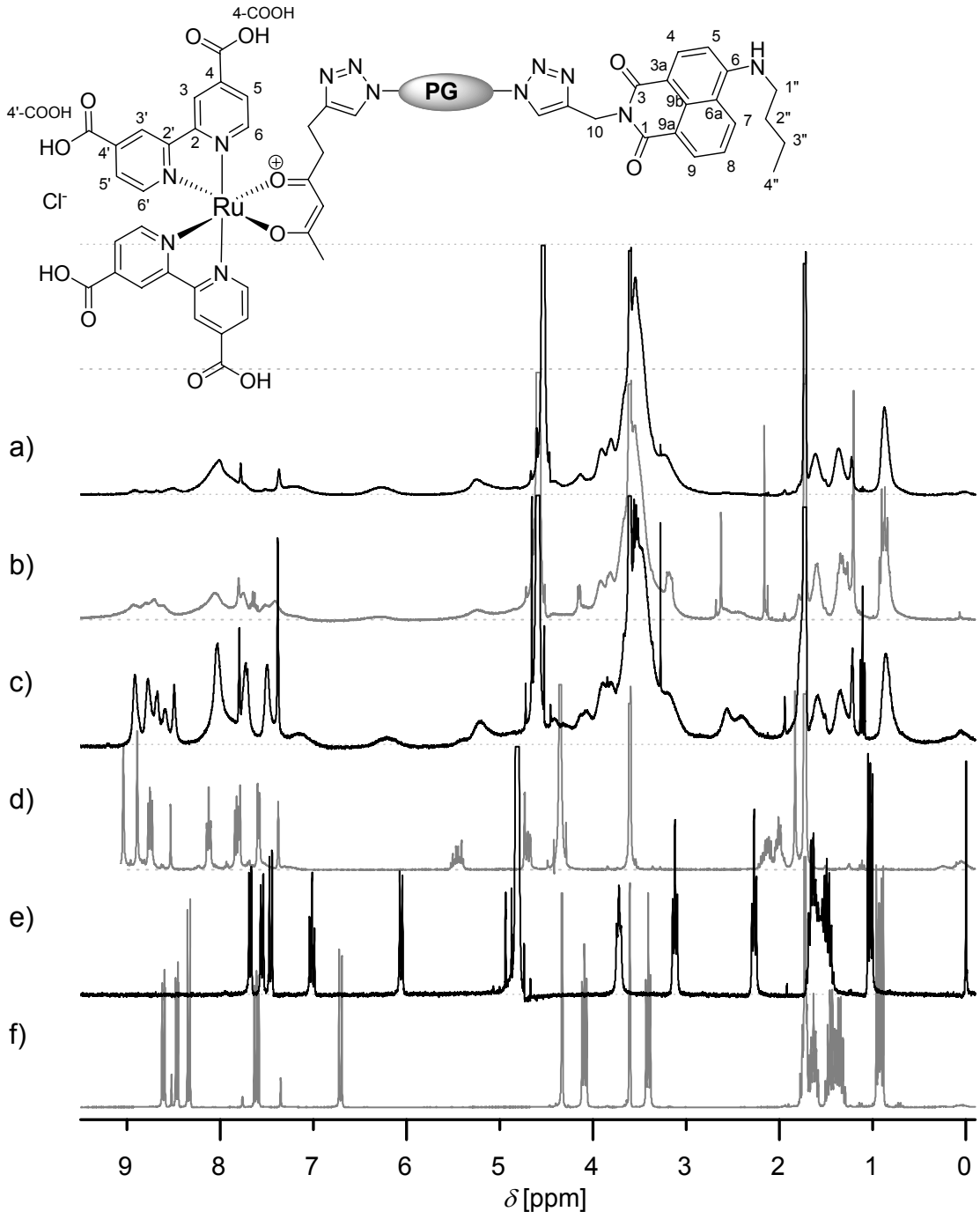

Figure 30. ^{1}H NMR-spectra of D-A-PG-N_3 derivatives that were soluble without the necessity of TBA-OH and respective model compounds. a) $D_{8.6}$-$A_{3\%}$-PG-$N_{3,\,30\%}$ (**66b**) in THF-d_8:D_2O:py-d_5 (11:7:1); b) $D_{0.8}$-$A_{5\%}$-PG-$N_{3,30\%}$ (**67c**) in THF-d_8:D_2O:py-d_5 (9:7:1); c) D_1-$A_{(20\%)}$-PG-$N_{3,\,40\%}$ (**64**) in THF-d_8:D_2O:py-d_5 (9:3:1); d) [Ru(dcbpy)$_2$allyl-acac]Cl (**57**) in THF-d_8:D_2O:py-d_5 (9:3:1); e) 4-Carboxybutyl butyl fluorol (**32**) (ca. 7 mM) in alkaline D_2O; f) Fluorol 7GA (**15**) in THF-d_8:D_2O:py-d_5 (9:3:1).

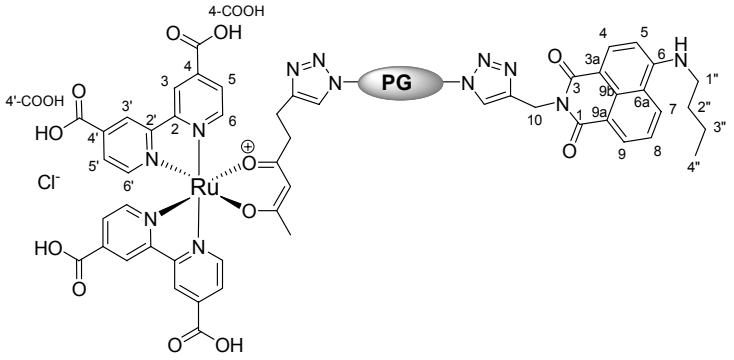

Table 16. Assignment of ^{1}H NMR resonances of D-A-PG-N_3 derivatives.

Entry	Region	Assignment	Reason
1	8.99 – 8.92	3-bpy-H	good agreement with model compound
2	8.84 – 8.79	3'-bpy-H	
3	8.71 – 8.65	6-bpy-H	
4	8.3 – 7.4	remaining signals of aromatic protons incl. triazole-H	
5	7.3 – 6.9	8-H	pronounced upfield shift compared to model compound due to chance in chemical environment *via* click coulpling
6	6.4 – 6.1	5-H	
7	5.5 – 4.9	10-CH_2, N-H and/or C=O-CH=C-O^-	good agreement with model compounds
8	4.4 – 2.9	1"-CH_2, PG-backbone, N-CH_2 of TBA^+	good agreement with model compounds
9	2.65 – 2.10	CH_2CH_2-linker between Ru-complex and triazole	in analogy to PG functionalized exclusively with acceptor units
10	1.7 – 1.5	2"-CH_2 + TBA^+	good agreement with model compound **15**
11	1.5 – 1.2	3"-CH_2 + TBA^+	
12	0.95 – 0.65	4"-CH_3 + TBA^+	

Table 17. Intensities from ^{1}H NMR characterization of selected D-A-PG-N_3 derivatives, loadings α_{Donor}, α_{Ru} and the donor acceptor ratio z_{DA} calculated thereof (see section 9.1.3 in the appendix on page 165 for details). Furthermore, z_{DA} as determined from UV-Vis spectra is shown in the last column. The samples are sorted with increasing $z_{DA,\ UV\text{-}Vis}$.

Entry	Polymer	^{1}H NMR			UV-Vis
		α_{Donor}	α_{Ru}	$z_{DA,\ HNMR}$	$z_{DA,\ UV\text{-}Vis}$
1	$D_{0.8}$-$A_{5\%}$-PG-$N_{3,\ 30\%}$ **67c**	6%	10%	0.56	0.8
2	D_1-$A_{(20\%)}$-PG-$N_{3,\ 40\%}$ **64**	4%	15%	0.26	1.0
3	$D_{3.7}$-$A_{8\%}$-PG-$N_{3,\ 60\%}$ **67g**	47%	9%	5.3	3.7
4	D_5-$A_{(10\%)}$-PG-$N_{3,\ 100\%}$ **65a**	65%	20%	3.2	5.0
5	D_7-$A_{(10\%)}$-*l*PG-$N_{3,\ 85\%}$ **65b**	113%	18%	6.4	7.0
6	$D_{8.6}$-$A_{3\%}$-PG-$N_{3,\ 30\%}$ **67b**	14%	1%	10	8.6

As a result, it is not possible to determine the polymer backbone's signal intensity with high accuracy. This leads in turn to inconclusive results for α_{Ru} and α_{Donor} as determined from ^{1}H NMR spectra (*vide infra*).

Based on the assignments stated in Table 16 the following strategy was applied in order to calculate the degree of loading with the respective chromophores. The signals of the acceptor moiety's 3- and 3'-bpy-Hs as well as the donor moiety's 5-H are the only ones which are clearly resolved and not overlapping with other resonances. Thus, the intensity of these signals was used for the calculation of the loading with the respective chromophore in combination of the intensity of the signal assigned to the PG backbone (see Section 9.1.3 in the Appendix on page 165 for details). Table 17 compiles the values for α_{Ru}, α_{Donor} and z_{DA} as deterined from ^{1}H NMR. These values are in some cases very sensitive to the phase correction applied to the ^{1}H NMR spectrum prior to integration. The agreement in z_{DA} determined from ^{1}H NMR and UV-Vis measurements is only fair, and the value for α_{Donor} in entry 5 is inconclusive. Thus, the values for α_{Ru} and α_{Donor} should not be overrated. The determination of the functionalization from ^{1}H NMR data in analogy to previous work using PG as polymeric support for hydrophobic substrates is not possible with the same precision.[78, 83, 91-93] The values deduced from ^{1}H NMR data in Table 17 should rather be understood as an order of magnitude.

3.6.5.3 ^{13}C NMR Spectra of D-A-PG-N_3

Figure 31b shows a ^{13}C NMR spectrum of $D_{3.7}$-$A_{8\%}$-PG-$N_{3,\ 60\%}$ (**67g**) in py-d_5:D_2O (4:1). 14000 scans were applied to the measurement of this spectrum. Under these conditions spectra with good signal to noise ratios are generally achieved. The noise in the spectrum displayed in Figure 31b was reduced using line broadening and a reduced number of points from the FID. This spectrum clearly reveals signals that are typical for the polymer backbone and the donor unit, however, the signals of the acceptor are not clearly resolved (see also Figure 31a and c for comparison with **45** and **66d**).

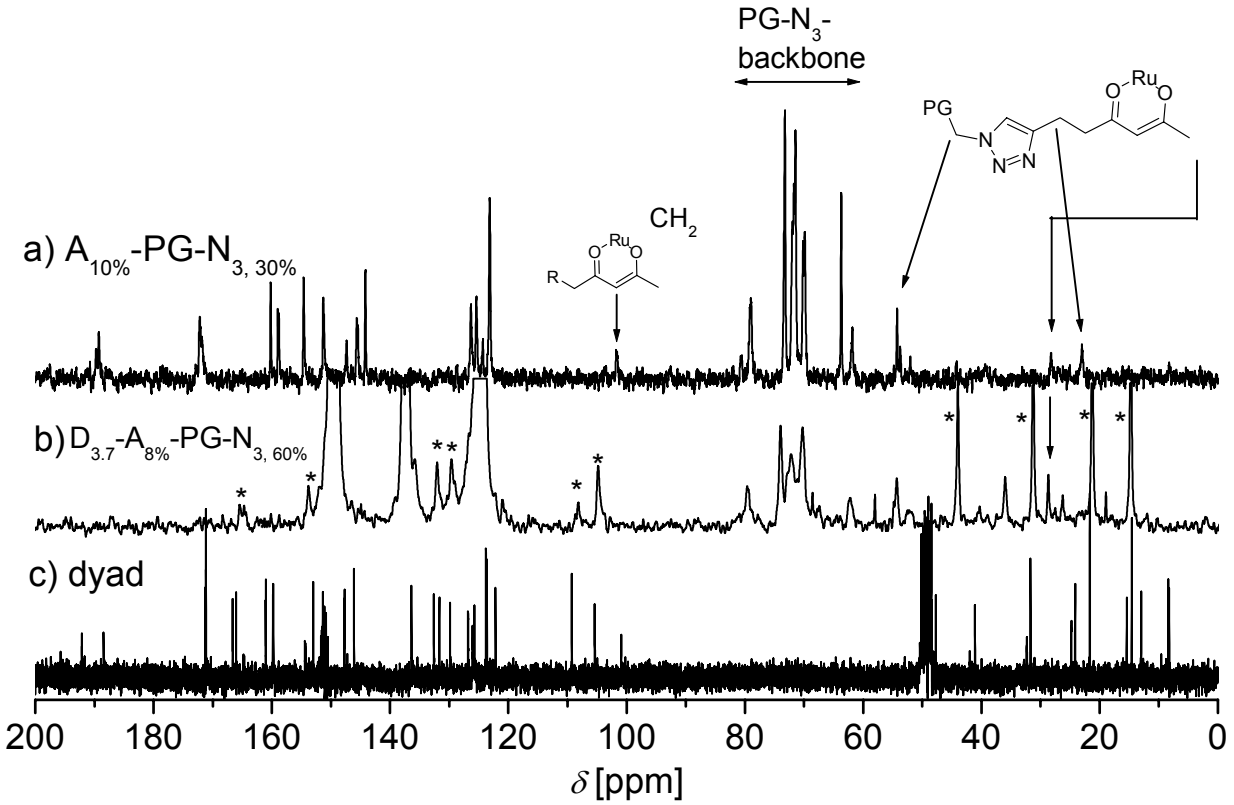

Figure 31. ^{13}C NMR spectra (75 MHz) of a) $A_{10\%}$-PG-$N_{3,\ 30\%}$, in D_2O/NaOD, b) $D_{3.7}$-$A_{8\%}$-PG-N_3 [45 mg in 0.7 ml py-d_5:D_2O (4:1), sum of a regular spectrum with 4000 scans and a DEPT spectrum with 10000 scans], the signals designated with an asterix in spectrum b) are characteristic for the donor unit. c) Dyad **45** in MeOD/NaOD.

3.6.6 D-A-PG-N_3 Conclusion

In conclusion, the syntheses described in Section 3.6 led to a series of donor acceptor functionalized polymers revealing a range of chromophore densities and ratios. The control of the molecular parameters α_{Ru}, α_{Donor} and z_{DA} *via* the stoichiometry of the reaction mixture was achieved in some cases, e.g., **64**, **67b**. However, in most cases the control was limited. Using one single solvent suitable for all reagents, namely, benzyl alcohol as supposed to a solvent mixture gave promising results towards an enhanced control over the molecular parameters *via* the reaction stoichiometry (Table 13). This procedure requires further optimization with respect to purification of the resulting polymers, e.g., by using different solvent mixtures for the column chromatography on Sephadex LH20. Furthermore, the compound's polarities and thereby solubilities were determined by α_{N3}. If α_{N3} was low, it was possible to purify the respective D-A-PG-N_3 derivatives in an alkaline aqueous solution (polymers **64** and **67**).[94] Otherwise mixtures of organic solvents and water with TBA-OH had to be used (polymers **65**). NMR measurements of samples with D-A-PG-N_3 derivatives gave spectra with a low signal to noise ratio and undefined baselines making the precise calculation of α_{Ru} and α_{Donor} impossible. The structure of the D-A-PG-N_3 derivatives was verified by the following two facts: (i) The precipitation of the reaction product from the reaction mixture and subsequent purification of the precipitate using column chromatography led to a product clearly showing the polymer backbone as well as donor *and* acceptor units in ^{1}H NMR and UV-Vis spectra and (ii) the shift of the signal assigned to the 5-H on the donor from δ = 6.8 to 6.2 ppm upon its immobilization to A-PG-N_3 is a clear evidence for the donor unit being forced into the polar vicinity of the $[Ru(dcbpy)_2acac]^+$ groups by the covalent attachement to the azide groups.

The series of polymers synthesized according to Scheme 14 encompassed compounds with donor acceptor ratios between zero and 8.6 and a variety of chromophore densities. The D-A-PG-N_3 derivatives **64**, **65a**, **65b**, **67b**, **67c**, and **67g** as well as $A_{29\%}$-PG-$N_{3,\ 40\%}$ (**66f**) were further tested towards their behavior as polymeric energy transfer sensitizers in the DSC. This work is described in Chapter 5.

4 Photophysical Behavior of Polymeric Fluorol Derivetives

In nature the enhancement of the light absorption cross section of the photosynthetic reaction center is achieved by the light harvesting complexes I and II, which basically represent an arrangement of specific chromophores.[32] This arrangement allows the funneling of excitonic energy taken up *via* light absorption to the reaction center by a multistep process consisting in energy migration, which is an energy hopping step within identical chromophores, and energy transfer, which is an energy hopping step within two different chromophores. In order to determine whether energy migration would contribute to light harvesting in the DSC, the series of D-Allyl-PG derivatives **48** was studied by photophysical methods in more detail.[95-97] The results of these studies are presented in this chapter. In analogy to similar studies with different chromophores immobilized to polymers[95] and dendrimers, e.g., porphyrin-[96] and perylene-decorated[98] structures, the photophysical experiments consisted in the measurement of absorption and emission spectra as well as in the characterization of the fluorescence lifetime and anisotropy decay *via* single photon counting experiments.[28] In these studies the key criteria for the proof of energy migration in respective artificial chromophore assemblies was a significant decrease in the anisotropy decay time ϕ.[96, 98] In this work the above-mentioned measurements were carried out with D-Allyl-PG derivatives that had a loading with the energy donor of 0.3, 3, 24 and 63% (**48a - d** see Chapter 3.4.2) in THF solution at room temperature. Fluorol 7GA (**15**) was used as monomeric model compound. In the following the results of steady state and time resolved measurements are presented and discussed. The characteristic photophysical properties of these of polymers are summarized in Table 18.

4.1 Steady State Measurements

Figure 32 shows the absorption and emission spectra of Fluorol 7GA **15** and polymers **48a - d** with different α_{Donor}. From Figure 32a it becomes obvious that the support of the chromophore to the polymer and α_{Donor} have only a minor influence on the absorption properties. The absorption maximum of the polymers increases from $\lambda_{abs,\,max}$ = 429 to 431 nm with an increasing α_{Donor}. In analogy to the latter behavior, the emission maximum changes very moderately from $\lambda_{exc,\,max}$ = 500 to 502 nm on enhancing α_{Donor} from 0.3 – 24%. The polymer $D_{63\%}$-Allyl-PG, however, reveals an emission maximum at $\lambda_{exc,\,max}$ = 515 nm. Figure

32b shows the fluorescence intensity for different α_{Donor}. This figure clearly reveals that the fluorescence intensity decreases (i) by the support of the chromophoric unit to the polymer and (ii) by an increase in α_{Donor}. The fluorescence intensity has been summarized in Table 18 using the ratio $\Phi(\alpha_{\text{Donor}}) \cdot \Phi_0^{-1}$ [$\Phi(\alpha_{\text{Donor}})$ and Φ_0 represents the integral of the fluorescence intensity of $D_{\alpha_{\text{Donor}}}$-Allyl-PG and Fluorol 7GA, respectively].

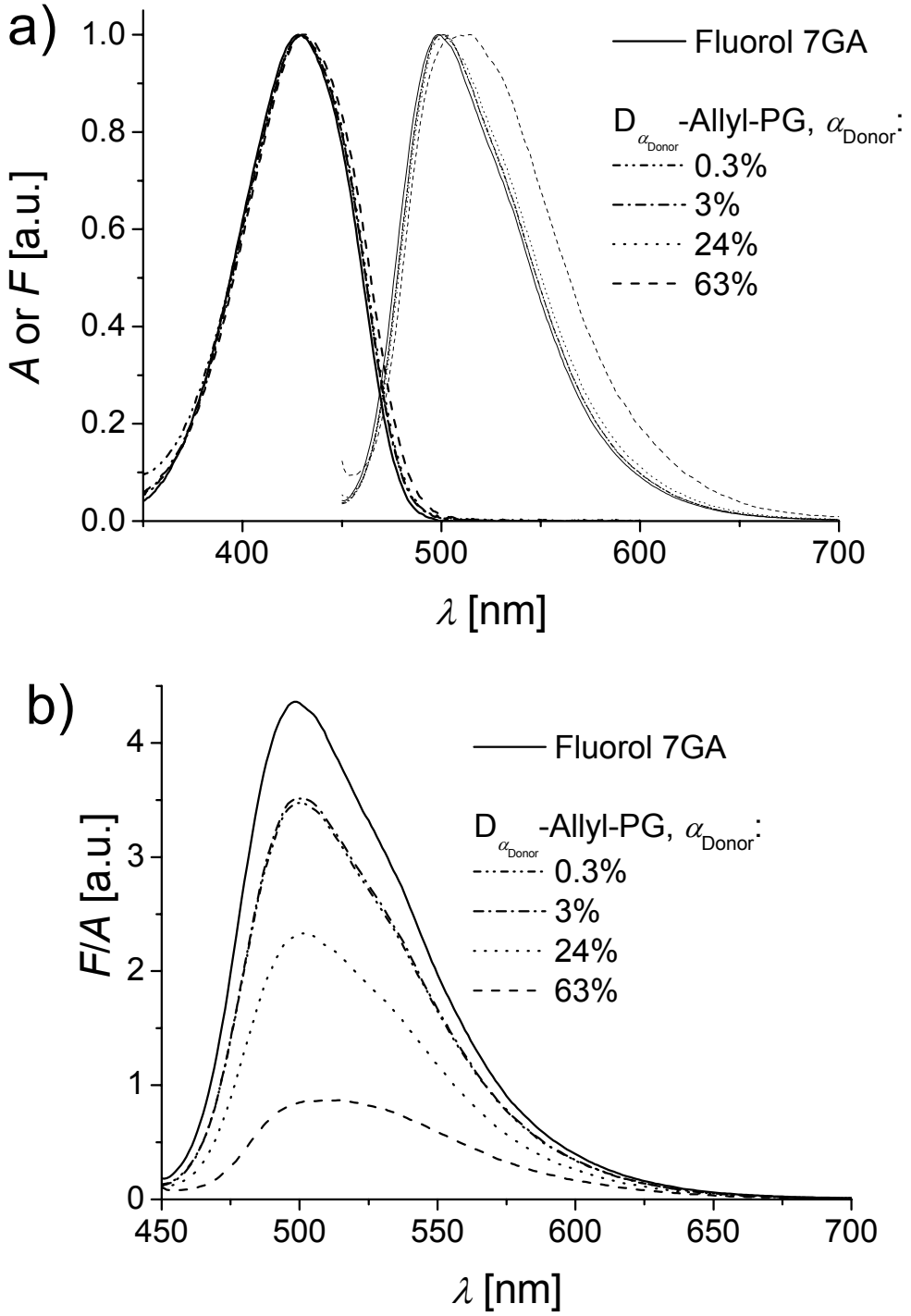

Figure 32. Normalized absorption and emission spectra of the different D-Allyl-PG derivatives and Fluorol 7GA in THF. a) Absorption and emission spectra normalized to unity ($\lambda_{\text{exc.}} = 430$ nm). b) Emission spectra ($\lambda_{\text{exc.}} = 430$ nm) normalized with respect to the amount of absorbed light.

4.2 Time-resolved Measurements

Figure 33 shows the time-resolved luminescence decay of the $D_{\alpha_{Donor}}$-Allyl-PG derivatives and Fluorol 7GA in THF. The characteristics of the luminescence and anisotropy decays *n*, A_i, τ_i and ϕ, respectively, were acquired from experimental data by fitting model exponential decay functions [eqs. (4.1) and (4.3)] to the experimental data *via* a deconvolution software (PicoQuant).

$$I(t) = \sum_{i=1}^{n} A_i e^{-\frac{t}{\tau_i}} \tag{4.1}$$

t	=	time
$I(t)$	=	intensity as a function of time
n	=	number of exponential components
A_i	=	amplitude of the component *i*
τ_i	=	luminescence lifetime of the component *i*

Eq. (4.2) is the definition of fluorescence anisotropy $r(t)$ in terms of the ratio of the fluorescence intensity components $I_{\parallel}(t)$ and $I_{\perp}(t)$ polarized in plane and perpendicular to the polarization of the excitation beam.[95, 96]

$$r(t) = \frac{I_{\parallel}(t) - I_{\perp}(t)}{I_{\parallel}(t) + 2I_{\perp}(t)} \tag{4.2}$$

$$r(t) = R_{INF} + R_1 e^{-\frac{t}{\phi_1}} \tag{4.3}$$

$r(t)$	=	anisotropy as a function of time
R_{INF}	=	residual anisotropy
R_1	=	initial anisotropy
ϕ_1	=	anisotropy decay time

The results of these fits are summarized in Table 18 and in Figure 34. The luminescence of Fluorol 7GA has a monoexponential decay in air-saturated EtOH solution. This behavior is typical for a monomeric fluorophore in solution. In air-saturated THF, however, a short component with a low amplitude (τ = 0.70 ns) had to be added to the model function in order to yield a satisfactory value for χ^2. In analogy to their parent chromophore the D-Allyl-PG derivatives' fluorescence decays have a component with a long ($6.3 < \tau_1 < 9.3$ ns) and short ($0.3 < \tau_3 < 1.0$ ns) lifetime. Additionally, another exponential component with an intermediate lifetime ($2.1 < \tau_2 < 6.0$ ns) is needed to fit the experimental decays appropriately. Thus the fluorescence decays of the polymers feature a 3-exponential decay with lifetimes (termed long for τ_1, intermediate for τ_2, and short for τ_3 in the following) in the same orders of magnitude irrespective of α_{Donor} (see Figure 34a). τ_2 is characteristic for the polymeric species, since the decay function of Fluorol 7GA lacks a component with a similar decay

time. In contrast to the moderate dependence of τ_1, τ_2, and τ_3 on α_{Donor} the amplitudes of the A_1, A_2 and A_3 depend strongly the polymer loading: A_1 decreases and A_3 increases with increasing α_{Donor}. $A_2(\alpha_{Donor})$ is maximal at 24% (see Figure 34b).

Table 18. Photophysical properties of D-Allyl-PG derivatives in air-saturated THF. The values from time-resolved experiments are the average of 3 measurements. The experimental error for A and τ was determined as the standard deviation of one set of measurements. The error in ϕ is the uncertainty given by the deconvolution software.

Entry	1	2	3	4	5
Compound	Fluorol 7GA[a)]	$D_{0.3\%}$-Allyl-PG	$D_{3\%}$-Allyl-PG	$D_{24\%}$-Allyl-PG[b)]	$D_{63\%}$-Allyl-PG
Loading	-	0.3%	3%	24%	63%
$\lambda_{abs,\,max}$ [nm]	428	429	429	430	431
$\lambda_{em,\,max}$ [nm]	499	500	500	502	515
$\Phi(\alpha_{Donor})\Phi_0^{-1}$ [%]	100%	84%	81%	55%	24%
A_1	0.918 ± 0.025	0.597 ± 0.010	0.561 ± 0.047	0.301 ± 0.019	0.062 ± 0.006
τ_1 [ns]	9.264 ± 0.033	9.096 ± 0.043	8.78 ± 0.27	8.025 ± 0.175	6.39 ± 0.15
A_2		0.286 ± 0.014	0.29 ± 0.11	0.538 ± 0.020	0.412 ± 0.005
τ_2 [ns]		4.936 ± 0.090	5.38 ± 0.67	4.137 ± 0.194	2.299 ± 0.046
A_3	0.082 ± 0.025	0.117 ± 0.018	0.151 ± 0.096	0.161 ± 0.012	0.526 ± 0.010
τ_3 [ns]	0.70 ± 0.16	0.499 ± 0.081	0.45 ± 0.25	0.90 ± 0.13	0.621 ± 0.009
χ^2	1.12	1.11	1.04	1.07	1.08
R_1	0.095 ± 0.012	0.252 ± 0.053	0.244 ± 0.071	0.161 ± 0.072	0.140 ± 0.031
ϕ_1 [ns][d)]	0.57 ± 0.11	0.714 ± 0.056	0.716 ± 0.056	0.72 ± 0.12	1.15 ± 0.10
G-factor[e)]	0.91	0.91	0.91	0.89	0.83
χ^2	1.09	1.36	1.29	1.15	1.23

a) This compound showed a monoexponential decay function with $\tau = 9.06$ ns in air-saturated EtOH ($\chi^2 = 1.124$). b) This compound showed a triexponential decay function in air-saturated EtOH ($\tau_1 = 8.00 \pm 0.14$ ns, $A_1 = 0.385 \pm 0.017$; $\tau_2 = 4.05 \pm 0.19$ ns, $A_2 = 0.437 \pm 0.022$; $\tau_3 = 0.82 \pm 0.16$ ns, $A_3 = 0.178 \pm 0.005$). d) Results of three measurements are shown. The error bars represent the uncertainty given by the deconvolution software. e) This factor takes into account differences in detection efficiencies for vertically and horizontally light.[95]

Fitting the anisotropy decay data $r(t)$ was possible with monoexponential models. The data quality, however, was poor for small t-values and the R_1-values acquired from the fits are therefore not reliable. The relevant result from the anisotropy measurements is that ϕ_1 increases somewhat *via* coupling the chromophore to the Allyl-PG-support (see ϕ_1 for Fluorol

7GA and D-Allyl-PG in the range α_{Donor} = 0.3 – 24%), however, for α_{Donor} = 63% a significant increase in ϕ_1 was observed with respect to lower α_{Donor} values (Figure 34c).

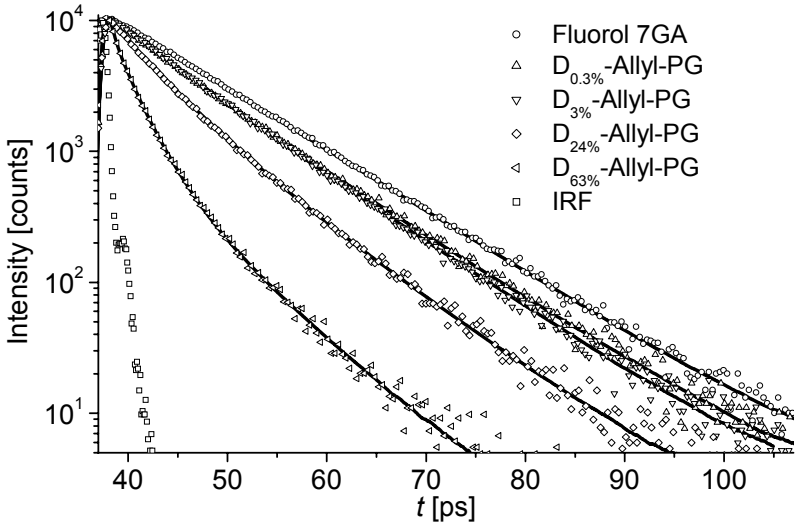

Figure 33. Semilogarithmic plot of the time-resolved photoluminescence decay of D-Allyl-PG derivatives and Fluorol 7GA in air-saturated THF and the instrument response function, IRF (symbols). The respective model function fitting the experimental data best is shown as solid black line. The parameters that were used to fit the function are summarized in Table 18.

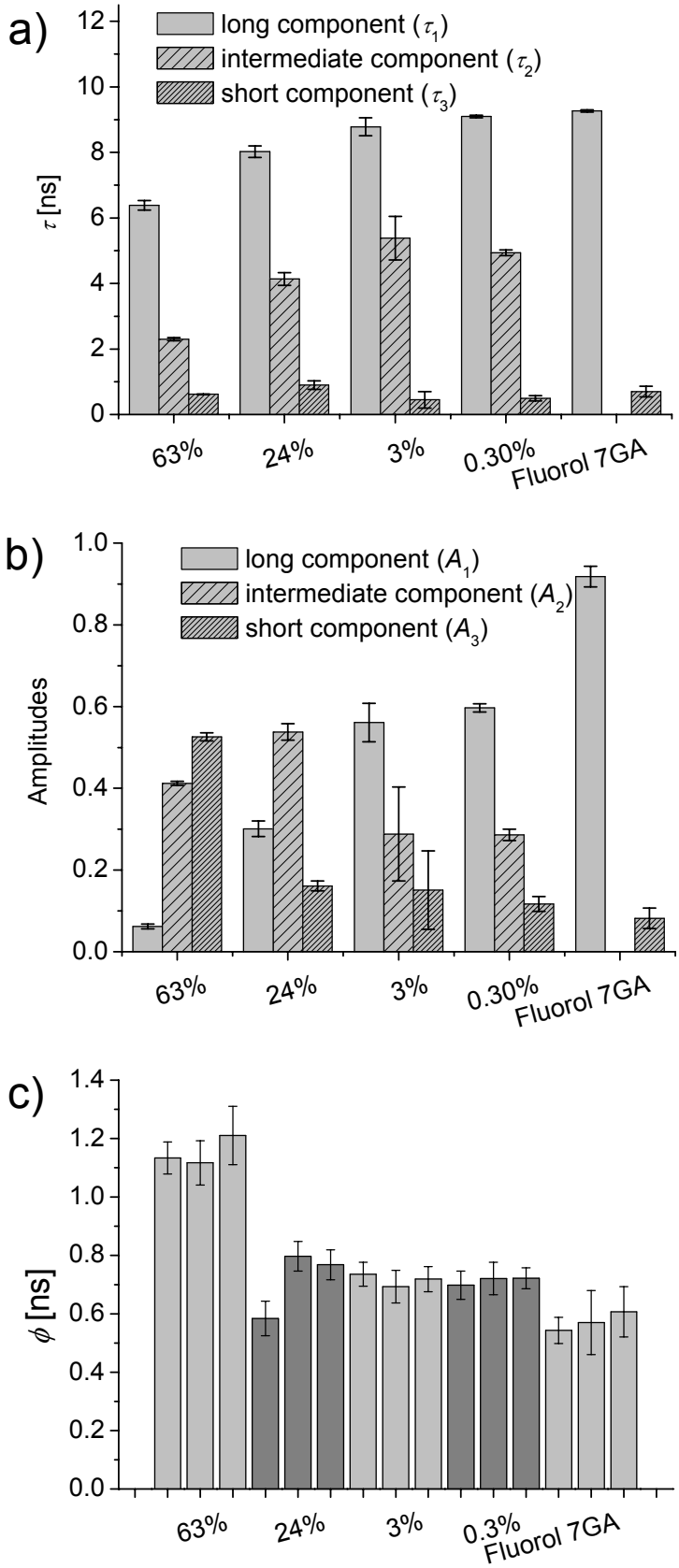

Figure 34. Graphical representation of the photophysical data of **48a - d** and **15** from Table 18 as column diagrams: a) Luminescence decay times $\tau_1 - \tau_3$, and b) their respective amplitudes $A_1 - A_3$. c) Anisotropy decay times ϕ (results of individual measurements).

4.3 Discussion

In the following, the key results of the individual photophysical characterization methods are summarized and associated. The absorption maximum for D-Allyl-PG derivatives and the monomolecular model compound Fluorol 7GA is nearly identical within this series, which is consistent with the chromophoric units being in a similar chemical environment in the ground state. The emission intensity and the other photophysical characteristics of the $D_{0.3\%}$-Allyl-PG and $D_{3\%}$-Allyl-PG is identical within the experimental error. This is consistent with the fact that these derivatives are a mixture of unfunctionalized Allyl-PG molecules that are photophysically inactive and D-Allyl-PG molecules functionalized with 1 – 2 chromophore moieties per polymer molecule in different ratios. The drop in fluorescence intensity upon immobilization of the chromophoric moiety to the polymer is in analogy to the typical behavior of fluorophores being immobilized to biomacromolecules. The latter also frequently leads to a drop in fluorescence intensity.[28][99] The further drop in fluorescence intensity for $\alpha_{Donor} > 3\%$ is consistent with concentration quenching on a microscopic level. Assuming an identical extinction coefficient the absolute chromophore concentration within the samples used for photophysical characterization are identical, however, the spatial distribution of the latter units within the solution, i.e., concentration of chromophore within the domain of a polymer molecule in solution, largely depends on α_{Donor}. An increasing α_{Donor} leads to an increasing microscopic chromophore concentration that in turn causes enhanced concentration quenching[100] and thus a decreasing emission intensity.

The fact that the fluorescence lifetime decay for Fluorol 7GA in EtOH is monoexponential is typical for solutions of diluted fluorophores. The reason for the appearance of the additional component in THF is unclear. One possibility would be the occurrence of an additional quenching mechanism based on a second order reaction, e.g., quenching by oxygen, proceeding in this solvent. The additional exponential component with an intermediate lifetime (τ_2) and slight increase in ϕ arising from the immobilization of the fluorol unit to the Allyl-PG is in consistence with the chromophore moieties having an additional decay pathway mediated *via* constraints in rotational diffusion by the covalent link to the polymer. The slight changes in τ for the individual components might be rationalized by changes in the molar mass of the chromophoric units as a function of α_{Donor}.[101] The rather drastic changes on A_1 and A_3 upon increasing α_{Donor} are in consistence with the molecular processes that are responsible for τ_3 which involving a second order reaction between the

chromophoric units, e.g., concentration quenching. The latter becomes predominantly more relevant with increasing α_{Donor}.

The motivation for the detailed photophysical characterization of the D-Allyl-PG derivatives was the question whether energy migration could contribute to light harvesting in the DSC. Based on the results presented in Sections 4.1 and 4.2 it turns out that energy migration does not take place in these polymers. The key result supporting this fact is the increase in ϕ_1 with increasing α_{Donor}, which stands in contrast to the behavior of chromophore-decorated dendrimers capable of performing energy migration. In such systems ϕ is typically decreased with respect to monomolecular model chromophores. The increased value for ϕ observed for $\alpha_{Donor} = 63\%$ supports the fact that the rotational diffusion is impeded and that no energy migration takes place.

In conclusion, the major influence of the increasing α_{Donor} on the D-Allyl-PG derivatives' photophysical properties are (i) drop in fluorescence intensity, (ii) occurrence of an additional exponential component in the fluorescence decay function, (iii) shifts in the weight of long and short components of the fluorescence decay function, (iv) shifts in τ, notably τ_1, (v) the shift in $\lambda_{em.,\,max}$, and (vi) increase in ϕ. Hypothetic mechanisms accounting for these observations are (i) the immobilization leading to a different behavior in rotational diffusion, an additional deactivation pathway of the excited state and a decrease in τ resulting from the alteration of the molecular mass of the chromophoric units, (ii) enhanced concentration quenching with increasing α_{Donor}, and (iii) contributions from excimer emission for $\alpha_{Donor} = 63\%$. Since an increasing instead of a decreasing ϕ was observed with increasing α_{Donor}, energy migration in D-Allyl-PGs may be ruled out. Thus only direct energy transfer from donor to acceptor contributes to current generation in the DSC.

5 Characterization of Donor Acceptor Systems in the DSC

The main goal of this work is to demonstrate that the photons, which are absorbed by the energy donor moiety, also contribute to current generation within the dye sensitized solar cell. Master plates, which comprised of 5 DSC test cells with an active area of 2.5 cm^2 per cell,[102, 103] were used in order to characterize the performance of different donor acceptor systems (Scheme 18). These consisted of (i) a mixture of donor and acceptor moieties coadsorbed onto the TiO_2 electrode, namely carboxybutyl-butyl-fluorol **32** and N719, (ii) donor acceptor dyad **45**, and (iii) donor acceptor polymers.

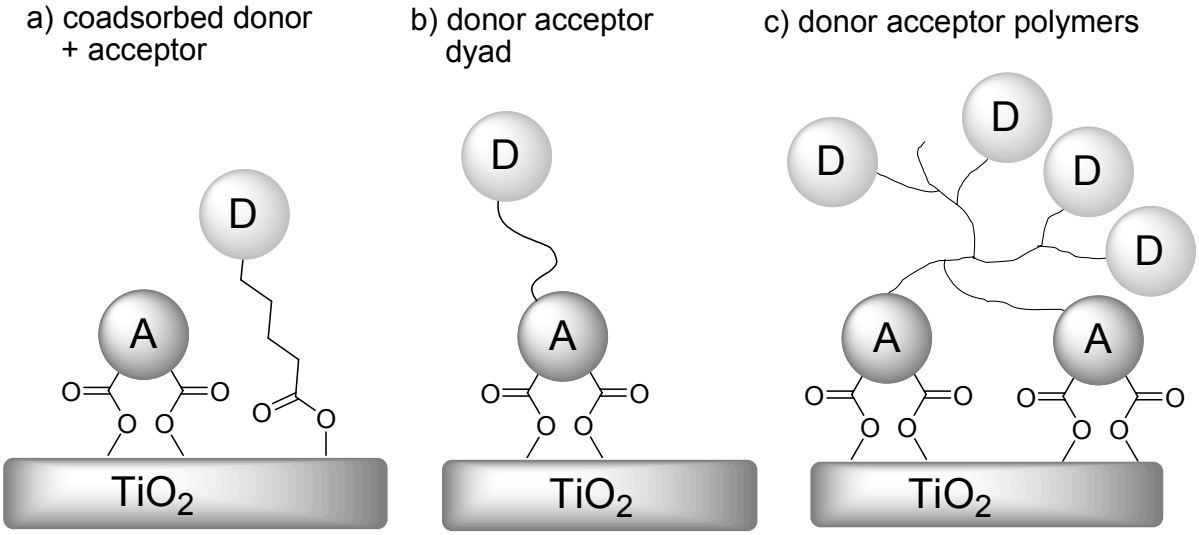

Scheme 18. Different energy transfer systems evaluated in the DSC in this chapter. TiO_2 represents the nanoporous photoelectrode of the DSC. a) Coadsorbed donor and acceptor chromophores. b) Donor acceptor dyad **45**. c) Donor acceptor polymers.

The experimental strategy to deliver the proof that the performance of efficient sensitizers may further be enhanced by resonant energy transfer was carried out *via* the following steps: (i) find a suitable standard cell setup, (ii) characterization of DSCs comprising either donor or acceptor model compounds as sensitizers, (iii) characterization of the different donor acceptor compounds synthesized in this work, and (iv) comparative evaluation of the results. In this chapter the methods of DSC characterization and methodology applied for the estimation of the energy transfer within the device are presented (Section 5.1) prior to the discussion of the experiments and results.

5.1 DSC Characterization Methods Used

The most self-evident characterization technique for solar cells is the IV measurement under illumination yielding the power conversion efficiency. This type of measurement was also carried out with the devices prepared in this work and is briefly described in sections 5.1.1 and 5.1.5. In order to determine whether the photons absorbed by the energy donor moiety from a donor acceptor sensitizer contribute to current generation, however, a detailed knowledge of the devices' spectral properties is necessary. This data allows the wavelength dependant comparison of the light-harvesting efficiency (*LHE*) with the current generated thereof, as determined by the external quantum efficiency (*EQE*). The latter comparison led to the estimation of the energy transfer efficiency (*ETE*) within the device.

5.1.1 Solar Cell Efficiency

The calibrated power conversion efficiencies of the test cells were measured under simulated AM1.5G conditions using a solar simulator with a halogen lamp field. The test cells were cooled during the measurement and a mask was applied in order to minimize scattering of light from the surrounding into the active cell area. From the IV measurements U_{oc}, j_{sc}, FF and η were extracted (see also Section 1.1.2 on page 3).

5.1.2 Light Harvesting Efficiency

The light harvesting efficiency used here is the percentage of incident light that is absorbed by the sensitizer. The determination of the cells' $LHE(\lambda)$ was based on transmission measurements of the stained ($T_{stained}$) and unstained ($T_{electrolyte}$) transparent devices. A DSC that was assembled identically to the test cells containing no sensitizer was used as a reference. The light harvesting efficiency [$LHE(\lambda)$] was calculated using the expression (5.1).

$$LHE(\lambda) = 1 - \frac{T_{stained}(\lambda)}{T_{electrolyte}(\lambda)} \tag{5.1}$$

The cell transmission was measured by means of an UV-Vis spectrometer in standard setup. The different layers in the cell were not perfectly planar and the positioning of the cell to the light beam was not necessarily perfectly perpendicular. These facts resulted in some transmission measurements revealing artefacts that were ascribed to interference at thin layers as well as the transmission in the red and IR part of the spectrum revealing slightly different

values. The correction methodology applied to enhance the transmission data is described in the experimental part (Section 8.4.2). Thus the values for *T* used for the calculation of *LHE* were averaged at each wavelength over different measurements.

5.1.3 External Quantum Efficiency

The external quantum efficiency $EQE(\lambda)$ is defined as the ratio between collected electrons and incident photons [eq. (5.2)], and is sometimes referred to as incident-photon-to-current-efficiency (IPCE).[1]

$$EQE = \frac{\text{number of collected electrons}}{\text{number of incident photons}} \tag{5.2}$$

The *EQE* of the test cells was measured by illuminating the test cell with bias light of an intensity comparable to the one under AM1.5G conditions. Monochromatic light was chopped with a frequency of around 15 Hz and the *EQE* at the respective wavelength was measured *via* a lock-in amplifier. In order to minimize artifacts resulting from high recombination at low light intensities and the lag between start of illumination and the respective current output, the bias light was chosen to be intensive while the chopping frequency was chosen to be as low as possible.[8, 104]

As mentioned in the introduction the external quantum efficiency at a specific wavelength is proportional to the light harvesting efficiency, the proportionality factor being the product of the injection and collection efficiencies. For brevity $\phi_{inj} \cdot \eta_{coll}$ in eq. (1.11) will be summarized as *k* in the following [eq. (5.3)].[8]

$$EQE(\lambda) = k \cdot LHE(\lambda) \tag{5.3}$$

k was estimated in this work by normalizing *EQE* so that the plot of EQE_{exp} fits with *LHE*. The respective normalization factor then corresponds to k^{-1} ($k = EQE \cdot LHE^{-1}$).

5.1.4 Energy Transfer Efficiency from the Spectral Properties of a DSC

The proportionality between *LHE* and *EQE* described in eq. (5.3) is valid for monomolecular sensitizers. In case of quantitative energy transfer from the donor to the acceptor chromophore, eq. (5.3) should also be valid for donor acceptor systems as sensitizer, notably in the wavelength area, where the donor chromophore adds significantly to *LHE*. However, if the energy transfer does not proceed to completion, light absorption of the donor does not contribute to the photocurrent to the same extent as light absorption by the acceptor. Simula-

ted *LHE* and *EQE* spectra for the different situations described above are displayed in Figure 35:[105] For an energy transfer efficiency (*ETE*) of unity *LHE* equals *EQE*. For *ETE* < 1 *EQE* is below *LHE* in the wavelength range of donor absorption, e.g., *ETE* = 80%. For very low *ETE*, e.g., *ETE* = 0% the resulting *EQE* of such a donor acceptor sensitized device would actually be below the *EQE* of a device exclusively sensitized with the respective acceptor. These examples show that the comparison of *LHE* and *EQE* data should allow the estimation of the energy transfer efficiency within the device.

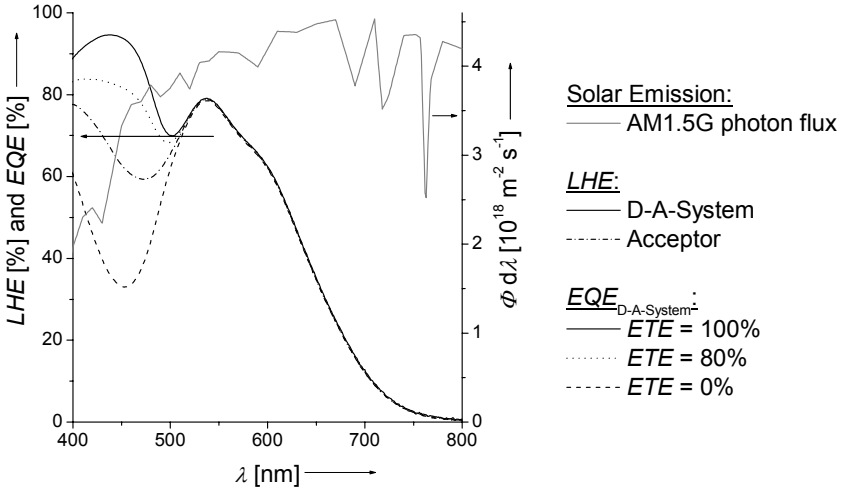

Figure 35. Simulated $LHE(\lambda)$ for DSCs stained with a donor acceptor sensitizer and a respective acceptor-only device and simulated $EQE(\lambda)$ for different energy transfer efficiencies (*ETE*). *The curves* $LHE_{\text{D-A-System}}$ *and* $EQE_{\text{D-A-System, }ETE = 100\%}$ *are identical.*

Thus a modified expression between *EQE* and *LHE* applicable to donor acceptor sensitizers was derived. The most important assumptions of this derivation are presented in the following (the details are in Section 9.2 of the Appendix). The energy transfer efficiency used in this work is defined as the fraction between the number of acceptor excitation events (and in turn electron injection events) due to resonant energy transfer (N_{RET}) and the number of photons that are absorbed by the donor [$N_{h\nu,\text{ Donor}}$, see eq. (5.4)].

$$ETE = \frac{N_{\text{RET}}}{N_{h\nu,\text{ Donor}}} \tag{5.4}$$

In order to get an approximate value for the *ETE*, $EQE(\lambda)$-functions were calculated based on the absorption spectra $A_{\text{D-A-System}}(\lambda)$ and $A_{\text{Acceptor}}(\lambda)$, as they prevail in the device. The latter were derived from $LHE(\lambda)$ of the respective devices stained with the donor acceptor sensitizer and acceptor, respectively, according to eq. (5.5).

$$A(\lambda) = -\log[1 - LHE(\lambda)] \tag{5.5}$$

In addition to eq. (5.3) the following assumptions were made for the simulation of $EQE_{\text{D-A-System}}$ as a function of *ETE*:

(i) $EQE_{\text{D-A-System}}$ is the sum of the *EQE* of the chromophoric units:

$$EQE_{\text{D-A-System}} = EQE_{\text{Donor}} + EQE_{\text{Acceptor}} \tag{5.6}$$

(ii) In analogy to the latter equation, the absorption spectrum of the donor acceptor sensitizer $A_{\text{D-A-System}}$ is the sum of the absorption spectra of the chromophoric units:

$$A_{\text{D-A-System}} = A_{\text{Donor}} + A_{\text{Acceptor}} \tag{5.7}$$

It is important to note that A_{Acceptor} is the absorbance of the acceptor proportion *within* the specific DSC stained with the respective D-A-system (this data was extrapolated from a device stained with the respective energy acceptor sensitizer, see Section 9.4.3 for details).

(iii) The fraction of light of a specific wavelength absorbed by the donor and acceptor, x_{Donor} and x_{Acceptor}, respectively, was assumed to be

$$x_{\text{Donor}}(\lambda) = \frac{A_{\text{Donor}}(\lambda)}{A_{\text{D-A-System}}(\lambda)}; x_{\text{Acceptor}}(\lambda) = \frac{A_{\text{Acceptor}}(\lambda)}{A_{\text{D-A-System}}(\lambda)} \tag{5.8}$$

Based on eqs. (5.3) and (5.6) – (5.8), expression (5.9) was derived allowing the simulation of $EQE_{\text{D-A-System}}$ as a function of *ETE* (see Section 9.2 of the Appendix for details).

$$EQE_{\text{D-A-System, sim}}(ETE) = LHE \cdot \left[\frac{A_{\text{Acceptor}}}{A_{\text{D-A-System}}} + ETE \cdot \left(1 - \frac{A_{\text{Acceptor}}}{A_{\text{D-A-System}}} \right) \right] \tag{5.9}$$

In order to determine the *ETE* for a given donor acceptor device $EQE_{\text{D-A-System, sim}}$ calculated according to eq. (5.9) was fitted to $EQE_{\text{D-A-System, exp}} \cdot k^{-1}$ by variation of the parameter *ETE*.

5.1.5 IV Measurements under Monochromatic Illumination

Some of the devices comprising donor acceptor as well as acceptor-only sensitizers investigated in this work had comparable performances under simulated one sun AM1.5G illumination. The halogen lamps used for the latter purpose had a relatively low photon flux in the blue area of the visible spectrum (see also Figure 35). The details for this behavior will be pointed out in the following sections. It is obvious, however, that the extent of current enhancement *via* RET is proportional to the integral of the product of $EQE(\lambda)$ and emission intensity of the light source [eq. (1.13)]. Thus, a halogen lamp field with very weak emission intensity in the blue, the wavelength where the donor moiety used in this work absorbs, is not the proper system to establish the proof of principle that energy donor acceptor dyes comprising Fluorol 7GA as a donor unit also yield a higher η in addition to a higher j_{sc} (see

Appendix, Section 9.3). The above-mentioned proof of principle would be best verified using light sources with emission maxima that allow selective excitation of the wavelength of maximal donor and acceptor absorption. Thus, in addition to the measurement of the IV characteristics under one sun (AM1.5G), current voltage measurements were carried out using a blue (green) LED array emitting between 465 and 475 nm with a maximum at 470 nm (515 and 535 nm with a maximum at 525 nm) as light sources. These light sources were chosen, since their emission maxima overlap well with the absorption of the lower energy metal-to-ligand charge transfer (MLCT) band of the Ru-complex as well as the π-π^*-absorption of the energy donor, respectively. A considerable fraction of the blue radiation will be absorbed by the donor, whereas the green light will be exclusively absorbed by the acceptor moiety. Thus, the influences originating from the energy transfer on DSC performance are best seen by comparing IV characteristics of different devices under these types of illumination. The calibration of the light source intensity was carried out by adjusting a DSC stained with an acceptor moiety (either N719 or [Ru(dcbpy)$_2$acac]Cl) so that the short circuit current output was identical to the one measured under simulated AM1.5G conditions. The results of these measurements are presented as the ratios $j_{\text{blue}} \cdot j_{\text{green}}^{-1}$ and $P_{\text{blue}} \cdot P_{\text{green}}^{-1}$, respectively. The current ratio shows to what extent the current per Ru-unit is increased *via* energy transfer. In addition, the absolute value for the current generated *via* RET under blue illumination was estimated using eq. (5.10).

$$j_{\text{blue, RET}} = \frac{EQE_{\text{D-A-System, sim}}(ETE, 470\text{ nm}) - EQE_{\text{Acceptor, sim}}(470\text{ nm})}{EQE_{\text{D-A-System, sim}}(ETE, 470\text{ nm})} \cdot j_{\text{blue}} \qquad (5.10)$$

$$EQE_{\text{Acceptor, sim}} = EQE_{\text{D-A-System, sim}}(ETE = 0)$$

The proof that RET is principally suitable for yielding additional current and a better device was established by the selective illumination experiments.

5.2 Design and Assembly of Test DSCs

Today's standard DSC setup for high efficiency cells consists of a relatively thick (10 – 15 µm) nanoporous TiO_2 layer functionalized with one sensitizer absorbing light between 300 and 700 nm. Additionally, a scattering layer is placed on top of the TiO_2 layers. Due to the efficient light-harvesting in and the opaqueness of this type of cells, the spectral characteristics of the sensitizer are not very pronounced: Such cells manage to absorb the incident light in the wavelength range where the sensitizer absorbs (between 300 and 650 nm

for Ru-based sensitizers) nearly quantitatively. Introducing an additional donor chromophore into such cells would not result in current and/or efficiency enhancement. On the other hand, a DSC comprising a TiO_2 photoelectrode that is transparent and thin enough to allow a small but measurable portion of the incident light to be transmitted is the ideal system for studying the influence of additional sensitizers onto DSC performance. Thus thin transparent photoelectrodes (1 print of TiO_2 paste resulting in an electrode thickness of 3.7 μm) which were manufactured by screen printing of a commercial anatase paste were used. If the performance of one monomolecular sensitizer was to be tested, 2 prints of TiO_2 were applied. The front electrode was stained with the sensitizers. EtOH was used as solvent for monomolecular sensitizers. However, for polymeric sensitizers aqueous solutions or THF-water mixtures, which were adjusted to a pH of 6 – 10 using ethylene diamine buffer and tetrabutylammonium hydroxide, were used. It was surprising that staining of the photoelectrode was possible from slightly alkaline solutions containing water since monomolecular sensitizers would desorb from TiO_2 under these conditions. The DSC assembly was completed by laminating front and back electrodes together using a hotmelt foil (Syrlin), filling the cell with electrolyte, and sealing of the holes. The transmission measurements of initially assembled cells did not deliver reliable data for $\lambda < 430$ nm since the DSC transmission was very low in this wavelength range. Reducing the iodine content of the electrolyte by one magnitude led to significantly better results considering the transmission measurements and no obvious drop in DSC performance. Thus in most cases an electrolyte with the reduced iodine concentration was used. In summary, the DSC test cells revealed the following characteristics deviating from the standard setup for high efficiency DSCs: (i) a thin photoelectrode and (ii) a reduced I_2 concentration in the electrolyte. These accordingly assembled devices showed a maximum light harvesting efficiency below 90% and a transmission above 5% at 400 nm. The individual solar cells that were assembled are summarized in Table 19. Different sets of DSCs were tested with the aim of (i) characterizing the behavior of the model chromophores (entries 1 – 3), and studying the energy transfer between (ii) coadsorbed donor and acceptor chromophores (entries 4 and 5), (iii) within the dyad (entries 6 and 7), and (iv) within donor acceptor polymers revealing different donor acceptor ratios (entries 8 – 14). It was attempted that the only parameter varied within a set of cells was the sensitizing dye. This criterion was fulfilled if DSCs with monomolecular sensitizers were assembled, but in case of the polymeric sensitizer, it was not possible to find a universal solvent mixture and pH at which all of them were soluble. Thus, photoelectrodes were stained with polymers in ethylene diamine (en) buffer or mixtures of en-buffer and THF.

The names of the resulting devices are given in the last column of Table 19. In the following the cell names will be represented in boldface. The results of all characterization techniques for the cells assembled for energy transfer studies are summarized in Table 24. Sections of this data are presented in the individual sections of this chapter. The structures of the sensitizers used here are summarized in Scheme 19.

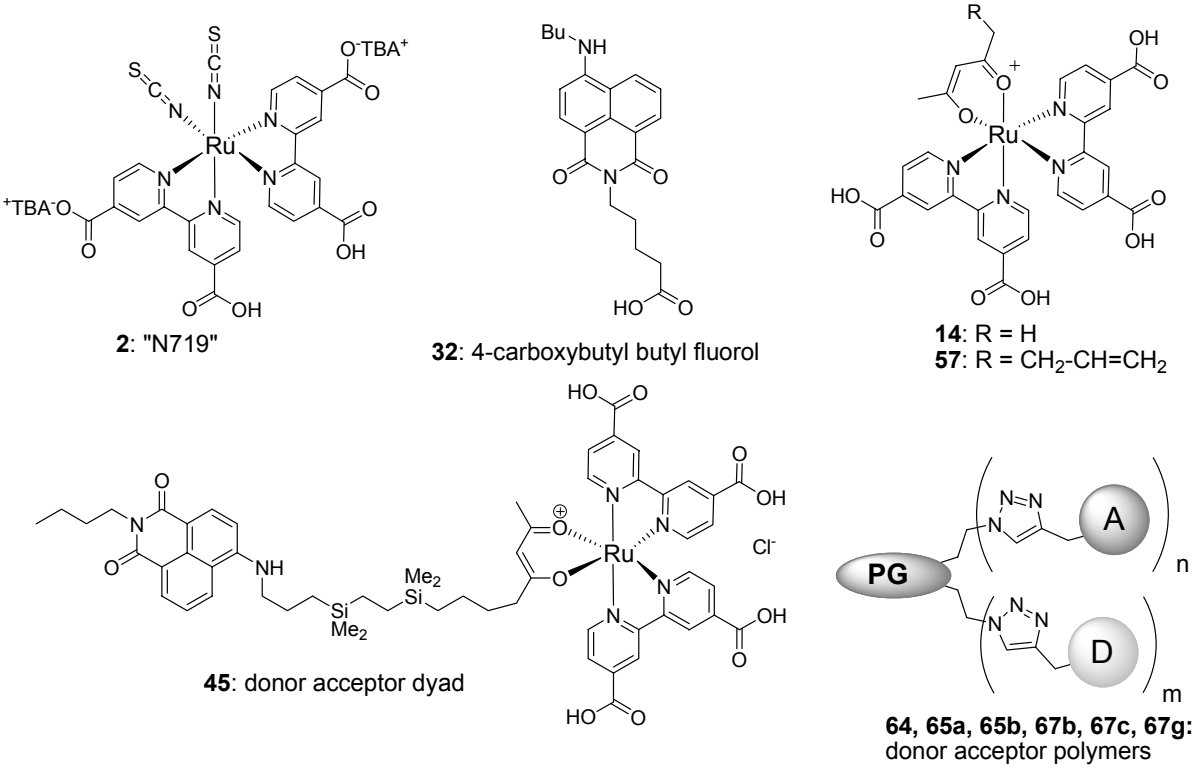

Scheme 19. Structures of the sensitizers investigated here.

Table 19. Overview of the dye solar cells that were assembled in this work. The table gives the type of sensitizer along with its donor acceptor ratio (z_{DA}), the staining conditions (solvent mixture and dye concentration c_{dye}), the number of screen-printing steps with TiO_2 paste applied for the photoelectrode preparation (number of prints, NP), the iodine concentration in the electrolyte (c_{I2}), and the resulting number of functional cells (NC). The last column gives an abbreviation for the specific devices that will be used to refer to the devices in the text.

Aim	Entry	DSC-#	Dye	z_{DA}	Staining Solvent	c_{dye} [mg ml^{-1}]	NP	c_{I_2} a)	NC	Device Name
model chromophores	1	CS 234-1	carboxybutyl-butyl-fluorol (**32**)	∞	EtOH	0.15	2	0.3	5	**D_{thick}**
	2	CS 234-2	[Ru(dcbpy)$_2$acac]Cl (**14**)	0	EtOH	0.16	2	0.3	1	**A_{thick}**
	3	CS 234-3	[Ru(dcbpy)$_2$allyl-acacH]Cl (**57**)	0	EtOH	0.19	2	0.3	5	**$A_{allyl, thick}$**
coadsorbed dyes	4	CS 240-3	N719 (**2**)	0	EtOH	0.92	1	0.03	2	**N719**
	5	CS 240-4	N719 (**2**) + carboxybutyl-butyl-fluorol (**32**)	0.45 b)	EtOH	0.92 0.86	1	0.03	2	**N719+D**
defined molecules	6	CS226-1	[Ru(dcbpy)$_2$acac]Cl (**14**)	0	EtOH	0.28	1	0.3	3	**A**
	7	CS226-2	donor acceptor dyad (**45**)	1.0	EtOH	0.14	1	0.3	3	**Dyad**
polymers in the DSC	8	CS226-3	$A_{29\%}$-PG-$N_{3,\ 30\%}$ (**66f**)	0	en-buffer c) 5.5 mM	0.39	1	0.3	3	**PA**
	9	CS 240-1	$D_{0.8}$-$A_{5\%}$-PG-$N_{3,\ 30\%}$ (**67c**)	0.8	en-buffer c) 4.8 mM	0.20	1	0.03	3	**$PDA_{0.8}$**
	10	CS 226-4	$D_{1.0}$-$A_{(20\%)}$-PG-$N_{3,\ 40\%}$ (**64**)	1.0	en-buffer c) 4.3 mM	0.29	1	0.3	3	**PDA_1**
	11	CS 241	$D_{3.7}$-$A_{8\%}$-PG-$N_{3,\ 60\%}$ (**67g**)	3.7	en-buffer c) 5.5 mM in THF:H_2O 9:1 adjusted to pH = 10 with TBA-OH	0.33	1	0.03	2	**PDA_4**
	12	CS 240-5	$D_{5.0}$-$A_{(10\%)}$-PG-$N_{3.\ 100\%}$ (**65a**)	5.0	en-buffer c) 6.8 mM in THF:H_2O 3:1 adjusted to pH = 8 with TBA-OH	0.19	1	0.03	1	**PDA_5**
	13	CS 240-6	$D_{7.0}$-$A_{(10\%)}$-*l*PG-$N_{3,\ 85\%}$ (**65b**)	7.0	en-buffer c) 6.8 mM in THF:H_2O 3:1	0.19	1	0.03	0	**PDA_7**
	14	CS 240-2	$D_{8.6}$-$A_{3\%}$-PG-$N_{3,\ 30\%}$ (**67b**)	8.6	en-buffer c) 20 mM in THF:H_2O 1:1	0.15	1	0.03	3	**PDA_9**

a) [mol l^{-1}]. b) Determined by fitting a simulated absorption spectrum to the experimental one of the DSC stained with N719 and carboxybutyl-butyl-fluorol assuming ε_{N719} = 13500 l mol^{-1} cm^{-1} and ε_{Donor} = 16000 l mol^{-1} cm^{-1}. c) ethylene diamine in water adjusted to a pH of 6 with HCl.

5.3 Results of DSC Characterization

The results of the different characterization methods described in Section 5.1 acquired with the devices summarized in Table 19 are presented here. Results of the device $\mathbf{D_{thick}}$, $\mathbf{A_{thick}}$ and $\mathbf{A_{Allyl,\ thick}}$ that were stained with the parent chromophores (entries 1 – 3) are shown and discussed in the next section. The results from methods investigating the IV and spectral properties that were obtained with donor acceptor sensitized cells along with cells containing exclusively the acceptor as reference are presented in Table 24 on page 110 and in Sections 5.3.2 and 5.3.3.

5.3.1 Model Chromophores

In order to assess the behavior of donor acceptor systems in the DSC the knowledge of the performance of the individual donor and acceptor chromophores as sensitizers in the DSC is crucial. The latter was the motivation for the assembly of the devices $\mathbf{D_{thick}}$, $\mathbf{A_{thick}}$, and $\mathbf{A_{Allyl,\ thick}}$ comprising carboxybutyl-butyl-fluorol **(32)**, [Ru(dcbpy)$_2$acac]Cl (**14)** and [Ru(dcbpy)$_2$allyl-acac]Cl (**57)** and as sensitizers in the DSC, respectively. **57** served as a model for [Ru(dcbpy)$_2$acac]Cl derivatives revealing a substitution in the α-position of the acac ligand. The IV characteristics of the devices mentioned above are summarized in Table 20.

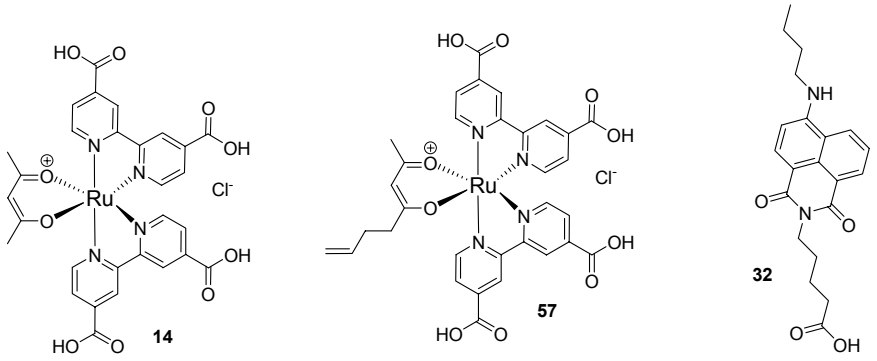

Table 20. IV characteristics of DSCs staine with model chromophores carboxybutyl-butyl-fluorol (**32**), [Ru(dcbpy)$_2$acac]Cl (**14**) and [Ru(dcbpy)$_2$allyl-acac]Cl (**57**).

Entry	Device Name	Dye	cells	U_{oc} [mV]	j_{sc} [mA cm^{-1}]	*FF* [%]	η [%]
1	$\mathbf{D_{thick}}$	**32**	5	379 ± 11	0.056 ± 0.002	51 ± 2	0.0108 ± 0.0004
2	$\mathbf{A_{thick}}$	**14**	1	685	6.1	74	3.1
3	$\mathbf{A_{allyl,\ thick}}$	**57**	5	634 ± 11	6.3 ± 0.3	72 ± 1	2.9 ± 0.1

DSCs featuring the compound carboxybutyl-butyl-fluorol (**D_{thick}**) were characterized in order to address the question whether the donor moiety is able to act as a sensitizer. It was possible to carry out IV measurements with corresponding cells, which showed that the cells are functional and that they reveal an open circuit voltage at around 400 mV but j_{sc} and as a result η was extremely low (Table 20, entry 1). In order to rule out that this extremely low performance was a result of the spectral mismatch between sensitizer absorption and the halogen lamp field of the solar simulator additional IV measurements were carried out under blue illumination (the calibration of light intensity was carried out as described in Section 5.1.5). Changing the illumination from white to blue brought about a 5.8-fold increase in j_{sc} and 8.2-fold increase in P_{max} of **D_{thick}**. Despite this increase the photocurrent represented only 5% of the one measured with **$A_{Allyl, thick}$** under identical illumination. The fact that **D_{thick}** does not produce a significant photocurrent, although a considerable amount of light is absorbed by the sensitizer, is caused by the disability of the aminonaphthalimide moiety to efficiently inject electrons into the nanoporous TiO_2 electrode.

The device efficiency of DSCs stained with [Ru(dcbpy)$_2$acac]Cl and [Ru(dcbpy)$_2$allyl-acac]Cl (devices **A_{thick}** and **$A_{thick, allyl}$**, respectively, Table 20, entries 2 and 3) were assembled in order to test whether the chemical modification on the terminal methyl group of the acac-ligand effectuates the behavior of [Ru(dcbpy)$_2$acac]$^+$ derivatives as sensitizer. This set of devices shows close to identical electrical properties under illumination with simulated AM1.5G light.

In addition to the results mentioned above, 2 entries from Table 24 are also interesting in the present context: The IV results from the devices **A** and **PA** (Table 24, entries 6 and 8) are equally close to identical indicating that supporting the acceptor chromophore to the polyglycerol azide does not interfere significantly with DSC performance.

The sets of devices presented here clearly demonstrate that the chemical modification on the acacH-ligand as carried out in this work does not markedly change the photovoltaic performance of the resulting sensitizer in itself.

5.3.2 Donor Acceptor Systems based on Monomolecular Sensitizers

In the following the results from DSCs characterization of devices that were assembled in order to study the energy transfer within monomolecular sensitizers are presented. These are namely the devices **N719**, **N719+D**, **A**, and **Dyad** (Table 19, entries 4 – 7, respectively). Due to their similarity, these results are presented together.

5.3.2.1 Results

The parameters that were varied within the set of devices mentioned above consisted exclusively of the type of dyes used for the staining step. The IV results are summarized in Table 21. From a comparison of the IV characteristics of both types of DSCs within the set, it is obvious that within the experimental error the efficiency is identical for the device sensitized with the energy acceptor unit or the energy donor acceptor systems. The expected current enhancement under this type of illumination effectuated by the presence of the donor moiety, however, is smaller than the experimental error (see Section 9.3 in the Appendix). Therefore, the IV data presented in Table 21 do not allow the discussion of the effect of the donor moiety.

Table 21. IV characteristics of DSCs stained with **2**, **32**, **14**, and **45**.

Entry	Device	U_{oc} [mV]	j_{sc} [mA cm^{-1}]	FF [%]	η [%]
1	**N719**	676 ± 7	4.1 ± 0.1	70 ± 1	2.0 ± 0.1
2	**N719+D**	666 ± 7	4.1 ± 0.1	70 ± 0	1.9 ± 0.1
3	**A**	654 ± 6	4.9 ± 0.4	73 ± 1	2.3 ± 0.2
4	**Dyad**	690 ± 10	5.0 ± 0.1	73 ± 3	2.5 ± 0.1

In order to determine whether the photons absorbed by the energy donor moieties in devices **N719+D** and **Dyad** contribute to current generation, a detailed knowledge of the spectral properties of the respective DSCs is necessary. Figure 36 summarizes the latter for the devices **N719** and **N719+D** as well as Figure 37 for the devices **A** and **Dyad**. The figures a) on pages 99 and 100 are averaged transmission spectra of several devices and the figures b) on those pages present $LHE(\lambda)$. One important difference in Figure 36a and Figure 37a is the transmission at low wavelengths: The devices comprising N719 as sensitizer were filled with an electrolyte containing 0.03 M iodine, whereas the others contained the 10-fold concentration. As a result, T_{DSC}(400 nm) is between 5 and 15% for the former set of devices allowing the reliable calculation of *LHE* down to short wavelengths. With the latter set of devices the calculation of *LHE* yields very large experimental errors for $\lambda < 430$ nm. The shapes of *LHE* of the donor acceptor systems are similar to that of their respective acceptor-only devices in the range > 550 nm. *LHE*, however, is significantly higher in the range from 400 – 500 nm if the donor moiety was present during the staining step (Figure 36b and Figure

37b). This behavior indicates that the donor group is also present and intact within the device. $LHE_{\mathbf{A}}$ and $LHE_{\mathbf{N719}}$ are somewhat larger than $LHE_{\mathbf{Dyad}}$ and $LHE_{\mathbf{N719+D}}$ for $\lambda > 520$ nm. This fact is consistent with the acceptor content being somewhat reduced by the spatial requirements of the respective donor unit. The figures c) on pages 99 and 100 show typical $EQE(\lambda)$ curves for DSCs stained with the respective acceptor sensitizers and donor acceptor systems.

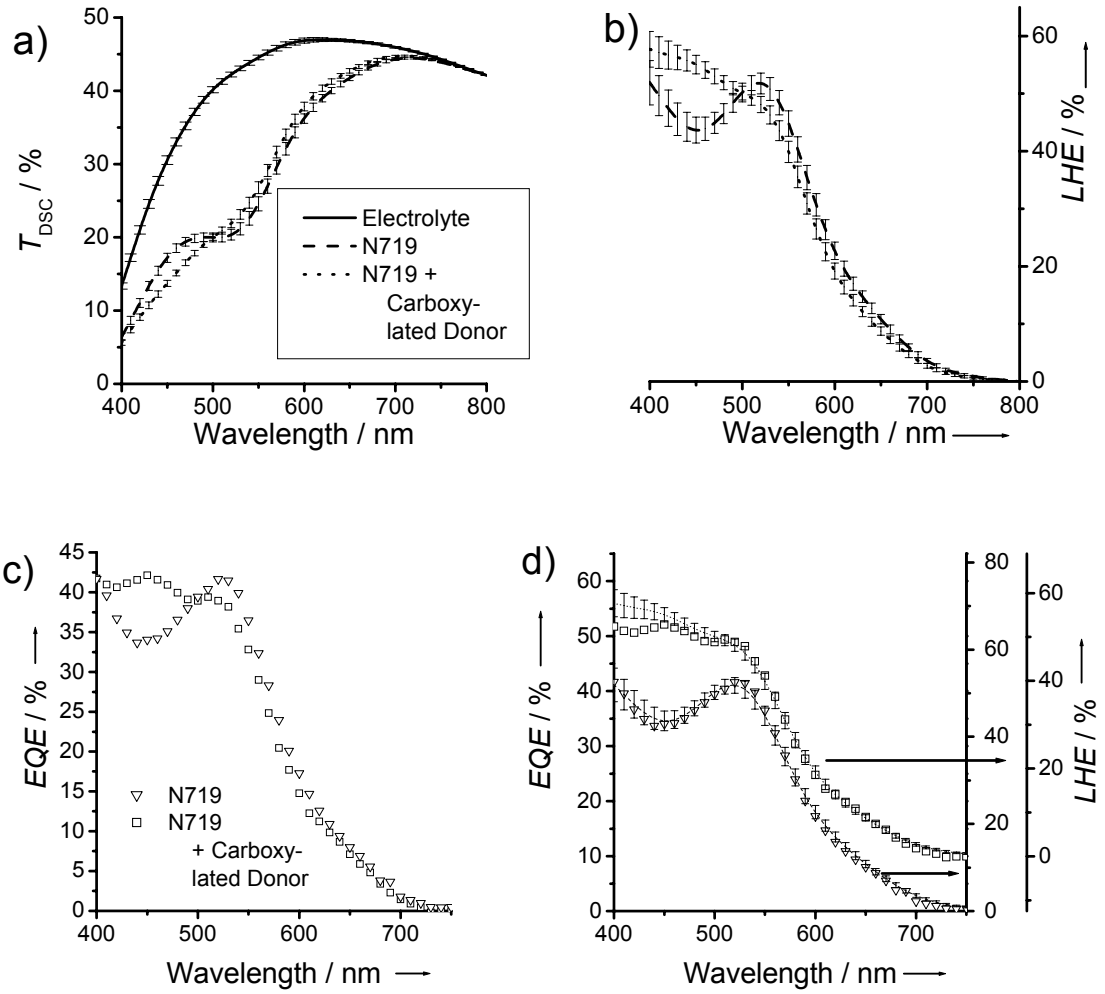

Figure 36. Results of different wavelength dependant characterization techniques applied to the devices **N719** and **N719+D**. a) Transmission as determined *via* an UV-Vis spectrometer in standard setup: **N719** (dashed) and **N719+D** (dotted). The transmission spectrum of unstained DSCs which were filled with electrolyte are presented as well (solid). All the spectra presented here were calculated averaging $T(\lambda)$-values of several cells after normalization to the red edge of the spectrum; the error bar is the standard deviation at each wavelength. b) Light harvesting efficiencies as calculated from the data presented in a). The error bars were calculated via the mean square method using the errors in $T_{\text{electrolyte}}$ and T_{stained}. c) Representative $EQE(\lambda)$-curves for the devices **N719** (▽) and **N719+D** (□), acquired using chopped monochromatic light and bias illumination (ca. 1 sun). d) Diagram superimposing the data presented in b) and c). For clarity an offset of 0.1 units is applied to the EQE(λ)-plot **N719+D**. $LHE(\lambda)$ was superimposed so that the part of the spectrum with $\lambda > 540$ nm overlaps with the EQE(λ)-curves in this spectral range.

The shape of the curve in the range of 520 to 800 nm is nearly identical in each set of measurements. e.g., the *EQE*(λ) curves for **14** and **45** both show maxima at 540 nm and a shoulder at 600 nm.[51] This part of the *EQE* curves is due to light absorption and electron injection of the energy acceptor. Furthermore there are maxima at 410 nm (400 nm) and 450 nm for [Ru(dcbpy)$_2$acac]Cl (N719) and dyad 45 or N719 carboxybutyl-butyl-fluorol mixture as sensitizer, respectively.

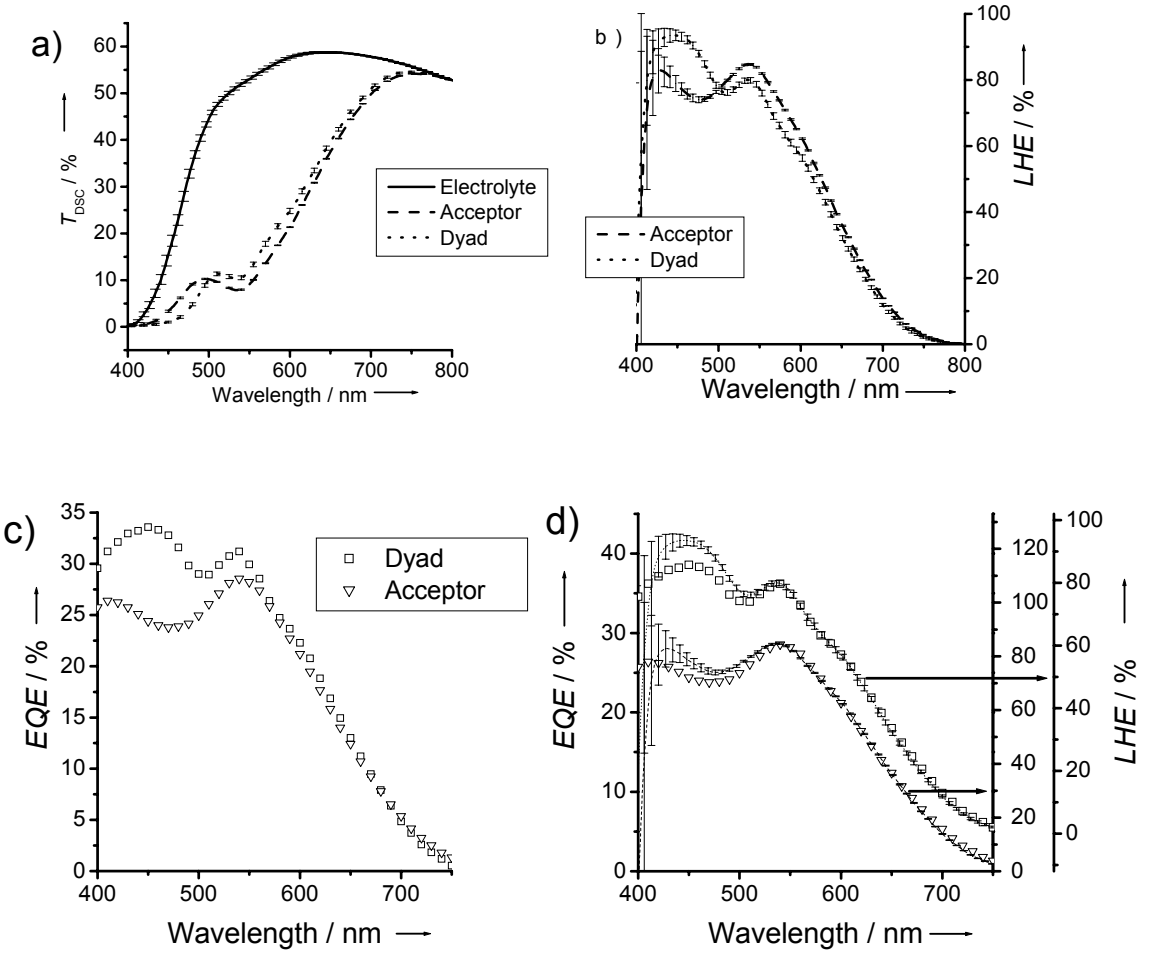

Figure 37. Results of different wavelength dependant characterization techniques applied to the devices **A** and **Dyad**. a) Transmission as determined *via* an UV-Vis spectrometer in standard setup: **A** (dashed) and **Dyad** (dotted). The transmission spectrum of unstained DSCs which were filled with electrolyte are presented as well (solid). All the spectra presented here were calculated averaging $T(\lambda)$-values of several cells after normalization to the red edge of the spectrum; the error bar is the standard deviation at each wavelength. b) Light harvesting efficiencies as calculated from the data presented in a). The error bars were calculated via the mean square method using the errors in $T_{electrolyte}$ and $T_{stained}$. c) Representative *EQE*(λ)-curves for the devices **A** ($\triangledown$) and **Dyad** ($\square$), acquired using chopped monochromatic light and bias illumination (ca. 1 sun). d) Diagram superimposing the data presented in b) and c). For clarity an offset of 0.05 units is applied to the EQE(λ)-plot **Dyad**. *LHE*(λ) was superimposed so that the part of the spectrum with $\lambda > 540$ nm overlaps with the EQE(λ)-curves in this spectral range.

In the case of acceptor-only sensitized devices, the maximum at 410 nm (400 nm) is less intensive, whereas in the devices comprising the D-A-systems, the maxima at 450 nm are significantly more intensive than the ones at around 540 nm. The maxima at 410 nm and 400 nm are consistent with the current generated from the blue MLCT band of the energy acceptor. The maxima at 450 nm, as well as the significantly higher intensity relative to the maxima at 540 nm, are in agreement with generation of current *via* the energy donor moieties. The *EQE* values for the set of measurements are identical within the experimental error for $\lambda > 520$ nm. Since the halogen lamps used for the IV characterization of the devices had a rather low emission intensity in the blue part of the spectrum, the overlapping EQE-curves are in good agreement with the identical j_{sc} as determined under the solar simulator (see Table 21). In addition to the identical curve form between the donor acceptor and acceptor-only devices in the range $\lambda > 550$ nm the figures c) on pages 99 and 100 clearly reveals their strong divergence for $\lambda = 400 - 550$ nm, the wavelength range, in which the energy donor absorbs. Figure 36d and Figure 37d superimpose the data presented in figures b) and c), respectively. This superimposition shows clearly that equation (5.3) is valid for **N719** over the entire spectral range displayed in Figure 36d: An excellent accordance between *LHE* and *EQE* is found for $k = 0.8$. For all further devices discussed in this section the accordance is given if $\lambda > 520$ nm. Below those wavelengths, the overlap of *EQE*- and *LHE*-data is only fair. Possible reasons for these deviations, which are valid for both devices stained with donor acceptor systems and acceptor-only devices, are discussed in further detail in the Appendix (Section 9.4 on page 169). However, the significant divergence between *LHE* and normalized *EQE*-data for the devices **Dyad** and **N719+D** (as judged on the data between 450 nm and 520 nm) are certainly due to incomplete energy transfer from excited donor moieties to the acceptor. Fitting $EQE_{exp} \cdot k^{-1}$ to $EQE_{sim}(ETE)$ according to (5.9) leads to $ETE = 89 \pm 10\%$ and $85 \pm 3\%$ for the devices **N719+D** and **Dyad**, respectively. Table 22 summarizes results from monochromatic illumination experiments. As already suggested by the *EQE* data, this data reveals that the devices stained with the donor acceptor systems are superior to the ones stained with the acceptor only as determined from the ratios $j_{blue} \cdot j_{green}^{-1}$ and $P_{blue} \cdot P_{green}^{-1}$. Under green light, the donor acceptor and acceptor-only devices largely give identical short circuit currents. Under blue illumination, however, j_{sc} is significantly higher for the cells comprising the energy donor moiety.

Table 22. Results from IV measurements under monochromatic illumination.

Entry	Device	$\frac{j_{blue}}{j_{green}}$	$j_{Donor,\ blue}$ [a)] $[mA\ cm^{-2}]$	$\frac{P_{blue}}{P_{green}}$
1	$\mathbf{D_{thick}}$	-	0.35	-
2	**N719**	1.04 ± 0.01 [b)]	-	1.01 ± 0.03 [b)]
3	**N719+D**	1.26 ± 0.01 [b)]	1.5	1.24 ± 0.01 [b)]
4	**A**	1.00 ± 0.01 [c)]	-	0.99 ± 0.02 [c)]
5	**Dyad**	1.24 ± 0.02 [c)]	2.5	1.21 ± 0.04 [c)]

a) calculated according to (5.10). b) Device $\mathbf{A_{Allyl,\ thick}}$ served as reference for light intensity calibration. c) Device **A** served as reference for light intensity calibration.

The same effect is also observed for the maximum output power P_{max}. The results obtained here are consistent with the fact that both types of DSCs have a similar $EQE(\lambda)$ for $\lambda > 520$ nm, but the light absorbed by the donor leads to a $EQE(\lambda < 520\ nm)$ which is higher for **Dyad** and **N719+D** than for **A** and **N719** within this wavelength range. Upon comparing data for η, j_{sc} and *LHE* it is striking that the devices **A** and **Dyad** are about as efficient as devices **N719** and **N719+D** (see Table 24 on page 110) despite the fact that $LHE_{\mathbf{A}}$ nearly doubles $LHE_{\mathbf{N719}}$. This behavior is also reflected in a lower value for *k* for **A** and **Dyad**. The latter fact is consistent with **14** and **45** forming aggregates or multilayers on the nanoporous TiO_2 electrode which leads to a lower injection efficiency (thus a lower *k*).

5.3.2.2 Discussion

The experimental evidence described so far clearly sustains the hypothesis that absorption of the energy donor contributes to current generation, which in turn might lead to a higher efficiency. In the following, the key results of the individual characterization methods are summarized and associated. The *LHE* spectra of devices investigated here (figures b on pages 99 and 100) clearly indicate that the donor chromophore absorbs in a wavelength range, where the acceptor chromophore only absorbs weakly. The introduction of the additional donor chromophre by either coadsorption with (as in device **N719+D**) or covalent coupling to a carboxylated Ru-polypyridine complex (as in device **Dyad**) provided a photoelectrode functionalized with two chromophoric units with a higher overall light absorption cross-section in the wavelength range where the donor absorbs. The spatial demands of the donor

unit, however, leads to a minor decrease in the acceptor content as proven by the slightly lower $LHE(\lambda)$ for $\lambda > 540$ nm with respect to the acceptor-only devices.

Energy transfer between donor and acceptor chromophores in solution is typically characterized by time-resolved fluorescence measurements or by the comparison of absorbtion and excitation spectra.[28] Attempts to carry out analogous experiments with dyad **45** were not successful due to the poor luminescence properties of the acceptor and the effective quenching of donor luminescence as a result of the interchromophoric distance well below the Förster radius. Efficient electron injection of the Ru-complex into TiO_2 is an adequate substitute to acceptor emission in order to detect electronic excitation. Therefore the comparison of $EQE(\lambda)$ and transmission measurements of DSCs comprising donor acceptor (devices **Dyad** and **N719+D**) and respective acceptor-only sensitizers (devices **A** and **N179**) was used as a method for the determination of *ETE*. The relevant EQE-measurement (Figure 38a and b, squares) showed clearly that light absorption by the energy donor in **Dyad** and **N719+D** contributes to current generation. This becomes apparent from the comparison of the $LHE(\lambda)$-spectra with the $EQE(\lambda)$-graphs (figures d on pages 99 and 100). All curves distinctively show the characteristic MLCT-band for the respective acceptor moiety. Furthermore, the curves belonging to **Dyad** and **N719+D** exceed the normalized $EQE(\lambda)$ and $LHE(\lambda)$-values of **A** and **N179** for 400 nm $< \lambda <$ 500 nm, the wavelength interval corresponding to donor absorption. This behavior clearly demonstrates that the higher *LHE* in this interval is converted into output current. Since it was shown that electron injection from the donor moiety can be ruled out (see Section 5.3.1), the gain in *EQE* in this region (relative to the long-wavelength part of the curve) was assigned to resonant energy transfer. In order to determine the extent of RET, simulations of the impact of *ETE* onto the shape of the $EQE_{Dyad}(\lambda)$-function were carried out. Figure 38 also shows the key results of the EQE simulation. In addition to the experimental EQE-data from Figure 36c and Figure 37c, which was normalized by fitting different values for k (resulting in $EQE_{exp.} \cdot k^{-1}$), three simulated curves $EQE_{sim,\, ETE = 0}$, $EQE_{sim,\, ETE = y}$ and $EQE_{sim,\, ETE = 100\%}$ are presented (y = 89% and 85% for **N719+D** and **Dyad**, respectively). These functions are shown as the upper edges of the dark gray and gray areas and as a black line, respectively. $EQE_{sim,\, ETE = 0\%}$ is tantamount to the light harvesting efficiency by the acceptor moiety within the donor acceptor system, while $EQE_{sim,\, ETE = 1}$ is synonymous with its overall light harvesting efficiency ($LHE_{\mathbf{Dyad}}$ and $LHE_{\mathbf{N719+D}}$). The approximation of EQE_{sim} to $EQE_{exp.} \cdot k^{-1}$ by a variation of *ETE* gave good agreement between the experimental and simulated data for $ETE_{\mathbf{N719+D}}$ = 89 % and $ETE_{\mathbf{Dyad}}$ = 85% (see plots of $EQE_{sim,ETE}$ and EQE_{exp}).

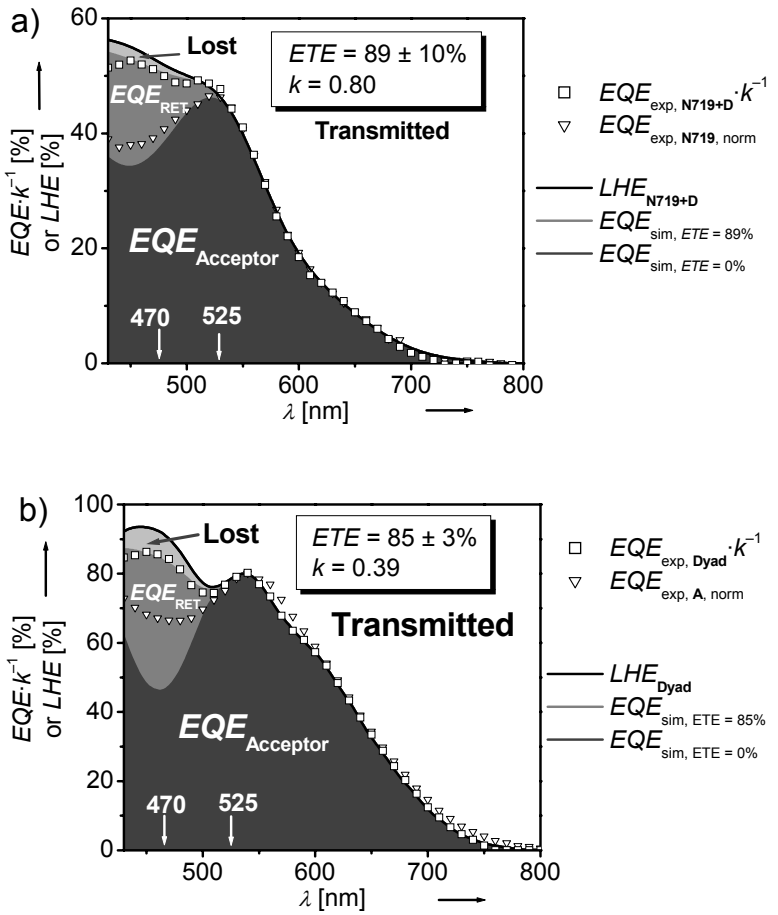

Figure 38. Summary of the conclusions drawn from the data presented in Figure 36 and Figure 37 for the set of devices a) **N719**/**N719+D** and b) **Dyad**/**A**. The black line represents $LHE_{\text{D-A-System}}$ which is identical to $EQE_{\text{sim, }ETE=1}$. The upper margins of the gray and dark gray areas correspond to $EQE_{\text{sim, }ETE=0.85}$ and $EQE_{\text{sim, }ETE=0}$, respectively. The latter curve also represents the fraction of light absorbed by the acceptor moiety within the respective donor acceptor system. The significance of the areas highlighted underneath the curves is presented. Normalized, experimental EQE-data $EQE_{\text{exp}} \cdot k^{-1}$ is also shown for the DSCs stained with the devices with donor acceptor systems (□) and acceptor-only cells (▽). The constant k summarizing injection and collection efficiencies was determined by fitting $EQE(\lambda)$ to the $LHE(\lambda)$ curve at $\lambda > 520$ nm ($k_{\textbf{Dyad}} = 0.39$; $k_{\textbf{N719+D}} = 0.80$). $EQE_{\text{exp, A}}$ and $EQE_{\text{exp, N719}}$ was normalized to fit with $EQE_{\text{exp,Dyad}} \cdot k^{-1}$ and $EQE_{\text{exp, N719+D}} \cdot k^{-1}$ for $\lambda > 520$ nm.

Thus, the energy transfer efficiency from the Fluorol unit to the respective acceptor unit within the devices was approximated to $89 \pm 10\%$ and $85 \pm 3\%$ for **N719+D** and **Dyad**, respectively. The considerations leading to the error in this value are presented in the Appendix. The EQE of a DSC is thus enhanced by donor absorption, even if the energy transfer efficiency is lower than unity. In order to summarize the circumstances prevalent in the DSCs discussed here the areas under the distinctive EQE_{sim}-functions were labeled in Figure 38. The proportion of photocurrent generated by direct acceptor absorption is represented by the dark gray area in Figure 38 (labelled as EQE_{Acceptor}). The gray area represents the proportion of photocurrent generated *via* donor-absorption and RET (labelled as EQE_{RET}), whereas the light gray area corresponds to the proportion of light absorbed by the

donor moiety which did not contribute to current generation due to a quenching mechanism other than RET (labelled as "Lost"). The white area depicts the proportion of light transmitted. The key conclusion from Figure 38 is that most of the photons absorbed by the donor also effectuate RET and charge injection into TiO_2. The highest proportion of current generated *via* donor absorption is prevalent in the device **Dyad** at 460 nm, where 45% of all the electrons collected at the front electrode were initially generated by donor absorption.
Choosing an illumination exclusively in the wavelength range, where the energy donor unit absorbs strongly, the fraction of electrons generated *via* RET is drastically enhanced compared to simulated AM1.5G illumination by halogen lights. Under illumination with λ_{max} = 470 nm, more than 40% of the current is generated due to RET in the donor acceptor device. Thus the motivation for performing IV measurements under monochromatic blue and green illumination was to test whether RET leads to a higher device performance. The crucial results from these measurements were presented as the ratios $j_{blue} \cdot j_{green}^{-1}$ and $P_{blue} \cdot P_{green}^{-1}$ in Table 22. They show that switching the mode of illumination from green to blue affords an increase in j_{sc} for the DSCs comprising donor acceptor systems as sensitizers. Since U_{oc} and *FF* did not depend significantly on the type of illumination, the increase in j_{sc} also results in a higher maximum output power P_{max}. Furthermore, the current under blue illumination generated *via* donor absorption ($j_{blue,\ Donor}$) is close to one magnitude larger in **Dyad** and **N719+D** as supposed to the donor-only device $\mathbf{D_{thick}}$. This result clearly sustains the work hypothesis that resonant energy transfer is a viable way for efficiency enhancement for dye solar cells.

5.3.3 Donor Acceptor Polymers

In the following the results from the DSCs that were stained with different chromophore functionalized polymers (device **PA** and $\mathbf{PDA_x}$) are presented (Table 19, Entries 8 – 14) and discussed. If suitable, the data presented in section 5.3.2 is referred to again.

5.3.3.1 Results

In contrast to monomolecular sensitizers the polymeric ones were not soluble in EtOH. Thus slightly acidic or basic aqueous solution or mixtures of the latter with THF were employed for the preparation of staining solutions. It turned out that these solvent mixtures were also suitable for the preparation of photoelectrodes. The characterization of devices **PA** and $\mathbf{PDA_x}$ by IV measurements under different types of illumination reveals the general trend that the

introduction of an increasing number of donor units leads to a significantly lower efficiency (Table 23). Devices **PDA$_{0.8}$** and **PDA$_1$** have identical efficiencies to **PA** within the experimental error. However, as soon as the donor acceptor ratio exceeds 1, η decreases considerably. On increasing z_{DA} from zero to 8.6, η drops about 86% with respect to **PA**, V_{oc} about 15% and j_{sc} about 85% (a plot of j_{sc} vs. z_{DA} is also show in Figure 41). The drastic decrease in efficiency is thus due to the decreasing current. Figure 39 shows the results of selective illumination experiments. Data points from all investigated devices (including devices **Dyad** and **A**) are plotted. An increasing donor acceptor ratio also leads to both, an increasing $j_{blue} \cdot j_{green}^{-1}$. Within the experimental error and range of donor acceptor ratios examined here, the trend is linear.

Table 23. IV characteristics of devices stained with (donor) acceptor polymers. Device **A$_{Allyl, thick}$** served as reference for light intensity calibration for the IV characteristics under monochromatic illumination (with some exceptions).

Entry[a]	Device	Polymeric Dye	z_{DA}	IV-Measurements[b]					
				U_{oc} [mV]	j_{sc} [mA cm^{-1}]	*FF* [%]	η [%]	$\frac{j_{blue}}{j_{green}}$	$\frac{P_{blue}}{P_{green}}$
5	**PA**	$A_{29\%}$-PG-$N_{3,\ 30\%}$ **66f**	0	714	4.7 ± 0.5	69	2.3	1.03	1.04
6	**PDA$_{0.8}$**	$D_{0.8}$-$A_{5\%}$-PG-$N_{3,\ 30\%}$ **67c**	0.8	677	4.6 ± 0.1	70	2.2	1.24	1.23
7	**PDA$_1$**	$D_{1.0}$-$A_{(20\%)}$-PG-$N_{3,\ 40\%}$ **64**	1.0	664	4.0 ± 0.5	71	1.9	1.13	1.14
8	**PDA$_4$**	$D_{4.0}$-$A_{8\%}$-PG-N_3 **67g**	4.0	616	0.85 ± 0.18	70	0.37	1.98	1.93
9	**PDA$_5$**	$D_{5.0}$-$A_{(10\%)}$-PG-$N_{3.\ 100\%}$ **65a**	5.0	662	1.7	64	0.74	2.15	1.96
10	**PDA$_7$**	$D_{7.0}$-$A_{(10\%)}$-*l*PG-$N_{3,\ 85\%}$ **65b**	7.0	2	1.9	-	-	2.26	-
11	**PDA$_9$**	$D_{8.6}$-$A_{3\%}$-PG-$N_{3,\ 30\%}$ **67b**	8.6	613	0.7 ± 0.1	75	0.32	2.79	2.89

a) The number corresponds to the entry in Table 24 on page 110 for the same set of data. b) See Table 24 on page 110 for details considering IV measurements.

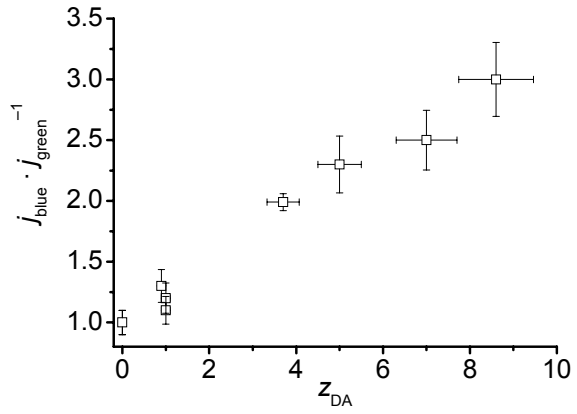

Figure 39. Plot of $j_{blue} \cdot j_{green}^{-1}$ vs. the donor acceptor ratio z_{DA}. The data is taken from Table 24.

The spectral properties (*LHE* and $EQE \cdot k^{-1}$) of the devices **PA** and $\mathbf{PDA_x}$ are shown in Figure 40. $LHE_{\mathbf{A}}$ was added to all spectra for comparison. It was not possible to measure $EQE(\lambda)$ with the device $\mathbf{PDA_7}$ due to a short circuit between the glass substrates. The light harvesting efficiency maxima of donor and acceptor absorption were taken from these spectra [$LHE_{\text{Donor}} = LHE(\lambda = 460\text{ nm})$, $LHE_{\text{Acceptor}} = LHE(\lambda = 535\text{ nm})$] and plotted against z_{DA} (Figure 41). The light harvesting efficiency of the acceptor moiety decreases strongly with increasing z_{DA}. Upon increasing z_{DA} from zero to 8.6, LHE_{Acceptor} drops about 85% with respect to **PA** (Figure 41a). LHE_{Donor} decreases only slightly or not at all (Figure 41b). The energy transfer efficiencies within the devices were estimated according to the method described in Section 5.1.4.

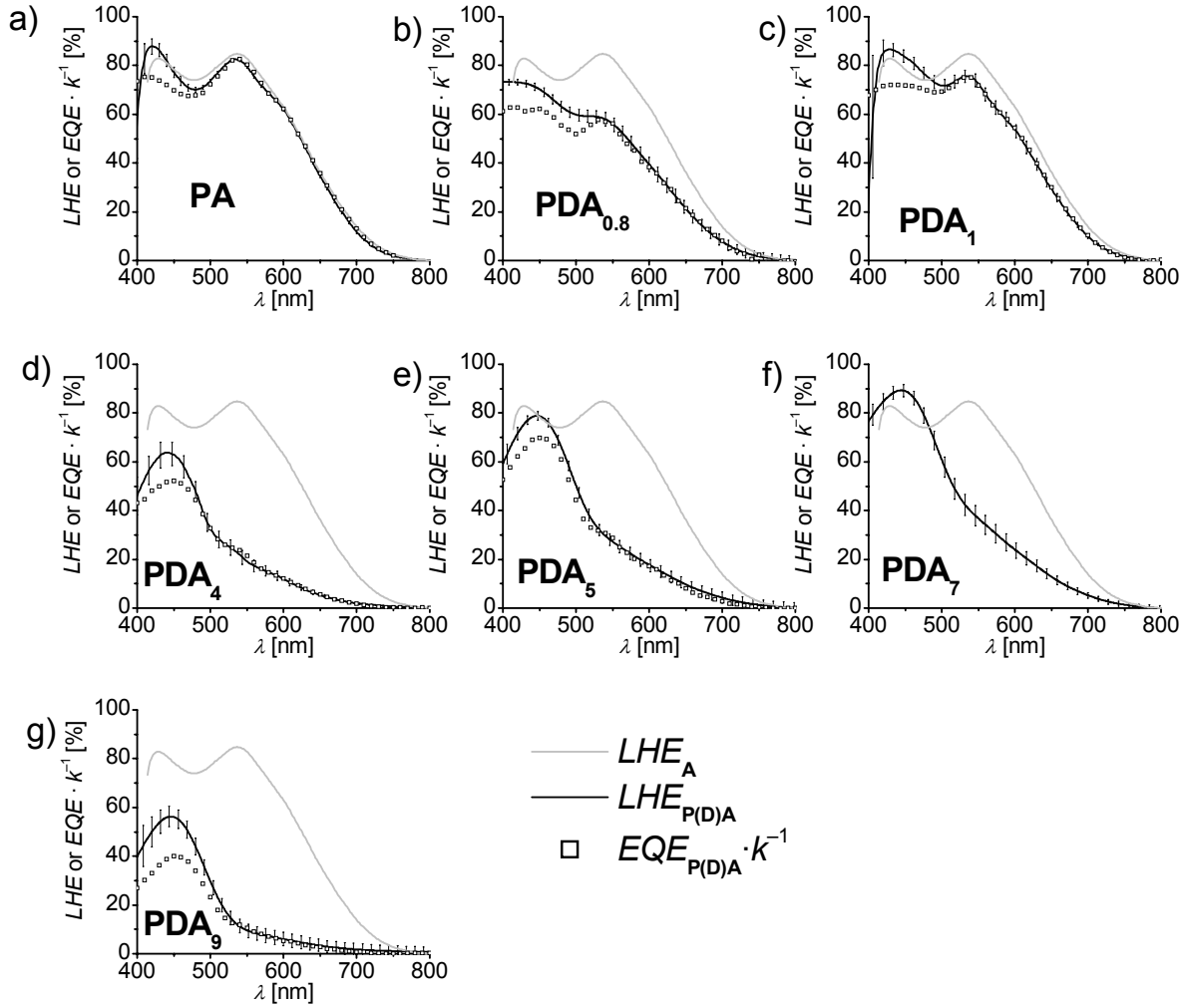

Figure 40. $LHE(\lambda)$ (solid black line) and $EQE(\lambda) \cdot k^{-1}$ (squares) for devices stained with polymeric sensitizers. For comparision $LHE(\lambda)$ of device **A** stained with $[Ru(dcbpy)_2acac]Cl$ is also displayed in all diagrams as solid light gray line. The devices used to measure the individual spectra are a) **PA**, b) $\mathbf{PDA_{0.8}}$, c) $\mathbf{PDA_1}$, d) $\mathbf{PDA_4}$, e) $\mathbf{PDA_5}$, f) $\mathbf{PDA_7}$, g) $\mathbf{PDA_9}$. It was not possible to measure $EQE(\lambda)$ with $\mathbf{PDA_7}$. Values for *LHE* and *EQE* at the wavelength of maximum donor and acceptor absorption [$LHE(\lambda = 445\text{ nm}) = LHE_{\text{Donor}}$ and $LHE(\lambda = 535\text{ nm}) = LHE_{\text{Acceptor}}$, respectively] of this series of devices are summarized in Table 24.

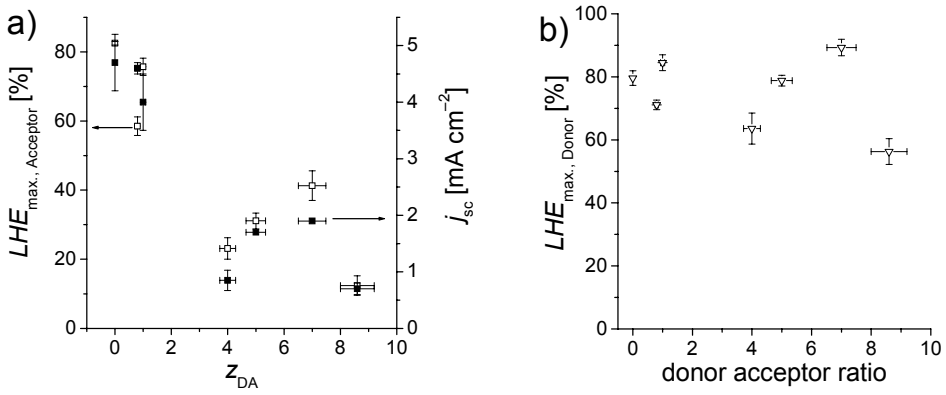

Figure 41. Plot of a) LHE_{Acceptor} (□) and $j_{\text{sc, AM1.5}}$ (■) as well as b) LHE_{Donor} (▽) vs. the donor acceptor ratio as determined by UV-Vis spectroscopy. The values were taken from Table 24.

The respective experimental ($EQE_{\text{exp}} \cdot k^{-1}$, *LHE*) and simulated datasets ($EQE_{\text{simulated, }ETE}$) are displayed in Figure 42. All devices revealed a significant contribution of donor absorption to $EQE(\lambda)$ with *ETE* values between 66 and 90%. No clear trend between z_{DA} and *ETE* is observed, except for the fact that *ETE* is lowest for z_{DA} at its largest.

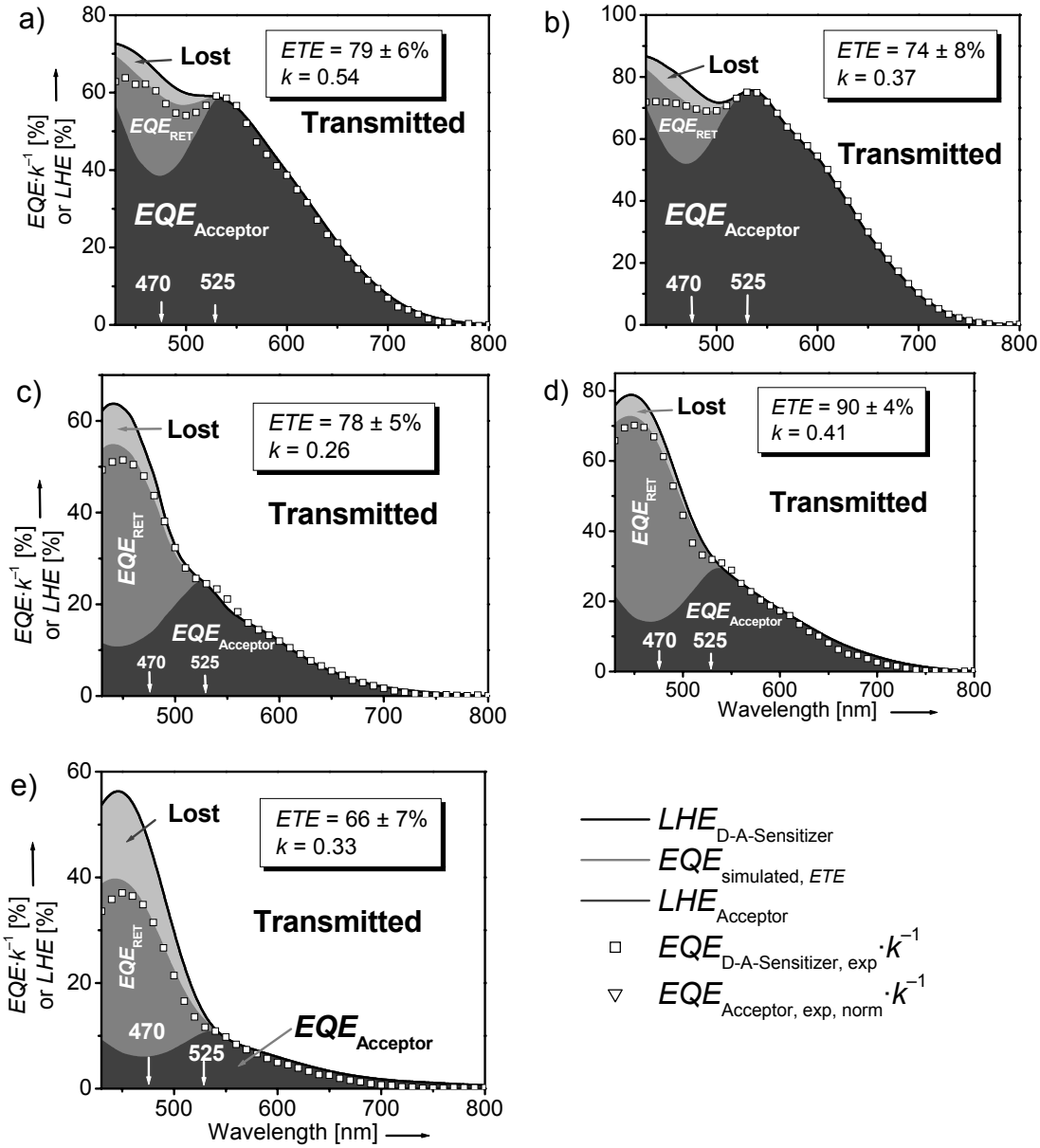

Figure 42. Juxtapositions of experimental results of the DSC's spectral properties ($LHE_{\text{D-A-Sensitizer}}$ and $EQE \cdot k^{-1}$) as well as simulated data derived thereof [LHE_{Acceptor} and $EQE_{\text{simulated,}}(ETE)$]. The *x*-axis shows the wavelength, the *y*-axis shows *LHE* and $EQE \cdot k^{-1}$. *The latter does not show the same range in all diagrams.* The devices used for the individual plots are a) **PDA$_{0.8}$**, b) **PDA$_1$**, c) **PDA$_4$**. d) **PDA$_5$**, e) **PDA$_9$**.

Table 24. Results of IV measurements under different types of illumination and characteristic *LHE* and *EQE* values obtained with the DSCs assembled according to Table 19, entries 4 – 14. The methodology for the calculation of *k* and *ETE* from the device's spectral properties is described in Section 5.1.4.

Aim	Entry	Device	z_{DA}	IV-Measurements[a]						Spectral Characteristics[b]				Result of Fit	
				U_{oc} [mV]	j_{sc} [mA cm^{-1}]	*FF* [%]	η [%]	$\frac{j_{blue}}{j_{green}}$	$\frac{P_{blue}}{P_{green}}$	LHE_D	LHE_A	EQE_D	EQE_A	*k*	*ETE* [%]
coad-sorbed dyes	1	**N719**	0	676 ± 7	4.1 ± 0.1	70 ± 1	2.0 ± 0.1	1.04 ± 0.01[e]	1.01 ± 0.03[e]	44%	52%	34%	42%	0.80	n.a.
	2	**N719+D**	0.45[a]	666 ± 7	4.1 ± 0.1	70 ± 0	1.9 ± 0.1	1.26 ± 0.01[e]	1.24 ± 0.01[e]	55%	48%	42%	39%	0.80	89 ± 10
defined molecules	3	**A**	0	654 ± 6	4.9 ± 0.4	73 ± 1	2.3 ± 0.2	1.00 ± 0.01[d]	0.99 ± 0.02[d]	80%	85%	24%	29%	0.32	n.a.
	4	**Dyad**	1.0	690 ± 10	5.0 ± 0.1	73 ± 3	2.5 ± 0.1	1.24 ± 0.02[d]	1.21 ± 0.04[d]	94%	80%	34%	31%	0.39	85 ± 3
Polymers in the DSC	5	**PA**	0	714 ± 15	4.7 ± 0.5	69 ± 1	2.3 ± 0.2	1.03 ± 0.01[d]	1.04 ± 0.00[d]	80%	83%	26%	31%	0.32	n.a.
	6	**PDA$_{0.8}$**	0.8	677 ± 6	4.6 ± 0.1	70 ± 1	2.2 ± 0.1	1.24 ± 0.03[e]	1.23 ± 0.04[e]	71%	59%	37%	34%	0.54	79 ± 6
	7	**PDA$_1$**	1.0	664 ± 15	4.0 ± 0.5	71 ± 1	1.9 ± 0.2	1.13 ± 0.09[d]	1.14 ± 0.06[d]	84%	76%	27%	28%	0.37	74 ± 8
	8	**PDA$_4$**	4.0	616 ± 12	0.85 ± 0.18	70 ± 1	0.37 ± 0.08	1.98 ± 0.05[f]	1.93 ± 0.05[f]	64%	23%	14%	6%	0.26	78 ± 5
	9	**PDA$_5$**	5.0	662	1.7	64	0.74	2.15[e]	1.96[e]	79%	31%	29%	13%	0.41	90 ± 4
	10	**PDA$_7$**	7.0	2	1.9	23	0.00	2.26[e]	n.d.	89%	41%	n.d.	n.d.	n.d.	n.d.
	11	**PDA$_9$**	8.6	613 ± 17	0.7 ± 0.1	75 ± 1	0.32 ± 0.04	2.79 ± 0.04[e]	2.89 ± 0.07[e]	56%	12%	13%	4%	0.33 (0.28)	66 ± 7 (85 ± 5)

a) IV curve measured under simulated AM1.5G conditions (halogen lamp field). For the determination of $j_{blue} \cdot j_{green}^{-1}$ and $P_{blue} \cdot P_{green}^{-1}$ LED arrays with λ_{max} = 470 and 525 nm were used as light sources, respectively. During the measurement of the IV characteristics under blue illumination, it was noticed that a drift in illumination intensity of ca. 10% occurred. Thus the measured j_{blue} values were reduced by 10% for the calculation of $j_{blue} j_{green}^{-1}$. If no errors are given, only one cell was characterized. b) Donor: *LHE*(λ = 445 nm), *EQE*(λ = 450 nm); Acceptor: for [Ru(dcbpy)$_2$acac]Cl-derivatives *LHE*(λ = 535 nm), *EQE*(λ = 540 nm); for N719 *LHE*(λ = 518 nm), *EQE*(λ = 520 nm). c) Determined by fitting a simulated absorption spectrum to the experimental absorption spectrum of the DSC stained with N719 and carboxybutyl-butyl-fluorol assuming ε_{N719} = 13500 l mol^{-1} cm^{-1} and ε_{Donor} = 16000 l mol^{-1} cm^{-1}. d) Device **A** served as reference for light intensity calibration. e) Device **A$_{Allyl,\ thick}$** served as reference for light intensity calibration. f) Device **N719** served as reference for light intensity calibration.

5.3.3.2 Discussion

The experimental evidence described in Section 5.3.3.1 clearly shows that absorption of the energy donor contributes to current generation also in polymeric donor acceptor sensitizers. In the following, the key results of the individual characterization methods are summarized and associated. The *LHE* spectra of the devices investigated here (Figure 40) clearly indicate that the introduction of the additional donor chromophore was also possible by means of adsorption of D-A-PG-N_3 derivatives. In contrast to results obtained with dyad **45** the spatial demands of the donor unit and polymer backbone lead to a significant decrease in the acceptor content, especially if z_{DA} is larger than one. The latter is illustrated by the decreasing $LHE_{Acceptor}$ in Figure 41a, which is directly responsible to the decrease in j_{sc} and η. In addition to the crowding out of the acceptor unit the staining conditions (especially the pH), the polarity of the polymer backbone and most importantly $\alpha_{Acceptor}$ may also influence the acceptor content: $LHE_{\mathbf{PDA5}}$ and $LHE_{\mathbf{PDA7}}$, resulting from devices stained with polymeric sensitizers based on a hydrophobic backbone and an estimated α_{Ru} of 10%, are overall higher than $LHE_{\mathbf{PDA4}}$ or $LHE_{\mathbf{PDA9}}$ (sensitizers comprising a rather hydrophilic backbone and α_{Ru} of 8% and 3%). All *LHE* spectra distinctively show the characteristic MLCT-band from $[Ru(dcbpy)_2acac]^+$ extending from ~750 nm to 520 nm. Furthermore, $LHE(400 < \lambda < 520$ nm) is larger than one would expect for a hypothetical acceptor-only device with identical acceptor loading, which proves the presence of the donor unit. The difference between LHE_{Donor} and $LHE_{Acceptor}$ (i.e. $LHE_{Donor} \cdot LHE_{Acceptor}^{-1}$) becomes much more pronounced with increasing z_{DA}, which clearly shows that it is possible to tune *LHE* by varying the reaction stoichiometry during the synthesis of polymeric sensitizers. This is possible despite the dispersity for α_{Donor} and α_{Ru} that is prevalent in D-A-PG-N_3 derivatives, and despite preferential adsorption for polymers with a larger α_{Ru} that is to be expected (this topic is covered in more detail in the Section 9.5 of the Appendix on page 170). The influence of the polymer architecture and molecular weight onto $LHE(\lambda)$ may be evaluated from the devices $\mathbf{PDA_5}$ and $\mathbf{PDA_7}$ that were stained with the hyperbranched and linear D-A-PG-N_3 derivatives **65a** and **65b**, respectively. A comparison of the respective *LHE* curves (Figure 40e and f) shows that $\mathbf{PDA_7}$ harvests light somewhat more efficiently, which points to the fact that linear, low molecular weight sensitizers might be better suited to sensitize the nanoporous photoelectrode, however, the different pH used for the staining might also have influenced $LHE(\lambda)$ of these devices.

The parameter connecting *LHE* and *EQE* of solar cells in general is *k* according to eq. (5.3). *k* varied between 0.26 and 0.54 for the devices stained with polymeric sensitizers. *k* being close to unity is a prerequisite for highly efficient solar cells. Thus, following up on optimizing this parameter is reasonable. The low value of $k = 0.26$ for **PDA$_4$** coincides with the highest pH during photoelectrode staining (pH = 10, see Table 19). Optimization of *k* could be realized by the further variation of the molecular parameters α_{Donor}, α_{Ru} and z_{DA} as well as by the systematic variation of staining solvent mixtures, concentrations and temperatures. In analogy to the monomolecular donor acceptor systems, $EQE(\lambda)$ showed clearly that light absorption by the energy donor in the devices stained with D-A-PG-N_3 derivatives contributes to current generation. This becomes apparent from the comparison of the $LHE(\lambda)$-spectra with the $EQE(\lambda)$-graphs (Figure 40). The increased *LHE* effectuated by the donor is reflected in an increased *EQE* with energy transfer efficiencies between 66 and 90% (Figure 42). Despite the fact that the measurement of $EQE(\lambda)$ was not possible for **PDA$_7$**, this device also reveals a high energy transfer efficiency as determined by $j_{blue} \cdot j_{green}^{-1} = 2.26$ which is very similar to the value measured with **PDA$_5$** (j_{sc} was the only result from electrical measurements that could be measured with **PDA$_7$** due to a short circuit on this masterplate). The only clear correlation between z_{DA} and *ETE* that was observed is the fact that *ETE* is lowest for z_{DA} at its largest. This would be consistent with some donor units that are far away from an acceptor unit, and therefore not able to transfer their excitation energy. The relatively low impact of the experimental parameters α_{Donor}, α_{Ru}, and z_{DA} on *ETE* underlines that using polymers as a support for different chromophores functioning as light-harvesting antennas is a viable concept for efficient light-harvesting in the DSC. Strikingly, the extent of current and power enhancement based on RET (as determined by $j_{blue} \cdot j_{green}^{-1}$) increased about nearly one magnitude by the use of D-A-PG-N_3 derivatives as sensitizers. The device **PDA$_9$** shows an increase in current of 179% on changing from green to blue illumination (as opposed to 24% with **Dyad**). The highest proportion of current generated *via* donor absorption is prevalent in this device at 460 nm, where 82% of all the electrons collected at the front electrode were initially generated by donor absorption. Another comparison attests the potential of the antenna effect *via* RET more impressively. Under blue illumination the RET-mediated short circuit current in devices **Dyad** and **PDA$_5$**, which both have comparable values for *k*, amounts to $j_{blue,\,RET} = 2.5$ and $2.9\ mA\ cm^{-2}$, respectively [estimated according to eq. (5.10)]. The higher $j_{blue,\,RET}$ for **PDA$_5$** stands in clear contrast to its significantly lower acceptor content (as indicated by the low value for LHE_A). This remarkable result highlights that the principle of energy funneling from multiple energy donor units in the vicinity of an electron injecting

energy acceptor may significantly enhance the current and power output of thin dye solar cells. The significantly decreased $LHE_{Acceptor}$ resulting by the displacement of the acceptor chromophore is compensated *via* the presence of donor effecting additional light absorption and energy transfer. The approximation of EQE_{sim} to $EQE_{exp.} \cdot k^{-1}$ showed that in some cases the majority of electrons collected at the front electrode have initially been generated by donor absorption under monochromatic illumination with blue light (Figure 42). The areas labeled as EQE_{RET} in Figure 42a – g become increasingly important to the overall *LHE* with increasing z_{DA}. Finally, in analogy to selective illumination experiments with monomolecular sensitizers, the increase based on the antenna effect in j_{sc} on changing from green to blue illumination leads proportionally to an increase in P_{max}. These results clearly sustain the work hypothesis that resonant energy transfer is a viable way for efficiency enhancement in (thin) dye solar cells and that $LHE(\lambda)$ may be tuned by the chromophore composition of donor acceptor polymers.

5.4 Conclusions

In conclusion, a simple concept for the increase of current generation of thin dye solar cells based on resonant energy transfer was devised. This was achieved by the introduction of a second chromophore acting as energy donor for the electron injecting acceptor chromophore. The criteria of choice for the donor chromophore were based on the Förster theory.[29-31] Although the use of multichromophoric dyes in the DSC has been described before, the novelty in the concept extensively evaluated in the present thesis consisted in the use of a purely organic dye as energy donor, namely Fluorol 7GA (**15**),[38, 54] and ruthenium complexes known to give efficient solar cells, namely [Ru(dcbpy)$_2$acac]Cl (**14**)[51, 52] and [Ru(dcbpy)$_2$(NCS)$_2$] (**1**)[9] as energy acceptors. Three different implementations of the above-mentioned concept were realized and evaluated. These consisted in (i) coadsorption of donor and acceptor chromophores onto TiO_2, (ii) introduction of the donor unit by its covalent immobilization to the energy acceptor, and (iii) covalent immobilization of both chromophores to a polymeric support. All three methods had in common that an identical or a lower device performance to respective reference devices was determined with the novel sensitizers under simulated sunlight. This behavior is consistent with the donor chromophore absorbing in a wavelength area where the (simulated) solar emission intensity is very low. Furthermore they had in common that high energy transfer efficiencies always led to a significant generation of current mediated by energy transfer. The pros and cons of the individual methodologies for the implementation of RET in the DSC will be discussed in the following. Comments

therein relating to significantly increased currents and efficiencies refer to the data acquired under selective illumination with blue light.

(i) Coadsorbed chromophores. This concept is fascinating because of its simplicity. The simple addition of **32**, which was accessible within two straight forward synthetic steps, to the staining solution comprising **2** led to a significant additional photocurrent ascribed to resonant energy transfer. Furthermore, it was possible to use today's standard sensitizer "N719" as energy acceptor, which results in good injection and collection efficiencies (as determined by $k = 0.8$) and a good global efficiency considering the high transmittance of the device. The downside to this concept is the limited control it gives over z_{DA}, which is dominated by the competitive adsorption of the sensitizers on the TiO_2 surface. Clearly, N719, bearing 4 carboxy groups, has a higher tendency to adsorb as indicated by $z_{DA} = 0.45$ for device **N719+D**, however, the considerably smaller molecule **32** is also adsorbed, presumably in corners of the rough TiO_2 electrode that are too small for the adsorption of N719. The latter hypothesis is also confirmed by the fact that the acceptor-content as determined by LHE_A is not significantly reduced by the addition of **32** to the staining solution (Table 24). Furthermore, only the surface of the nanoporous TiO_2 is used as an effective light-absorbing volume. In this concept the advantage that the donor chromophore does not need to be in direct contact with the TiO_2 electrode for efficient electron injection is not made use of.

(ii) Defined donor acceptor sensitizers. The concept involving dyad **45** as a defined molecule offers the advantage of a precise control on z_{DA}. The additional spatial requirement of the donor chromophore and linker only led to a minor decrease in acceptor content as determined by LHE_A. The synthesis of such systems, however, is very involved, notably for defined compounds with $z_{DA} > 1$ (e.g., a dendron carrying several donor units in the periphery and one acceptor suitable for DSC applications in the focal point). Nevertheless, this sensitizer was the first one based on an organic fluorophore and an efficient Ru-based sensitizer to be evaluated in such detail in the DSC.[106]

(iii) Donor acceptor polymers. The characterization of devices with polymeric sensitizers with a high donor acceptor ratio ($z_{DA} > 3$) clearly showed that this parameter allows tuning of *LHE* and *EQE* by the chemical composition of the polymer. The latter behavior is made possible by the high *ETE* at high z_{DA}, thus by the antenna effect. The pronounced spatial requirement of the hyperbranched polymer backbone and donor is manifested in a significant crowding out of the acceptor unit resulting in a decreasing LHE_A. This method, however, offers the potential of maintaining LHE_A at a higher level by optimizing the molecular parameters α_{Ru}, α_{Donor}, z_{DA} and most importantly the molecular architecture. This set of

parameters offers diverse opportunities to further optimize the present concept. E.g., a linear polymer that carries one sensitizing acceptor unit at the chain end and several donor units on or within the chain would allow for a more efficient use of the TiO_2 surface (thus a system with low α_{Ru}, high α_{Donor} and z_{DA}). The crowding out of the acceptor unit should be less pronounced with such an architecture.[42]

Despite the considerable initial success at implementing resonant energy transfer in the dye solar cell by the three concepts mentioned above, the following factors remain unclear or need to be optimized: (i) Considering the Förster radius of the donor acceptor pair comprising **15** and **14** (R_0 = 4.6 nm) *ETE* should be close to unity assuming a donor acceptor distance in **45** below 2 nm. The facts accounting for the missing 15% in *ETE* are unidentified. (ii) A lot of light is wasted in cells with [Ru(dcbpy)$_2$acac]Cl derivatives due to inefficient electron injection (low *k*). Optimizing the staining conditions might be a viable way of enhancing *k*. (iii) The wavelength range of donor absorption (400 – 500 nm) is irrelevant for practical applications. Ru-based sensitizers are also able to harvest this light without antenna systems (Figure 45a on page 124). Thus the donor acceptor sensitizers described here should be considered model compounds proving the general feasibility of the concept. Conditions under which the principle described here could prove useful for practical applications are outlined in the outlook of this thesis (Chapter 7 as of page 123).

6 Summary

In this work, three different donor acceptor systems effectuating an improvement of light harvesting and energy conversion at the wavelength of donor absorption were assembled and evaluated. The aminonaphthalimide Fluorol 7GA (**15**) and the Ru-complex [Ru(dcbpy)$_2$acac]Cl (**14**) were referred to as donor and acceptor chromophores, respectively. A prerequisite to these studies consisted in the synthesis of donor acceptor dyad **45** and polymers **64**, **65**, and **67** as well as model chromophores **14**, and **32**.

The initial synthetic methodology for linking the donor and acceptor molecules was based on a set of olefin functionalized chromophores, which were coupled in subsequent hydrosilylation steps to 1,2-bis(dimethylsilyl)ethane (Scheme 20).

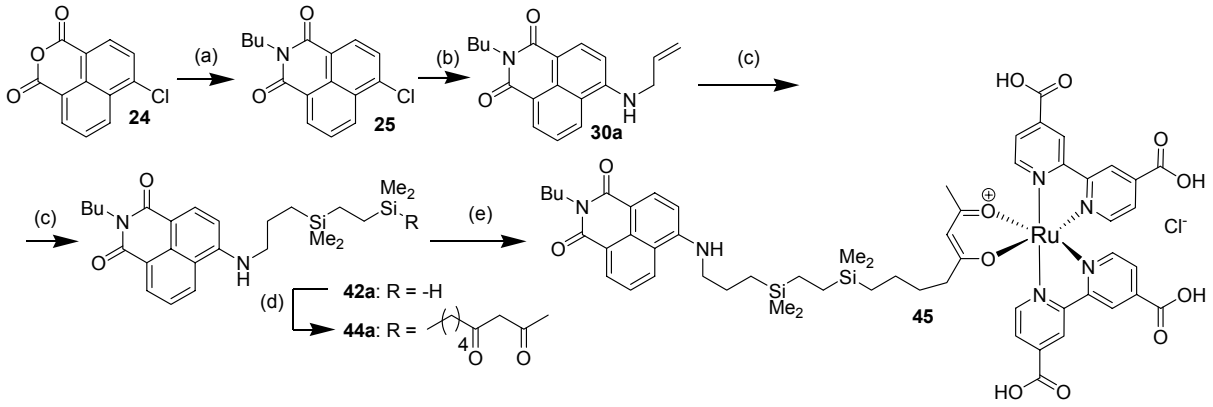

Scheme 20. Synthesis of donor acceptor dyad: *via* a sequence consisting of two condensation and hydrosilylation reactions, respectively and finally a complex forming reaction: (a) $BuNH_2$, EtOH, reflux 80%; (b) excess CH_2=$CHCH_2NH_2$, NMP 60 °C, 92%; (c) $HSiMe_2CH_2CH_2SiMe_2H$, Pt-catalyst, CH_2Cl_2, reflux, 77%; (d) Oct-7-en-2,4-dione, Pt-catalyst, CH_2Cl_2, reflux, 90%; (e) [Ru(di-Me-dcbpy)$_2$Cl$_2$], KO*t*Bu, MeOH/DMF, reflux, then purification *via* column chromatography using alkalinke water on Sephadex LH20, 32%.

The resulting link between the energy donor and acceptor is only constituted of alkyl- and Si-C-groups, both of which are known to possess excellent chemical stability. Due to their insolubility in organic solvents [Ru(dcbpy)$_2$acac]$^+$ derivatives could not be subjected to hydrosilylation reactions directly. Thus the synthetic route proceeded *via* the 2 step hydrosilylation sequence of butyl allyl fluorol (**30a**) with (i) an excess of 1,2-bis(dimethylsilyl)ethane (**39**) giving the respective Si-H functionalized chromophore **42a** and (ii) Oct-7-en-2,4-dion yielding the *β*-diketonato functionalized energy donor **44a**. The subsequent complex formation was carried out by reacting [Ru(di-Me-dcbpy)$_2$Cl$_2$] (**56**) with the ligand **44a** in presence of KO*t*Bu in MeOH. Isolation of dyad **45** after the column chromatography step was performed by precipitation from aqueous solution with HCl. Figure

43 shows ^{1}H-NMR and electronic spectra of the compounds Fluorol 7GA, [Ru(dcbpy)$_2$acac]Cl and the dyad in (basic) MeOH.

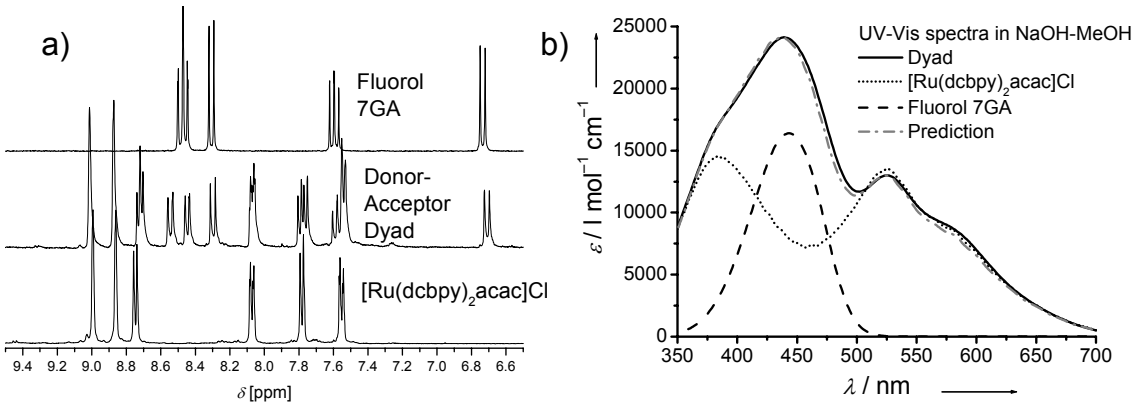

Figure 43. a) ^{1}H-NMR-spectra (300 MHz, MeOD/NaOD) of the aromatic region of Fluorol 7GA **15**, dyad **45** and [Ru(dcbpy)$_2$acac]Cl (**14**). b) UV-Vis spectra of donor acceptor dyad (**45**) (solid), the energy acceptor [Ru(dcbpy)$_2$acac]Cl (**14,** dot), and the energy donor Fluorol 7GA (**15**, dash) in NaOH/MeOH. Furthermore, a theoretical spectrum calculated according to $\varepsilon_{Dyad} = 0.99 \cdot \varepsilon_{Donor} + 0.96 \cdot \varepsilon_{Acceptor}$ is shown (light gray, dash-dot).

The ^{1}H NMR spectrum of the dyad in Figure 43a clearly shows both the signals of the donor unit and the aromatic protons of the dcbpy ligands. From the integral of the signals belonging to the donor and acceptor group respectively, the 1:1 donor acceptor ratio was confirmed. Additionally, the 1:1 ratio was independently confirmed by UV-Vis spectra (Figure 43b) showing that the extinction coefficients of **45** are the sum of its individual chromophoric components. Furthermore, it was observed that the acacH derivatives used in this work were subjected to decomposition under the conditions applied for the complex formation. This fact accounts for the low yields.

Scheme 21 summarizes the sequence of reactions leading to alkyne functionalized donor and acceptor chromophores and their subsequent support to a polymeric azide *via* "Click-Chemistry." The alkyne functionalized ligand **55** was synthesized by monoalkylation of the dianion resulting from the treatment of penta-2,4-dion (**51**) with NaH and *n*-BuLi with trimethylsilylpropargylbromide in a 78% yield. The latter ligand was then incorporated into [Ru(dcbpy)$_2$propargyl-acac]Cl (**58)** by refluxing the ligand in presence of [Ru(di-Me-dcbpy)$_2$Cl$_2$] and KO*t*Bu in MeOH. Under these conditions, the TMS-group was cleaved. The alkyne functionalized donor chromophore propargyl butyl fluorol (**31**) resulted in analogy to **30a** by the two-step sequence comprising imide formation and chloride substitution on chloronaphthalic anhydride **24** in a 69% yield over two steps.

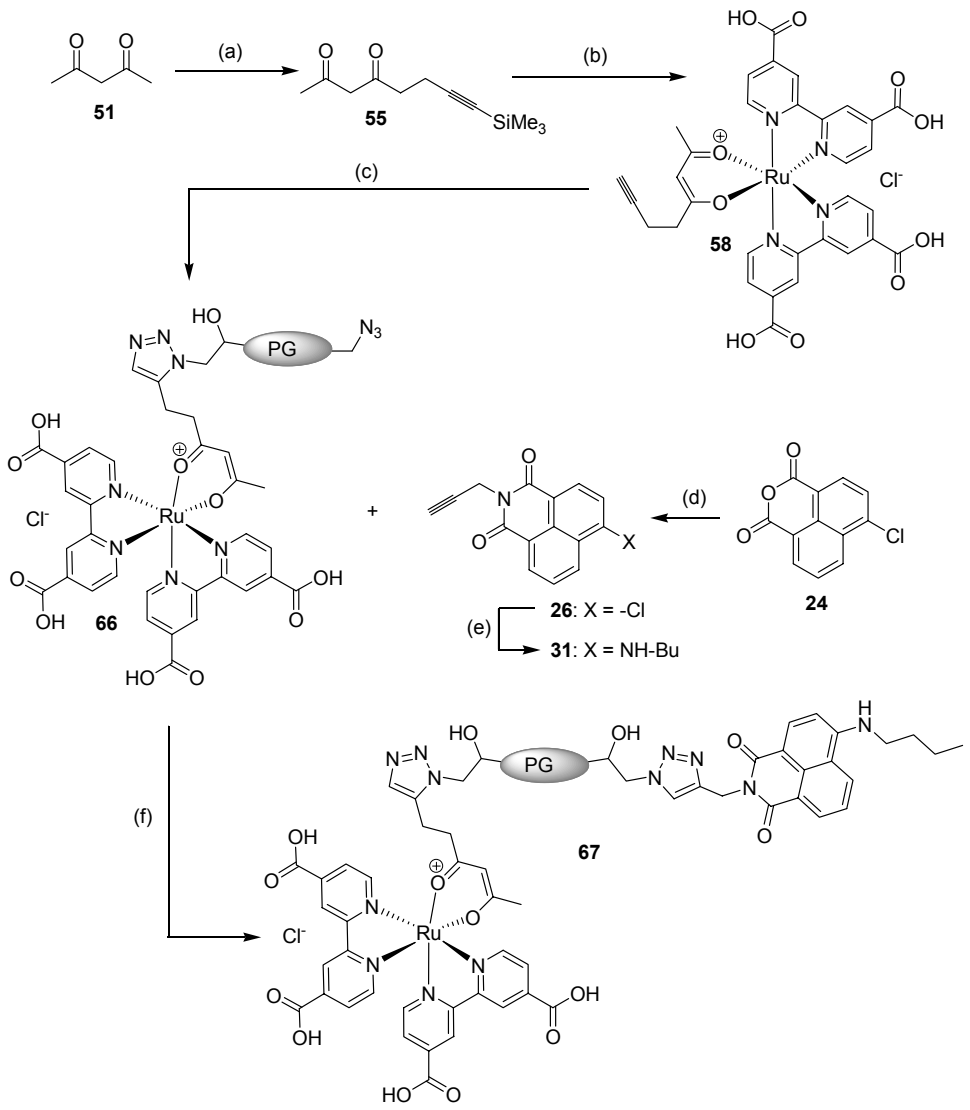

Scheme 21. Synthesis of donor acceptor functionalized polymers. (a) 1.) NaH in THF, 2.) *n*-BuLi, -20 °C, 3.) $Me_3Si\text{-}C{\equiv}CCH_2\text{-}Br$, 78%; (b) $[Ru(di\text{-}Me\text{-}dcbpy)_2Cl_2]$, KO*t*Bu, MeOH/DMF, reflux, 55%; (c) $PG\text{-}N_3$, $CuSO_4$. Sodium ascorbate, DMF/Water, < 67%; (d) $HC{\equiv}CCH_2NH_2$, EtOH, reflux, 81%; (e) $Bu\text{-}NH_2$, NMP, 60 – 80 °C, 85%; (f) $CuSO_4$. Sodium ascorbate, DMSO/water, up to 69% yield.

The difficulty in supporting both chromophores onto one polymer consisted in finding an appropriate solvent system that would allow the formation of a homogeneous reaction mixture with all reaction partners. While the solubility of the polyglycerol azide highly depends on the degree of azide functionalization α_{N_3}, **58** is soluble in basic water and alcohols and **31** is soluble in organic media. Supporting both chromophores simultaneously to the $PG\text{-}N_{3,\,40\%}$ was possible in a DMSO-water-mixture with $CuSO_4$ and sodium ascorbate as catalyst. Alternatively, the simultaneous support of **58** and **31** to $PG\text{-}N_{3,\,100\%}$ (**62e**) and *l*$PG\text{-}N_{3,\,85\%}$ (**62f**) in benzyl alcohol using diisoproply-ethyl-amine and $[Cu(PPh_3)_3Br]$ as catalytic system led to a better control over the donor acceptor ratio and higher conversions.

The characterization of the highly amphiphilic D-A-PG derivatives *via* ^{1}H NMR spectroscopy was not a reliable method for determining the loading of the polymer with the respective chromophoric units. Thus, in some cases D-A-PG derivatives were synthesized in a 2-step sequence *via* (i) the addition of **58** to different PG-N_3 derivatves **62** in DMF-water mixtures, isolation, characterization and calculation of α_{Ru} of the respective A-PG-N_3 and (ii) the addition of **31** to the remaining azide groups in DMSO-water mixtures. By the syntheses described in Scheme 20 and Scheme 21 a variety of donor acceptor sensitizers suitable for the application in the DSC were made. The molecular parameters of these newly synthesized sensitizers are summarized in Table 25 in combination with results considering their performance in the DSC.

Table 25. Molecular parameters of donor acceptor sensitizers and results of their performance in the device. z_{DA} = donor acceptor ratio. For polymers: α_D = loading with donor, α_{Ru} = loading with acceptor, α_{N3} = initial azide functionalization of PG-backbone. η = global power conversion efficiency under simulated AM1.5G conditions. LHE_A = light harvesting efficiency at the longest-wavelength absorption maximum of the acceptor sensitizer. $j_b\, j_g^{-1} = j_{blue} \cdot j_{green}^{-1}$ = current ratio determined by monochromatic illumination experiments. *ETE* = energy transfer efficiency within the device. $k = \phi_{inj} \cdot \eta_{coll}$ = product of injection and collection efficiencies.

Entry	Molecular Parameters[a]					Performance of resulting DSC[b]					
	Dye	α_D [%]	α_{Ru} [%]	z_{DA}[c]	α_{N3} [%]	Device	η[d] [%]	LHE_A [%]	$j_b j_g^{-1}$	*ETE* [%]	*k*
1	**2**			0		**N719**	2.0	52	1.04		0.8
2	**2** + **32**			0.45		**N719+D**	1.9	48	1.26	89	0.8
3	**14**			0		**A**	2.3	85	1		0.32
4	**45**			1		**Dyad**	2.5	80	1.24	85	0.39
5	**66f**	0	29	0	30	**PA**	2.3	83	1.03		0.32
6	**67c**	4	5	0.8	30	**$PDA_{0.8}$**	2.2	59	1.24	79	0.54
7	**64**	20	20	1.0	40	**PDA_1**	1.9	76	1.13	74	0.37
8	**67g**	32	8	3.7	60	**PDA_4**	0.37	23	1.98	78	0.26
9	**65a**	40[e]	10[e]	5.0	100	**PDA_5**	0.74	31	2.15	90	0.41
10	**65b**	40[e]	10[e]	7.0	85	**PDA_7**	0	41	2.26	n.d.	n.d.
11	**67b**	26	3	8.6	30	**PDA_9**	0.32	12	2.79	66	0.33

a) See Table 13 on page 59 and Table 15 on page 67 for synthetic results of the polymeric sensitizers. b) See Table 24 on page 110 for details towards the characterization of the devices. c) Determined from UV-Vis spectra. d) The experimental error is 10%. e) According to the initial reaction stoichiometry.

In addition to the synthetic work, dye solar cells using the novel donor acceptor systems were assembled (Table 25). The detailed characterization of these cells consisted in IV

measurements under simulated AM1.5G conditions as well as monochromatic illumination and the characterization of the cell's spectral properties resulting in $LHE(\lambda)$ and $EQE_{exp}(\lambda)$ data. The energy transfer efficiency within the device (*ETE*) was estimated from the latter two spectra by fitting a simulated *EQE* curve calculated according to eq. (7.1) to $EQE_{exp}(\lambda) \cdot k^{-1}$. k was determined relating $EQE(\lambda)$ to $LHE(\lambda)$ for $\lambda > 520$ nm.

$$EQE_{\text{D-A-System, sim}}(ETE) = LHE \cdot \left[\frac{A_{\text{Acceptor}}}{A_{\text{D-A-System}}} + ETE \cdot \left(1 - \frac{A_{\text{Acceptor}}}{A_{\text{D-A-System}}} \right) \right] \qquad (7.1)$$

A_{Acceptor} = Acceptor absorbance of *within the respective D-A-sensitized device*
$A_{\text{D-A-System}}$ = Absorbance of the D-A-sensitized device [$A = -\log(1 - LHE)$]

The key results from DSC characterization are presented in Table 25. This dataset allowed the evaluation of the different methodologies for the implementation of resonant energy transfer within the DSC. These consisted in (i) coadsorption of donor and acceptor chromophores onto TiO_2 (device **N719+D**), (ii) introduction of the donor unit by its covalent immobilization to the energy acceptor (device **Dyad**) and (iii) covalent immobilization of both chromophores to a polymeric support (devices $\mathbf{PDA_x}$). All three methods had in common that high energy transfer efficiencies led to a significant generation of current mediated by energy transfer in any case. Comments relating to significantly increased currents and efficiencies in the following refer to the data acquired under selective illumination with blue light ($j_b j_g^{-1}$).

Figure 44 shows a selection of spectral properties and respective fits. The methodology for the determination of *ETE* devised here served as a tool to clearly distinguish between contributions of donor and acceptor absorption to the photocurrent (see areas labeled EQE_{RET} and $EQE_{Acceptor}$ in Figure 44).

Coadsorbing chromophores **2** and **32** onto the TiO_2 photoelectrode was the most straightforward method. This concept fascinates by its simplicity. The addition of **32** to the staining solution comprising **2** led to a significant additional photocurrent ascribed to resonant energy transfer. Furthermore, it offered the advantage that today's standard sensitizer "N719" was used as energy acceptor, resulting in good injection and collection efficiencies (as determined by $k = 0.8$) and a good global efficiency considering the high transmittance of the device. The downside to this concept was the limited control it gives over z_{DA}.

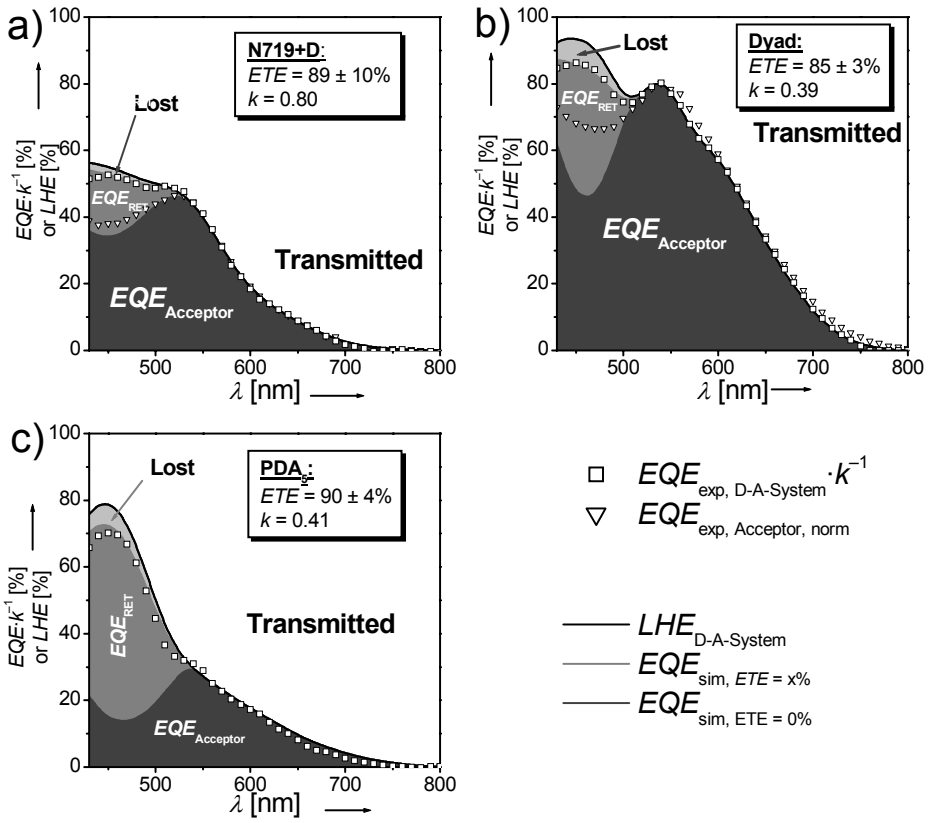

Figure 44. Selected results from spectral properties and *EQE* simulations of devices a) **N719+D** stained with N719 and 4-carboxybutyl butyl fluorol, b) **Dyad** stained with **45** and c) **PDA$_5$** stained with D_5-$A_{(10\%)}$-PG-$N_{3,\ 100\%}$ (**65a**).

Dyad **45** presented a defined molecule which allowed better control of z_{DA} in the device. The additional spatial requirement of the donor chromophore and linker only led to a minor decrease in acceptor content as determined by LHE_A. The synthesis of **45**, however, was very involved. Nevertheless, this sensitizer was the first one based on an organic fluorophore and an efficient Ru-based sensitizer to be evaluated in such detail in the DSC.[106]

The characterization of devices with polymeric sensitizers having a high donor acceptor ratio ($z_{DA} > 3$) clearly showed that this parameter allows one to tune *LHE* and *EQE* by the chemical composition of the polymer. The latter behavior is made possible by the high value for *ETE* (in most cases >> 70%) at high z_{DA}, thus due to energy transfer from multiple donor units per acceptor unit (the antenna effect). The devices **PDA$_x$** revealed an increasing current ratio $j_{blue} \cdot j_{green}^{-1}$ with increasing z_{DA} which indicates that the current generated per Ru-complex is enhanced by RET (an increase of up to 179% was achieved, see Table 25, entry 11). The pronounced spatial requirements of the hyperbranched polymer backbone and donor are manifested in a significant crowding out of the acceptor unit which obviously results in a decreasing acceptor-mediated light-harvesting efficiency (LHE_A). In turn, this is the cause for the decreasing global efficiency η. This is obvious from Figure 44b and c:

LHE_A (corresponding to the curve $EQE_{sim,\ ETE\ =\ 0\%}$) is significantly decreased in polymeric sensitizers with large z_{DA}. Remarkably, the presence of the donor unit keeps *LHE* and *EQE* at a high level within the wavelength range λ = 440 – 460 nm. The latter fact clearly proves the potential of the concept of RET-mediated light-harvesting in the DSC: The presence of organic chromophores is capable of making up for the low *LHE* of the Ru-complex. Due to the fact that wavelength range of donor absorption was narrow and in the blue (λ = 400 – 500 nm), no efficiency enhancement could be shown under practically relevant conditions. However, the donor acceptor sensitizers described here are model compounds proving the general feasibility of the concept.

7 Outlook

Despite the considerable initial success at implementing resonant energy transfer in the dye solar cell the following factors remain to be optimized:

(i) Suppression of sacrificial light absorption. Many photons that were absorbed are wasted in cells relying on [Ru(dcbpy)$_2$acac]Cl derivatives due to inefficient electron injection (low k). This behavior is possibly linked to aggregate formation of the dye. A suppression of aggregate formation could be achieved by optimizing the staining conditions with respect to solvent compositions, additives and temperature.

(ii) Crowding out of acceptor units. In case of polymeric sensitizers with a low degree of loading for the ruthenium complex (α_{Ru}) the spatial requirements of the polymers and donor units brought about a significant crowding out of the electron injecting acceptor unit which also accounted for the light-harvesting for $\lambda > 520$ nm. Using polymers as a platform for photoelectrode functionalization, however, offers the potential of maintaining LHE_A at a higher level by optimizing the molecular parameters of the polymers. These consist in α_{Ru}, α_{Donor}, z_{DA} and most importantly the molecular architecture. This set of parameters open diverse opportunities to further optimize the present concept. E.g., a linear polymer that carries one sensitizing acceptor unit at the chain end and several donor units on or within the chain (thus a system having low α_{Ru}, high α_{Donor} and z_{DA}) would allow for a more efficient use of the TiO_2 surface for acceptor adsorption. The crowding out of the acceptor unit should be less pronounced with such an architecture.[42] Polymeric systems also have the potential of making efficient use of the pores in the nanoporous TiO_2 electrode for additional light harvesting: Energy donors extending into the electrolyte without significantly reducing the diffusion of the redox couple could funnel light energy to the acceptor adsorbed onto the TiO_2 surface, notably if these donor units are also capable of energy hopping *via* energy migration.[29] Additionally, the acceptor content, and efficiency reduction thereby, could also be compensated by an energy donor revealing a low Stokes-shift that absorbs and emits in a similar wavelength range as the acceptor (e.g., perylene tetracarboxylic acid diimides could prove useful as energy donor for the Ru complexes described here).

(iii) "Catching the Blue Sun."[107] The latter heading expresses that the wavelength range of donor absorption has a low relevancy for the global efficiency of the DSCs (Figure 45a). The energy transfer does not contribute to an enhancement of η under practically relevant illumination (AM1.5G conditions). Furthermore, the [Ru(dcbpy)$_2$acac]$^+$ is also capable of

light harvesting in the range of donor absoption. Thus the present results should be considered a model study. The concept of RET in the DSC, however, could prove useful if an efficient sensitizer for the near-IR emission were available that is incapable of absorption in the visible range (Figure 45b). In such a case, antenna systems could be designed with multiple donor chromophores covering the visible part of the solar emission spectrum, e.g., donors based on perylene derivatives, thus transferring the energy to a red or near IR absorbing acceptor chromophore, which then would effectuate electron injection. Squaraine **6**[26] presents such a red-absorbing sensitizer, although a dye extending further into the red would be desirable (up to ~ 1000 nm could be beneficial in the DSC). The methodology for the determination of *ETE* from the device's spectral properties could prove useful in evaluating the contribution of energy transfer in future antenna systems.

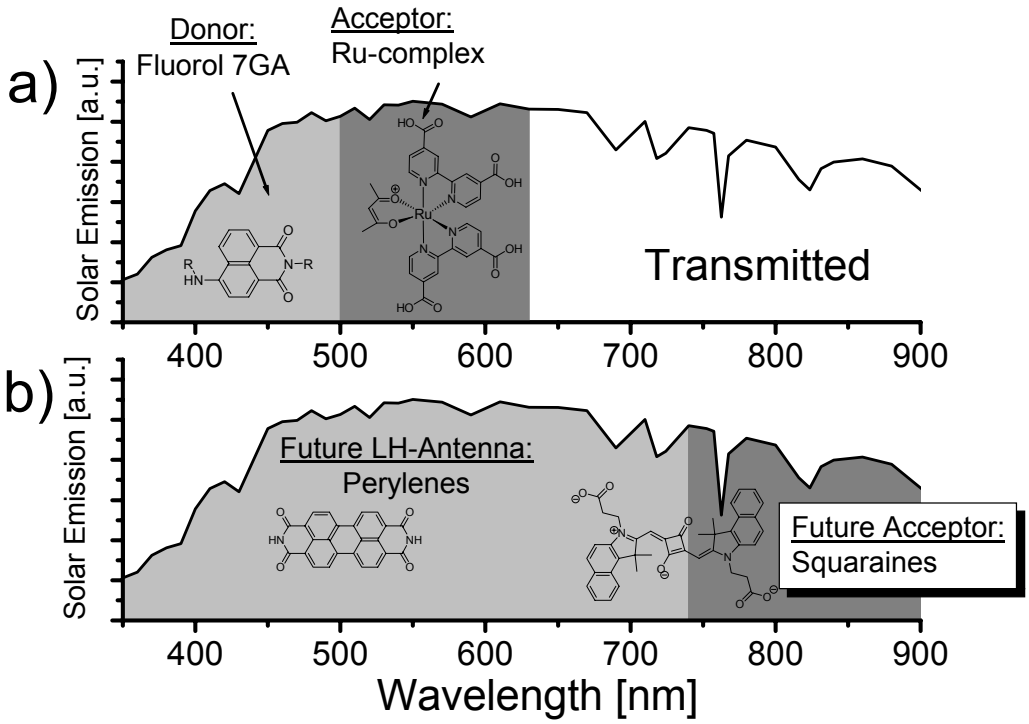

Figure 45. Spectral ranges of donor acceptor absorption a) in the present work and b) the way they should be designed if practical relevance should be found.

8 Experimental

8.1 Equipment used

^{1}H NMR and ^{13}C NMR spectra were recorded on a BRUKER ARX 300 spectrometer, operating at 300 and 75 MHz, respectively. The solvent signals were used as internal standard. The NMR samples comprised 3 to 50 mg dissolved in 600 – 1000 µl NMR solvent.
FT-IR spectra were recorded on a BRUKER Vector22 FT-IR spectrometer on/in KBr between 4000 and 500 cm^{-1}.
UV-Vis spectra were recorded on a PERKIN ELMER Lambda 20 spectrometer using PMMA or PS cuvettes if possible. Alternatively quarz cuvettes were used.
Photoluminescence spectra were measured on a J&M TIDAS diode-array spectrometer and normalized with respect to sample absorption and integration time.
Time-resolved fluorescence measurements proceeded *via* single-photon counting. The samples had an absorbance below 0.1 in a 0.5 cm quartz cuvette and were excited with a 459 nm laser diode. The fluorescence response of the sample was recorded at 536 nm with a photomultiplier. The decay profile of the sample and the instrument response (IRF) was recorded using the software TIME HARP. The maximum number of counts collected for one fluorescence decay profile was at least 10000. The fluorescence decay and instrument response was measured without polarizers in the light path. The anisotropy decay was determined with polarizers for the excitation and emission beams by the measurement of the fluorescence decay under parallel [$I_{VV}(t)$] and perpendicular [$I_{VH}(t)$] adjustment of the polarizers applying identical measuring times. The measurements were corrected by the *G*-factor *via* tail-matching [see eq. (9.1)].[28]

$$G = \frac{I_{VV}(t)}{I_{VH}(t)} \tag{9.1}$$

The anisotropy decay was calculated from experimental data according to eq. (9.2).

$$r(t) = \frac{GI_{VV}(t) - I_{VH}(t)}{GI_{VV}(t) + 2I_{VH}(t)} \tag{9.2}$$

The decay profiles for the intensity and anisotropy decays were fitted to linear combinations of exponential functions [see eq. (4.1) and (4.3)] using the software package FluoroFit from PICO QUANT minimizing χ^2 according to the Levenberg-Marquard algorithm.

IV measurements were carried out by exposing the devices to a halogen lamp field with a calibrated intensity. The solar cells were exposed to the lamp field on a copper block that was thermostated at 13 °C.

Selective illumination during IV measurements was carried using a set of 2 BL3000 Blue and BL3000 Green LED arrays from LAMINA CERAMICS mounted onto a cooled copper block.

Thermogravimetric Analysis measurements were carried out under air using a STA 409 from NETZSCH heating between 50 and 650 °C at 10 K min^{-1}.

Particle sized distributions were measured on a HORIBA particle size analyzer.

8.2 Chemicals

All chemicals were used as received unless stated otherwise. 4-Chloro-1.8-naphthalic anhydride (technical grade, ACROS, 50 w%), sodium hydride (95%, ALDRICH), allyl amine (ALDRICH), propargyl amine (ALDRICH), diethylsilane (ABCR) 1,2-bis-dimethylsilanylethane ($HSiMe_2CH_2CH_2SiMe_2H$) (ABCR). N-methy-pyrrolidone (NMP, FLUKA), *n*-butyl amine (FLUKA), 5-aminovaleric acid (FLUKA), 2,6-diisopropyl aniline (ACROS), $RuCl_3 \cdot x\ H_2O$ (*x* ca. 3, ABCR), NH_4PF_6 (ABCR), methanesulfonic acid chloride (ACROS), functional silanes (ABCR). TiO_2 particles (TIONA 568, a rutile pigment, coated with Al_2O_3 and SiO_2 from MILLENIUM CHEMICALS)

dcbpy (**49**),[71, 72] [Ru(di-Me-dcbpy)$_2$Cl$_2$] (**56**),[73] [Ru(dcbpy)$_2$Cl$_2$] (**50**),[9] allyl-acacH (**36**)[53, 108] 8-trimethylsilyloct-7-yne-2,4-dione (**55**)[53, 108] and 4-Azido-1-amino butane[109] were prepared according to published procedures. $Si(CH_2CH_2CH_2SiMe_2H)_4$ was synthesized and kindly supplied by Dr. Harald Hahn from the group of Prof. Dr. Heinrich Lang, TU Chemnitz. Linear polyglycerol was prepared from its ethoxyethyl protected form having M_n = 3100 g mol^{-1}. The latter was prepared and kindly supplied by Heidemarie Weinhart from the group of Prof. Dr. Rainer Haag, FU Berlin. Hyperbranched polyglycerol (SB 134, M_n = 5000 g mol^{-1}) was available from previous studies of Dr. Holger Türk.

Toluene was extracted three times with H_2SO_4 and Na_2CO_3 and distilled prior to its use for hydrosilylation reactions.

8.3 Synthetic Procedures

Butyl chloro fluorol (25)

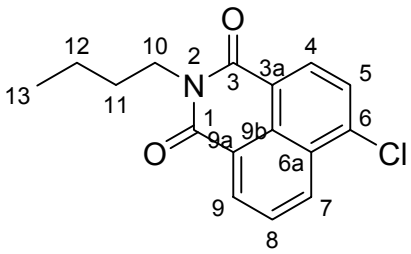

$C_{16}H_{14}ClNO_2$
Exact Mass: 287.0713
Mol. Wt.: 287.7409

4-Chloro-1.8-naphthalic anhydride (50 wt%, 20 g, 43 mmol, 1 eq.) was dissolved in EtOH (technical grade, 1600 ml) at 80°C. This solution was cooled to 70°C and then *n*-Butylamine (6.3 g, 86 mmol, 2 eq.) was added. After keeping the reaction mixture for 10 min at 60°C, the solvent was evaporated to dryness and the residue was recrystallized from EtOH (240 ml) and washed with cold EtOH and water to yield Butyl-Chloro-Fluorol **25** (10.1 g, 35 mmol, 82%). This product contained traces of aromatic impurities, which were not removed prior to further synthetic steps.

^{1}H-NMR ($CDCl_3$, 300 MHz, spectrum contains signals of impurities at δ = 8.42, 8.39, 8.26, 8.08, 7.90, 1.16 and 0.68) δ (ppm) = 8.57 (dd, 1H, $^3J_{9,8}$ = 7.3 Hz, $^4J_{9,7}$ = 1.1 Hz, 9-H), 8.49 (dd, 1H, $^3J_{7,8}$ = 8.5 Hz, $^4J_{7,9}$ = 1.0 Hz, 7-H), 8.40 (d, 1H, $^3J_{4,5}$ = 8.0 Hz, 4-H), 7.77 (dd, 1H, $^3J_{8,9}$ = 7.3 Hz, $^3J_{8,7}$ = 8.4 Hz, 8-H), 7.73 (d, 1H, $^3J_{5,4}$ = 8.0 Hz, 5-H), 4.12 (t, 2H, $^3J_{10,11}$ = 7.6 Hz, 10-H), 1.68 (m, 2H, 11-H), 1.41 (qt, 2H, $^3J_{12,11}$ = 7.5 Hz, $^3J_{12,13}$ = 7.5 Hz, 12-H), 0.94 (t, 3H, $^3J_{13,12}$ = 7.3 Hz, 13-H).

^{13}C-NMR ($CDCl_3$, 75.4 MHz, spectrum contains signals of impurities at δ = 133.68, 133.01, 131.45, 130.03, 127.95, 126.81, 122.17) δ (ppm) = 163.57 (1-C), 163.32 (3-C), 138.80 (6-C), 131.83 (9-C), 130.93 (4-C), 130.39 (7-C), 129.13 (8-C), 128.89 (5-C), 127.72 (6a-C), 127.24 (9b-C), 123.02 (9a-C), 121.53 (3a-C), 40.29 (10-C), 30.10 (11-C), 20.32 (12-C), 13.78 (13-C).

MS (EI, 70 eV): *m*/*z* (%) = 287.1 [M^+].

IR(KBr): $\tilde{\nu}$ = 1733, 1558, 1262, 781, 638, 480 cm^{-1}.

Propargyl chloro fluorol (26)

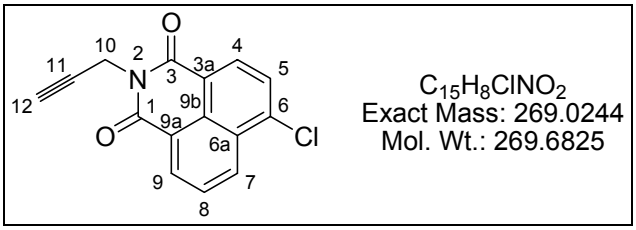

This compound was synthesized analogously to butyl-chloro-fluorol **25** using propargyl amine in stead of butyl amine. Yield: 81%.

^{1}H-NMR ($CDCl_3$, 300 MHz, spectrum contains signals of water, ethanol and impurities at δ = 8.42, 8.39, 8.02, 8.00, 5.27, 3.46, 1.21, 1.01) δ (ppm) = 8.66 (dd, 1H, $^{3}J_{7,8}$ = 7.3 Hz, $^{4}J_{7,9}$ = 1.1 Hz, 9-H), 8.57 (dd, 1H, $^{3}J_{9,8}$ = 8.6 Hz, $^{4}J_{9,7}$ = 1.1 Hz, 7-H), 8.50 (d, 1H, $^{3}J_{4,5}$ = 8.0 Hz, 4-H), 7.83 (dd, 1H, $^{3}J_{8,9}$ = 7.3 Hz, $^{3}J_{8,7}$ = 8.4 Hz, 8-H), 7.80 (d, 1H, $^{3}J_{5,4}$ = 8.0 Hz, 5-H), 4.92 (d, 2H, $^{4}J_{10,12}$ = 2.4 Hz, 10-H), 2.18 (t, 1H, $^{4}J_{12,10}$ = 2.5 Hz, 12-H).

^{13}C-NMR ($CDCl_3$, 75.4 MHz) δ (ppm) = 163.57 (1-C), 163.32 (3-C), 138.80 (6-C), 131.83 (9-C), 130.93 (4-C), 130.39 (7-C), 129.13 (8-C), 128.89 (5-C), 127.72 (6a-C), 127.24 (9b-C), 123.02 (9a-C), 121.53 (3a-C), 40.29 (10-C), 30.10 (11-C).

MS (EI, 70 eV): *m*/*z* (%) = 268.9 (100) [M^+].

4-Carboxybutyl-chloro-fluorol (27)

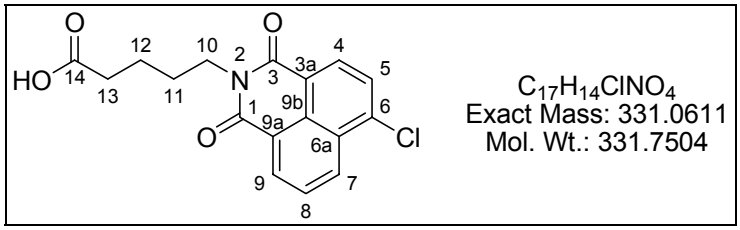

4-Chloro-1.8-naphthalic anhydride (50 w%, 6.00 g, 12.9 mmol, 1 eq.) was dissolved in EtOH (technical grade, 600 ml) at 80°C. This solution was cooled to 70°C and then 5-aminovaleric acid (1.81 g, 15.5 mmol, 1.2 eq.) and $NaHCO_3$ (1.30 g, 15.5 mmol, 1.2 eq.) were added. After keeping the reaction mixture for 3 h at 60°C, the solvent was evaporated to dryness. The conversion was 56% and the reaction product contained starting material.

^{1}H-NMR ($CDCl_3$, 300 MHz, spectrum contains signals of starting material, ethanol and impurities) δ (ppm) = 8.70 – 7.30 (aromatic signals of product and starting material), 4.16 (t, 2H, 10-H), 2.37 (m, 2H, 13-H), 1.75 (m, 4H, 11 and 12-H), 7.80 (d, 1H, $^{3}J_{5,4}$ = 8.0 Hz, 5-H), 4.92 (d, 2H, $^{4}J_{10,12}$ = 2.4 Hz, 10-H), 2.18 (t, 1H, $^{4}J_{12,10}$ = 2.5 Hz, 12-H).

4-Azidobutyl-chloro-fluorol (28)

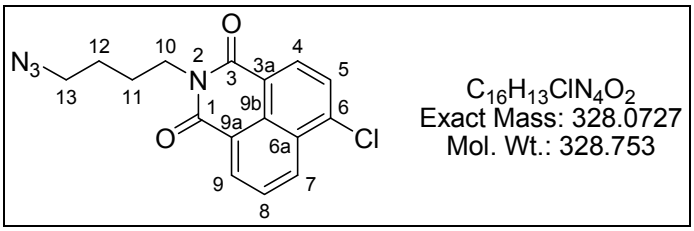

This compound was synthesized analogously to butyl-chloro-fluorol **25** using 4-azidobutyl amine in stead of butyl amine.

^{1}H-NMR ($CDCl_3$, 300 MHz, spectrum contains signals from the starting material, ethanol and from impurities at δ = 1.0 – 1.4 and 2.5 – 3.0 ppm) δ (ppm) = 8.59 – 7.57 (m, 5H, aromatic H), 4.08 (t, 2H, $^{3}J_{10,11}$ = 7.1 Hz, 10-H), 3.26 (dd, 1H, $^{3}J_{13,12}$ = 6.9 Hz, 13-H), 1.79 – 1.53 (m, 4H, 11- and 12-H).

^{13}C-NMR ($CDCl_3$, 75.4 MHz) δ (ppm) = 163.46 (1-C),163.20 (3-C), 138.93 (6-C), 131.88 (9-C), 130.97 (4-C), 130.47 (7-C), 129.03 (8-C), 128.74 (5-C), 127.72 (6a-C), 127.22 (9b-C), 122.71 (9a-C), 121.22 (3a-C), 51.02 (13-C), 39.63 (10-C), 26.37 (11-C), 25.21 (12-C).

2,6-Diisopropylphenyl-imidazolo-fluorol (29)

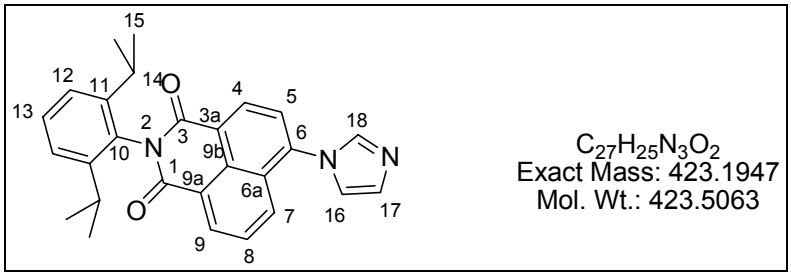

This reaction was carried out under nitrogen. 4-Chloro-1,8-naphtalic anhydride (50w%, 5 g, 10.75 mmol, 1 eq.) and imidazole (42 g) were placed in a 500-ml two neck flask. 2,6-Diisopropyl aniline (92%, 4.97 g, 25.8 mmol, 2.4 eq.) were added and the mixture was heated to 140 °C for 3 h. After cooling to room temperature HCl (0.2 M, 360 ml) was added and the mixture was stirred for 20 h after which a precipitate was formed. The title compound was isolated from the precipitate *via* column chromatography using an isohexane/ethyl acetate (1:1) with silica gel as stationary phase. Yield: 3.2 g, 5.67 mmol, 72%.

^{1}H-NMR ($CDCl_3$, 300 MHz) δ (ppm) = 8.73 (m, 2H, Ar-H), 8.14 (dd, 1H, J = 0.9 Hz, J = 8.6 Hz, Ar-H), 7.88 – 7.83 (m, 2H, Ar-H), 7.76 (d, 1H, J = 7.7 Hz, 5-H), 7.47 (dd, H, $J_{8,9}$ = 8.0 $J_{8,7}$ = 7.5 Hz, 8-H), 7.37 – 7.30 (m, 4H, 13-, 12- and 17-H), 2.71 (septet, 2H, J = 6.9 Hz, 14-H), 1.14 (d, 12H, J = 6.9 Hz, 15-H).

^{13}C-NMR ($CDCl_3$, 75.4 MHz) δ (ppm) = 163.70 (1-C), 163.21 (3-C), 145.52 (Ar-C), 139.36 (Ar-C), 138.03 (Ar-C), 132.61 (Ar-C), 131.52 (Ar-C), 130.62 (Ar-C), 129.67 (Ar-C), 129.04 (Ar-C), 128.46 (Ar-C), 127.74 (Ar-C), 124.21 (Ar-C), 124.05 (Ar-C), 123.13 (Ar-C), 123.00 (Ar-C), 121.41 (Ar-C), 29.14 (14-C), 23.90 (15-C).

MS (EI, 70 eV): *m/z* (%) = 423.1 (94) [M^+], 380.1 (100) [M – propyl$^+$], 365.2 (12) [M – propyl - CH_3 + H^+].

Butyl allyl fluorol (30a)

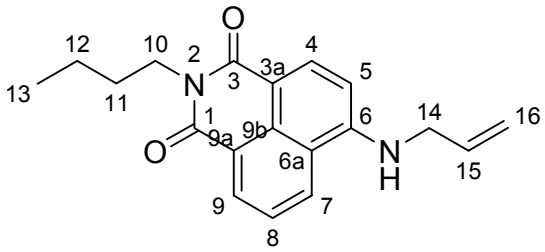

$C_{19}H_{20}N_2O_2$
Exact Mass: 308.1525
Mol. Wt.: 308.3743
C, 74.00; H, 6.54; N, 9.08; O, 10.38

25 (7.19 g, 25 mmol, 1 eq.) was dissolved in NMP (60 ml) and allyl amine (14.3 g, 250 mmol, 10 eq.) was added. The mixture was heated to 60°C for 3 days, after which the major part of the solvent was removed *in vacuo*. The residue was separated from traces of remainig starting material by column chromatography on silica gel using an isohexane/ethyl acetate gradient to afford compound **30a**. Yield: 7.10 g, 23 mmol, 92%.

^{1}H-NMR ($CDCl_3$, 300 MHz) δ (ppm) = 8.54 (dd, 1H, $^3J_{9,8}$ = 6.7 Hz, $^3J_{9,7}$ = 0.7 Hz, 9-H), 8.41 (d, 1H, $^3J_{7,8}$ = 8.4 Hz, 7-H), 8.11 (d, 1H, $^3J_{4,5}$ = 7.9 Hz, 4-H), 7.57 (dd, 1H, $^3J_{8,7}$ = 7.5 Hz, $^3J_{8,9}$ = 8.2 Hz, 8-H), 6.68 (d, 1H, $^3J_{5,4}$ = 8.4 Hz, 5-H), 6.00 (ddt, 1H, $^3J_{14,15}$ = 5.2 Hz, $^3J_{15,16(cis)}$ = 10.3 Hz, $^3J_{15,16(trans)}$ = 17.2 Hz, 15-H), 5.52 (t, 1H, $^3J_{NH,14}$ = 5.2 Hz, N-H), 5.35 (dd, 1H, $^3J_{gem}$ = 1.3 Hz, $^3J_{15,16}$ = 17.2 Hz, 16-H), 5.27 (dd, 1H, $^2J_{gem}$ = 1.3 Hz, $^3J_{15,16}$ = 10.3 Hz, 16-H), 4.13 (t, 2H, $^2J_{10,11}$ = 7.5 Hz, 10-H), 4.05 (m, 2H, 14-H), 1.68 (m, 2H, $^3J_{16,17}$ = 7.4 Hz, 11-H), 1.41 (tq, 2H, $J_{12,11}$ = 7.7 Hz, $^3J_{12,13}$ = 7.7 Hz, 12-H), 0.93 (t, 3H, $^3J_{13,12}$ = 7.3 Hz, 13-H).

^{13}C-NMR ($CDCl_3$, 75.4 MHz) δ (ppm) = 163.70 (1-C), 163.21 (3-C), 145.52 (Ar-C), 139.36 (Ar-C), 138.03 (Ar-C), 132.61 (Ar-C), 131.52 (Ar-C), 130.62 (Ar-C), 129.67 (Ar-C), 129.04 (Ar-C), 128.46 (Ar-C), 127.74 (Ar-C), 124.21 (Ar-C), 124.05 (Ar-C), 123.13 (Ar-C), 123.00 (Ar-C), 121.41 (Ar-C), 29.14 (14-C), 23.90 (15-C).

MS (EI, 70 eV): *m/z* (%) = 308.2 (100) [M^+], 291.2 (56) [M – CH_4^+] 252.1 (44) [M – Bu + H^+].

Anal. Cald. for $C_{19}H_{20}N_2O_2$: C, 74.00; H, 6.54; N, 9.08. Found: C, 73.61; H, 6.60; N 8.90.

IR $\tilde{\nu}$ = 3388, 3001, 2953, 2861, 1677, 1639, 1578, 1434, 1391, 1345, 1244, 1119, 1076, 770 cm^{-1}.

Propargyl-butyl-fluorol (31)

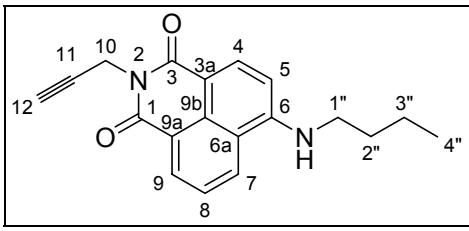

$C_{19}H_{18}N_2O_2$
Exact Mass: 306.1368
Mol. Wt.: 306.3584
C, 74.49; H, 5.92; N, 9.14; O, 10.44

26 (2.765 g, 10.3 mmol, 1 eq.) was dissolved in NMP (50 ml). Butylamine (3.75 g, 51.3 mmol, 5 eq.) was added and the mixture was stirred at 60°C for 12 h. The solvent was removed at high vacuum and the crude product was recrystallized from ethanol. Yield: 2.69 g, 8.77 mmol, 85%.

^{1}H-NMR ($CDCl_3$, 300 MHz) δ (ppm) = 8.55 (dd, 1H, $^3J_{9,8}$ = 7.30 Hz, $^4J_{9,7}$ = 0.65 Hz, 9-H), 8.44 (d , 1H, $^3J_{9,8}$ = 8.38 Hz, 4-H), 8.06 (d, 1H, $^3J_{7,8}$ = 7.95 Hz, 7-H), 7.58 (dd, 1H, $^3J_{8,7}$ = 7.52, $^3J_{8,9}$ = 8.38 Hz, 8-H), 6.68 (d, 1H, $^3J_{5,4}$ = 8.6 Hz, 5-H), 5.30 (m, 1H, N-H), 4.92 (d, 2H, ^4J = 2.58 Hz, C*H*$_2$C≡CH), 3.38 (m, 2H, 1'-H), 2.15 (t, 1H, ^3J = 2.58 Hz, ≡C*H*), 1.79 (m, 2H, 2'-H), 1.52 (m, 2H, 3'-H), 1.01 (t, 3H, $^3J_{4',3'}$ = 7.31 Hz, 4'-H).

^{13}C-NMR ($CDCl_3$, 75.4 MHz) δ (ppm) = 163.8 (1-C), 163.0 (3-C), 149.8 (6-C), 134.7 (4-C), 131.2 (9-C), 129.6 (9a-C), 126.3 (7-C), 124.4 (9b-C), 122.3 (6a-C), 120.0 (8-C), 109.2 (3a-C), 104.2 (5-C), 79.3 (12-C), 70.0 (11-C), 43.4 (1"-C), 30.8 (2"-C), 29.0 (10-C), 20.3 (3"-C), 13.8 (4"-C)

IR $\tilde{\nu}$ = 3380, 3293, 3261, 2994, 2953, 2929, 2867, 2123, 1688, 1642, 1576, 1547, 1465, 1416, 1395, 1369, 1336, 1300, 1246, 1186, 1171, 1153, 1097, 1068, 949, 770, 677, 515 cm^{-1}.

Anal. Cald. for: $C_{19}H_{18}N_2O_2 \cdot 0.125\ H_2O$: C, 73.95; H, 5.96; N, 9.08 . Found: C, 73.96; H, 5.95; N 9.10.

MS (EI, 70 eV): *m*/*z* (%) = 306.0 (100) [M$^+$], 263.0 (10) [M – propyl$^+$].

4-carboxybutyl butyl fluorol (32)

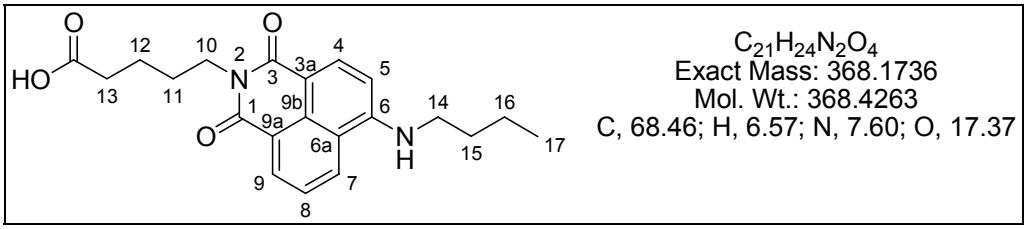

$C_{21}H_{24}N_2O_4$
Exact Mass: 368.1736
Mol. Wt.: 368.4263
C, 68.46; H, 6.57; N, 7.60; O, 17.37

The crude mixture containing 4-carboxybutyl-chloro-fluorol and 4-chloro-1,8-naphthalic anhydride (3 g) was dissolved in NMP (80 ml). Butyl amine (2.65 g) was added and the mixture was heated to 80 °C for 44 h. The solvent was removed *in vaccuo*. In order to

separated Dibutyl-fluorol from 4-carboxybutyl butyl fluorol, the residue was taken up in CH_2Cl_2 (100 ml) and extracted into aq. NaOH (2M). The org. phase was discardesd. The aq. phase was acidified with HCl (20%) and extracted with CH_2Cl_2. The resulting organic phase was dried over $MgSO_4$ and the solvent was evaporated. Recrystallization from EtOH afforded the title compound. Yield: 0.40 g, 1.1 mmol, 10% over 2 steps.

^{1}H-NMR (MeOD/NaOD, 300 MHz) δ (ppm) = 8.49 (dd, 1H, $^3J_{9,8}$ = 8.5 Hz, $^4J_{9,7}$ = 1.1 Hz, 9-H), 8.45 (dd, 1H, $^3J_{7,8}$ = 7.4 Hz, $^4J_{7,9}$ = 1.0 Hz, 7-H), 8.30 (d, 1H, $^3J_{4,5}$ = 8.5 Hz, 4-H), 7.59 (dd, 1H, $^3J_{8,7}$ = 7.4 Hz, $^3J_{8,9}$ = 8.3 Hz, 8-H), 6.72 (d, 1H, $^3J_{5,4}$ = 8.7 Hz, 5-H), 4.13 (t, 2H, $^3J_{10,11}$ = 6.6 Hz, 10-H), 3.43 (t, 2H, $^3J_{14,15}$ = 7.2 Hz, 14-H), 2.22 (t, 2H, $^3J_{13,12}$ = 7.0 Hz, 13-H), 1.82 - 1.66 (m, 6H, 11-, 12- and 15-H), 1.51 (tq, 2H, $^3J_{16,17}$ = $^3J_{16,15}$ = 7.4 Hz, 16-H), 1.05 (t, 3H, $^3J_{17,16}$ = 7.4 Hz, 17-H).

^{13}C-NMR (MeOD/NaOD, 75.4 MHz) δ (ppm) = 183.06 (COONa), 166.39 (1-C), 165.80 (3-C), 152.72 (6-C), 136.06 (4-C), 132.24 (7-C), 131.17 (9a-C), 129.48 (9-C), 125.38 (8-C), 123.24 (6a-C), 121.73 (9b-C), 109.14 (3a-C), 105.05 (5-C), 44.49 (14-C), 41.24 (10-C), 39.32 (13-C), 31.93 (15-C), 29.64 (11-C), 25.68 (12-C), 21.75 (16-C), 14.60 (17-C).

MS (EI, 70 eV): *m/z* (%) = 368.0 (100) [M^+], 351.0 (23) [M – OH^+], 309.0 (18) [M – $CH_2CO_2H^+$].

Anal. Cald. for: $C_{21}H_{24}N_2O_4 \cdot 0.25\ H_2O$: C, 67.63; H, 6.62; N, 7.51. Found: C, 67.82; H, 6.66; N 7.44.

UV-Vis (EtOH): λ_{max} (nm) [ε (l mol^{-1} cm^{-1})] = 445 (15920).

UV-Vis (aq. NaOH, 0.1M): λ_{max} (nm) [ε (l mol^{-1} cm^{-1})] = 455 (15610).

4-Azidobutyl-butyl-fluorol (33)

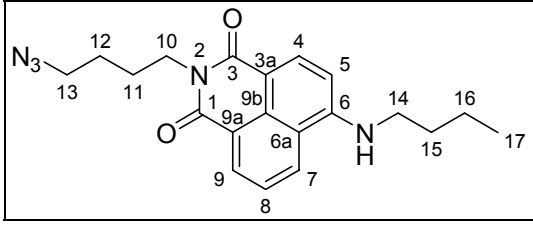

$C_{20}H_{23}N_5O_2$
Exact Mass: 365.1852
Mol. Wt.: 365.4289
C, 65.73; H, 6.34; N, 19.16; O, 8.76

4-Azidobutyl-chloro-fluorol (0.3 g, 0.92 mmol, 1 eq.), butyl amine (46 mg, 8.2 mmol, 10 eq.) and NMP (17 ml) were stirred at 80 °C for 3 d. The solvent was removed *in vaccuo* and the residue was further purified *via* column chromatography on silica gel using isohexane/EE (3:1) as eluent to afford the title compound (0.3 g, 0.82 mmol, 90%).

^{1}H-NMR ($CDCl_3$, 300 MHz, spectrum contains signals of impurities at δ = 2.01, 1.22 and 0.88 ppm) δ (ppm) = 8.53 (dd, 1H, $^3J_{9,8}$ = 7.4 Hz, $^4J_{9,7}$ = 0.9 Hz, 9-H), 8.41 (d , 1H, $^3J_{9,8}$ = 8.5

Hz, 4-H), 8.06 (dd, 1H, $^3J_{7,8}$ = 8.3 Hz, $^4J_{7,9}$ = 0.9 Hz, 7-H), 7.56 (dd, 1H, $^3J_{8,7}$ = 8.2 Hz, $^3J_{8,9}$ = 7.3 Hz, 8-H), 6.68 (d, 1H, $^3J_{5,4}$ = 8.5 Hz, 5-H), 5.29 (bs, 1H, N-H), 4.16 (t, 2H, $^3J_{16,17}$ = 7.0 Hz, 10-H), 3.38 (t, 2H, $^3J_{21,22}$ = 7.2 Hz, 14-H), 3.31 (t, 2H, J = 6.8 Hz, 13-H), 1.85 – 1.60 (m, 6H, 11-, 12- and 15-H), 1.51 (tq, 2H, $^3J_{16,17}$ = 7.4 Hz, $^3J_{16,15}$ = 7.4 Hz, 16-H), 1.00 (tq, 2H, $^3J_{17,16}$ = 7.3 Hz, 17-H).

^{13}C-NMR ($CDCl_3$, 75.4 MHz) δ (ppm) = 164.66 (1-C), 164.07 (3-C), 149.52 (6-C), 134.54 (4-C), 131.11 (9-C), 129.78 (9a-C), 125.84 (7-C), 124.60 (9b-C), 122.98 (6a-C), 120.10 (8-C), 109.95 (3a-C), 104.30 (5-C), 51.21 (13-C), 43.40 (14-C), 39.29 (10-C), 30.99 (15-C), 26.48 (11-C), 25.40 (12-C), 20.30 (16-C).

MS (EI, 70 eV): m/z (%) = 365.2 (70) [M^+], 323.0 (20) [$M - N_3^+$], 293.2 (87) [$M - CH_3(CH_2)_3NH$], 182.1 (100) [$M - CH_3(CH_2)_3NH - N_3(CH_2)_4N - H^+$].

HRMS (EI): m/z = 365.185201. Calc. for $C_{20}H_23N_5O_2$: 365.185175. Derivation: 0.1 ppm.

2,6-Diisopropylphenyl-allyl-fluorol (34)

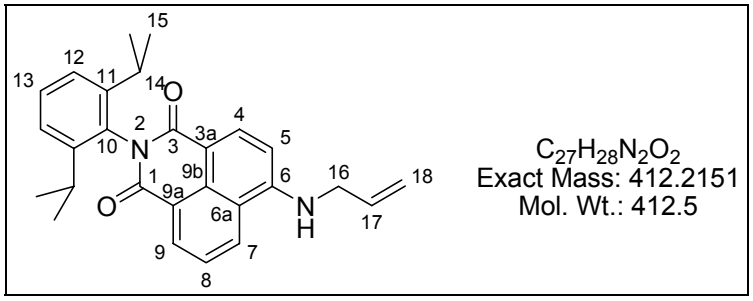

2,6-Diisopropylphenyl allyl fluorol (**29**) (1.0 g, 2.4 mmol, 1 eq.) and allyl amine (2.7 g, 47 mmol, 20 eq.) were dissolved in NMP (33 ml). The mixture was stirred at 40 °C for 20 h. Then water and DCM were added and the organic phase was extracted 7 times with acidic water. The organic phase was dried over $MgSO_4$, the solvent evaporated and the residue was purified by chromatography over silica gel using a ishexane:ethyl acetate 1:1. Yield: 0.6 g, 1.45 mmol, 60%.

^{1}H-NMR ($CDCl_3$, 300 MHz, spectrum contains impurities at δ = 0.8 and 1.5 ppm) δ (ppm) = 8.60 (dd, 1H, $^3J_{9,8}$ = 6.7 Hz, $^3J_{9,7}$ = 0.7 Hz, 9-H), 8.47 (d, 1H, $^3J_{7,8}$ = 8.4 Hz, 7-H), 8.14 (d, 1H, $^3J_{4,5}$ = 7.9 Hz, 4-H), 7.63 (dd, 1H, $^3J_{8,7}$ = 7.5 Hz, 8-H, $^3J_{8,9}$ = 8.2 Hz, 8-H), 7.39 (m, 1H, 13-H), 7.24 (m, 2H, 12-H), 6.74 (d, 1H, $^3J_{5,4}$ = 8.6 Hz, 5-H), 6.00 (m, 1H, 17-H), 5.44 (m, 1H, N-H), 5.36 (dd, 1H, $^3J_{gem}$ = 1.1 Hz, $^3J_{15,16}$ = 17.2 Hz, 18-H), 5.28 (dd, 1H, $^2J_{gem}$ = 1.3 Hz, $^3J_{15,16}$ = 10.3 Hz, 18-H), 4.07 (m, 2H, 16-H), 2.70 (sept, 2H, $^3J_{14,15}$ = 7.4 Hz, 14-H), 1.10 (d, 6H, $^3J_{15,14}$ = 6.9 Hz, 15-H) overlapping with 1.09 (d, 2H, $J_{15,14}$ = 6.9 Hz, 15-H).

Dibutyl allyl fluorol (30b)

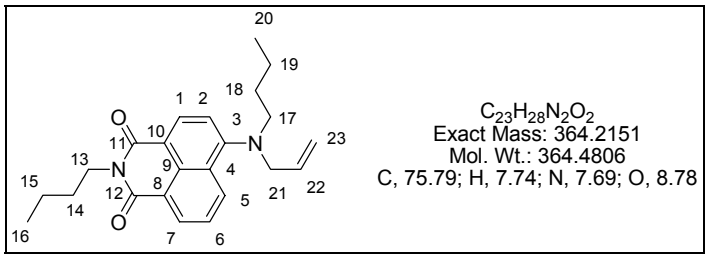

Dibutyl-fluorol (0.987 g, 3.04 mmol, 1 eq.) was dissolved in DMF (abs., 50 ml). NaH (0.188 g, 7.84 mmol, 2.6 eq.) was added, after which the color of the solution turned from bright yellow to dark purple. Then allyl bromide (0.442 g, 3.65 mmol, 1.2 eq.) was added and the solution was stirred at room temperature for 2 h. Then, excess NaH was quenched by the addition of MeOH and the solvents were evaporated. The residue was dissolved in $CHCl_3$ and extracted with aqueous NH_4Cl, twice, and brine. The combined aqueous extracts were extracted with $CHCl_3$ and the combined organic extracts were dried over $MgSO_4$. Purification of the crude product over silica gel using isohexane/ethyl acetate (5:1) as solvent afforded 0.886 g dibutyl allyl fluorol **30b** (2.43 mmol, 80%).

^{1}H-NMR ($CDCl_3$, 300 MHz) δ (ppm) = 8.54 (dd, 1H, $^3J_{7,6}$ = 7.2 Hz, $^4J_{7,5}$ = 1.0 Hz, 7-H), 8.46 (d, 1H, $^3J_{1,2}$ = 8.3 Hz, 1-H), 8.43 (dd, 1H, $^3J_{5,6}$ = 8.3 Hz, $^3J_{5,7}$ = 1.2 Hz, 5-H), 7.63 (dd, 1H, $^3J_{6,7}$ = 7.4 Hz, $^3J_{6,5}$ = 8.3 Hz, 6-H), 7.18 (d, 1H, $^3J_{2,1}$ = 8.3 Hz, 2-H), 5.89 (ddt, 1H, $^3J_{trans}$ = 17.1 Hz, $^3J_{cis}$ = 10.1 Hz, $^3J_{22,21}$ = 5.8 Hz, 22-H), 5.31 (dd, 1H, $^3J_{trans}$ = 17.1 Hz, $^4J_{23,21}$ = 1.4 Hz, 23-H (trans)), 5.23 (dd, 1H, $^3J_{cis}$ = 10.3 Hz, $^4J_{23,21}$ = 1.2 Hz, 23-H (cis)), 4.14 (t, 2H, $^3J_{13,14}$ = 7.4 Hz, 13-H), 3.91 (d, 2H, $^3J_{21,22}$ = 5.8 Hz, 21-H), 3.31 (t, 2H, $^3J_{17,18}$ = 10.3 Hz, 17-H), 1.68 (m, 2H, *J* = Hz, 14-H), 1.55 (m, 2H, *J* = Hz, 18-H), 1.42 (qt, 2H, $^3J_{15,16}$ = 7.4 Hz, $^3J_{15,14}$ = 7.4 Hz, 15-H), 1.29 (qt, 2H, $^3J_{19,18}$ = 7.4 Hz, $^3J_{19,20}$ = 7.4 Hz, 19-H), 0.95 (t, 3H, $^3J_{16,15}$ = 7.4 Hz, 16-H), 0.85 (t, 3H, $^3J_{20,19}$ = 7.4 Hz, 20-H).

^{13}C-NMR ($CDCl_3$, 75.4 MHz) δ (ppm) = 164.52 (12-C), 164.02 (11-C), 154.92 (3-C), 133.97 (22-C), 131.91 (7-C), 130.96 (5-C), 130.51 (1-C), 130.11 (6-C), 126.92 (4-C), 125.22 (8-C), 123.16 (9-C), 117.88 (10-C), 116.60 (2-C), 115.79 (23-C), 58.00 (17-C), 51.73 (21-C), 39.97 (13-C), 30.21 (14-C), 28.86 (18-C), 20.35 (15-C), 20.29 (19-C), 13.80 (16- and 20-C).

MS (EI, 70 eV): *m*/*z* (%) = 364.2 (42) [M^+], 321.2 (100) [M – propyl$^+$], 265.1 (7) [M – propyl – butyl$^+$], 237.1 [M – propyl – butyl – $C_2H_4^+$].

Anal. Cald. for $C_{23}H_{28}N_2O_2$: C, 75.79; H, 7.74; N, 7.69. Found: C, 75.66; H, 7.79; N 7.65

UV-Vis (EtOH): λ_{max} (nm) [ε (l mol^{-1} cm^{-1})] = 261 (14960), 417 (10960).

IR $\tilde{\nu}$ = 3078, 2958, 2931, 2871, 1694, 1652, 1614, 1588, 1513, 1466, 1427, 1389, 1352, 1267, 1187, 783, 760 cm^{-1}.

Butyl hydrosilyl fluorol (42a)

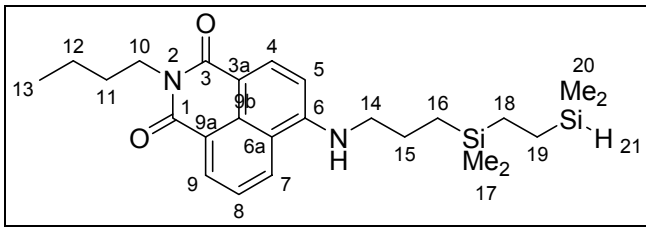

$C_{25}H_{38}N_2O_2Si_2$
Exact Mass: 454.25
Mol. Wt.: 454.75
C, 66.03; H, 8.42; N, 6.16;
O, 7.04; Si, 12.35

Butyl allyl fluorol **30a** (1.75g, 5.675 mmol, 1 Eq.) was dissolved in DCM (150 ml) under a nitrogen atmosphere. To this solution 1,2-Bis-dimethylsilanylethane (3.00 g, 20.49 mmol, 3.6 Eq.) and the platinium catalyst solution (100 µl) was added. The mixture was stirred under reflux for 3 h after which the solvent was evaporated. Purification by chromatography on silica gel using isohexane/ethyl acetate (5:1) as eluant yielded 1.998 g (4.393 mmol, 77%) of the title compound as orange crystals. ^{1}H-NMR ($CDCl_3$, 300 MHz) δ (ppm) = 8.52 (d, 1H, $^3J_{1,2}$ = 6.9 Hz, 9-H), 8.40 (d, 1H, $^3J_{3,2}$ = 8.4 Hz, 7-H), 8.08 (d , 1H, $^3J_{9,8}$ = 8.4 Hz, 4-H), 7.54 (dd, 1H, $^3J_{2,1}$ = 7.5 Hz, $^3J_{2,3}$ = 8.2, 8-H), 6.66 (d, 1H, $^3J_{8,9}$ = 8.6 Hz, 5-H), 5.42 (s, 1H, N-H), 4.13 (t, 2H, $^3J_{16,17}$ = 7.5 Hz, 10-H), 3.79 (m, 1H, Si-H), 3.36 (t, 2H, $^3J_{21,22}$ = 6.7 Hz, 14-H), 1.75 (m, 2H, 11-H) overlapping with 1.68 (m, 2H, 15-H), 1.40 (tq, 2H, $^3J_{18,19}$ = 7.4 Hz, $^3J_{18,17}$ = 7.4 Hz, 12-H), 0.93 (t, 3H, $^3J_{19,18}$ = 7.4 Hz, 13-H), 0.64 (m, 2H, 16-H), 0.45 (s, 4H, 18- and 19-H), 0.02 (d, 6H, $^3J_{27,28}$ = 3.7 Hz, 20-CH_3), -0.02 (s, 6H, 17-CH_3).

^{13}C-NMR ($CDCl_3$, 75.4 MHz) δ (ppm) = 164.65 (1-C), 164.10 (3-C), 149.37 (6-C), 134.40 (4-C), 130.98 (9-C), 129.76 (9a-C), 125.76 (7-C), 124.52 (9b-C), 123.11 (6a-C), 120.10 (8-C), 110.10 (3a-C), 104.23 (5-C), 46.86 (14-C), 39.92 (10-C), 30.28 (11-C), 23.53 (15-C), 20.39 (12-C), 13.84 (13-C), 12.21 (16-C), 7.77 (18-C), 6.33 (19-C), -3.98 (20-CH_3), -4.90 (17-CH_3).

IR $\tilde{\nu}$ = 3367, 2955, 2904, 2876, 2789, 2105, 1684, 1636, 1617, 1574, 1245, 1175, 888, 835, 772 cm^{-1}.

MS (EI, 130 eV): *m*/*z* (%): 454.3 (19) [M^+], 367.2 (100) [$M^+ - HSiMe_2CH_2CH_2$].

Anal. Cald. for $C_{25}H_{38}N_2O_2Si_2$: C, 66.03; H, 8.42; N, 6.16. Found: C, 65.90; H, 8.31; N 5.99.

Dibutyl hydrosilyl fluorol (42b)

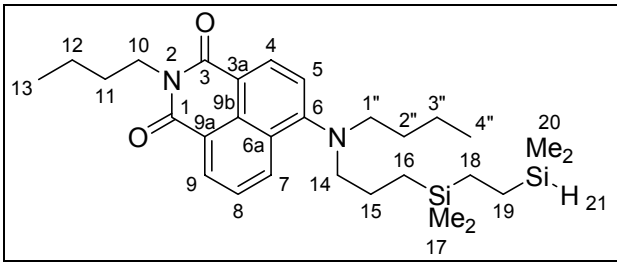

$C_{29}H_{46}N_2O_2Si_2$
Exact Mass: 510.31
Mol. Wt.: 510.86
C, 68.18; H, 9.08; N, 5.48; O, 6.26; Si, 11.00

1,2-Bis-dimethylsilanylethane (0.602 g, 4.115 mmol, 5 equiv.) were dissolved in toluene (4 ml) under argon atmosphere. Dibutyl Allyl Fluorol **30b** (0.301 g, 0.823 mmol, 1 equiv.) in toluene (4 ml) and Pt-catalyst (30 µl) were added. After 18 h the solvent was removed *in vaccuo* and the residue was purified by chromatography on silica gel using isohexane/ethyl acetate (10:1) as eluant to yield 0.260 g (61%) of the title compound as orange oil.

^{1}H-NMR ($CDCl_3$, 300 MHz) δ(ppm) = 8.53 (dd, 1H, $^3J_{9,8}$ = 7.2 Hz, $^4J_{9,7}$ = 0.9 Hz, 9-H), 8.43 (m, 2H, 7- and 4-H), 7.61 (dd, 1H, $^3J_{8,9}$ = 7.31 Hz, $^3J_{8,7}$ = 8.38 Hz, 8-H), 7.16 (d , 1H, $J_{5,4}$ = 8.17 Hz, 5-H), 4.13 (t, 2H, $^3J_{10,11}$ = 7.4 Hz, 10-H), 3.72 (m, 1H, Si-H), 3.33 (t, 2H, $^3J_{14,15}$ = 7.3 Hz, 14-H) overlapping with 3.31 (t, 2H, $^3J_{1",2"}$ = 7.3 Hz, 1"-H), 1.68 (m, 2H, 11-H), 1.54 (m, 4H, 15- and 2"-H), 1.41 (tq, 2H, $^3J_{12,13}$ = 7.5 Hz, $^3J_{12,11}$ = 7.5 Hz, 12-H), 1.23 (tq, 2H, $^3J_{3",2"}$ = 7.5 Hz, $^3J_{3",4"}$ = 7.5 Hz, 3"-H), 0.93 (t, 3H, $^3J_{13,12}$ = 7.3 Hz, 13-H), 0.83 (t, 3H, $^3J_{4",3"}$ = 7.4 Hz, 4"-H), 0.41 (m, 2H, 16-H), 0.34 (m, 4H, 18- and 19-H), -0.04 (d, 6H, $^3J_{20\text{-}CH3,\ Si\text{-}H}$ = 3.7 Hz, 20-CH_3), -0.13 (s , 6H, 17-CH_3).

^{13}C-NMR ($CDCl_3$, 75.4 MHz) δ(ppm) = 164.51 (1-C), 164.00 (3-C), 155.34 (6-C), 131.92 (4-C), 130.90 (9-C), 130.72 (7-C), 130.23 (9a-C), 127.04 (9b-C), 124.96 (6a-C), 123.19 (8-C), 116.65 (5-C), 115.47 (3a-C), 57.10 (14-C), 53.27 (1"-C), 39.92 (10-C), 30.22 (2"-C), 29.15 (11-C), 21.43 (15-C), 20.34 (12-C), 20.27 (3"-C), 13.79 (13-C), 13.77 (4"-C), 11.97 (16-C), 7.70 (18-C), 6.24 (19-C), -3.99 (20-C), -4.98 (17-C).

IR $\tilde{\nu}$ = 2956, 2873, 2107, 1696, 1657, 1588, 1465, 1427, 1392, 1352, 1248, 1087, 891, 834, 782, 761 cm^{-1}.

MS (EI, 70 eV): *m*/*z* (%): 510.2 (18) [M^+], 467.3 (7) [$M^+ - CH_2CH_2CH_3$], 337.2 (100) [$M^+ - HSiMe_2CH_2CH_2SiMe_2CH_2CH_2$].

Butyl-3-(diethylsilyl)propyl-fluorol (43)

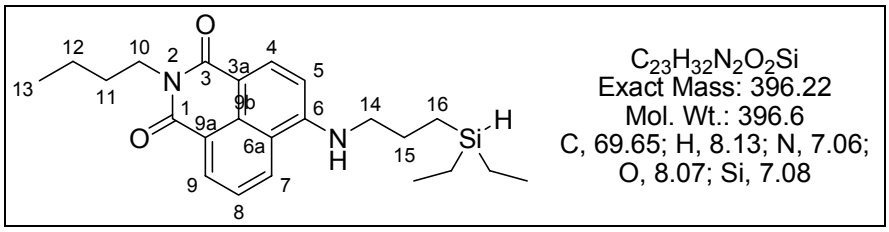

Butyl allyl fluorol (0.972 g, 3.15 mmol, 1 eq.) was dissolved in DCM (50 ml) under argon. Diethylsilane (3.0 ml, 2.04 g, 23 mmol, 7.3 eq.) and the Pt-catalyst solution (200 µl) was added and the mixture was refluxed for 12 h. Then the solvent was evaporated and the crude product was separated by column chromatography on silica gel using isohexane:EE (gradiet from 5:1 to 2:1) as eluent. In addition to the title compound several side products were isolated, one of which was shown to be butyl-propyl-fluorol by ^{1}H NMR and MS spectroscopy. Yield: 0.34 g, 0.85 mmol, 27%.

^{1}H-NMR ($CDCl_3$, 300 MHz) δ (ppm) = 8.51 (dd, 1H, ^{3}J = 7.3 Hz, ^{4}J = 0.9 Hz, 9-H), 8.39 (d , 1H, ^{3}J = 8.4 Hz, 7-H), 8.08 (dd, 1H, ^{3}J = 8.4 Hz, ^{4}J = 0.6 Hz, 4-H), 7.53 (dd, 1H, ^{3}J = 7.5 Hz, ^{3}J = 8.4 Hz, 8-H), 6.65 (d, 1H, ^{3}J = 8.4 Hz, 5-H), 5.48 (t, 1H, ^{3}J = 4.9 Hz, N-H), 4.12 (t, 2H, ^{3}J = 7.7 Hz, 10-H), 3.69 (quint., 1H, ^{3}J = 3.2 Hz, Si-H), 3.37 (m, 2H, 14-H), 1.82 (m, 2H, 11-H), 1.67 (m, 2H, 15-H), 1.40 (tq, 2H, ^{3}J = 7.5 Hz (2x), 12-H), 0.94 (m, 9H, 3 x CH_3), 0.73 (m, 2H, 16-H), 0.58 (m, 4H, Si-CH_2CH$_3$).

^{13}C-NMR ($CDCl_3$, 75.4 MHz) δ (ppm) = 164.65 (1-C), 164.11 (3-C), 149.39 (6-C), 134.38 (4-C), 130.97 (9-C), 129.74 (9a-C), 125.83 (7-C), 124.52 (9b-C), 123.06 (6a-C), 120.12 (8-C), 110.08 (3a-C), 104.21 (5-C), 46.53 (14-C), 39.92 (10-C), 30.28 (11-C), 24.18 (15-C), 20.38 (12-C), 13.83 (13-C), 8.13 (16-C), 8.08 (Si-CH_2-CH_3), 2.64 (Si-CH_2-CH_3).

MS (EI, 70 eV): *m*/*z* (%): 396.2 (96) [M^+], 379.2 (44) [M – CH_3 – H_2^+], 367.1 (83) [M – $CH_2CH_3^+$], 182.0 (100).

Butyl acacH fluorol (44a)

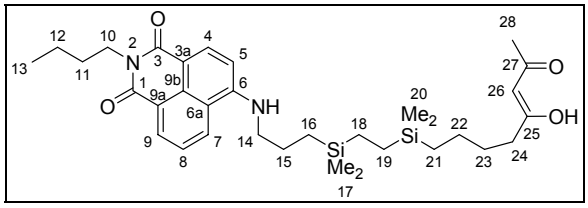

Butyl Hydrosilyl Fluorol **42a** (0.815 g, 1.792 mmol, 1 Eq.) was dissolved in DCM. Oct-7-en-2,4-dion (0.318 g, 2.111 mmol, 1.18 Eq.) and the Pt-catalyst (100 µl) were added and the

mixture was stirred for 6 h under reflux under a nitrogen atmosphere. Purification by chromatography on silica gel using isohexane/ethyl acetate (3:1) as eluant yielded 0.963 g (1.619 mmol, 90%) of the title compound as yellowish-orange waxy material. ^{1}H-NMR ($CDCl_3$, 300 MHz) δ (ppm) = 15.49 (s , 1H Enol-OH), 8.52 (d, 1H, $^{3}J_{9,8}$ = 7.3 Hz, 9-H), 8.41 (d, 1H, $^{3}J_{9,7}$ = 8.4 Hz, 7-H), 8.09 (d, 1H, $^{3}J_{4,5}$ = 8.4 Hz, 4-H), 7.55 (dd, 1H, $^{3}J_{8,9}$ = 7.7 Hz, $^{3}J_{8,7}$ = 7.7 Hz, 8-H), 6.66 (d, 1H, $^{3}J_{5,4}$ = 8.4 Hz, 5-H), 5.45 (m, 2H, N-H and 26-CH, Enol form), 4.13 (t, 2H, $^{3}J_{10,11}$ = 7.5 Hz, 10-H), 3.53 (s, 1H, 26-CH_2, Keto form), 3.36 (td, 2H, $^{3}J_{14,N\text{-}H}$ = 5.2 Hz, $^{3}J_{14,15}$ = 6.9 Hz, 14-H), 2.47 (t, 2H, $^{3}J_{24,23}$ = 7.2 Hz, 24-H, Keto form), 2.23 (t, 2H, $^{3}J_{24,23}$ = 7.5 Hz, 24-H, Enol form), 2.19 (s, 3H, 28-H, Keto form), 2.01 (s, 3H, 28-H, Enol form), 1.75 (m, 2H, 11-H), 1.68 (m, 2H, 15-H), 1.58 (m , 2H, 23-H), 1.40 (tq, 2H, $^{3}J_{12,13}$ = 7.5 Hz, $^{3}J_{12,11}$ = 7.5 Hz, 12-H), 1.27 (m, 2H, 22-H), 0.93 (t, 3H, $^{3}J_{13,12}$ = 7.4 Hz, 13-H), 0.63 (m, 2H, 16-H), 0.47 (m, 2H, 21-H), 0.35 (s, 4H, 18- and 19-H), -0.03 (s, 6H, 17-CH_3), -0.09 (s, 6H, 20-CH_3).

^{13}C-NMR ($CDCl_3$, 75.4 MHz) δ (ppm) = 204.33 (25-C, Keto), 202.18 (27-C, Keto), 194.33 (25-C, Enol), 191.39 (27-C, Enol), 164.64 (3-C), 164.08 (1-C), 149.39 (6-C), 134.39 (4-C), 130.97 (9-C), 129.78 (9a-C), 125.80 (7-C), 124.50 (9b-C), 123.12 (6a-C), 120.13 (8-C), 110.10 (3a-C), 104.22 (5-C), 99.72 (26-C, Enol), 57.84 (26-C, Keto), 46.88 (14-C), 43.48 (24-C, Keto), 39.90 (10-C), 37.91 (24-C, Enol), 30.85 (23-C, Keto), 30.28 (11-C), 29.48 (23-C, Enol), 27.14 (28-C, Keto), 24.92 (28-C, Enol), 23.55 (15-C and 22-C, Enol), 23.40 (22-C, Keto), 20.38 (12-C), 14.43 (21-C, Keto), 14.39 (21-C, Enol), 13.84 (13-C), 12.15 (16-C), 7.09 (18-C), 7.02 (19-C), -3.99 (Si-CH_3), -4.04 (Si-CH_3)

IR $\tilde{\nu}$ = 3385, 3076, 2954, 2926, 2871, 2507, 1685, 1638, 1580, 1546, 1428, 1395, 1245, 1150, 1131, 1104, 1077, 833, 774 cm^{-1}.

MS (EI, 70 eV): *m*/*z* (%): 594.4 (7) [M^+], 367.2 (100) [M^+ – Me-CO-CH_2-CO-$(CH_2)_4$-$SiMe_2CH_2CH_2$]. Anal. Cald. for $C_{37}H_{58}N_2O_4Si_2 \cdot 0.5\ H_2O$: C, 65.63; H, 8.51; N, 4.64. Found: C, 65.97; H, 8.53; N 4.61.

Dibutyl acacH fluorol (261b)

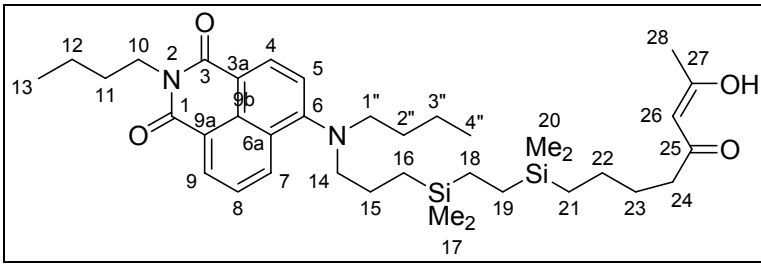

$C_{37}H_{58}N_2O_4Si_2$
Exact Mass: 650.39
Mol. Wt.: 651.04
C, 68.26; H, 8.98; N, 4.30;
O, 9.83; Si, 8.63

Dibutyl Hydrosilyl Fluorol **30b** (0.242 g, 0.475 mmol, 1.1equiv) and Oct-7-en-2,4-dion (0.060 g, 0.431 mmol, 1.0 equiv.) were dissolved in toluene (6 ml) under argon. After addition of the Pt-catalyst solution (30 µl) the mixture was heated to 60-70°C. After 40 h the solvent was evaporated. The residue was purified by chromatography on silica gel using isohexane/ethyl acetate (10:1) as eluant to yield 0.107 g (34%) of the title compound.

^{1}H-NMR ($CDCl_3$, 300 MHz) δ (ppm) = 15.47 (s , 1H Enol-OH), 8.52 (d , 1H, $^3J_{9,8}$ = 7.3 Hz, 9-H), 8.43 (d , 1H, $^3J_{4,5}$ = 8.2 Hz, 4-H), 8.40 (d , 1H, $^3J_{7,8}$ = 8.6 Hz, 7-H), 7.60 (dd, 1H, $^3J_{8,9}$ = 7.5 Hz, $^3J_{8,7}$ = 8.4 Hz, 8-H), 7.16 (d, 1H, $^3J_{5,4}$ = 8.2 Hz, 5-H), 5.43 (s, 1H, 26-H, Enol), 4.13 (t, 2H, $^3J_{10,11}$ = 7.5 Hz, 10-H), 3.53 (s, 2H, 26-H, Keto), 3.32 (m, 4H, 14- and 1"-H), 2.45 (t, 2H, $^3J_{24,23}$ = 7.4 Hz, 24-H, Keto), 2.20 (m, 2+3H, 24-H, Enol and 28-H, Keto), 2.00 (s, 3H, 28-H, Enol), 1.67 (m, 2H, 11-H), 1.54 (m, 6H, 15-, 23- and 2"-H), 1.40 (tq, 2H, $^3J_{18,19}$ = 7.5 Hz, $^3J_{18,17}$ = 7.5 Hz, 12-H), 1.24 (m, 4H, 22- and 3"-H), 0.93 (t, 3H, $^3J_{19,18}$ = 7.3 Hz, 13-H), 0.83 (t, 3H, $^3J_{39,38}$ = 7.3 Hz, 4"-H), 0.41 (m, 4H, 16- and 21-H), 0.24 (s, 4H, 18- and 19-H), -0.14 (s, 6H, 17-CH_3) overlapping with -0.15 (s, 6H, 20-CH_3).

^{13}C-NMR ($CDCl_3$, 75.4 MHz) δ (ppm) = 204.17 (25-C, Keto), 202.10 (27-C, Keto), 194.19 (25-C, Enol), 191.30 (27-C, Enol), 164.52 (1-C), 164.00 (3-C), 155.40 (6-C), 131.94 (4-C), 130.90 (9-C), 130.76 (7-C), 130.21 (9a-C), 126.95 (9b-C), 124.93 (6a-C), 123.14 (8-C), 116.56 (5-C), 115.32 (3a-C), 99.63 (26-C, Enol), 57.82 (26-C, Keto), 57.04 (14-C), 53.24 (1"-C), 43.43 (24-C, Keto), 39.90 (10-C), 37.87 (24-C, Enol), 30.78 (23-C, Keto), 30.19 (2"-C), 29.45 (11-C), 29.12 (23-C, Enol), 27.14 (28-C, Keto), 24.87 (28-C, Enol), 23.52 (22-C), 21.42 (15-C), 20.32 (12-C), 20.26 (3"-C), 14.33 (21-C), 13.79 (13- and 4"-C), 11.88 (16-C), 7.01 (18-C), 6.96 (19-C), -4.07(17- and 20-CH_3).

IR $\tilde{\nu}$ = 2956, 2930, 2870, 1694, 1656, 1587, 1462, 1427, 1392, 1355, 1249, 1087, 832 cm^{-1}.

MS (EI, 70 eV): m/z (%) 510.4 (16) [M^+]; 467.3 (6) [M – $CH_2CH_2CH_3^+$] 337.2 (100) [M – $(CH_2)_2SiMe_2(CH_2)_2SiMe_2H^+$].

Tetra-acacH-dendrimer (46)

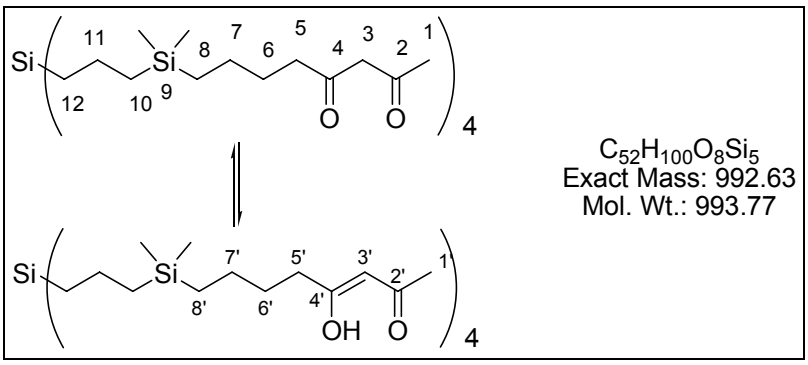

$Si(CH_2CH_2CH_2SiMe_2H)_4$ (182 mg, 0.42 mmol, 1 eq.), allyl-acacH (298 mg, 2.12 mmol, 5.1 eq.) and the Pt-cat. solution (50 µl) were stirred in toluene (5 ml) under nitrogen atmosphere at 60°C for 2 days. Then the mixture was evaporated, taken up on silica gel and purified *via* column chromatography using isohexane:ethyl acetate 5:1. Yield: 113 mg, 0.112 mmol, 27%.

^{1}H-NMR ($CDCl_3$, 300 MHz, samples contains signals of impurities at δ = 0.85, 0.07 and -0.02 ppm) δ (ppm) = 15.45 (s , 4H, 4'-OH), 5.44 (s, 4H, 3'-H), 3.52 (s, 8H, 3-H), 2.45 (t, 8H, $^3J_{5,6}$ = 7.3 Hz, 5-H), 2.22 (t, 8H, $^3J_{5,6}$ = 8.3 Hz, 5'-H), 2.06 (s, 16H, 1-H), 2.00 (s, 16H, 1'-H), 1.54 (m, 8H, ^3J = 7.5 Hz, 6-CH_2), 1.25 (m, 16H, 7- and 11-H), 0.47 (m, 24H, 8-, 10- and 12-H), -0.10 (s, 24H, Si-CH_3).

^{13}C-NMR ($CDCl_3$, 75.4 MHz, spectrum contains signals of impurities at δ = 52.87, 35.69, 33.81, 28.52, 21.80, 15.12 and 14.11) δ (ppm) = 204.16 (4-C), 202.07 (2-C), 194.14 (4'-C), 191.38 (2'-C), 99.63 (3'-C), 57.81 (3-C), 43.50 (5-C), 37.92 (5'-C), 30.78 (6-C), 29.52 (6'-C), 27.18 (1-C), 24.92 (1'-C), 23.61 (7'-C), 23.41 (7-C), 20.58 (11-C), 20.15 (11'-C), 18.48 (10- and 10'-C), 17.46 (12- and 12'-C), 15.56 (8-C), 15.18 (8'-C), -3.39 (Si-CH_3).

MS (CI, NH_3 130 eV): *m*/*z* (%): 1010.6 (19) [M + NH_4^+], 993.6 (35) [M + H^+], 851.5 (50) [M – $(CH_2)_4(CO)CH_2(CO)CH_3$ – H^+], 199.0 (100) [$Me_2Si(CH_2)_4(CO)CH_2(CO)CH_3^+$].

Donor-Allyl-PG (48)

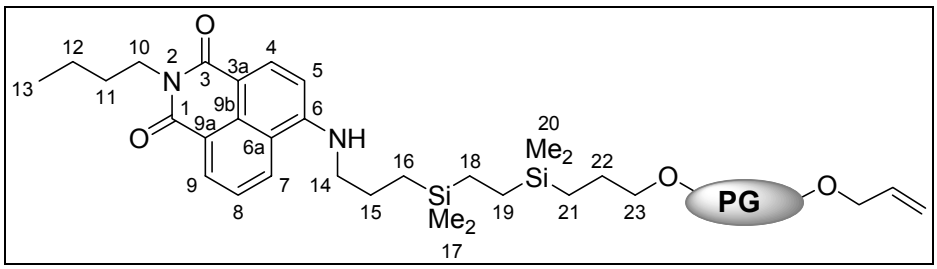

$D_{63\%}$-Allyl-PG: Allyl-PG (59 mg, 0.52 mmol based on allyl units, 1 eq.), **42a** (216 mg, 0.48 mmol, 0.92 eq.) and the Pt-cat. solution (50µl) were dissolved in CH_2Cl_2 (10 ml) under argon. The solution was refluxed for 18 h. Then the solvent was evaporated and the residue was taken up on toluene:acetone (10 ml, 3:1) and precipitated into MeOH (80 ml). The precipitation was repeated twice by precipitating from CH_2Cl_2 solution into MeOH. Yield: 187 mg, 90% assuming a degree of loading of 63%.

^{1}H-NMR ($CDCl_3$, 300 MHz) δ (ppm) = 8.45 (1H, 9-H), 8.34 (1H, 7-H), 8.16 (1H, 4-H), 7.46 (1H, 8-H), 6.58 (1H, 5-H), – 5.60 (CH_2-C*H*=CH_2 + NH), 5.25 – 5.00 (2H, CH_2-CH=C*H*$_2$), 4.10 (2H, *J* = Hz,), 3.97 (2 + 2H, C*H*$_2$-CH=CH_2 + 10-H), 3.80 – 3.00 (5 + 2H, PG-backbone + 14-H), 1.65 (4H, 15- and 11-H), 1.45 (2H, 22-H), 1.36 (2H, 12-H), 0.88 (3H, 13-H), 0.57 (2H, 16-H), 0.45 – 0.15 (6H, 18-, 19- and 21-H), -0.13 (12H, 17- and 20-CH_3).

^{13}C-NMR ($CDCl_3$, 75.4 MHz) δ (ppm) = 164.59 (1-C), 164.05 (3-C), 149.60 (6-C), 135.30 (-*C*H=CH_2), 134.80 (-*C*H=CH_2), 134.34 (4-C), 130.93 (9-C), 129.74 (9a-C), 126.22 (7-C), 124.38 (9b-C), 122.85 (6a-C), 120.14 (8-C), 116.70 (-CH=*C*H$_2$), 109.77 (3a-C), 104.05 (5-C), 78.59 , 77.82 , 74.61 , 73.56 , 72.23 , 71.84 , 71.62 , 71.27 , 70.25 (PG-backbone + 23-C), 46.88 (14-C), 39.89 (10-C), 30.28 (11-C), 24.47 (22-C on secondary OR), 24.04 (22-C on primary OR), 23.40 (15-C), 20.37 (12-C), 13.85 (13-C), 12.12 (16-C), 10.53 (21-C), 6.99 (18- and 19-C), -4.04 (Si-CH_3).

$D_{25\%}$-Allyl-PG: Allyl-PG (151 mg, 1.31 mmol, 1 eq.), **42a** (150 mg, 0.33 mmol, 0.25 eq.) and the Pt-cat. solution (100 µl) were dissolved in CH_2Cl_2 (5 ml) under an argon atmosphere. The solution was refluxed for 18 h and evaporated. The residue was purified *via* ultrafiltration in toluene and acetone. Yield 227 mg, 76% assuming a degree of loading of 25%.

$D_{3\%}$-Allyl-PG: This compound was synthesized analogously. The purification consisted in dialysis in $CHCl_3$.

^{1}H-NMR ($CDCl_3$, 300 MHz) δ (ppm) = 8.53 (1H, 9-H), 8.40 (1H, 7-H), 8.06 (1H, 4-H), 7.54 (1H, 8-H), 6.66 (1H, 5-H), 5.85 (1H, CH_2-C*H*=CH_2 + NH), 5.32 – 4.99 (2H, CH_2-CH=C*H*$_2$),

4.15 – 3.90 (2 + 2H, C*H*$_2$-CH=CH$_2$ + 10-H), 3.90 – 2.99 (5 + 2H, PG-backbone + 14-H), 1.80 – 1.05 (2H, 15-, 11-, 22- and 12-H), 0.91 (3H, 13-H), 0.62 (2H, 16-H), 0.50 – 0.26 (6H, 18-, 19- and 21-H), -0.04 (6H, 17-CH$_3$), -0.09 (6H, 20-CH$_3$).

^{13}C-NMR ($CDCl_3$, 75.4 MHz) δ (ppm) = 164.57 (1-C), 164.02 (3-C), 149.32 (6-C), 135.15 (-*C*H=CH$_2$), 134.68 (-*C*H=CH$_2$), 134.35 (4-C), 130.92 (9-C), 129.75 (9a-C), 125.80 (7-C), 124.48 (9b-C), 123.13 (6a-C), 120.08 (8-C), 116.64 (-CH=*C*H$_2$), 109.97 (3a-C), 104.16 (5-C), 78.78 , 77.24 , 72.18 , 71.72 , 71.58 , 71.28 , 70.15 (PG-backbone + 23-C), 46.81 (14-C), 39.84 (10-C), 30.21 (11-C), 24.45 (22-C on secondary OR), 23.98 (22-C on primary OR), 23.51 (15-C), 20.32 (12-C), 13.78 (13-C), 12.10 (16-C), 10.47 (21-C), 7.01 (18- and 19-C), -4.07 (Si-CH$_3$).

4,4'-Dicarboxy-2,2'-bipyridine dimethyl ester (54)

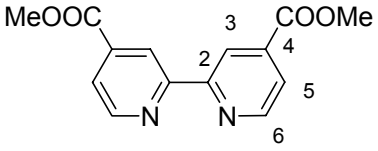

$C_{14}H_{12}N_2O_4$
Exact Mass: 272.0797
Mol. Wt.: 272.2561
C, 61.76; H, 4.44; N, 10.29; O, 23.51

This compound was synthesized according to literature procedures.[72] Yield: 89% based on recovered starting material.

^{1}H-NMR ($CDCl_3$, 300 MHz) δ (ppm) = 8.93 (m, 2H, 3-H), 8.83 (d, 2H, $^3J_{6,5}$ = 4.9 Hz, 6-H), 7.87 (dd, 2H, $^3J_{5,6}$ = 4.9 Hz, $^4J_{5,3}$ = 1.72 Hz, 5-H), 3.97 (s, 3H, COOCH$_3$). ^{13}C-NMR ($CDCl_3$, 75.4 MHz) δ (ppm) = 165.58 (COOCH$_3$), 156.45 (2-C), 150.11 (6-C), 138.56 (4-C), 123.21 (3-C), 120.52 (5-C), 52.72 (COOCH$_3$).

MS (EI): m/z (%) 272.1 (10) [M]$^+$, 241.2 (7) [M - CH$_3$O]$^+$, 214.2 (100) [M - CO$_2$Me]$^+$, 183.1 (5) [M - CO$_2$Me - CH$_3$O]$^+$, 155.2 [M-2x(CO$_2$Me)]$^+$.

Anal. Cald. for $C_{14}H_{12}N_2O_4$: C, 61.76; H, 4.44; N, 10.29. Found: C, 61.59; H, 4.62; N 10.26.

8-Trimethylsilyloct-7-yne-2,4-dione (55)

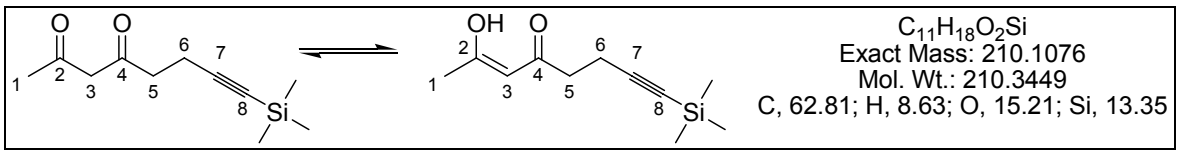

This compound was synthesized according to publishe procedures.[53] Work-up *via* column chromatography led to a yield of 78%.

^{1}H-NMR ($CDCl_3$, 300 MHz) δ (ppm) = 15.28 (s, 0.76H, -OH), 5.51 (s, 0.78H, =CH-), 3.58 (s, 0.31H, CO-CH_2-CO), 2.73 (t, 0.33H, ^3J = 7.3 Hz, -CO-CH_2CH_2 keto-form), 2.49 (s, 3.67H, -CO-CH_2CH_2 enol-form and -CO-CH_2CH_2 keto-form), 2.22 (s, 0.44H, CH_3-CO keto-form), 2.04 (s, 2.36H, CH_3-CO enol-form), 0.12 (s, 9H, Si-CH_3).

^{13}C-NMR ($CDCl_3$, 75.4 MHz) δ (ppm) = 201.9 (4-C, enol), 201.5 (2-C, enol), 192.0 (4-C, keto), 190.5 (2-C, keto), 105.2 (8-C, enol), 105.0 (8-C, keto), 99.9 (3-C, enol), 85.4 (7-C, enol), 85.3 (7-C, keto), 57.7 (3-C, keto), 42.4 (5-C, keto), 37.2 (5-C, enol), 30.7 (1-C, keto), 24.6 (1-C, enol), 15.9 (6-C, enol), 14.2 (6-C, keto), -0.1 (Si-*C*H_3).

GC/MS (CI, NH_3, 130 eV): *m*/*z* (%) = 228.1 (17) [M + NH_3^+]; 211.1 [M + H^+]; 195.1 [M – CH_3^+].

Anal. Cald. for $C_{11}H_{18}O_2Si$: C, 62.81; H, 8.63. Found: C,62.66; H, 8.50.

IR $\tilde{\nu}$ = 2960, 2901, 2177, 1709, 1618, 1422, 1359, 1250, 1208, 1135, 1046, 1012, 956, 890, 844, 760, 699, 639, 552, 508 cm^{-1}.

Dichloro-ruthenium(II)-bis-4,4'-dicarboxy-2,2'-bipyridine (56)

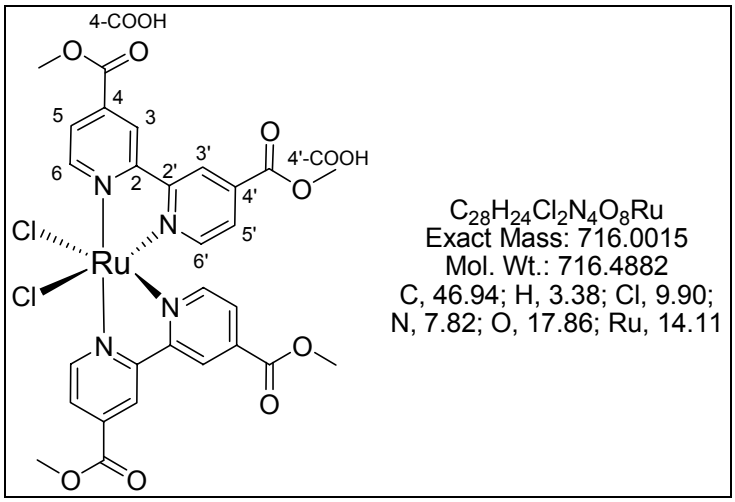

Di-Me-dcbpy **54** (4.26 g, 15.6 mmol, 2.1 eq.) and $RuCl_3$ (36% Ru, 2.12 g, 7.54 mmol, 1 eq.) was refluxed in ethanol (200 ml) under a nitrogen atmosphere for 18 h. The reaction mixture

was cooled to room temperature and filtered through a sintered glass crucible (G4). The residue was dried to give the pure title compound.[73] Yield: 5.25 g, 7.33 mmol, 97%.

^{1}H-NMR ($CDCl_3$, 300 MHz, spectrum contained signals of traces of the ethyl ester derivative of the title compound) δ (ppm) = 10.42 (d, 2H, $^3J_{6,5}$ = 5.8 Hz, 6-H), 8.82 (d, 2H, $^4J_{3,5}$ = 1.1 Hz, 3-H), 8.65 (d, 2H, $^4J_{3',5'}$ = 1.1 Hz, 3'-H), 8.15 (dd, 2H, $^3J_{5,6}$ = 5.9 Hz, $^4J_{5,3}$ = 1.4 Hz, 5-H), 7.68 (d, 2H, $^3J_{6',5'}$ = 5.8 Hz, 6'-H), 7.47 (dd, 2H, $^3J_{5',6'}$ = 5.9 Hz, $^4J_{5',3'}$ = 1.4 Hz, 5'-H), 4.09 (s, 6H, J = Hz, $COOCH_3$), 3.94 (s, 6H, J = Hz, $COOCH_3$).

The measurement of a ^{13}C-NMR spectrum was not possible due to the aggregation of the compound in $CHCl_3$.

MS (ESI, 4.5 kV): m/z (%) = 715.9 (100) [M^+].

Ruthenium(II)-bis-4,4'-dicarboxy-2,2'-bipyridine-acetylacetonato chloride (14)

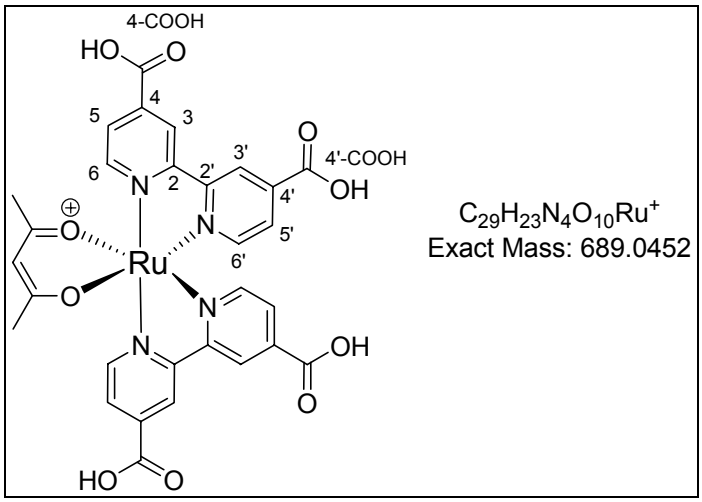

This compound was synthesized according to published procedures.[51] Yield: 11%.

^{1}H-NMR (D_2O/NaOD, 300 MHz, TPS-standard, spectrum contains one signal of an impurity at δ = 3.37 PPM) δ (ppm) = 8.91 (s, 2H, 3-H), 8.81 (d , 2H, $^3J_{6,5}$ = 5.8 Hz, 6-H), 8.75 (s, 2H, 3'-H), 8.02 (dd, 2H, $^3J_{5,6}$ = 5.8 Hz, $^4J_{5,3}$ = 1.5 Hz, 5-H), 7.85 (d, 2H, $^3J_{6',5'}$ = 6.0 Hz, 6'-H), 7.44 (dd, 2H, $^3J_{5',6'}$ = 6.0 Hz, $^4J_{5',3'}$ = 1.5 Hz, 5'-H), 5.61 (s, 1H, J = Hz, Alkene-H), 1.94 (s, 6H, CH_3), 1.86 (m, 6H, CDH_2, CD_2H).

^{13}C-NMR (D_2O/NaOD, 75.4 MHz) δ (ppm) = 191.22 (Me-*C*=O), 174.53 (4-COOH), 174.39 (4'-COOH), 162.26 (4-C), 160.91 (4'-C), 156.55 (6'-C), 153.40 (6-C), 147.38 (2-C), 146.01 (2'-C), 128.12 (5-C), 127.20 (5'-C), 125.01 (3- and 3'-C), 103.67 (*C*H(COMe)$_2$).

MS (ESI, 4.5 kV): m/z (%) = 711.0 (7) [M + Na – H^+]; 689.0 (100) [M - Cl^+]; 242.2 (61) [dcpby – $2H^+$].

Ruthenium(II)-bis-4,4'-dicarboxy-2,2'-bipyridine-α-propargylacetylacetonato chloride (58)

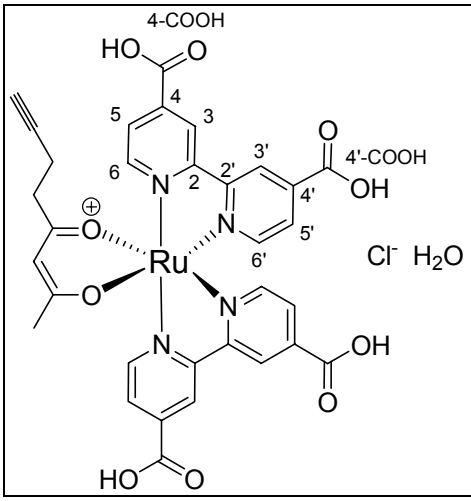

Complete compound:
$C_{32}H_{27}ClN_4O_{11}Ru$
Mol. Wt.: 780.1
C, 49.27; H, 3.49; Cl, 4.54;
N, 7.18; O, 22.56; Ru, 12.96

Cationic Complex:
$C_{32}H_{25}N_4O_{10}Ru^+$
Exact Mass: 727.0609

Procedure in MeOH: [Ru(di-Me-dcbpy)$_2$Cl$_2$] (1.00 g, 1.40 mmol, 1 eq.) and 8-trimethylsilyl-oct-7-yne-2,4-dione (0.44 g, 2.09 mmol, 1.5 eq.) were placed in a flask with MeOH (abs., 200 ml). This mixture was purged with argon for 10 min and then heated under reflux for 90 min. Then a solution KO*t*Bu (168 mg, 1.50 mmol, 1.1 eq.) in MeOH (5 ml) was added and the reaction mixture was stirred under reflux for another 1.5 h. The resulting reaction mixture was slightly acidic, thus another portion of KO*t*Bu (168 mg, 1.50 mmol, 1.1 eq.) in MeOH (5 ml) was added and the reaction stirred for one more hour. The solvent was removed *in vaccuo* and the residue was taken up in NaOH (20 ml, 1M). The resulting deep red solution was eluted with water over Sephadex LH20. The individual fractions collected on elution were characterized *via* UV-Vis spectroscopy in alkaline water and the fractions containing the product were unified and titrated to a pH of 2 with diluted HCl. It turned out that the title compound eluted last from the column. Yield: 597 mg, 1.28 mmol, 55%.

^{1}H-NMR (D$_2$O/NaOD, 300 MHz) δ (ppm) = 8.90 (d, 2H, $^4J_{3,5}$ = 1.3 Hz, 3-H), 8.87 (d, 2H, $^4J_{3,5}$ = 1.3 Hz, 3-H), 8.83 (d, 2H, $^3J_{6,5}$ = 5.8 Hz, 6-H), 8.79 (d, 2H, $^3J_{6,5}$ = 5.6 Hz, 6-H), 8.75 (d, 2H, $^4J_{3',5'}$ = 1.5 Hz, 3'-H), 8.72 (d, 2H, $^4J_{3',5'}$ = 1.3 Hz, 3'-H), 7.98 (dd, 2H, $^3J_{5,6}$ = 5.8 Hz, $^4J_{5,3}$ = 1.3 Hz, 5-H), 7.91 (d, 2H, $^3J_{6',5'}$ = 5.8 Hz, 6'-H), 7.82 (d, 2H, $^3J_{6',5'}$ = 5.8 Hz, 6'-H), 7.43 (dd, 2H, $^3J_{5',6'}$ = 5.8 Hz, $^4J_{5',6'}$ = 1.7 Hz, 5'-H) overlapping with 7.41 (dd, 2H, $^3J_{5',6'}$ = 5.8 Hz, $^4J_{5',6'}$ = 1.7 Hz, 5'-H), 5.63 (s, 1H, Alkene-H), 2.35 – 2.11 (m, 4H, CH_2CH_2), 1.91 (s, 3H, CH_3).

^{13}C-NMR (D$_2$O/NaOD, 75.4 MHz) δ (ppm) = 191.92 (Me-*C*O-), 191.54 (CH_2-*C*O-), 174.56 (COOH), 174.49 (COOH), 174.41 (COOH), 162.23 (4'-C), 160.91 (4-C), 160.89 (4-C), 156.73 (6'-C), 156.63 (6'-C), 153.59 (6-C), 153.49 (6-C), 147.45 (2-C), 147.43 (2-C), 146.05

(2'-C), 146.02 (2'-C), 128.17 (5-C), 128.04 (5-C), 127.20 (5'-C), 127.07 (5'-C), 125.02 (3-C), 124.96 (3'-C), 103.66 (Me-CO-*C*H), 85.92 (*C*≡CH), 51.72 (*C*H_2-CO), 18.54 (*C*H_2-C≡CH).

Anal. Cald. for $C_{32}H_{25}ClN_4O_{10}Ru \cdot H_2O$: C, 49.27; H, 3.49; N, 7.18. Found: C, 49.38; H, 3.48; N 7.06.

UV-Vis (0.1M NaOH/): λ_{max} (*A*) = 309 (1.967), 381 (0.571), 515 nm (0.5).

IR $\tilde{\nu}$ = 3427, 3305, 3109, 2923, 2853, 2616, 2501, 2114, 1938, 1696, 1602, 1547, 1513, 1462, 1435, 1404, 1311, 1256, 1234, 1130, 1017, 895, 772, 684, 469 cm^{-1}.

MS (ESI, 4.0 kV): *m*/*z* (%) = 727.0 (100) [M - Cl^+].

Ruthenium(II)-bis-4,4'-dicarboxy-2,2'-bipyridine-α-allylacetylacetonato chloride (57)

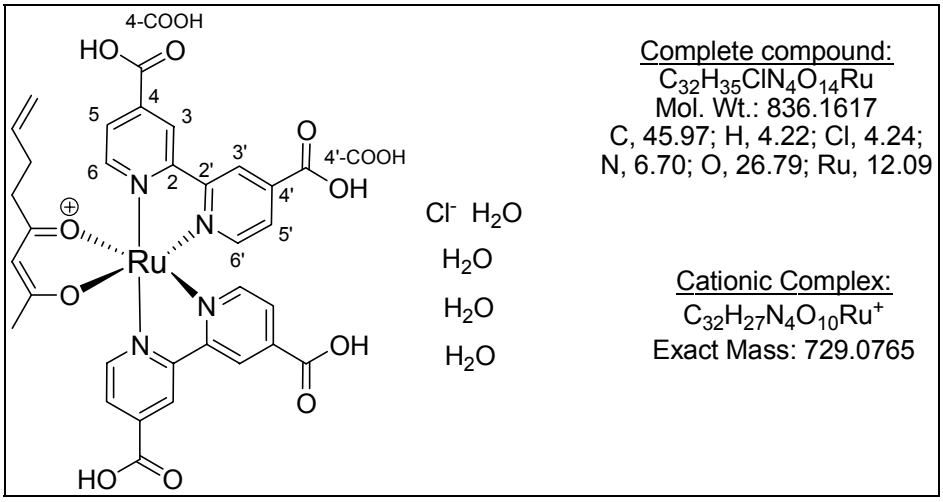

[Ru(dcbpy)$_2$Cl$_2$] (1.72 g, 2.61 mmol, 1 eq.), Na_2CO_3 (2.76 g, 26 mmol, 10 eq.), DMF (100 ml) and water (50 ml) were placed in a two-neck-flask with dropping funnel and strirred at 60°C. Oct-7-ene-2,4-dione (0.51 g, 3.9 mmol, 1.5 eq.) in DMF (20 ml) were added dropwise to the reaction mixture. After completion of the addition the reaction mixture was stirred for 90 min at 60°C and for another 60 min at 100°C. The solvent mixture was removed *in vaccuo*. The remaining crude product was isolated by three column chromatography steps using water (twice) and a methanol water mixture (3:1) as eluents. The individual fractions were characterized by UV-Vis-spectroscopy and the fractions having identical absorption spectra were unified. The methanol from the basic methanolic solution containing the product was removed using a rotary evaporator and the remaining aq. solution was titrated with HCl. At a pH of 3.6, the formation of a precipitate begun. The solution was further titrated to a pH of 3. After storing the suspension at room temperature for 18 h the precipitate was isolated by filtration. The residue was washed with acetone and diethylether and dried to afford the title compound. Yield: 1.321 g, 1.73 mmol, 66%.

^{1}H-NMR (D_2O/NaOD, TPS-standard, 300 MHz) δ (ppm) = 8.90 (m, 2H, 3-H), 8.76 (m, 4H, 3'- and 6-H), 8.00 (m, 2H, 5-H), 7.93 (d, 1H, ^3J = 5.81 Hz, 6'-H), 7.82 (d, 1H, ^3J = 5.81 Hz, 6'-H), 7.43 (m, 2H, 5'-H), 5.62 (s, 1H, Me-CO-CH), 5.30 (ddt, 1H, ^3J = 17.1 Hz, ^3J = 10.4 Hz, -C*H*=CH_2 ^3J = 6.5 Hz, -C*H*=CH_2), 4.56 (m, 2H, -CH=C*H*$_2$), 2.30 (m, 1H, CO-CH_2), 2.17 (m, 1H, CO-CH_2), 1.99 (m, 2H, C*H*$_2$-CH=CH_2), 1.91 (s, 3H, CH_3-CO).

^{13}C-NMR (D_2O/NaOD, TPS-standard, 75.4 MHz) δ (ppm) = 191.56 (Me-*C*O-), 189.37 (CH_2-*C*O-), 172.56 (4-COOH), 172.41 (4'-COOH), 160.19 (4'-C), 160.15 (4'-C), 158.89 (4-C), 154.73 (6'-C), 154.63 (6'-C), 151.60 (6-C), 151.34 (6-C), 145.40 (2-C), 145.38 (2-C), 144.02 (2'-C), 143.98 (2'-C), 137.65 (-*C*H=CH_2), 126.07 (5-C), 126.03 (5-C), 125.17 (5'-C), 125.04 (5'-C), 123.00 (3-C), 122.91 (3'-C), 115.66 (-CH=*C*H$_2$), 101.63 (Me-CO-*C*H), 40.30 (*C*H$_2$-CO-), 31.76 (*C*H$_2$-CH=CH_2),27.91 (*C*H$_3$-CO).

MS (ESI, 2.8 kV): *m*/*z* (%) = 729.1 (100) [M - Cl^+].

Anal. Cald. for $C_{32}H_{27}ClN_4O_{10}Ru \cdot 4\ H_2O$: C, 45.97; H, 4.22; N, 6.70. Found: C, 46.02; H, 4.00; N 6.86.

Ruthenium(II)-bis-4,4'-carboxy-2,2'-bipyridine-α-allylacetylacetonato chloride tetramethyl ester (35)

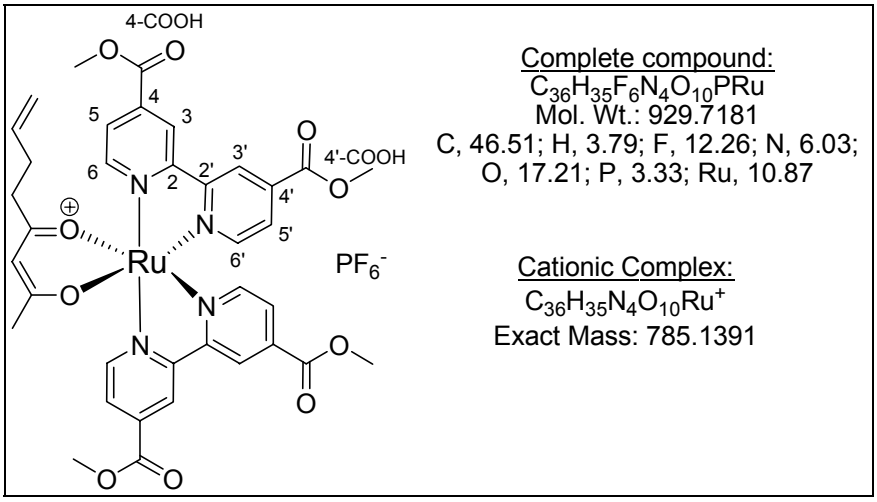

KOH (310 mg, 14.7 mmol, 20 eq.) was dissolved in DMSO (10 ml) and [Ru(dcbpy)$_2$allyl-acac]Cl (**57**) (0.565 g, 0.739 mmol, 1 eq.) was added. The reaction mixture was cooled to 0°C, upon which it solidified. Then CH_3I (0.946 g, 18.5 mmol, 25 eq.) were added and the mixture was allowed to warm to room temperature. After 3.5 h excessive CH_3I was removed *in vaccuo* and the reaction mixture was poured onto cold HCl (0.5 M, 400 ml). The resulting solution was extracted 5 times with CH_2Cl_2. A black organic phase and a reddish aq. phase resulted. From the aqueous phase some starting material (114 mg) was recovered *via* precipitation on acidification. The phases were separated and the organic phase was extracted

with saturated $NaHCO_3$. It was observed that the $NaHCO_3$-solution immediately became intensely red, pointing to the hydrolysis of the methyl ester in the slightly alkaline medium (*repetition of this extraction is thus not advised*). Then the organic phase was dried over $MgSO_4$ and the solvent was evaporated. The residue was eluted over a column comprising Sephadex LH20 using acetone/water (1:2) as eluent. The product did not elute properly and smeared over the column. Addition of NaCl to the eluent effectuated the elution of the $[Ru(dcbpy)_2allyl\text{-}acac]^+$-species. The acetone was distilled off from the solution and addition of KPF_6 (544 mg) lead to a black precipitate which was collected on a filter, taken up in acetone and transferred to a flask and dried to afford 0.227 g of the title compound. Yield: 0.227 g, 0.244 mmol, 41% based on recovered starting material.

^{1}H-NMR (Acetone-d_6, 300 MHz, spectrum contains signals of impurities at δ = 2.64 and 1.24 ppm) δ (ppm) = 9.30 (m, 2H, 3-H), 9.17 (m, 2H, 3'-H), 9.07 (d, 1H, $^3J_{6,5}$ = 6.0 Hz, 6-H) overlapping with 9.04 (d, 1H, $^3J_{6,5}$ = 6.0 Hz, 6-H), 8.35 – 8.20 (m, 4H, 5- and 6'-H), 7.71 (m, 2H, 5'-H), 5.56 (s, 1H, Me-CO-C*H*), 5.48 (m, 1H, -C*H*=CH_2), 4.80 – 4.66 (m, 2H, -CH=CH_2), 4.12 (s, 6H, 4-$COOCH_3$), 4.00 (s, 3H, 4'-$COOCH_3$) overlapping with 4.00 (s, 3H, 4'-$COOCH_3$), 2.35 – 2.00 (m, 4H, CO-CH_2CH_2-), 1.92 (s, 3H, CO-CH_3).

^{13}C-NMR (Acetone-d_6, 75.4 MHz) δ (ppm) = 190.37 (Me-*C*O-), 188.69 (CH_2-*C*O-), 165.20 (4-COO), 165.15 (4-COO), 164.97 (4'-COO), 164.94 (4'-COO), 160.57 (4'-C), 160.54 (4'-C), 159.13 (4-C), 155.44 (6-C), 155.36 (6-C), 152.28 (6'-C), 152.09 (6'-C), 138.73 (2-C), 138.22 (2'-C), 137.25 (-*C*H=CH_2), 126.42 (3-C), 126.37 (3-C), 125.27 (3'-C), 125.15 (3'-C), 123.72 (5-C), 123.67 (5-C), 123.59 (5'-C), 123.54 (5'-C), 115.12 (-CH=*C*H_2), 100.52 (Me-CO-*C*H), 53.71 (4-COO*C*H_3), 53.54 (4'-COO*C*H_3), 40.33 (*C*H_2-CO-), 31.02 (*C*H_2-CH=CH_2), 28.06 (*C*H_3-CO).

MS (ESI, 5.0 kV): *m*/*z* (%) = 785.0 (100) $[(M - PF_6^-)^+]$.

Donor Acceptor Dyad (45)

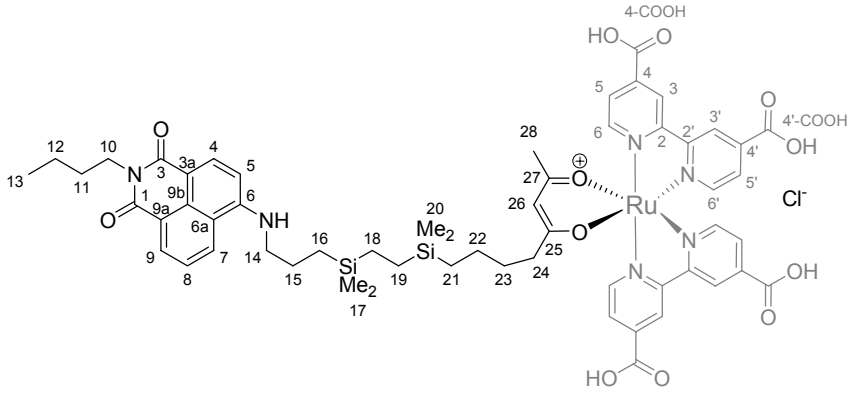

$C_{57}H_{65}ClN_6O_{12}RuSi_2$
Exact Mass: 1218.2931
Mol. Wt.: 1218.853
C, 56.17; H, 5.38; Cl, 2.91; N, 6.90;
O, 15.75; Ru, 8.29; Si, 4.61

By hydrosilylation: **35b** (30 mg, 32 mmol, 1 eq.), **42a** (16 mg, 35 mmol, 1.1 eq.) and the Pt-cat. solution (10 µl, 0.03 eq.) were refluxed for 20 h in CH_2Cl_2 (8 ml). Then the solvent was evaporated and the residue was taken up in a mixture of acetone and diluted NaOH. The resulting solution was loaded onto Sephadex LH20 and the product was eluted with water. The product containing fraction had a pH of 10.4 after the chromatography. It was acidified to pH = 2.0 with diluted HCl upon which the precipitation of the product occurred which was islolated by centrifugation and drying. Yield: 7 mg, 5.7 µmol, 18%.

Butyl acacH fluorol (**44a**, 108 mg, 0.0182 mmol 1 Eq.) was dissolved in MeOH abs. (20 ml) and KO*t*Bu (25 mg, 0.228 mmol, 1.25 Eq.) was added as a solid and the mixture was heated under reflux. In a separate vessel, [Ru(di-Me-dcbpy)$_2$Cl$_2$] (143 mg, 0.200 mmol, 1.1 Eq. were dissolved in DMF abs. (10 ml). This solution was added to the reaction mixture in several portions over 7 h. Then, NaOH aq. (1M, 1.5 ml) was added and the solvents were evaporated. The residue was dissolved in water and eluted over Sephadex LH 20. The combined fractions containing the product were concentrated *in vaccuo* and titrated to a pH of 2 with diluted HCl. Upon acidification, a precipitate formed, which was isolated by centrifugation. This procedure yielded the desired compound, which still contained mostly NaCl. A second chromatography step was carried out over Sephadex LH 20 in NaOH/MeOH. The combined fractions containing the product were dried, dissolved in water and titrated to a pH of 2 with diluted HCl. Upon acidification, a precipitate formed, which was isolated by centrifugation. The precipitate was taken up in MeOH and dried *in vaccuo* to yield the analytically pure product (38 mg, 0.0312 mmol, 17%).

^{1}H-NMR (MeOD/NaOD, 300 MHz) δ (ppm) = 9.00 (s, 2H, 3-bpy-H), 8.85 (s, 2H, 3'-bpy-H), 8.70 (m, 2H, 6-bpy-H), 8.49 (d, 1H, $^3J_{9,8}$ = 8.38 Hz, 9-H), 8.39 (d, 1H, $^3J_{7,8}$ = 7.31 Hz, 7-H), 8.23 (d, 1H, $^3J_{4,5}$ = 8.6 Hz, 4-H), 8.07 (m, 2H, 5-bpy-H), 7.75 (m, 2H, 6'-bpy-H), 7.57 (m, 3H,

8- and 5'-bpy-H), 6.65 (d, 1H, $^3J_{5,4}$ = 8.6 Hz, 5-H), 5.34 (s, 1H, 26-H), 4.05 (t, 2H, $^3J_{10,11}$ = 7.4 Hz, 10-H), 3.39 (t, 2H, $^3J_{14,15}$ = 6.9 Hz, 14-H), 1.90 (m, 2H, 24-H), 1.80 (s, 3H, 28-H), 1.68 (m, 2H, 15-H), 1.60 (m, 2H, 11-H), 1.35 (m, 2H, 12-H), 1.11 (m, 2H, 23-H), 0.92 (m, 5H, 22- and 13-H), 0.62 (m, 2H, 16-H), 0.3 – 0.1 (m, 6H, 19- 18- and 21-H), –0.08 (s, 6H, 17-CH_3), –0.28 (s, 6H, 20-CH_3).

^{13}C-NMR (MeOD/NaOD, 100 MHz) δ (ppm) = 192.15 (25-C), 188.44 (27-C), 171.27 (COOH), 171.14 (COOH), 171.12 (COOH), 166.63 (1-C), 166.06 (3-C), 161.04 (4-bpy-C), 161.02 (4-bpy-C), 159.85 (4'-bpy-C), 159.74 (4'-bpy-C), 154.39 (6'-bpy-C), 154.29 (6'-bpy-C), 153.01 (6-C), 151.54 (6-bpy-C), 151.43 (6-bpy-C), 147.77 (2'-bpy-C), 147.75 (2'-bpy-C), 146.16 (2-bpy-C), 146.15 (2-bpy-C), 136.39 (4-C), 132.59 (7-C), 131.68 (9-C), 129.86 (9a-C), 126.82 (5-bpy-C), 126.79 (5-bpy-C), 126.07 (5'-bpy-C), 126.01 (5'-bpy-C), 125.74 (8-C), 123.79 (3-bpy + 3'-bpy-C), 123.63 (6a-C), 122.19 (9b-C), 109.29 (3a-C), 105.41 (5-C), 100.88 (26-C), 47.75 (14-C), 41.09 (10-C), 32.28 (23-C), 31.71 (11-C), 24.79 (22-C), 24.17 (15-C), 21.66 (12-C), 15.44 (21-C), 14.56 (13-C), 13.01 (16-C), 8.41 (18-C), 8.26 (19-C), -3.48 (17- and 20-CH_3). Signals of 28- and 24-Cs are missing due to H-D-exchange. These signals appear, if one uses CH_3OH instead of CD_3OD as NMR-solvent at δ = 28.1 and 41.0 ppm, respectively.

IR $\tilde{\nu}$ = 3395 (br), 3080, 2954, 2928, 2873, 1723, 1684, 1639, 1609, 1580, 1552, 1515, 1467, 1433, 1400, 1328, 1248, 1020, 775 cm^{-1}.

UV-Vis (NaOH/MeOH): λ_{max} (ε) = 309 (52400), 439 (24100), 525 nm (13000 l mol^{-1} cm^{-1}).

MS (ESI): *m*/*z* (%): 1183.2 (100) [M^+ – Cl].

Anal. Cald. for $C_{57}H_{65}ClN_6O_{12}RuSi_2 \cdot H_2O$: C, 55.35; H, 5.46; Cl, 2.87; N, 6.79. Found: C, 55.27; H, 5.61; N 6.53.

Butyl-Dyad (59)

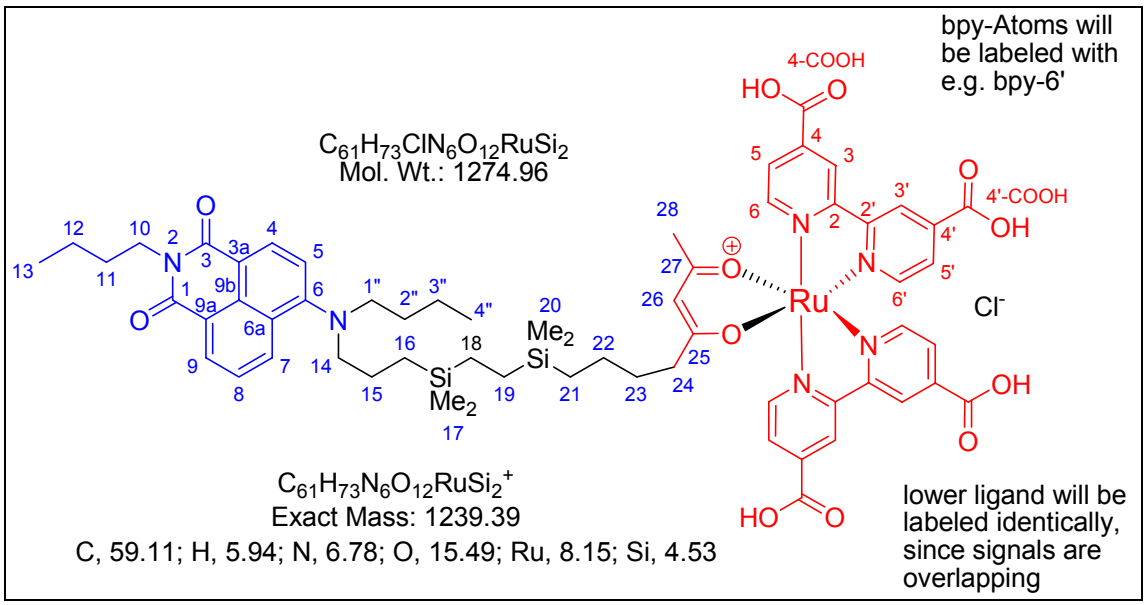

44b (0.167 g, 0.257 mmol, 1 eq.) and $[Ru(dcbpy)_2Cl_2]$ (0.433 g, 0.282 mmol, 1.1 equiv.) were dissolved in DMF/H_2O (2:1, 10 ml). Na_2CO_3 (0.269 g, 2.570 mmol, 10 equiv.) was added and the mixture was stirred under reflux for 2 h. Then, the solvent was evaporated. Workup and purification of the crude product in analogy to **45** afforded 17 mg (0.013 mmol, 5%) of the title compound.

^{1}H-NMR (MeOD, 400 MHz, spectrum contains one signal of an impurity at δ = 1.28 ppm) δ (ppm) = 9.02 (s, 2H, 3-bpy-H), 8.88 (s, 2H, 3'-bpy-H), 8.74 (m, 2H, 6-bpy-H), 8.50 (m, 2H, 9- and 7-H), 8.41 (d, 1H, $^3J_{4,5}$ = 8.2 Hz, 4-H), 8.07 (m, 2H, 5-bpy-H), 7.79 (m, 2H, 6'-bpy-H), 7.69 (dd, 1H, $^3J_{8,9}$ = 7.45 Hz, 8-H), 7.69 (dd, 1H, $^3J_{8,7}$ = 8.5 Hz, 8-H), 7.55 (m, 2H, 5'-bpy-H), 7.30 (d, 1H, $^3J_{5,4}$ = 8.2 Hz, 5-H), 5.40 (s, 1H, 26-H), 4.12 (t, 2H, $^3J_{10,11}$ = 7.5 Hz, 10-H), 3.42 (m, 4H, 14- and 1"-H), 1.99 (m, 2H, 24-H), 1.89 (s, 3H, 28-H), 1.61 (m, 8H, 10-, 11-, 2"- and 15-H), 1.40 (m, 2H, 12-H), 1.31 (m, 2H, 3"-H), 1.19 (m, 2H, 23-H), 0.95 (m, 5H, 22- and 13-H), 0.86 (t, 3H, $^3J_{4",3"}$ = 7.3 Hz, 4"-H), 0.48 (m, 2H, 16-H), 0.20 – 0.05 (m, 6H, 18-, 19- and 21-H), -0.15 (s, 6H, 17-CH_3), -0.30 (s, 6H, 21-CH_3).

^{13}C-NMR (MeOH/NaOD, 100 MHz) δ (ppm) = 192.19 (27-C), 188.47 (25-C), 171.30 (COOH), 171.18 (COOH), 171.15 (COOH), 171.13 (COOH), 166.32 (1-C), 165.87 (3-C), 161.05 (4-bpy-C), 159.86 (4'-bpy-C), 159.77 (4'-bpy-C), 157.52 (6-C), 154.39 (6'-bpy-C), 154.30 (6'-bpy-C), 151.54 (6-bpy-C), 147.78 (2'-bpy-C), 147.73 (2'-bpy-C), 146.15 (2-bpy-C), 133.66 (4-C), 132.83 (9-C), 132.60 (7-C), 131.84 (9a-C), 128.56 (9b-C), 126.83 (5-bpy-C), 126.59 (8-C), 126.09 (5'-bpy-C), 126.05 (5'-bpy-C), 124.39 (6a-C), 123.81 (3- and 3'-bpy-C),

118.35 (5-C), 116.19 (3a-C), 100.87 (26-C), 57.68 (1"-C), 55.50 (14-C), 41.22 (10-C), 32.31 (11-C), 31.68 (15-C), 31.07 (28-C), 31.04 (28-C), 30.91 (2"-C), 24.88 (23-C), 24.02 (22-C), 22.94 (3"-C), 21.66 (12-C), 15.37 (21-C), 14.58 (13-C), 14.51 (4"-C), 12.98 (16-C), 8.31 (18-C), 8.13 (19-C), -3.49 (Si-Me), -3.56 (Si-Me), -3.57 (Si-Me).

IR $\tilde{\nu}$ = 3425 (br), 3087, 2953, 2925, 2869, 1760, 1722, 1651, 1585, 1568, 1514, 1465, 1404, 1382, 1331, 1308, 1256, 1228, 1018, 829, 779 cm^{-1}.

UV-Vis (NaOH/EtOH): λ_{max} (nm) [ε (l mol^{-1} cm^{-1})] = 310 (50600), 385 (15300), 527 (12200).

UV-Vis (EtOH): λ_{max} (nm) [ε (l mol^{-1} cm^{-1})] = 313 (46200), 421 (19100), 527 (12200)

Allylated Polyglycerol (47)

$PG_{TMP,\ 5000}$ (10 g, 135 mmol, 1 eq.) and NaOH (27 g, 675 mmol, 5 eq.) were vigorously stirred in a mixture of water (50 ml) and toluene (135 ml) at 50°C until the reagents had dissolved. Tetrabutylammonium hydrogensulfate (4.58 g, 13.5 mmol, 0.1 eq.) was added and the mixture was stirred for 30 min. Subsequently allyl bromide (81.7 g, 675 mmol, 5 eq.) was added dropwise and the reaction mixture was stirred at 50°C for 24 h. Water and toluene were added, the phases were separated and the aq. phase was extracted with toluene three times. The combined organic extracts were dried over Na_2SO_4 and the solvent was removed *in vaccuo*. The crude product was purified *via* column chromatography on silica gel using isohexane/ethyl acetate (5:1) as eluent.

^{1}H-NMR ($CDCl_3$, 250 MHz, spectrum contains signal of impurities at δ = 2.78, 2.31, 1.97, 1.19 and 0.77 ppm) δ (ppm) = 5.83 (m, 1H, =CH-), 5.20 (m, 1H, CH_2=CH-), 5.08 (m, 1H, CH_2=CH), 4.07 (d, 2H, CH_2=CH-CH_2O), 3.93 (d, 2H, CH_2=CH-CH_2O), 3.7 – 3.3 (m, 5H, PG-backbone).

^{13}C-NMR ($CDCl_3$, 75.4 MHz) δ (ppm) = 135.14 (=CH-), 134.66 (=CH-), 116.66 (H_2C=), 116.56 (H_2C=), 116.43 (H_2C=), 78.76, 78.52, 77.24, 76.96, 72.14, 71.68, 71.55, 71.22, 71.16, 71.09, 70.17 (PG-Backbone).

IR $\tilde{\nu}$ = 3078, 2867, 1646, 1458, 1421, 1347, 1133, 1075, 996, 924 cm^{-1}.

Polyglycerol mesylates (63)

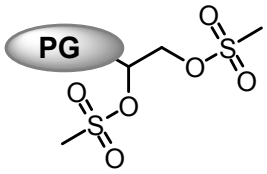

General procedure for the mesylation of hyperbranched polyglycerol (**d**: BO 539; **c**: BO 540; **b**: BO 553; **a** BO 565; **e** BO 564): PG_{5000}-TMP (**d**, **c,** **b** 4.0 g, 54 mmol; **a** 2.0 g, 27 mmol, 1 eq.; **e** 5.0 g; 68 mmol, 1 eq.) was dissolved in pyridine (abs. 35 ml) and cooled to -5°C. Methylsulfonyl chloride (**d**: 3.7 g, 32 mmol, 0.6 eq.; **c**: 2.5 g, 22 mmol, 0.4 eq; **b** 1.9 g, 16 mmol, 0.3 eq.; **a** 301 mg, 2.7 mmol, 0.1 eq.; **e** 8.5 g, 74 mmol, 1.1 eq.) were dissolved in pyridine (abs. 10 ml) and added dropwise to the polyglycerol solution such that the temperature stayed below 0°C. The reaction mixture was stirred overnight at room temperature. Then, the reaction mixture was poured onto ice and concentrated *in vaccuo*. In cases of **d** and **c** the residue was dialysed using acetone/water (7:3) yielding the mesylated polymer (**d**: 4.6 g, 71%; **c** 4.6 g, 81%). Otherwise, the residue was dried under high vacuum and used for the next reaction step without further purification.

Spectra from BO 541-2: ^{1}H-NMR (acetone-d_6, 250 MHz, spectrum contains signals of pyH^+) δ (ppm) = 5.10 – 3.35 (m, 6H, PG-backbone and –OH with peaks at δ = 5.06, 4.9, 4.78, 4.56, 4.44, 4.35, 4.29, 4.08, 3.94, 3.76, 3.63, 3.43, 3.33 ppm), 3.19 (s, 3H, CH_3), 1.48 (m, 2H, CH_2 from starter), 0.94 (m, 3H, CH_3 from starter).

^{13}C-NMR (acetone-d_6, 75.4 MHz, spectrum contains signals of pyridine, CH_3SO_3H and of impurities at δ = 109.56 and 105.25 ppm) δ (ppm) = 83.19, 81.17, 79.34, 77.94, 75.62, 75.51, 73.68, 73.13, 72.59, 72.34, 72.07, 71.57, 71.19, 70.53, 70.39, 70.04, 69.15, 68.9, 68.84, 67.24, 64.16, 62.31, 61.94 (PG-backbone), 38.79, 37.35 (Me).

BO 581: ^{1}H-NMR (DMSO-d_6, 250 MHz, spectrum contains signals of pyridine and CH_3SO_3H) δ (ppm) = 7.20 (d, 2H, Ar-H of initiator), 6.84 (d, 2H, Ar-H of initiator), 4.55 – 4.15 (m, CH_2O-SO_2-), 3.90 – 3.55 (PG-Backbone), 3.55 – 3.40 (m, 2H, CH_2OH), 3.23 (s, 3H, O-SO_2CH_3), 3.18 (s, 3H, O-SO_2CH_3).

^{13}C-NMR (DMSO-d_6, 75.4 MHz, spectrum contains signals of pyridine, CH_3SO_3H and of an impurity at δ = 44.66 ppm) δ (ppm) = 78.44, 76.99, 69.79, 68.46 (PG-backbone), 38.56 (Me).

Polyglycerol azides (62)

Representative procedure (BO 542): PG-OMs_{40} (4.4 g, 17 mmol OMs, 1 eq.) was dissolved in DMF (50 ml) and sodium azide (5.5 g, 85 mmol, 5 eq.) were added to the solution. The mixture was stirred for 3 days at 60°C. The reaction mixture was filtered in order to remove excessive azide and the filtrate was evaporated. The residue was taken up in MeOH and dialysed to yield 1.5 g PG-N_3.

BO 542: ^{1}H-NMR (MeOD; 250 MHz, spectrum contains the signal of MeOH) δ (ppm) = 4.0 – 3.2 (PG-Backbone), 1.42 (m, 2H, CH_2 from starter), 0.91 (m, 3H, CH_3 from starter).

^{13}C-NMR (MeOD; 75.4 MHz, spectrum contains the signal of MeOH) δ (ppm) = 81.69, 80.18, 74.27, 73.85, 73.19, 72.71, 72.48, 71.88, 71.32, 71.1, 71.01, 70.92, 64.75, 63.05 (PG-Backbone) 62.61, 62.42, (CH-N_3) 55.13, 53.18, 53.02 (CH_2N_3).

BO 582: ^{1}H-NMR (DMSO-d_6, 250 MHz, spectrum contains signals of DMF, CH_2Cl_2, H_2O, pyH^+ and signals of impurities at δ = 1.22 ppm) δ (ppm) = 7.20 (d, 2H, Ar-H of initiator), 6.84 (d, 2H, Ar-H of initiator), 3.90 – 3.20 (PG-Backbone).

^{13}C-NMR (DMSO-d_6, 75.4 MHz, spectrum contains signals of DMF, CH_2Cl_2, pyH^+ and signals of impurities at δ = 113.70, 34.79 and 29.99 ppm) δ (ppm) = 78.06, 78.02 (CHRO), 68.69 (CH_2O), 60.48, 60.43 (R_2CH-N_3 on terminal position), 51.07 (CH_2N_3).

$A_{\alpha Ru}$-PG-$N_{3,\ \alpha N3}$ (66)

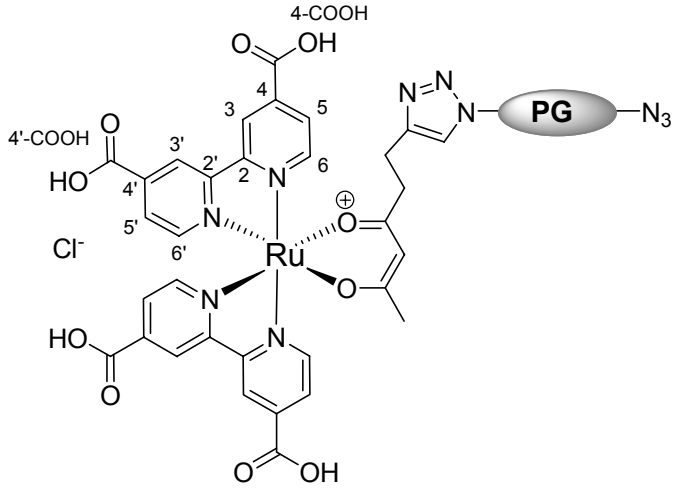

Series with varying acceptor ratio (**66e**, **c**, **b,** charge CS 233a - c): [Ru(dcbpy)$_2$propargyl-acac]Cl (260 mg) and Na_2CO_3 (225 mg) were dissolved in water (10 ml) and the pH of this solution was adjusted from 10.2 to 6.8 using HCl. PG_{5000}-$N_{3,\ 30\%}$ (292 mg) was dissolved in a mixture of water (15 ml) and DMF (3 ml). A clear solution resulted, which was divided into 3

equal portions (resulting in 3 batches containing 0.26 mmol N_3-groups, each). To these solutions the solution of the Ru-complex (**e.** 3775 µl, **c.** 2515 µl, **b.** 1885 µl corresponding to **e.** 0.5 eq., **c.** 0.33 eq. and **b.** 0.25 eq of Ru with respect to azide groups), $CuSO_4$ (0.1 M, **e.** 64 µl, **c.** 43 µl, **b.** 32 µl, corresponding to 0.05 eq. with respect to alkyne groups) and Sodium Ascorbate (0.35 M; **e.** 93 µl, **c.** 62 µl; **b.** 46 µl, corresponding to 0.25 eq. with respect to alkyne groups) was added. These solutions were stirred at room temperature in the dark for 6 days. Then, the mixture was loaded onto a column (diameter 5 cm, Sephadex LH20) and eluted with water. Two fractions were collected in each case (The volumes of the fraction 1: **e.** 100 ml; **c.** 125 ml; **b.** 100 ml; and fraction 2 **e.** 230 ml; **c.** 230 ml; **b.** 135 ml), which were characterized by UV-Vis-spectroscopy. Fraction 1 contained the polymer-bound Ru-complex, Fraction 2 [Ru(dcbpy)$_2$propargyl-acac]Cl. Acidifying the solutions to pH = 2 – 2.5 lead to the formation of a precipitate, however, with a deeply colored supernatant, pointing to incomplete precipitation. Precipitation from aqueous solution into methanol or acetone did not give complete precipitation either. Thus, the product was isolated *via* azeotropic distillation of the solvent with toluene and was likely to contain salts. Yield: **e.** 115 mg, **c.** 338 mg and **b.** 166 mg.

Series with varying N_3-loading (**66a**, **d**, **i, charge CS 233e, f, h**): [Ru(dcbpy)$_2$propargyl-acac]Cl (206 mg) and Na_2CO_3 (158 mg) were dissolved in water (7.1 ml) and the pH of this solution was adjusted to 6.2 using HCl. The polyglycerol azides (**a.** PG_{5000}-$N_{3,\ 10\%}$, 115.6 mg, 0.15 mmol N_3; **d.** PG_{5000}-$N_{3,\ 30\%}$, 71.4 mg, 0.26 mmol N_3; **i.** PG_{5000}-$N_{3,\ 100\%}$, 24 mg, 0.25 mmol N_3) were dissolved in **a.** a mixture of water (4 ml) and DMF (3.75 ml); **d.** in DMF (2 ml); and **i.** DMF (57 ml). To the solutions of the polymers, the solution of the Ru-complex (**a.** 4.20 ml, **d.** 7.30 ml, **i.** 6.99 ml corresponding to 0.4 eq. with respect to N_3-groups), $CuSO_4$ (0.1 M in H_2O, **a.** 30 µl, **d.** 52 µl, **i.** 50 µl corresponding to 0.05 eq. with respect to alkyne groups) and Sodium Ascorbate (0.211 M in H_2O, **a.** 72 µl, **d.** 124 µl, **i.** 119 µl, corresponding to 0.25 eq. with respect to alkyne groups) were added. Then the solutions were stirred at room temperature in the dark for 14 days. The mixtures were loaded onto a column (diameter 5 cm, Sephadex LH20, in case of reaction **i.** the solvent was evaporated prior to further work-up) and eluted with water. Two fractions were collected in each case (The volumes of the fraction 1: **a:** 100 ml; **d:** 100 ml; **i:** 130 ml; and fraction 2 **a:** 100 ml; **d:** 230 ml; **i:** 190 ml;), which were characterized by UV-Vis-spectroscopy. Fraction 1 contained the polymer-bound Ru-complex, Fraction 2 [Ru(dcbpy)$_2$propargyl-acac]Cl. The solvent of the first fraction of reactions **a.** and **d.** was removed in vacuo. To the first fraction of reaction **h.**, HCl was added until pH = 2, upon which a dense precipitate and a nearly colorless supernatant formed. The

products were further isolated *via* evaporation of the solvent and freeze-drying. Yield: **a.** 144 mg, **d.** 49 mg and **i.** 30 mg.

^{1}H-NMR (D_2O, 300 MHz) δ (ppm) = 8.89 (2H, 3-H), 8.74 (2H, 3'-H), 8.63 (3H, 6-H), 7.95 (2H, 5-H), 7.79 (2H, 6'-H), 7.43 (2H, 5'-H), 5.51 (1H, Alkene-H), 4.43 (2H, CH_2-N), 4.0 – 3.0 (5H, PG-backbone with peaks at δ = 4.15, 3.99, 3.88 and 3.62 ppm) 2.57 (4H, CO-C*H*$_2$-C*H*$_2$-$C_{Triazole}$), 1.81 (3H, CH_3-CO), 1.34 (2H, initiator-CH_2), 0.80 (3H, initiator-CH_3).

^{13}C-NMR (D_2O/NaOD, 75.4 MHz) δ (ppm) = 191.82 (Me-*C*O-), 191.33 (CH_2-*C*O-), 174.22 (COOH), 162.23 (4'-C), 161.05 (4-C), 160.87 (4-C), 156.65 (6'-C), 153.37 (6-C), 149.38 (quart. Triazole-C), 147.70 (2-C), 147.50 (2-C), 146.22 (2'-C), 128.36 (5-C), 127.47 (5'-C), 126.36 (tert. triazole-C), 125.20 (3- and 3'-C), 103.85 (Me-CO-*C*H), 82.74, 81.03, 75.28, 73.99, 73.75, 73.48, 72.19, 71.94, 65.73, 63.88 (PG-Backbone incl. remaining CH-N_3), 56.30, 55.77 (CH_2-N_3 and CH_2-$N_{Triazole}$), 46.21 (*C*H_2-CO-), 30.27 (*C*H_3-CO-), 25.05 (*C*H_2-$C_{Triazole}$).

UV-Vis (0.1M NaOH/H_2O): λ_{max} (*A*) = 312 (1.906), 386 (0.575), 519 nm (0.5).

D-A-PG-N_3 (64, 65, 67)

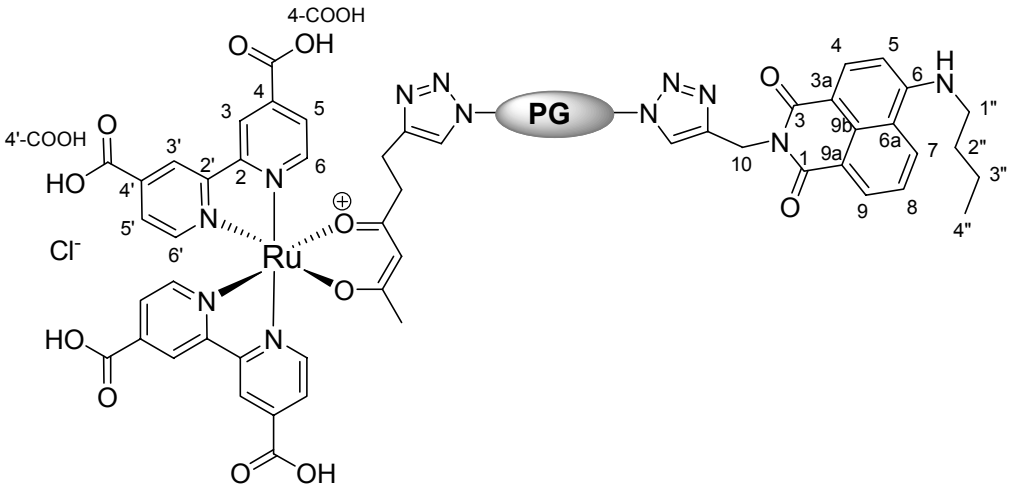

Simultaneous addition of donor and acceptor chromophore in DMSO-water (D_1-$A_{(20\%)}$-PG-$N_{3,\ 40\%}$, **64**, CS 217-9). [Ru(dcbpy)$_2$propargyl-acac]Cl (96.5 mg, 0.127 mmol, 0.5 eq.) and $NaHCO_3$ (80 mg, 0.95 mmol, 3.75 eq.) were dissolved in water (2.2 ml). Solutions of PG-$N_{3,\ 40\%}$ (50 mg, 0.25 mmol N_3, 1 eq.) in DMSO (25 ml), $CuSO_4$ (15.8 mg, 0.063 mmol, 0.25 eq.) in water (0.4 ml) and sodium ascorbate (100 mg, 0.5 mmol, 2 eq.) in water (1.2 ml) were added. Upon combination of the solutions mentioned above, the reaction mixture turned inhomogeneous. The addition of water (20 ml) lead to a homogeneous reaction mixture again. After 3 h a solution of propargyl-butyl-fluorol (42 mg, 0.139 mmol, 0.55 eq.) in DMSO (20 ml) and the reaction mixture was stirred for 7 days at room temperature in the

dark. Then the solvents were removed under high vacuum and the residue was taken up with water (35 ml). The resulting solution was extracted with DCM. The extraction resulted in a yellowish organic phase and a brown emulsion. The emulsion was frozen, brought back to room temperature and titrated from an initial pH of 7.1 to 1.9. The titration resulted in the formation of a precipitate which was isolated by centrifugation. The precipitate was dissolved in NaOH (1M) and purified *via* column chromatography over Sephadex LH20 using water as eluent. The fraction containing the product was precipitated again by addition of diluted HCl to a pH of 1.1. The precipitate was isolated *via* centrifugation and freeze-dried. Yield: 89 mg, 47%.

^{1}H-NMR (THF-d_8:D_2O:py-d_5 9:3:1, 300 MHz, spectrum contains signals of EtOH) δ (ppm) = 8.92 (2H, 3-bpy-H), 8.78 (2H, 3'-bpy-H), 8.68 (2H, 6-bpy-H), 8.59, 8.49, 8.03, 7.80, 7.73 (further aromatic hydrogen atoms), 7.16 (1H, 8-H), 6.20 (1H, 5-H), 5.23 (3H, 10-H and CO-CH-CO), 4.05 ($N_{triazole}$-CH_2), 3.95 – 3.10 (PG-backbone and 1"-H), 2.56, 2.42 (4H, CH_2CH_2 linking Ru to PG), 1.36 (2H, 2"-H), 1.21 (2H, 3"-H), 0.86 (3H, 4"-H).

Simultaneous addition of donor and acceptor chromophore in benzyl alcohol (**65a**, CS 237h; **65b**, CS 237l). The polyglycerol azides (**a**. PG-$N_{3,\ 100\%}$, 94 mg, 0.95 mmol, 1eq.; **b**. PG-$N_{3,\ 85\%}$, 21 mg, 0.21 mmol, 1eq.), [Ru(dcbpy)$_2$propargyl-acac]Cl (**a**: 72.4 mg, 0.095 mmol, 0.1 eq.; **b**. 16.2 mg, 0.021 mmol, 0.1 eq.), *i*Pr_2NEt (**a**. 123 mg, 0.949 mmol, 1 eq.; **b**. 27 mg, 0.021 mmol, 1 eq.) and [Cu(PPh_3)$_3$Br] (**a**. 88 mg, 0.095 mmol, 0.1 eq.; **b**. 20 mg, 0.021 mmol, 0.1 eq.) were dissolved in benzyl alcohol (**a**. 5 ml, **b**. 3 ml). A homogeneous solution formed which was stirred at 50 °C for 12 h. Then propargyl butyl fluorol (**a**. 116 mg, 0.38 mmol, 0.4 eq.; **b**. 26 mg, 0.085 mmol, 0.4 eq.) and another portion of [Cu(PPh_3)$_3$Br] (same amounts as stated above) were added and the mixture was stirred for 18 h and stored at -18 °C for 5 days. Then the reaction mixture was warmed to RT and THF (**a**. 20 ml; **b**. 15 ml) and TBA-OH (0.12 M in water, **a**. 10 ml; **b**. 5 ml) and eluted over Sephadex LH20 with THF:water (3:1). Work up with **a**.: The fractions containing the product were stored at -18 °C. Brown crystals formed in a yellowish solution. The solution was discarded and the crystals melted upon warming to room temperature. The THF in the resulting deep brown solution was evaporated and the remaining aqueous solution was titrated from pH = 11.5 to 3.4 with HCl. The resulting precipitate was dried to give 188 mg (67%) donor acceptor polymer **65a**.

^{1}H-NMR (THF-d_8:D_2O3:1 with TBA-OH, 300 MHz, spectrum contains signals of an impurity between δ = 7.75 and 7.40 ppm and of NBu_4^+ at δ = 3.20, 1.61, 1.35, 0.90 ppm) δ (ppm) = 8.97 (2H, 3-bpy-H), 8.83 (2H, 3'-bpy-H), 8.65 (2H, 6-bpy-H), 8.40 – 7.40 (further aromatic hydrogen atoms), 7.14 (1H, 8-H), 6.20 (1H, 5-H), 5.35 – 4.80 (3H, 10-H and CO-CH-CO),

4.0 ($N_{triazole}$-CH_2), 3.95 – 3.10 (PG-backbone and 1"-H overlapping with NBu_4^+), 2.57, 2.40 (4H, CH_2CH_2 linking Ru to PG), 1.80 – 0.5 (misc. signals overlapping with NBu_4^+)

Work-up with **b**.: The THF was evaporated from the fractions containing the product. A suspension resulted which was redissoved by addition of THF. The THF-water mixture (ca. 1:1) containing the product was then added to diethylether. 2 phases resulted. The brown aqueous phase was titrated to pH = 3.8 upon which a precipitate formed which was isolated and further washed *via* redispersion and centrifugation. 34 mg (54%) polymer resulted.

The products were further purified by dissolving a sample in THF-water-TBA-OH mixtures and precipitation into acidic acetone. Some impurities leading to signals in the aromatic region of the ^{1}H NMR spectra were still prevailing. And an additional purification *via* Sephadex LH20 was conducted.

^{1}H-NMR (THF-d_8:D_2O:py-d_5 12:4:1 with TBA-OH, 300 MHz, spectrum contains signals of impurities at δ = 7.75 – 7.40, 4.17 ppm and of NBu_4^+ at δ = 3.20, 1.61, 1.35, 0.90 ppm) δ (ppm) = 8.96 (2H, 3-bpy-H), 8.82 (2H, 3'-bpy-H), 8.65 (2H, 6-bpy-H), 8.50 – 7.40 (further aromatic hydrogen atoms), 7.18 (1H, 8-H), 6.20 (1H, 5-H), 5.35 – 4.80 (3H, 10-H and CO-CH-CO), 4.0 ($N_{triazole}$-CH_2), 3.95 – 3.10 (PG-backbone and 1"-H overlapping with NBu_4^+), 2.60, 2.44 (4H, CH_2CH_2 linking Ru to PG), 1.80 – 0.5 (misc. signals overlapping with NBu_4^+)

Series with varying donor acceptor ratio (**67e**, **c**, **b,** charge CS 233-2a - c) The further functionalization of the products with the donor chromophore was carried out as follows. The polymers were dissolved in diluted NaOH (**e.** 4 ml, **c.** 4 ml, **b.** 4 ml), the resulting solution was adjusted with HCl (**e.** pH = 7.3, **c.** pH = 5.5, **b.** HCl-adition omitted) and then diluted with DMSO (**e.** 11 ml, **c.** 11 ml, **b.** 13 ml). Then a solution of Propargyl-Butyl-Fluorol (35.4 mg ml^{-1}) was added (**e.** 1.11 ml, 0.5 eq. **c.** 1.48 ml, 0.67 eq. **b.** l.72 ml, 0.75 eq., eq. is referring to initially prevailing azide groups prior to the first reaction). After addition of $CuSO_4$ (0.1 M, **e.** 322 µl, **c.** 429 µl, **b.** 483 µl, corresponding to 0.25 eq. with respect to alkyne groups) and Sodium Ascorbate (0.26 M, **e.** 373 µl, **c.** 479 µl, **b.** 544 µl, 0.75 eq. with respect to alkyne groups) the solutions were stirred at room temperature in the dark for 7 days. Addition of HCl to the reaction mixture lead to the precipitation of the polymers, which were separated from the solvent by centrifugation. The work-up of these products is described individually in the following. **e.** The precipitate was taken up in diluted NaOH, loaded onto a column (diameter 5 cm, Sephadex LH20) and eluted with water. One brown fraction was collected (*V* = 150 ml, pH = 11.1) and acidified with HCl to a pH of 2.8 upon which complete precipitation of the polymer occurred. The product was isolated *via* centrifugation and freeze-drying. Yield: 52 mg. **c.** The precipitate was taken up in NaOH (1 M, 15 ml) and MeOH (5

ml), loaded onto a column (diameter 1 cm, Sephadex LH20) and initially eluted with a water methanol mixture (3:1). Two 50-ml-fractions were collected and acidified with HCl to pH = 2.4 upon which complete precipitation of the polymer occurred. The products were isolated *via* centrifugation and freeze-drying. Yields, F1: 38 mg, F2 3.6 mg. **b.** The precipitate had a brown, slimy consistency. It was taken up in NaOH (1 M, 15 ml) and extracted with CH_2Cl_2 in order to remove unreacted donor chromophore. No clear phase separation appeared after letting the emulsion rest in the separation funnel over night, the organic phase was bright yellow, the aqueous phase was a brown emulsion and there was brown slime at the organic aqueous phase interface. Addition of water to the emulsion lead to the dissolution of the slimy material and a good phase separation. The solvent of the organic phase was evaporated and the residue was dried and characterized by ^{1}H-NMR. The aqueous phase was loaded onto a column (diameter 5 cm, Sephadex LH20) and eluted with water. 7 fractions were collected (25 ml) and characterized *via* UV-Vis spectroscopy. Fractions 1 – 6 were combined and acidified to pH = 2, upon which complete precipitation of the polymer occurred. The product was isolated *via* centrifugation and freeze-drying. Yield: 47 mg.

Series with varying Donor acceptor-Distance (CS 233 e, f and h): [Ru(dcbpy)$_2$propargyl-acac]Cl (LB 19 F7-10, 206 mg) and Na_2CO_3 (158 mg) were dissolved in water (7.1 ml) and the pH of this solution was adjusted to 6.2 using HCl. The polyglycerol azides (**e.** PG_{5000}-$N_{3,\ 10\%}$, BO 567, 115.6 mg, 0.15 mmol N_3; **f.** PG_{5000}-$N_{3,\ 30\%}$ BO 556, 71.4 mg, 0.26 mmol N_3; **h.** PG_{5000}-$N_{3,\ 100\%}$, BO 573, 24 mg, 0.25 mmol N_3) were dissolved in **e.** a mixture of water (4 ml) and DMF (3.75 ml); **f.** in DMF (2 ml); and **h.** DMF (57 ml). To the solutions of the polymers, the solution of the Ru-complex (**e.** 4.20 ml, **f.** 7.30 ml, **h.** 6.99 ml corresponding to 0.4 eq. with respect to N_3-groups), $CuSO_4$ (0.1 M in H_2O, **e.** 30 µl, **f.** 52 µl, **h.** 50 µl corresponding to 0.05 eq. with respect to alkyne groups) and Sodium Ascorbate (0.211 M in H_2O, **e.** 72 µl, **f.** 124 µl, **h.** 119 µl, corresponding to 0.25 eq. with respect to alkyne groups) were added. Then the solutions were stirred at room temperature in the dark for 14 days. Then, the mixtures were loaded onto a column (diameter 5 cm, Sephadex LH20, in case of reaction **h.** the solvent was evaporated prior to further work-up) and eluted with water. Two fractions were collected in each case (The volumes of the fraction 1: **e:** 100 ml; **f:** 100 ml; **h:** 130 ml; and fraction 2 **e:** 100 ml; **f:** 230 ml; **h:** 190 ml;), which were characterized by UV-Vis-spectroscopy. Fraction 1 contained the polymer-bound Ru-complex, Fraction 2 [Ru(dcbpy)$_2$propargyl-acac]Cl. The solvent of the first fraction of reactions **e.** and **f.** was removed in vacuo. To the first fraction of reaction **h.**, HCl was added until pH = 2, upon which a dense precipitate and a nearly colorless supernatant formed. The products were

further isolated *via* evaporation of the solvent and freeze-drying. Yield: **e.** 144 mg, **f.** 49 mg and **h.** 30 mg.

$D_{3.7}$-$A_{8\%}$-PG-$N_{3,\ 60\%}$ (**67g**): ^{1}H-NMR (py-d_5:D_2O 4:1, 300 MHz, spectrum contains signals of EtOH) δ (ppm) = 9.40 – 8.70 (3-, 3′- and 6-bpy-Hs), 8.70 – 7.70 (further aromatic hydrogen atoms), 7.40 (1H, 8-H), 6.39 (1H, 5-H), 5..00 (10-H, CO-CH-CO, $N_{triazole}$-CH_2, PG-backbone and 1"-H), 2.72, 2.54 (4H, CH_2CH_2 linking Ru to PG), 1.89 (3H, CO-CH_3), 1.71 (2H, 2"-H), 1.40 (2H, 3"-H), 0.86 (3H, 4"-H).

$D_{8.6}$-$A_{3\%}$-PG-$N_{3,\ 30\%}$ (**66b**): ^{1}H-NMR (THF-d_8:D_2O:py-d_5 11:7:1, 300 MHz) δ (ppm) = 8.92 (2H, 3-bpy-H), 8.79 (2H, 3'-bpy-H), 8.68 (2H, 6-bpy-H), 8.50, 8.01, 7.51 (further aromatic hydrogen atoms), 7.20 (1H, 8-H), 6.27 (1H, 5-H), 5.25 (3H, 10-H and CO-CH-CO), 4.13 ($N_{triazole}$-CH_2), 3.95 – 3.10 (PG-backbone and 1"-H), 2.58, 2.45 (4H, CH_2CH_2 linking Ru to PG), 1.95 (3H, CO-CH_3), 1.61 (2H, 2"-H), 1.37 (2H, 3"-H), 0.87 (3H, 4"-H).

8.4 Dye Solar Cells Assembly and Characterization

8.4.1 DSC Manufacture

The DSC test cells were manufactured as follows. Front electrode: Onto a glass substrate coated with fluorine doped tin oxide one print of TiO_2 screen printing paste (Ti-Nanoxide HT/SP, SOLARONIX) resulting in 5 5 × 0.5 cm TiO_2 rectangles and silver lines were deposited *via* screen printing. Back electrode: Onto a glass substrate coated with fluorine doped tin oxide one print of Pt-paste was deposited *via* screen printed. Alternatively, Pt was sputtered onto the glass substrate. Additionally, silver lines were screen printed. The electrodes were dried at 150 °C after the printing steps and sintered at 450 °C for 30 min under air. The front electrode was immersed into the respective dye solution overnight after which it was rinsed and dried in a stream of air. The composition of the staining solutions is summarized in Table 19. A syrlin gasket was laminated onto the front electrode (1 min at 110 – 130 °C), the protection foil was removed and the back electrode was positioned onto the front electrode. Fusing the front and back electrodes together was performed by laminating at 130°C for 3 min. The electrolyte was injected into the cells and the holes were sealed with either syrlin coated glass cover slips or aluminum foil. The cells were contacted by soldering a wire onto the TCO glass using an ultrasound soldering rod.[102, 103]

8.4.2 Calculation of the Light Harvesting Efficiency

LHE was determined according to eq. (9.3)

$$LHE = 1 - \frac{T_{\text{stained}}}{T_{\text{electrolyte}}} \tag{9.3}$$

T_{stained} = transmission of the stained DSC
$T_{\text{electrolyte}}$ = transmission of an identical DSC without sensitizer filled with electrolyte

T_{stained} and $T_{\text{electrolyte}}$ were determined from several transmission measurements using a UV-Vis spectrometer in standard setup. At least 4 transmission spectra were averaged. The error ΔT was determined *via* the standard deviation of the measurements. The error in *LHE* was calculated by the mean square method according to eq. (9.4).

$$\Delta LHE = \sqrt{\left(\frac{\Delta T_{\text{stained}}}{T_{\text{electrolyte}}}\right)^2 + \left(\frac{T_{\text{stained}} \cdot \Delta T^2_{\text{electrolyte}}}{T^2_{\text{electrolyte}}}\right)^2} \tag{9.4}$$

The different layers in the cell were not perfectly planar and the positioning of the cell to the light beam was not necessarily perfectly purpendicular. These facts resulted in some transmission measurements revealing artefacts that were ascribed to interference at thin layers as well as the transmission in the red and IR part of the spectrum revealing slightly different values. The following methodology was applied in order to enhance the quality of transmission data:

1.) smoothing of the transmission data using Oringin 6.1 (Savitzky-Golay, 25 points, polynomial degree = 1)

2.) normalization of the different transmission spectra at λ = 800 nm

3.) averaging of the spectra and calculation of the error as standard deviation

The averaged spectra and the respective standard deviation were used for the calculation of *LHE* and ΔLHE.

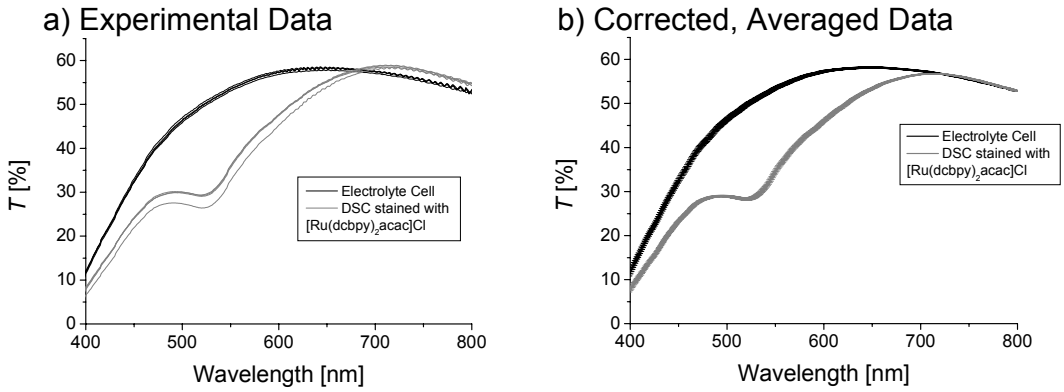

Figure 46. Transmission data prior and after correction.

8.4.3 Determination of *k* and *ETE* from *LHE*(λ) and *EQE*(λ)

The methodology for the determination of the wavelength-independant constants *k* and *ETE* from the results of the spectral characterization of the DSCs consisted in the following steps: (i) plotting the *LHE* calculated from transmission spectra, (ii) normalizing EQE_{exp} so that it fits with *LHE* for $\lambda > 540$ nm (in analogy to the procedure for the determination of *k* described in chapter 5.1.3), (iii) normalizing $A_{Acceptor}$ acquired from the *LHE* of a DSC containing exclusively the energy acceptor as sensitizer so that it matches with $A_{D\text{-}A\text{-}System}$ for $\lambda > 540$ nm and (iv) choosing *ETE* so that the plot of $EQE_{D\text{-}A\text{-}System,\ sim}$ calculated according to eq. (5.9) fits with $EQE_{exp} \cdot k^{-1}$.

9 Appendix

9.1 Calculation of Loadings from ^{1}H NMR data

The intensity of ^{1}H NMR signals, the area under the peaks A between 2 chemical shifts used here is defined according to eq. (9.1).

$$A_{b;e} = \int_{\delta=b}^{e} I(\delta) d\delta \tag{9.1}$$

N^H = number of hydrogen atoms responsible fort he respective signal
i = Index
N_i^H = number of hydrogen atoms of the structural unit i
A_i = area
δ = chemical shift [ppm]
$I(\delta)$ = intensity of ^{1}H NMR-spectrum as a function of δ
b_i = lower integration limit
e_i = upper integration limit

Relating the signal intensity of the respective functionality FG to the one of the polymer backbone according to eq. (9.2) gives the respective loading α_{FG}.

$$\alpha_{FG} = \frac{A_{FG}}{N_{FG}^H} \cdot \frac{N_{PG}^H}{A_{PG}} \tag{9.2}$$

α_{FG} = loading with the respective functional group FG
A_{FG} = integral area of the signal of FG
N^H_{FG} = number of hydrogens accounting for A_{FG}
A_{PG} = integral area from PG-backbone and remaining OH-groups
N^H_{PG} = number of hydrogens accounting for A_{PG}

9.1.1 D-Allyl-PG

$$A_{Alkene} = \frac{A_{4.2-3.8} - 2A_{Fluorol}}{2} \tag{9.3}$$

$$A_{Fluorol} = \frac{A_{9.0-6.5} + A_{0.7-0.1}}{13} \tag{9.4}$$

$$A_{PG} = \frac{A_{3.8-3.0} - 4 \cdot A_{Fluorol}}{5} \tag{9.5}$$

$$\alpha_{FG} = \frac{A_{FG}}{A_{PG}} \tag{9.6}$$

Table 26. Integral intensities ($I_{\delta 1 - \delta 2}$) from ^{1}H NMR spectra of D-Allyl-PGs, the normalized intensities (I_{Fluorol}, I_{Allyl}, I_{CH3}, and I_{PG}) and degree of loading with the respective functional groups (α_{FG}) calculated thereof.

	$D_{63\%}$-Allyl-PG	$D_{24\%}$-Allyl-PG	$D_{3\%}$-Allyl-PG	$D_{0.3\%}$-Allyl-PG	Allyl-PG
$I_{9.0-6.5}$	88121	68428	10027	1805	
$I_{6.0-5.5}$	19083	44584	68568	103638	81468
$I_{5.4-4.9}$	31607	93438	144258	210681	172695
$I_{4.2-3.8}$	45751	123284	155774	223084	186214
$I_{3.8-3.0}$	216038	385683	393501	540680	441149
$I_{2.0-1.1}$	284759	260390	28883	17063	
$I_{1.0-0.7}$	84392	72442	12744	8070	
$I_{0.7-0.1}$	147371	131763	18314	3005	
$I_{0.1--0.1}$	229370	231440	56693	10964	
I_{Fluorol}	18115	15399	2180	370	0
I_{Alkene}	4761	46243	75707	111172	93107
I_{CH3}	10016	8748	2068	2320	0
I_{PG}	28716	64817	76956	107840	88230
α_{Fluorol}	63.1%	23.8%	2.8%	0.3%	0.0%
α_{Allyl}	16.6%	71.3%	98.4%	103.1%	105.5%
α_{Pr}	34.9%	13.5%	2.7%	2.2%	0.0%
$\Sigma\alpha$	114.5%	108.6%	103.9%	105.6%	105.5%

9.1.2 PG-OMs

The spectra of PG-OMs were measured in solvents, where no quick exchange of acidic protons is expected, thus an unfunctionalized PG group provides 6 protons giving rise to resonances in the area 5.3 – 3.25 ppm. *Via* the mesylation the protons on the OH-groups are substituted by SO_2CH_3. The latter provides a signal between 3.25 and 3.15 ppm. From these considerations the loading of PG with mesyl groups α_{OMs} was calculated according to eq. (9.7).

$$\alpha_{\text{OMs}} = \frac{\frac{A_{\text{OMs}}}{3}}{\frac{A_{\text{PG}} + \frac{A_{\text{OMs}}}{3}}{6}} \tag{9.7}$$

α_{OMs} = loading with OMs
A_{OMs} = integral area of CH_3 group from OMs
A_{PG} = integral area from PG-backbone and remaining OH-groups (5.3 – 3.25 ppm)

9.1.3 D-A-PG-N_3

The calculation of loading with the donor and acceptor unit was based on the following signals: (i) the 3- and 3′-bpy-H (A_{byp}, N^{H}_{bpy} = 4), (ii) the 5-H on the fluorol unit (A_D; N^{H}_{D} = 1), (iii) the range from 4.3 – 3.0 ppm comprising the PG-backbone N(C$\underline{H_2}$-Pr)$_4^+$ and THF-d_8 and the 1"-CH_2 on the fluorol unit ($A_{4.3–3.0}$) , and (iv) the signal of THF, N(CH_2-C$\underline{H_2}$-Et)$_4^+$ ($A_{1.9–1.5}$). From these considerations the area of the PG-bacbone results to

$$A_{PG} = A_{4.3–3.0} - A_{1.9–1.5} - 2A_D . \tag{9.8}$$

α_{Donor} and α_{Ru} were calculated according to eq. (9.2).

Table 27. Intensities from ^{1}H NMR characterization of D-A-PG-N_3 derivatives, loadings α_{Donor}, α_{Ru} and the donor acceptor ratio z_{DA} calculated thereof.

#	Polymer	^{1}H NMR						
		A_{bpy}	A_D	$A_{4.5\text{-}3.0}$	A_{misc}	α_{Donor}	α_{Ru}	z_{DA}
1	$D_{0.8}$-$A_{5\%}$-PG-$N_{3,\ 30\%}$ **67c**	7.10	1.00	111.0	23.8	6%	10%	0.56
2	D_1-$A_{(20\%)}$-PG-$N_{3,\ 40\%}$ **64**	14.9	0.97	205	77.5	4%	15%	0.26
3	$D_{3.7}$-$A_{8\%}$-PG-$N_{3,\ 60\%}$ **67g**	0.76	1.00	12.88	0.44	47%	9%	5.3
4	D_5-$A_{(10\%)}$-PG-$N_{3,\ 100\%}$ **65a**	1.77	1.42	47.1	33.4	65%	20%	3.2
5	D_7-$A_{(10\%)}$-*l*PG-$N_{3,\ 85\%}$ **65b**	0.32	0.51	24.27	21.0	113%	18%	6.4
6	$D_{8.6}$-$A_{3\%}$-PG-$N_{3,\ 30\%}$ **67b**	0.39	1.00	45.03	8.48	14%	1%	10

9.2 Simulation of EQE data as a function of *ETE*

The EQE of a donor acceptor system ($EQE_{D\text{-}A\text{-}Syste}$) comprises contributions of the acceptor and the donor chromophores ($EQE_{Acceptor}$ and EQE_{Donor}, respectively).

$$EQE_{D\text{-}A\text{-}System} = EQE_{Acceptor} + EQE_{Donor} \tag{9.9}$$

Furthermore, $EQE_{Acceptor}$ was assumed to be proportional to $LHE_{Acceptor}$

$$EQE_{Acceptor} = k \cdot LHE_{Acceptor} \tag{9.10}$$

Assuming that the energy donor does not inject electrons into TiO_2, equation (9.10) is not applicable to the energy donor. In this case electron injection resulting from donor absorption only takes place after resonant energy transfer. Thus the energy transfer efficiency needs to be taken into consideration for the calculation of EQE_{Donor}.

$$EQE_{Donor} = k \cdot ETE \cdot LHE_{Donor} \tag{9.11}$$

Substituting the expressions (9.11) and (9.10) in eq. (9.9) gives

$$EQE_{\text{Dyad}} = k \cdot LHE_{\text{Acceptor}} + k \cdot ETE \cdot LHE_{\text{Donor}}. \tag{9.12}$$

In analogy to *EQE*, the light harvesting efficiecncy (*LHE*) also has contributions of the individual chromophores.

$$LHE_{\text{D-A-System}} = LHE_{\text{Acceptor}} + LHE_{\text{Donor}} \tag{9.13}$$

LHE_{Acceptor} and LHE_{Donor} are the product of LHE_{Dyad} and the fractions of absorbed light, absorbed by the chromophoric moieties, x_{Acceptor} and x_{Donor}, respectively.

$$LHE_{\text{Acceptor}} = LHE_{\text{D-A-System}} \cdot x_{\text{Acceptor}} \tag{9.14}$$

$$LHE_{\text{Donor}} = LHE_{\text{D-A-System}} \cdot x_{\text{Donor}} \tag{9.15}$$

The fractions of absorbed light are calculated from the absorbance *A* of the donor acceptor system, acceptor and donor, respectively.

$$x_{\text{Acceptor}} = \frac{A_{\text{Acceptor}}}{A_{\text{D-A-System}}} \tag{9.16}$$

$$x_{\text{Donor}} = \frac{A_{\text{Donor}}}{A_{\text{D-A-System}}} = 1 - x_{\text{Acceptor}} \tag{9.17}$$

Introduction of expressions (9.14) to (9.17) into (9.13) yields

$$EQE_{\text{D-A-System}} = k \cdot LHE_{\text{D-A-System}} \cdot \frac{A_{\text{Acceptor}}}{A_{\text{D-A-System}}} + k \cdot ETE \cdot LHE_{\text{D-A-System}} \cdot \frac{A_{\text{Donor}}}{A_{\text{D-A-System}}}. \tag{9.18}$$

Since $A_{\text{D-A-System}}$ is the sum of A_{Donor} and A_{Acceptor}, eq. (9.18) can be simplified to

$$EQE_{\text{D-A-System}} = k \cdot LHE_{\text{D-A-System}} \cdot \left[\frac{A_{\text{Acceptor}}}{A_{\text{D-A-System}}} + ETE \cdot \left(1 - \frac{A_{\text{Acceptor}}}{A_{\text{D-A-System}}} \right) \right] \tag{9.19}$$

$EQE_{\text{D-A-System}}$ was simulated using experimental values for $LHE_{\text{D-A-System}}$, $A_{\text{D-A-System}}$ and A_{Acceptor}, which were in turn obtained from $LHE_{\text{D-A-System}}$ and the light harvesting effiency of a device that was exclusively stained with the respective acceptor unit ($LHE_{\text{Acceptor-only}}$) according to eq. (9.20).

$$A = -\log(1 - LHE) \tag{9.20}$$

In order to determine the error in $EQE_{\text{D-A-System}}$ equation was further rearranged to (9.22) (see next paragraph).

$$EQE_{\text{D-A-System}} = k \cdot LHE_{\text{D-A-System}} \cdot \left[x_{\text{Acceptor}} + ETE \cdot \left(1 - x_{\text{Acceptor}} \right) \right] \tag{9.21}$$

$$EQE_{\text{D-A-System}} = k \cdot LHE_{\text{D-A-System}} \cdot \left[x_{\text{Acceptor}} (1 - ETE) + ETE \right]. \tag{9.22}$$

The error $\Delta EQE_{\text{D-A-System}}$ was calculated using the mean square method taking into account equation (9.22) and the error ΔLHE_{Dyad} [see Eq. (S23)]. $\Delta x_{\text{Acceptor}}$ turned out not to add significantly to $\Delta EQE_{\text{D-A-System}}$.

$$\Delta EQE_{\text{D-A-System}} = k \cdot \left[x_{\text{Acceptor}} (1 - ETE) + ETE \right] \cdot \Delta LHE_{\text{D-A-System}} \,. \tag{S23}$$

Finally, *ETE* was estimated by evaluation of the fit of $EQE_{\textbf{Dyad},\,\text{experimental}} \cdot k^{-1}$ and $EQE_{\textbf{Dyad},\,\text{simulated}}$ (assuming $k = 1$ for the simulation), as a function of the parameter *ETE*. For $k = 0.39$ and $ETE = 0.83$ (0.87) the upper (lower) margin of the error bars of $\Delta EQE_{\textbf{Dyad},\,\text{simulated}}$ were coinciding with $EQE_{\textbf{Dyad},\,\text{experimental}} \cdot k^{-1}$ in the area between 470 and 490 nm. Thus, the value determined for *ETE* is 85 ± 3%. The estimation in *ETE* was carried out accordingly for the other donor acceptor systems.

9.3 Magnitude of Current Generated by Donor Absorption under AM1.5G

From Table 21 on page 98 it becomes obvious that the presence of the donor in the DSC did not effectuate a significant increase in current and efficiency under simulated sunlight using halogen lamps. The reasons for this behaviour will be outlined in the following. From Figure 35 on page 90 it becomes obvious that *EQE* at 520 – 530 nm for DSCs sensitized with **45** and **14** are approximately the same. Thus, for the following considerations, EQE_{Acceptor} from Figure 35c was normalized so that it equals EQE_{Dyad} at 530 nm (Figure 47). Based on these normalized EQE-functions and the photon flux $\Phi(\lambda)$ under AM1.5G conditions, the short circuit current of the devices was calculated according to eq. (9.24) (see also Figure 47 and Figure 48).

$$j_{sc} = \frac{F}{N_A} \int_{300\text{ nm}}^{800\text{ nm}} EQE(\lambda) \cdot \Phi(\lambda) \mathrm{d}\lambda \tag{9.24}$$

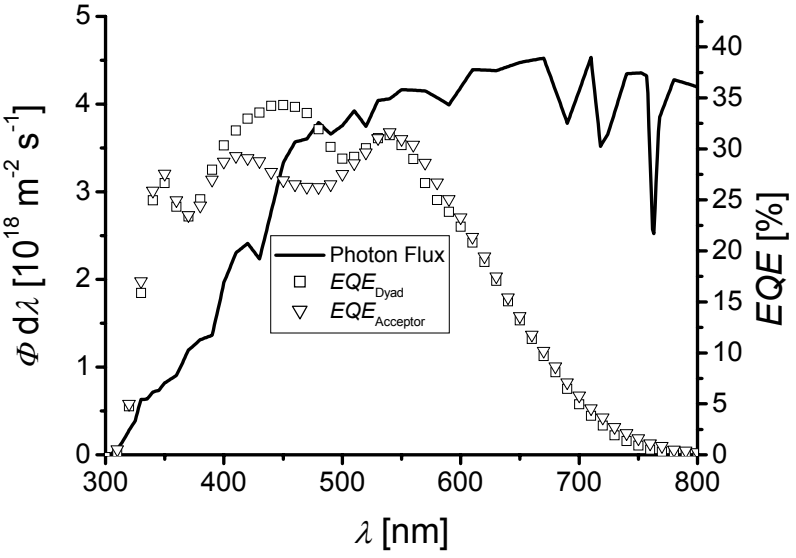

Figure 47. EQE-data and photon flux under AM1.5G conditions used for the calculation of j_{sc}.

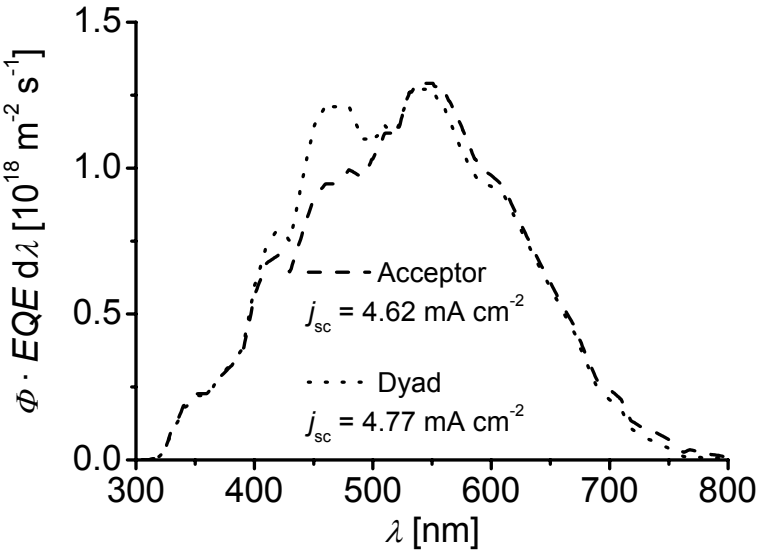

Figure 48. Plot of $EQE(\lambda) \cdot \Phi(\lambda)d\lambda$ versus λ. The area under these curves are proportional to the current generated by the DSCs sensitized with 45 and **14** under illumination with AM1.5G-light.

The thus calculated j_{sc} is 4.77 and 4.62 mA cm^{-2} for the dyad and the acceptor, respectively, which corresponds to a current enhancement of merely 3.1% by the presence of the donor under this type of illumination. Considering that the results presented in Table 21 were determined under illumination with halogen lights, which have a weaker photon flux in the area where the donor moiety absorbs with respect to the AM1.5G-irradiance, the coinciding j_{sc} for cells with **262** and **14** as sensitizer is plausible despite their significant difference in $EQE(\lambda)$. The errors in the IV-characteristics, which are mainly due to inhomogenities

between different cells and instability of the solar simulator, are surpassing the expected current gain under this illumination. Due to the circumstance mentioned above the IV-characteristics were also determined under monochromatic blue and green light. These measurements delivered the proof of principle

9.4 Deviation between *ETE* and *EQE*

The following factors could account for the divergence of *LHE* and *EQE* functions in Figure 3d in case of devices stained with either dye 2 or 5: (i) Although identical cells were used for the *EQE*- and T_{DSC}-measurements, it was impossible to use the identical spot on the cell for the respective measurements. Inhomogeneities in the photoelectrode and/or overall cell thickness might lead to different scattering behavior which is increasingly important with decreasing wavelength; (ii) The data quality in $T_{electrolyte}$ might be too inferior at low wavelengths to allow for reliable calculation of *LHE* (This could account for the drastic divergence for $\lambda < 420$ nm); (iii) $T_{electrolyte}$ is a function of the I_3^--concentration in the electrolyte and especially in the nanoporous photoelectrode, which is subject to change as a function of time and illumination intensity. The gradient in I_3^--concentration prevalent under the conditions applied for the measurement of $EQE(\lambda)$ is expected to yield somewhat lower *EQE*-values than predicted according to $LHE(\lambda)$. Such a behavior is also observed in Figure 37d. In fact, it was shown that the transmission of the DSC is altered by the application of bias illumination under short circuit conditions. This experiment was carried out using a reference solar cell, which was covered by a DSC stained with [Ru(dcbpy)$_2$acac]Cl. Thus, the DSC serves as a filter between the monochromatic light source and the reference solar cell. In an initial measurement, the EQE of the reference solar cell was determined in the dark ($EQE_{RC,\ dark}$) and a second measurement was conducted after having kept the DSC, which was being operated under short circuit conditions, for 30 min under constant white illumination ($EQE_{RC,\ bright}$, see Figure 49a). The change in transmittance of the DSC (ΔT_{DSC}) was calculated using eq. (9.25) (see Figure 49b, the relative error in EQE_{RC} was estimated from the data points between $540 < \lambda < 600$ nm to be = 5‰. The error in ΔT_{DSC} was calculated according to the mean square method).

$$\Delta T_{DSC} = \frac{EQE_{RC,\ bright}}{EQE_{RC,\ dark}} - 1 \tag{9.25}$$

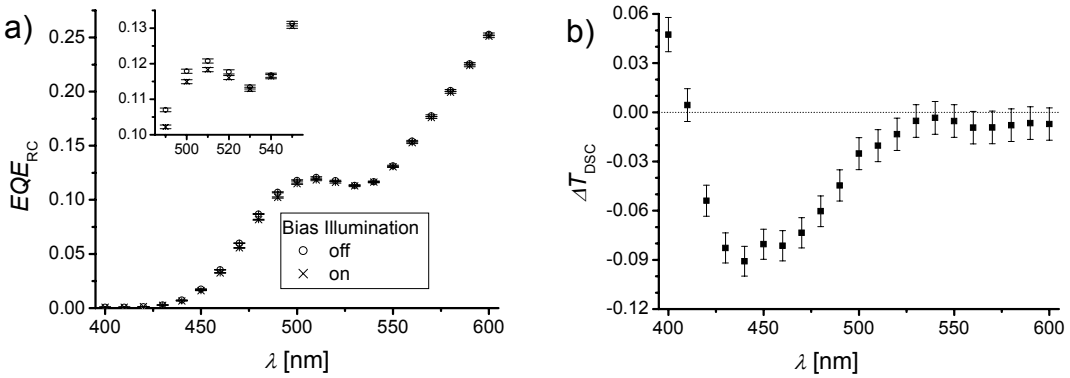

Figure 49. Results of experiments carried out towards the characterization of the change in transmission of a DSC by the application of bias illumination. The external quantum efficiency of a reference solar cell (EQE_{RC}), which was covered by a DSC stained with [Ru(dcbpy)$_2$acac]Cl and being operated under short circuit conditions, was determined without and during bias illumination. **a)** $EQE_{RC}(\lambda)$ before (○) and during (×) the application of bias illumination (for clarity, the inset shows a magnification of the data between 500 and 550 nm). **b)** Change in transmission of the DSC (ΔT_{DSC}) as calculated using eqation **(9.25)** The relative error in EQE_{RC} was estimated from the data points between 540 < λ < 600 nm to be = 5‰. The error in ΔT_{DSC} was calculated according to the mean square method.

Figure 49b shows clearly that the application of bias illumination brings about a change in T_{DSC} for λ < 500 nm. This observation is consistent with a slight change in triiodide concentration induced by the current generated by the DSC.

9.5 Donor Acceptor Ratio in the Device

Figure 50 shows the absorbance of a selection of DSCs (A_{DSC}) calculated according to eq. (9.26). Normalized absorption spectra of the staining solutions were added to the diagrams.

$$A_{DSC} = -\log(1 - LHE) \tag{9.26}$$

Figure 50a reveals relatively good agreement between the absorption spectrum of dyad **45** in solution and on the photoelectrode with respect to the intensity of the band around 450 nm.[111] By desorbing **45** and the measurement of an absorption spectrum of the desorbed dye it was shown that the donor acceptor ratio decreased by 10% *via* the staining and laminating process as well as the exposure to the electrolyte. In conclusion a good agreement between z_{DA} in **45** and on the photoelectrode was achieved using the monomolecular, thus monodisperse sensitizer **45**. Figure 50b – d reveals a significant deviation between A_{DSC} and the absorption spectrum in solution with respect to the intensity of the donor absorption. The donor acceptor ratio after adsorption to the photoelectrode is significantly lower than in the staining solution. This fact is rationalized by the polydispersity of the sensitizers. In contrast to **45** donor acceptor polymers are polydisperse with respect to their molecular weight as well

as α_{Donor}, $\alpha_{Acceptor}$ and z_{DA}. Polymers with a higher $\alpha_{Acceptor}$ will adsorb with a higher probability which is obviously resulting in a reduced z_{DA}. Thus, z_{DA} within the device is lower than z_{DA} as determined from UV-Vis spectra of D-A-PG-N_3 derivatives. Nevertheless, Figure 50 proofs that it was possible to influence the light-harvesting characteristics by the composition of the polymer, namely z_{DA}. It was attempted to estimate z_{DA} in the device by fitting simulated to experimental A_{DSC} curves, however, this did not lead to conclusive results.

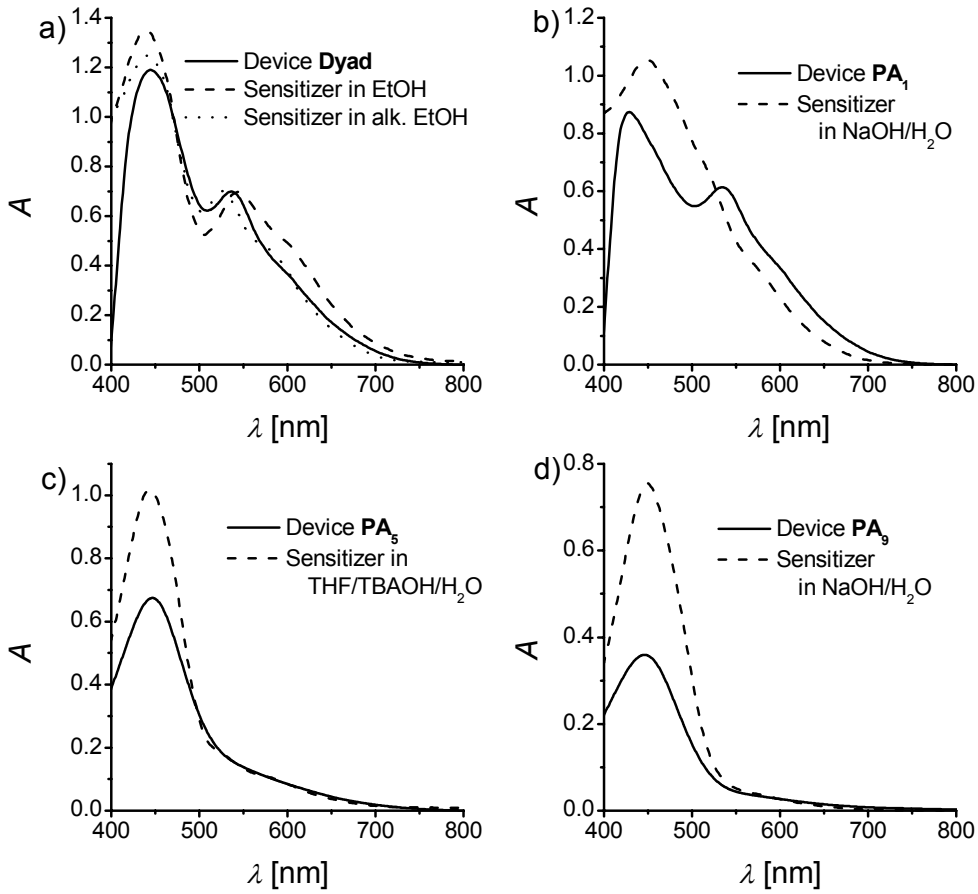

Figure 50. Comparison of absorption spectra of donor acceptor sensitizers in solution and within the device. a) dyad **45** (Device **Dyad**), b) $D_{1.0}$-$A_{(20\%)}$-PG-$N_{3,\ 40\%}$ **64** (Device **PDA_1**), c) $D_{5.0}$-$A_{(10\%)}$-PG-$N_{3.\ 100\%}$ **65a** (Device **PDA_5**), d) $D_{8.6}$-$A_{3\%}$-PG-$N_{3,\ 30\%}$ **67b** (Device **PDA_9**).

9.6 Modified TiO_2 Particles for Electrophoretic Ink

Another important trend prevailing in recent years has been the increasing importance of information technology which is ubiquitous in today's modern societies due to the increased portability of devices. The latter is a result of the optimization of energy management in the production and operation of respective devices (mobile computers, cell phones and organizers). A considerable part of the energy of, e.g., mobile computers is consumed by the display. The second topic investigated in this thesis is a contribution to the development of an alternative, power-saving display technology known as electrophoretic ink. In the larger scheme, this topic is thus related to the enhancement of the energy efficiency of today's lifestyle. The contribution consisted in experiments towards the modification of TiO_2 particles for electrophoretic ink applications.

9.6.1 Electrophoretic Ink

Liquid-crystalline displays (LCD)[112] are one of today's most widely applied display technologies, however, this technology still presents some disadvantages consisting in the strong dependence of the visibility on the viewing angle and the necessity of an interior light source requiring high power consumption. These disadvantages spur interest in the development of alternative display technologies.[113] Electrophoretic displays are one alternative being very distinct from LCDs.[114-116] This display's setup and working principle is shown in Figure 51. The operation is based on the electrophoretic migration of oppositely charged and colored micro-particles upon a change in the polarity of the voltage at the condenser sandwiching the particle dispersion. The micro-particles should be strongly absorbing (black) or highly scattering (white) and have a size between 0.1 and 5 μm. Alternatively, white micro-particles may be dispersed in black oil. Displays based on this principle may potentially be manufactured flexibly at low cost. They are marked by the following properties: (i) intrinsic bistability, (ii) low power consumption, (iii) a high contrast and reflectivity, and (iv) near-lambertian viewing characteristics, i.e., a low dependence of viewing angle on the quality of the image. Since such displays' appearance are close to ink on paper, this concept has also been termed "electrophoretic ink."[117]

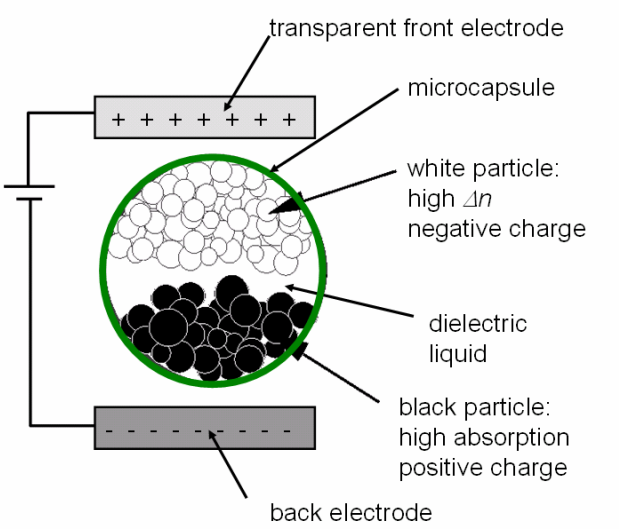

Figure 51. Principle of one pixel of the electrophoretic display. The key component is the dispersion of oppositely charged white and black particles in a dielectric medium. This dispersion is located in a capacitor comprising one transparent electrode. Upon changing the polarity of the voltage applied to the condenser the particles migrate through the medium to the respective opposite side of the condenser thus effecting a color change of the pixel.

Such a display may potentially be fabricated by printing and thus satisfy the practical requirements of electronic paper.[114] One strategy to charge particles is presented in Scheme 22 relies on acidic, white and basic, black particles. Combining these two kinds of particles should lead to interparticle neutralization and thereby charged particles.[118]

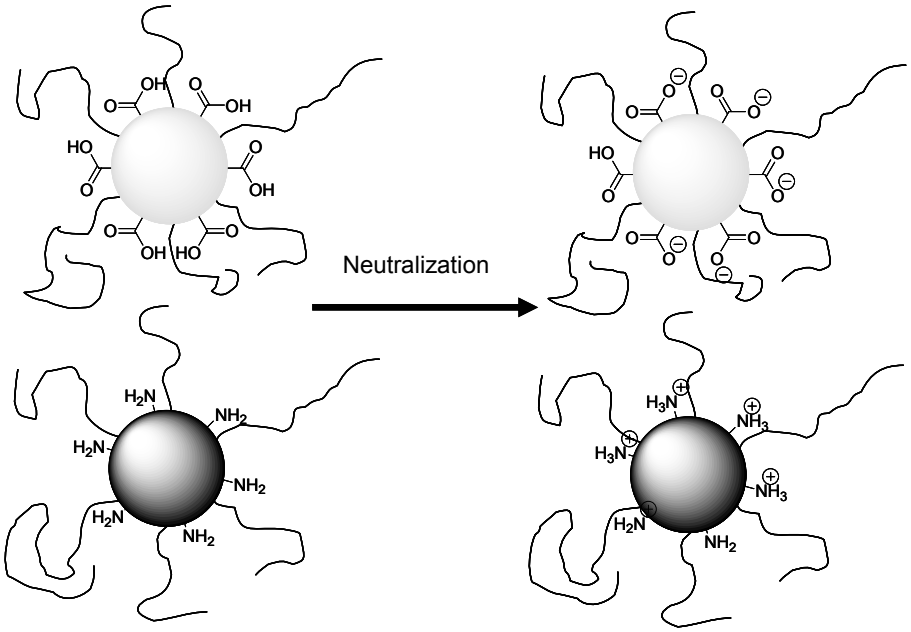

Scheme 22. Principle of formation of oppositely charged particles according to G. Hadziioannou: Combining white acidic and black basic particles leads *via* neutralization to negatively charged white particles and positively charged black particles.

9.6.2 Motivation for TiO_2 Particle Modification

In a side project this thesis dealt with the modifications of TiO_2 particles for electrophoretic ink applications. The requirements for white pigment particles in this application emerge from the work principle shown in Figure 51 and Scheme 22. Such particles should efficiently scatter light, have a low density in order to attenuate sedimentation in the pixel and should possess acidic groups. These requirements would be met by the encapsulation of a TiO_2 particle functionalized with acidic groups into a polymer shell.

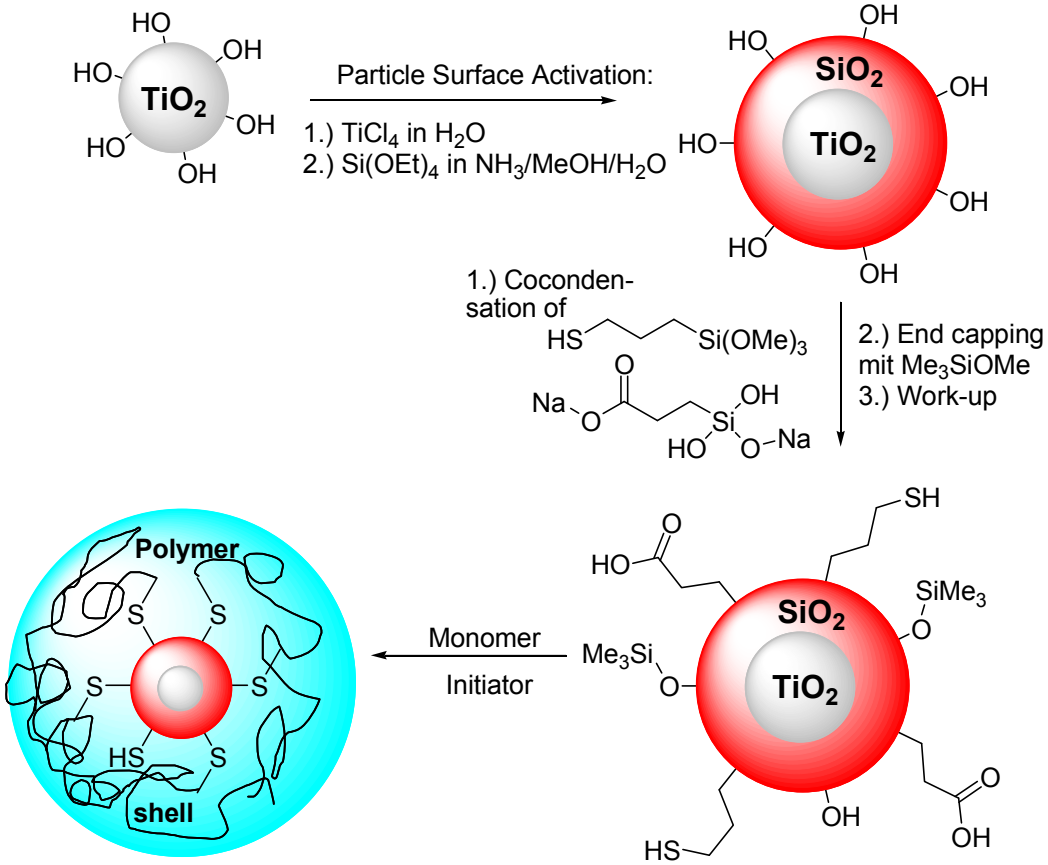

Scheme 23. Modification of TiO_2 with functional groups allowing the subsequent encapsulation into a polymeric shell.

The introduction of functional groups *via* functional silanes and subsequent grafting of polymers to the resulting functional TiO_2 particles according to Scheme 23 could be one viable way of meeting the requirements for pigment particles mentioned above. The following approach was to be followed in order to evaluate the latter approach:

(i) Surface functionalization of TiO_2-particles

(ii) Grafting of polymers to functional TiO_2-particles

(iii) Characterization of polymer-modified TiO_2-particles

Results towards the modification of TiO_2 particles are presented in the following.

9.6.3 Results and Discussion of TiO_2 Modification

The requirements that TiO_2 particles should fulfill follow from the functional principle of electrophoretic ink described in the introduction (section 9.6.1). The particles should comprise (i) a high density of COOH groups on the surface, a shell providing (ii) a considerable decrease in density, and (iii) steric stabilization. These requirements could be met by encapsulating COOH-bearing TiO_2 particles into a thick polymer shell. The synthetic concept that was devised here in order to modify TiO_2-particles accordingly for electrophoretic ink applications is shown in Scheme 24. Conducting experiments towards this scheme was motivated by the following considerations: Although the direct functionalization of TiO_2 particles with methacrylate bearing titanates (e.g., **68**) and subsequent polymerization has been described,[119] the availability of titanates comprising different functional units is limited. In contrast incorporation of functional silanes of the type $(RO)_{3-n}SiR'_n$ onto silica or into siloxane particles is a versatile, straight forward and broadly applied method.[120-124] Its application is also fuelled by the wide range of commercially available alkoxy silanes.[125] Furthermore, the modification of silica spheres[126] featuring polymerizable groups at the surface has also been described[121] and resulted in the hypothesis that the assembly of a SiO_2 shell around TiO_2 and its further functionalization according to Scheme 24 would be a more robust and flexible method for the synthesis of functional TiO_2 pigments. The first step of the synthetic concept in Scheme 24 consisted in the surface activation and incorporation of functionalities. This treatment aimed at achieving a high loading with carboxy groups, e.g., by the introduction of silan **69**, and moieties that will allow the grafting of polymers (e.g., by the introduction of silanes **70** and **71**) as well as a hydrophobization of the TiO_2 particles (*via* Me_3SiOEt). The second one consisted in the grafting of polymers to the functional TiO_2.

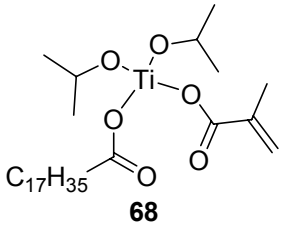

68

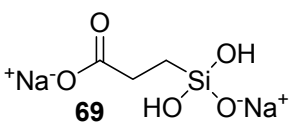

69

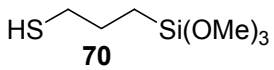

70

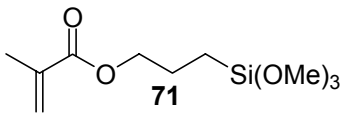

71

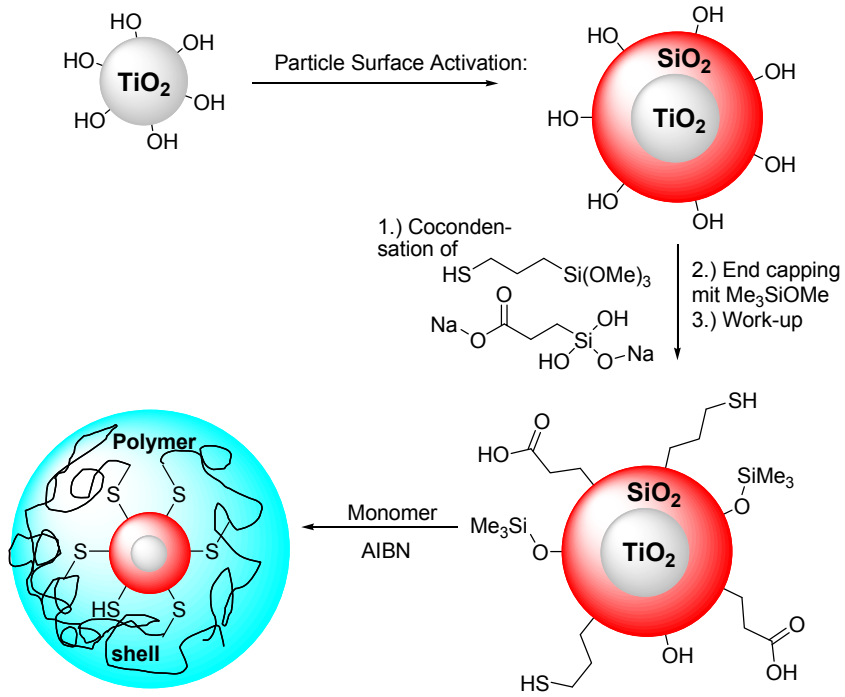

Scheme 24. Synthesis of polymer-grafted COOH-functionalized rutile particles.

In more detail the work towards modified TiO_2 particles comprised of the following steps:

1. Surface activation of TiO_2 *via* the growth of a SiO_2 shell using $Si(OEt)_4$.[126]
2. Condensation of functional Tri(alkoxy)silanes: (i) **70**[120, 121] or **71** in order to allow grafting of polymer chains by radical polymerization and (ii) **69** in order to incorporate a functionality, which will allow to generate a charge on the particle.
3. Passivation of the particle surface: *via* condensation of Me_3SiOEt.
4. Work-up by centrifugation and redispersion-steps. Characterization of modified particles by TEM, particle size measurements, TGA, Elemental Analysis.
5. Dispersion polymerization of different monomers and monomer mixtures in solution or bulk with functionalized particles.
6. Work-up by dissolving unbound polymer, centrifugation and redispersion-steps. Characterization by TEM, particle size measurements, TGA, Elemental Analysis.

Steps 1-4 in Scheme 24 will be referred to as particle functionalization, steps 5-6 as grafting.

9.6.3.1 Particle Functionalization

Several conditions for surface activation were evaluated: (i) Dispersion of the TiO_2-particles in an alcoholic/aqueous NH_3 solution and subsequent addition of tetraethoxysilane (TEOS, **73**) and subsequently Me_3SiOEt, and (ii) Dispersion of the TiO_2-particles in water, addition of $TiCl_4$, after 30 min an alcoholic/aqueous NH_3 solution then TEOS/aq. NH_3/EtOH and subsequently a mixture of functional silanes and Me_3SiOEt. The former conditions are also

applied for the synthesis of SiO_2 particles from $Si(OEt)_4$.[126] The latter conditions were inspired by a modification procedure applied by Grätzel *et al.* for the modification of nanoporous TiO_2 photoelectrodes.[127][25, 128, 129] Since preliminary experiments showed that the latter conditions proved to be more efficient in particle functionalization, most reactions were carried out according to these conditions. An overview of the experiments towards surface functionalization and incorporation of functional groups is presented in Table 28; the precise stoichiometry of the individual reaction runs is summarized in Table 32 in the experimental part. In general, the particle surface activation according to the $TiCl_4$ method consisted in dispersing TiO_2 in a 0.5 M solution of $TiCl_4$ in H_2O. The dispersion is stirred for 30 min at 60 °C. Then the hydrolytic mixture comprising MeOH, NH_3 and H_2O (the amount of NH_3 was chosen so that it overcompensates the HCl formed by the hydrolysis of $TiCl_4$) is added. To this dispersion TEOS was added dropwise from EtOH solution. The rational for the latter consisted in keeping the concentration of species resulting from TEOS hydrolysis low thereby favoring the condensation of SiO_2 onto the activated TiO_2 particle surface. The dispersion was stirred for 12 h after completion of TEOS addition. Subsequently functional silanes **70** or **71** and **69** and finally Me_3SiOEt were added dropwise in a stepwise manner. Only after the condensation of Me_3SiOEt the particle dispersion is worked-up by sedimentation and redispersion. Runs BO 441 – 444 (entries 8a – 8d in Table 28) started from the same batch considering the TiO_2-activation. After addition of $Si(OEt)_4$ the batch was split up into 4 portions, which were functionalized with different combinations of silanes.

Table 28. Overview of experiments carried out towards the functionalization of TiO_2 particles. All the runs were terminated by the addition of Me_3SiOEt in order to passivate the particle surface.

Entry	Run	$TiCl_4$	$Si(OEt)_4$	functional silanes used for surface functionalization
1	BO 375		✓	none (except Me_3SiOEt)
2	BO 385	✓	✓	none (except Me_3SiOEt)
3	BO 386	✓	✓	$(MeO)_3Si(CH_2)_3SH$
4	BO 389	✓	✓	$(MeO)_3Si(CH_2)_3SH$
5	BO 412	✓	✓	$(MeO)_3Si(CH_2)_3SH$
6	BO 416	✓	✓	$(MeO)_3Si(CH_2)_3OCO\text{-}CMe{=}CH_2$
7	BO 420	✓	✓	$(MeO)_3Si(CH_2)_3SH$, $Me_2Si(OEt)_2$, $MeSi(OMe)_3$
8	BO 441 – 444[a)]	✓	✓	↓
8a	BO 441			$(MeO)_3Si(CH_2)_3SH$, $NaOSi(OH)_2(CH_2)_2COONa$[b)]
8b	BO 442			$(MeO)_3Si(CH_2)_3SH$
8c	BO 443			$NaOSi(OH)_2(CH_2)_2COONa$
8d	BO 444			none (except Me_3SiOEt)

a) In run 8 the surface activation with $TiCl_4$ and $Si(OEt)_4$ proceeded in one batch which was then split into 4 portions and functionalized individually with different combinations of silanes in runs 8a – 8d. b) When **70** and **69** were added together, two separate dropping funnels were used in order to avoid the beginning of condensation of the two silanes in the dropping funnel.

The products were characterized *via* transmission electron microscopy (TEM), thermogravimetric analysis (TGA), elemental analysis, thiol content *via* the photometric Ellman test, and particle size measurement in MeOH. Some representative samples were also characterized by ^{13}C CP MAS NMR spectroscopy.

9.6.3.2 Transmission Electron Microscopy

Figure 52 shows micrographs of the TiO_2 particles that were employed as substrate for modification procedures. The compact particles reveal a relatively smooth surface. Figure 53 shows micrographs of the TiO_2 particles during and after the modification according to run BO 375 (Table 28, Entry 1). Activation of TiO_2 with TEOS yields no change in overall

particle morphology. However, the growth of a thin SiO_2 shell around the TiO_2 particle can be inferred from the TEM-micrographs a). Further treatment with Me_3SiOEt leads to particles, which comprise of a big core with a dense shell of small particles clustered around (see Figure 53b + c).

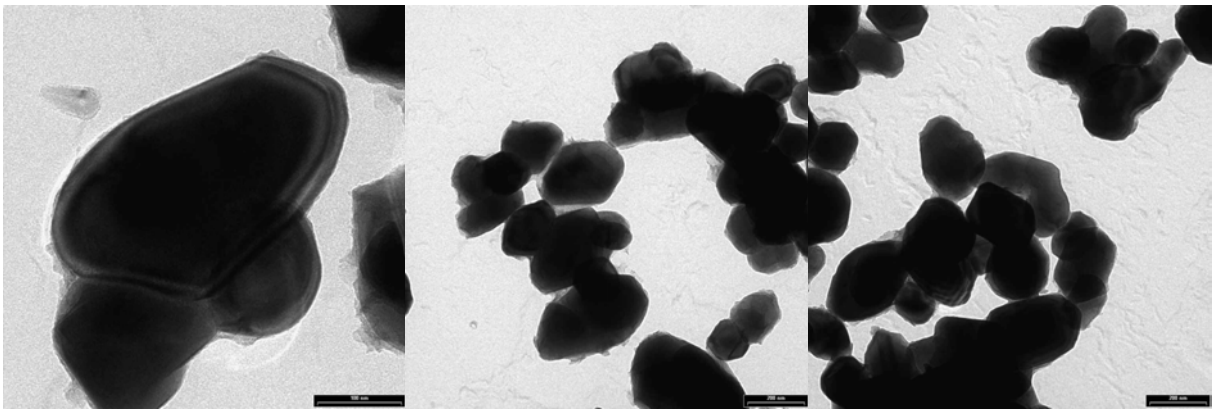

Figure 52. TEM micrographs of the TiO_2 particles used prior to modification.

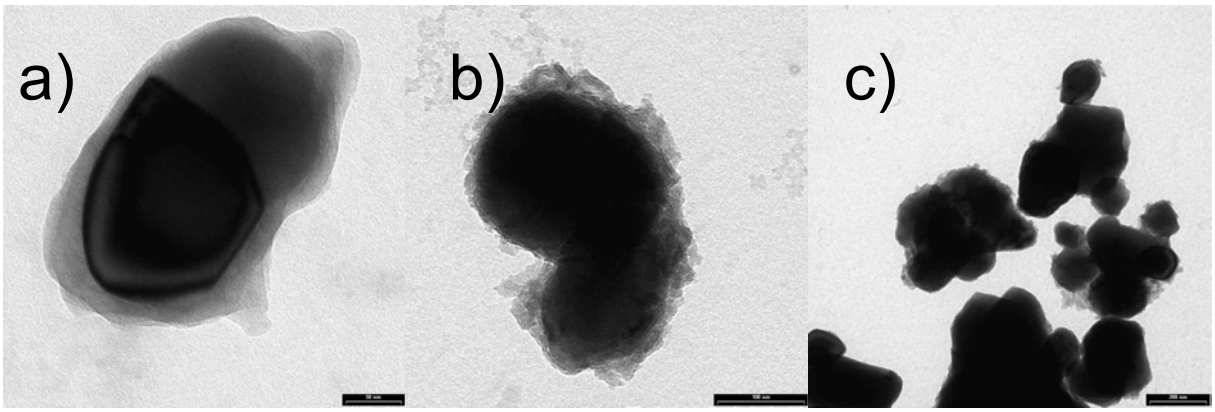

Figure 53. TEM micrograph of TiO_2 during and after run BO 375 (Table 28, entry 1). a) after $Si(OEt)_4$ treatment and b) further modification with Me_3SiOEt. The scale bar corresponds to 50, 100, and 200 nm in a), b), and c), respectively.

Figure 54 through Figure 56 show micrographs from different runs of particle activation *via* $TiCl_4$ in H_2O. This procedure leads to the growth of needle-like structures on the particle surface (Figure 54a and b). This effect is less pronounced in later runs (notably BO 389 Figure 56a and b), which may be ascribed to different sample storage times prior to the TEM measurement. Transferring the $TiCl_4$-activated particles from the acidic to the basic environment of the hydrolytic mixture does not effectuate a change in the surface morphology (Figure 54c). After the condensation of TEOS the modified particles show a pronounced core, which is surrounded by a shell of clustered small particles. The addition of functional silanes and the surface passivation *via* Me_3SiOEt does not affect the particle morphology significantly.

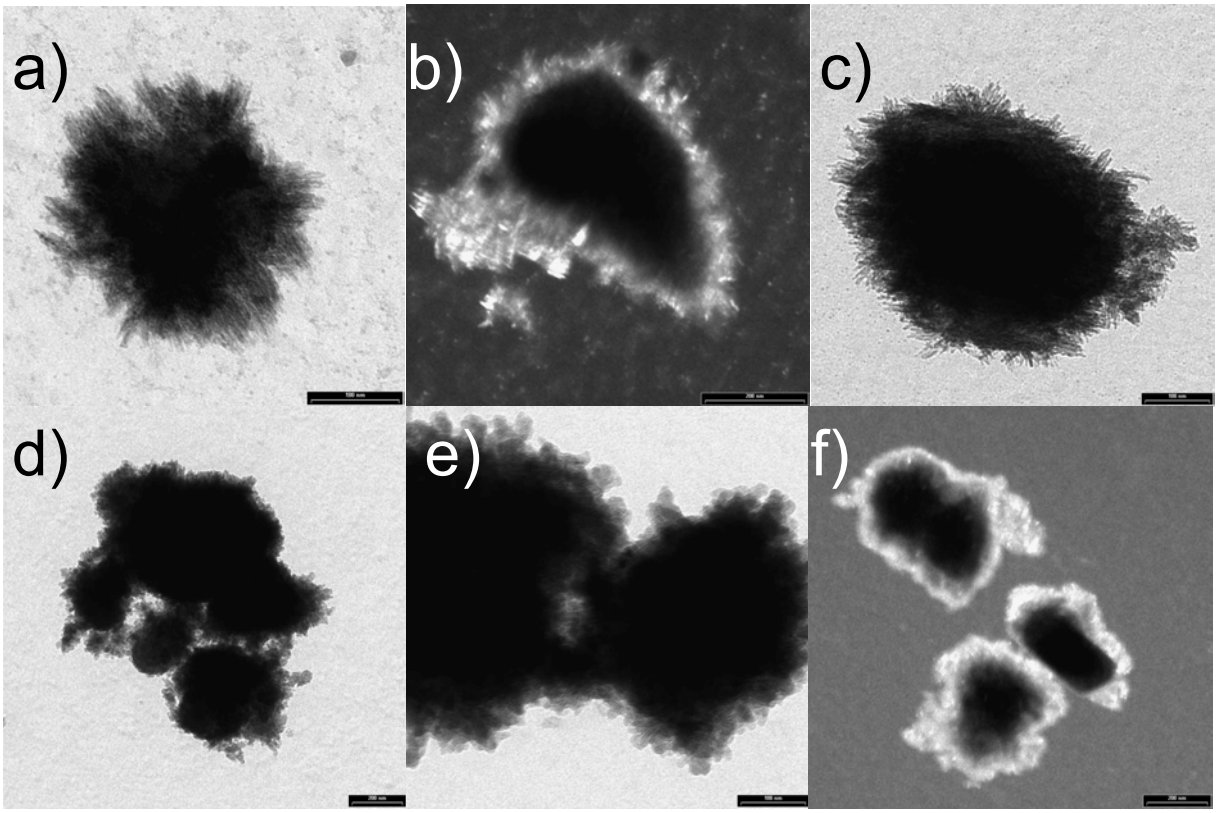

Figure 54. TEM micrograph of TiO_2 during and after run BO 385 (Table 28, entry 2). a) After $TiCl_4$ treatment, b) df-TEM after $TiCl_4$ treatment, c) after immersion into $MeOH/NH_3$, d) after TEOS treatment, e) final product, f) final product df-TEM. The scale bar corresponds to 100 nm in a, c and e and 200 nm in b, d and f.

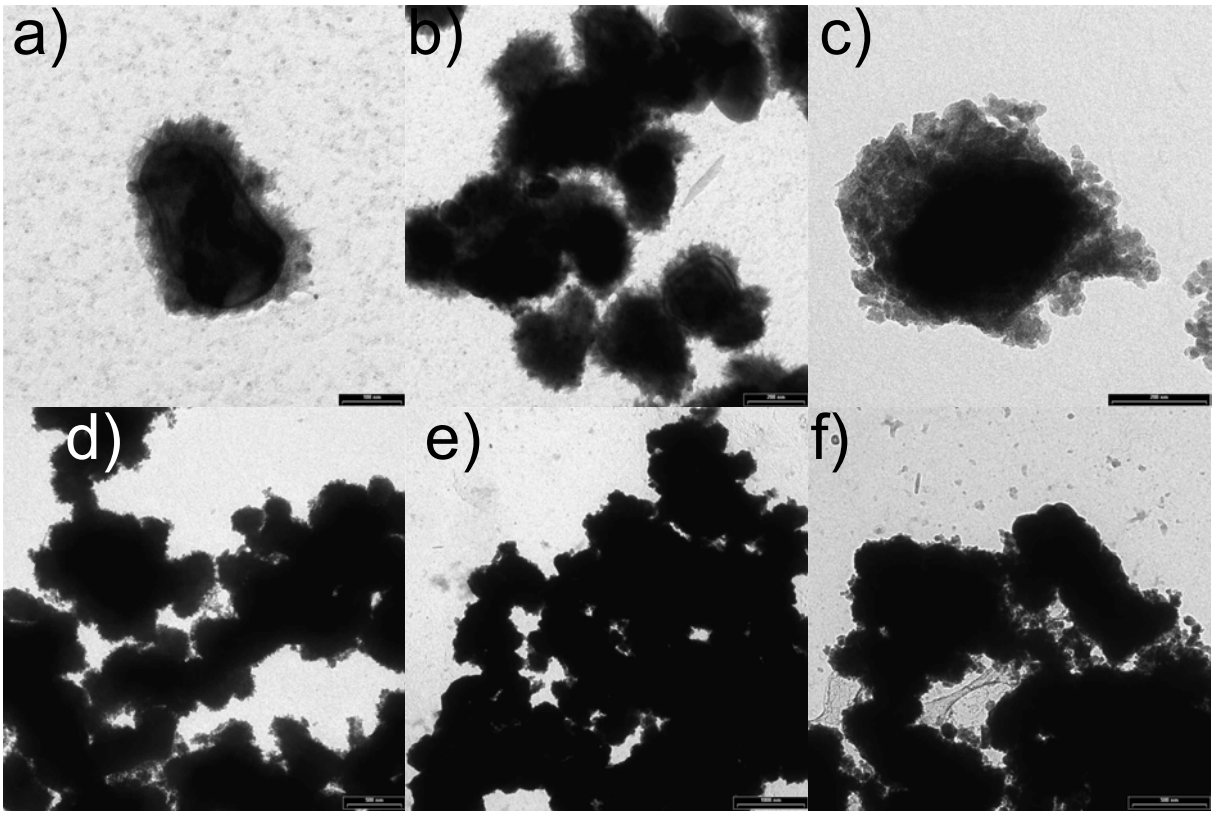

Figure 55. TEM micrograph of TiO_2 during and after run BO 386 (Table 28, entry 3). a + b) After $TiCl_4$ treatment, c + d) after TEOS treatment, e + f) final product after redispersion in MeOH. The scale bar corresponds to 100 nm in a, 200 nm in b + c, 500 nm in d and f and 1000 nm in e.

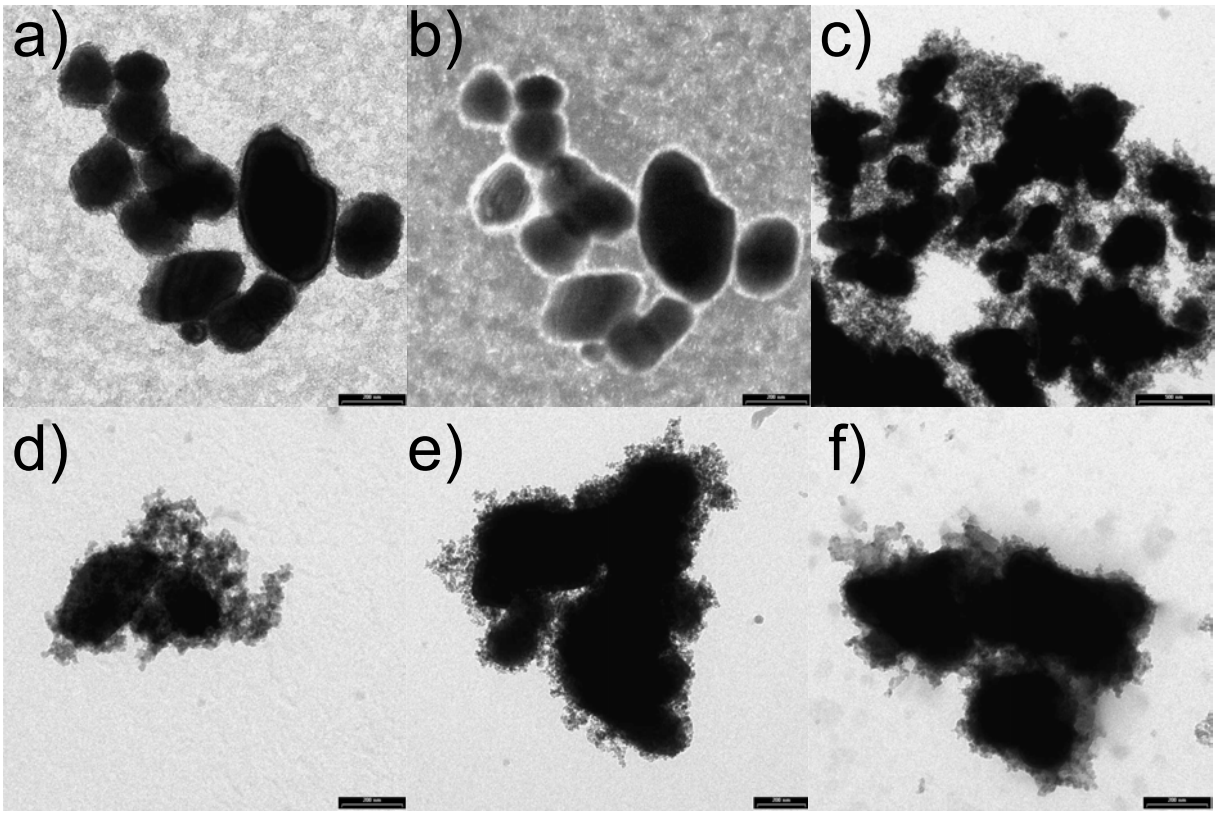

Figure 56. TEM micrograph of TiO_2 during and after run BO 389 (Table 28, entry 4). a + b) After $TiCl_4$ treatment (b: df-TEM), c + d) after treatment with TEOS and $(MeO)_3Si(CH_2)_3$-SH, e) after Me_3SiOEt treatment, f) final product after redispersion in MeOH. The scale bar corresponds to 200 nm in all micrographs except for c (500 nm).

The appearance of the modified particles after the TEOS treatment is very similar in all the runs. The ratio between the amount of small clustered particles and the core is subject to variability. In some TEM micrographs, domains of clustered small particles are visible, which are not bound to the big TiO_2 particles. It can be inferred from the TEM-micrographs that the surface activation route *via* $TiCl_4$ yields to a much higher particle surface area than the treatment with TEOS alone (Table 28, entry 1).

9.6.3.3 Chemical Composition of Functionalized Particles

The chemical composition of the functionalized particles was estimated *via* TGA, elemental analysis, and the photometric Ellman test allowing the quantification of thiol groups. The results from this set of characterization methods are displayed in Table 29. Exemplary TGA-diagrams are displayed in Figure 57. The unmodified TiO_2-particles reveal a mass loss of 2.5% in the TGA and elemental analysis shows that the particles do not contain N, H, or S (only 0.4% of C). After modification with TEOS and Me_3SiOEt (BO 375), the mass loss as determined by TGA under air does not provide any significant change from the unmodified material. In runs where the particle surface activation proceded *via* $TiCl_4$, however, the mass

loss was determined to be between –4% and –8%. This can be ascribed to post condensation of the clustered SiO_2 particles as well as the combustion of the functional groups and thereby mass loss during the TGA measurement.

Table 29. Results of elemental analysis, Ellman test, and TGA and particle size measurements of TiO_2 particles.

Entry	Run	Elemental Analysis					Ellman test S [%]	TGA $\Delta m \cdot m_0$ [%]	Particle size[a] [µm]
		C [%]	H [%]	N [%]	S [%]	Sum			
0	TiO_2	0.41	-	-	-	0.41	n.d.	-2.46	0.58 ± 0.36
1	BO 375	n.d.	n.d.	n.d.	n.d.	n.d.	n.d.	-2.86	0.58[b]
2	BO 385	0.88	0.5	0.4	0	1.78	n.d.	-5.57	1.8 ± 0.8
3	BO 386	1.7	0.54	0.3	0.4	2.94	0.12	-6.65	2.6 ± 1.4
4	BO 389	n.d.	n.d.	n.d.	n.d.	n.d.	0.29	n.d.	2.2
5	BO 412	1.45	0.71	-	0.61	2.77	0.48	-6.37	3.3 ± 1.4
6	BO 416	0.80	1.10	2.10	-	4.00	n.d.	-6.58	2.8 ± 1.5
7	BO 420	1.1	0.35	-	0.2	1.65	0.18	-8.30	21 ± 20[c]
8a	BO 441	1.35	0.3	-	-	1.65	0.11	-4.67	9.2 ± 7.0
8b	BO 442	1.26	0.35	-	0.34	1.95	0.19	-4.19	8.1 ± 5.0
8c	BO 443	1.26	0.32	-	-	1.58	-	-5.72	6.2 ± 4.5
8d	BO 444	0.68	0.29	-	-	0.97	-	-4.05	11.8 ± 7.7

a) Determined *via* quasi elastic light scattering on an HORIBA particle size analyzer after redispersion of the final product in MeOH. The value given is the average particle size and the standard deviation as calculated by the HORIBA software. b) This value was determined using the particle size analyzer "ZETA SIZER". c) This measurement was performed right after the final treatment with Me_3SiOEt.

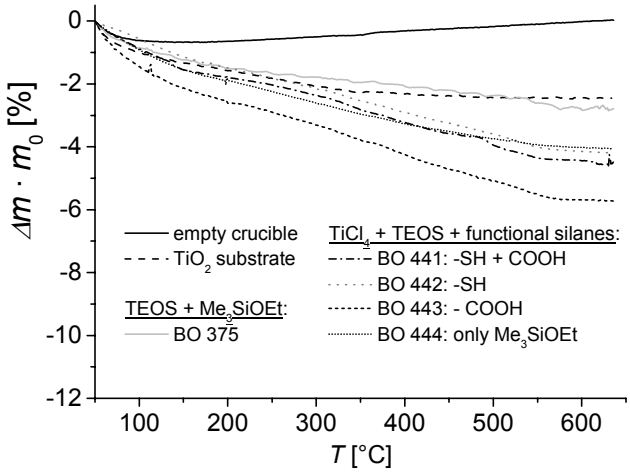

Figure 57. TGA traces of an empty cruscible, the TiO_2 substrate and selected functionalized particles.

A comparison of the carbon content of Runs BO 441 to BO 444 shows that the treatment with TEOS and Me_3SiOEt effectuates a slight increase which is more pronounced, if the functional silanes were used prior to the surface passivation (BO 441 - 443). This clearly points towards the incorporation of the functional silanes. The photometric determination of thiol groups *via* the Ellman test also points to the fact that thiol is present in the modified particles, however, the sulphur content determined by this method is lower than the one determined by elemental analysis. In order to test whether the thiol is indeed covalently bound to the particle surface the following control experiment was conducted: A mixture of TiO_2 with $(MeO)_3Si(CH_2)_3SH$ was sedimented and redispersed in MeOH in analogy to the work-up of the experiments from Table 28. The washed particles did not contain any thiol which was revealed by a negative Ellman test. This demonstrates that unbound thiol is efficiently removed from the reaction mixture by the applied purification method.

9.6.3.4 Particle size

The particle sizes were measured in most cases by redispersion of the modified particles in MeOH and characterization of the resulting dispersion *via* quasi-elastic light scattering (HORIBA particle size analyzer). In some cases the particle size was also determined after each modification step (Figure 58a). The surface activation with TEOS only resulted in a moderate increase in particle size (Table 29, Entry 1). Activation with $TiCl_4$ leads to a much more pronounced initial increase in particle size. The subsequent treatment with TEOS in an alcoholic ammonia solution effects a 2- to 20-fold increase in particle size and in broad particle size distributions which results in the large error given in Table 29. In some cases the particle size decreases slightly upon treatment with Me_3SiOEt.

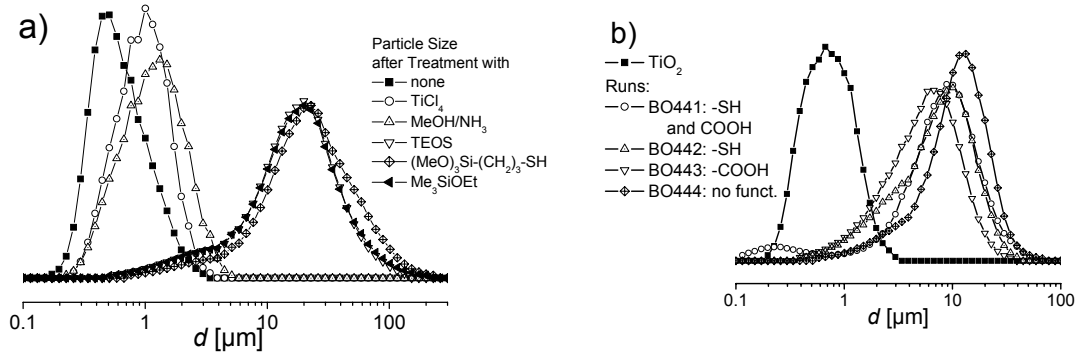

Figure 58. Histograms of particle size distribution a) after each modification step of Run BO 420, and b) after redispersion of reaction products BO 441 – 444 in MeOH.

9.6.3.5 ^{13}C-CP-MAS NMR

Figure 59 shows the ^{13}C-MAS NMR spectra of the reaction products of runs BO 441 – BO 444. These spectra clearly reveal that the groups which were introduced by the functional silanes are present in the particles. The presence of CO_2H is verified by the peak at 175 ppm; its α-CH_2 group resonates at 28 ppm. The signals of further CH_2 groups reveal chemical shifts between 5 and 15 ppm. Furthermore the spectra show that the hydrolysis of the Si-OMe and Si-OEt-functionalities has not been completed during the reaction (signals at around 53 and 60 ppm).

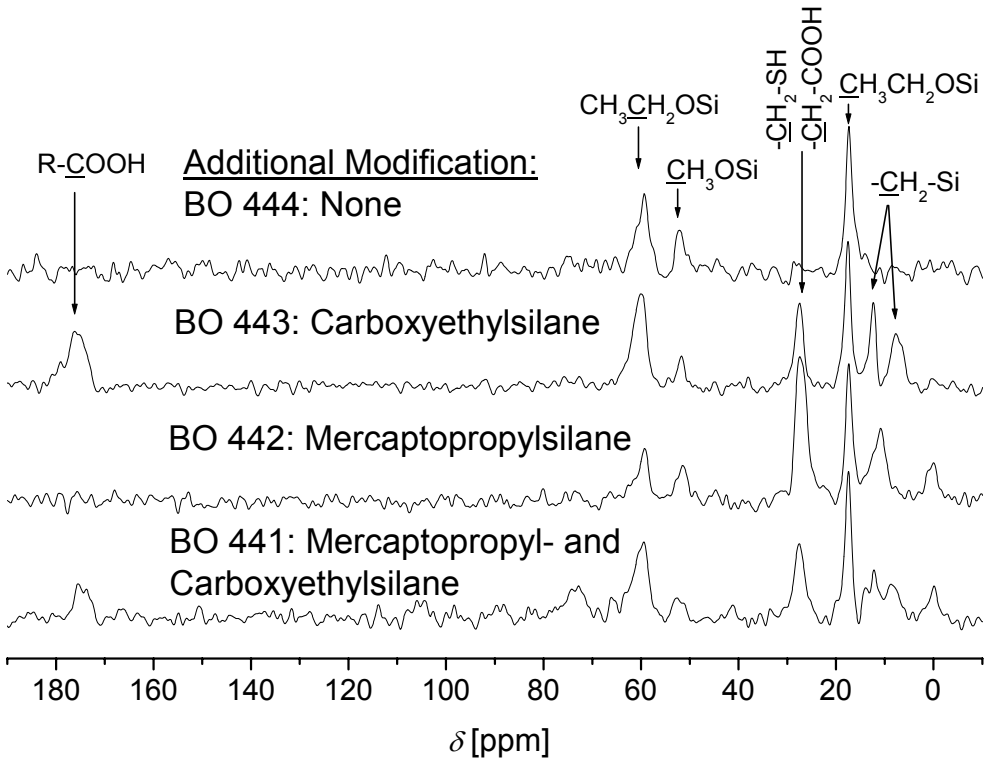

Figure 59. ^{13}C CP MAS NMR spectra of the final products of runs BO 441 – 444.

9.6.4 Grafting Vinyl Monomers to Functional TiO_2 Particles

The modified TiO_2 particles that were obtained according to the conditions from Table 28 were dispersed in monomers and monomer mixtures, which were then polymerized. These syntheses and the characterization of the resulting products are described in the next sections. The results allow evaluation of the question whether the procedure according to Scheme 23 (page 174) is a viable method for the preparation of modified TiO_2 particles for electrophoretic ink applications.

9.6.4.1 Synthesis

The functionalized particles were used in a further reaction to examine the grafting of polymers to the thiol or methacryloyl group *via* a radical polymerization of different monomers. The polymerization experiments comprising the functionalized particles resulting from runs of Table 28 were carried out by dispersing the respective particles in a solution of AIBN in the respective monomer. The individual experimental conditions are summarized in Table 30. Oxygen was excluded from the reaction flask and the dispersion was heated to 65 °C (in some cases to 100 °C). The mixture solidified within 30 min to 2 h. The work-up consisted in redispersion of the residue in THF (or toluene for PS) and three centrifugation-redispersion steps.

Runs 1 – 6 were conducted in order to evaluate the influence of the functional units towards the grafting behavior. In runs 7 – 14 the monomer-initiator ratio was varied for methyl acrylate, methyl methacrylate and *tert*-butyl acrylate. Furthermore methacrylic acid and acrylic acid were employed as comonomer. Runs 15 – 17 aimed at comparing whether the addition of $Me_2Si(OEt)_2$ and $MeSi(OEt)_3$ as surface functionalization reagents (Table 28, Run 7) or the use of a solvent in the polymerization would be beneficial to the grafting procedure. By introducing the more hydrophobic monomer *n*-butyl acrylate in runs 18 – 22 the enhancement of the dispersibility in hydrophobic media was anticipated.

The products resulting from the grafting polymerization were characterized *via* TEM, elemental analysis and TGA as well as towards their dispersability in various solvents. These results are presented in the next sections.

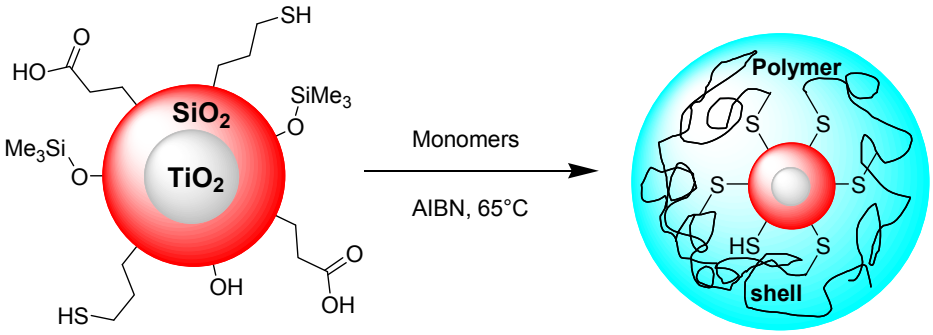

Table 30. Composition of reactions carried out towards the grafting of polymers to functional TiO_2 particles. The functional TiO_2 particles were dispersed in the solution of initiator in monomer (MMA = methyl methacrylate, MA = methyl acrylate, MMAA = methacrylic acid, MAA = methyl methacrylic acid). The dispersion was heated to 65°C, in some cases to 100 °C. After the solidification of the reation mixture THF was added and the particles were isolated and purified *via* three centrifugation-redispersion steps.

#	Run	Substrate			Reaction Conditions			
		Charge	Functionality	m [g]	$m_{Monomer}$ [g]	m_{Init} [a]	Monomers	Yield [g]
1	BO 423	BO 385	none	0.2	1	14.3	MMA	0.5
2	BO 450	BO 444	none	0.5	2.5	35.7	MMA	0.6
3	BO 449[b]	BO 443	-COOH	0.5	2.5	35.7	MMA	0.7
4	BO 448[b]	BO 442	-SH	0.5	2.5	35.7	MMA	0.7
5	BO 447[b]	BO 441	-COOH + -SH	0.5	2.5	35.7	MMA	0.8
6	BO 421[b]	BO 416	-O-CO-CMe=CH_2	1	5	71.4	MMA	1
7	BO 401	BO 389	-SH	1	5	71.4	MA	1
8	BO 404	BO 389	-SH	1	2	71.4	MA	1
9	BO 407	BO 389	-SH	1	1.8 + 0.2	71.4	MA + MAA	1
10	BO 402	BO 389	-SH	1	5	71.4	MMA	0.9
11	BO 405	BO 389	-SH	1	2	71.4	MMA	0.9
12	BO 408	BO 389	-SH	1	1.8 + 0.2	71.4	MMA + MMAA	1
13	BO 403	BO 389	-SH	1	5	71.4	*t*Bu-Acr	0.8
14	BO 406	BO 389	-SH	1	2	71.4	*t*Bu-Acr	0.8
15	BO 415[c]	BO 412	-SH	1	5	71.4	Styrene	1.1
16	BO 424[c]	BO 420	-SH	1	5	71.4	Styrene	1
17	BO 425[c, d]	BO 420	-SH	1	5	71.4	Styrene	1.3
18	BO 465	BO 441	-COOH + -SH	0.5	2.5	35.7	BA	0.7
19	BO 466	BO 442	-SH	0.5	2.5	35.7	BA	0.6

a) Mass of the radical initiator AIBN used in mg. b) The mixture was heated to 100 °C. c) Toluene was used for the work-up. d) 10 g of benzene were added as solvent to the reaction mixture.

9.6.4.2 Thermogravimetric Analysis, Elemental Analysis, and TEM

Table 31 summarizes results from elemental analysis and TGA measurements under air. If oxygen was present in the monomer, the O content was extrapolated from the C content and the sum formula of the respective monomer.

Table 31. Elemental analysis and thermogravimetric data acquired with the reaction products from Table 30. If no value is given for the N or S content it was below the detection limit.

#	Run	Initial functiona-lization	Elemental Analysis						TGA under air		
			C [%]	H [%]	N [%]	S [%]	O [%][a]	Sum[b] [%]	$\Delta m/m$ [%]	T_1 [°C]	T_2 [°C]
1	BO 423	none	1.71	0.63	0.40	-	-	2.74	-8.13		
2	BO 450	none	1.41	0.40	-	-	-	1.81	-4.59		
3	BO 449	-COOH	2.10	0.46	-	-	-	2.56	-6.1		
4	BO 448	-SH	7.16	1.21	-	0.30	3.82	12.49	-14.2		343
5	BO 447	-COOH + -SH	10.91	1.76	-	-	5.81	18.48	-19.4	144	349
6	BO 421	-MPS	18.07	2.41	0.13	0.05	9.63	30.29	-31.8	142	344
7	BO 401	-SH	21.68	2.98	0.12	0.45	12.84	38.07	-39.2		356
8	BO 404	-SH	21.25	2.93	0.13	0.48	12.58	37.37	-30.1		354
9	BO 407	-SH	19.61	2.70	0.13	0.42	11.61	34.47	-39.1		340
10	BO 402	-SH	19.78	2.88	0.12	0.50	10.54	33.82	-34.2	150	343
11	BO 405	-SH	16.44	2.44	0.12	0.46	8.76	28.22	-28.2	131	345
12	BO 408	-SH	16.85	2.55	0.13	0.47	8.98	28.98	-29.4	145	353
13	BO 403	-SH	19.05	2.96	0.14	0.54	9.52	32.21	-22.2	217	337
14	BO 406	-SH	20.54	3.13	0.13	0.49	10.26	34.55	-32.8	214	331
15	BO 415	-SH	17.49	1.94		0.60		20.03	-23		334
16	BO 424	-SH	14.89	1.54				16.43	-17.8		338
17	BO 425[b]	-SH	5.58	0.75				6.33	-8.69		
18	BO 465	-COOH + -SH	8.75	1.44		0.10		13.62	-15.1		287
19	BO 466	-SH	10.34	1.66		0.29		16.23	-18.3		316

a) This value was extrapolated from the C content and the sum formula of the respective monomer if oxygen was present in the monomer. Only the C/O ratio of the major monomer was considered if monomer mixtures were grafted. b) Sum of weight percent of all determined elements.

The most striking result from comparing data from TGA measurements and elemental analysis in Table 31 is that the content of combustible material increases by the polymerization procedure exclusively, if a polymerizable group, namely, the thiol- or acrylate-moiety, was immobilized to the TiO_2 particles prior to the polymerization. Runs BO

423, BO 449 and BO 450 (entries 1 – 3) show a C-content that is not significantly different from the respective starting materials (see entries 2, 8c, and 8d in Table 29 on page 182; BO 385, BO 443, and BO444, respectively). On the other hand, if a group capable of mediating the grafting is present, a significant amount of polymer remains in the reaction product after the work-up. Grafting of MMA to functional particles without covalent attachment should result in a small mass loss as determined by TGA (below 10%). The grafting experiments in bulk monomer with TiO_2-SH derivatives give $\Delta m/m_0$ values between –14 and –39%. Also an onset temperature only prevails if a thiol or methacryloyl moiety is present on the substrates (Figure 60a). The weight percent of combustible elements and the weight loss determined *via* TGA are mostly in good agreement.

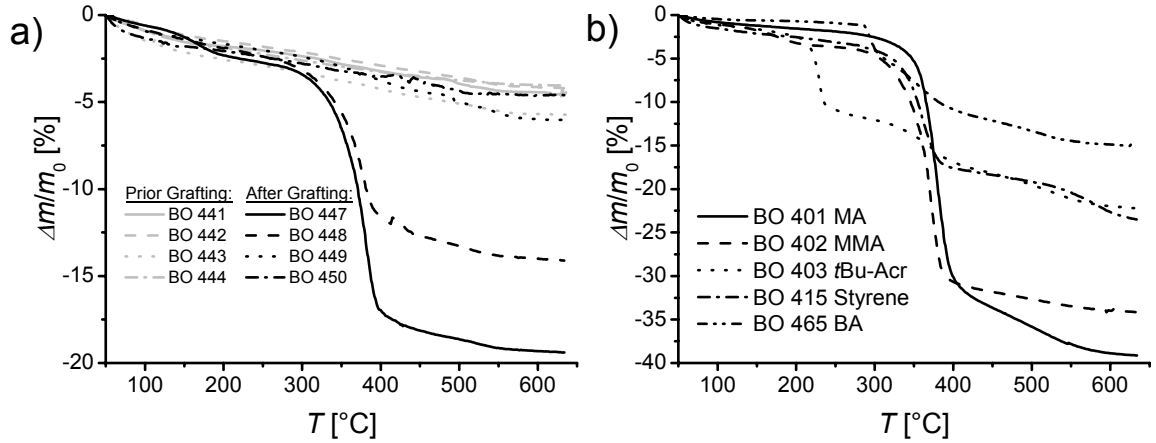

Figure 60. a) TGA traces of modified TiO_2 particles prior (gray) and after (black) subjecting them to the grafting procedure (prior to grafting: Table 28, entries 8a – d, after grafting: Table 30, entries 2 - 5). Only the products BO 447 and BO 448 (Entries 5 and 4, Table 30) that have also been modified with a thiol group show an onset temperature of 349 °C and 343 °C, respectively. In case of BO 449 and BO 450 the grafting step did not influence the TGA result. b) TGA traces of functionalized TiO_2 particles that were subjected to the grafting procedure with different monomers (Table 30, entries 7, 10, 13, 15, 18).

Theoretically, a decrease in initiator concentration should result in an increase in the degree of polymerization, thus also in an increase in the amount of polymer on the particles after grafting. This theoretical predicton is only fulfilled for MMA. The particles emerging from the modification with a mixture of $Me_2Si(OEt)_2$, $MeSi(OMe)_3$, and $(MeO)_3Si(CH_2)_3SH$ do not show an enhanced functionalization with polystyrene (Table 31, entries 15 and 16), Neither does the addition of benzene lead to augmented polymer content (Table 31, entries 17, and 16). The amount of grafted polymer is actually decreased.

A comparison of TEM micrographs prior and after grafting shows that there is no change in particle morphology (not shown). Furthermore, it was not possible to detect a shell or coating that could be ascribed to the polymer grafted onto the particles.

9.6.4.3 Dispersability and Particle Size

Figure 61a-c shows particle size distributions of a dispersion of thiol- and carboxy-modified particles (BO 441 and BO 442) in MeOH and a dispersion of these particles after modification by radical dispersion polymerization with different monomers in different hydrophobic solvents, namely octane and toluene.

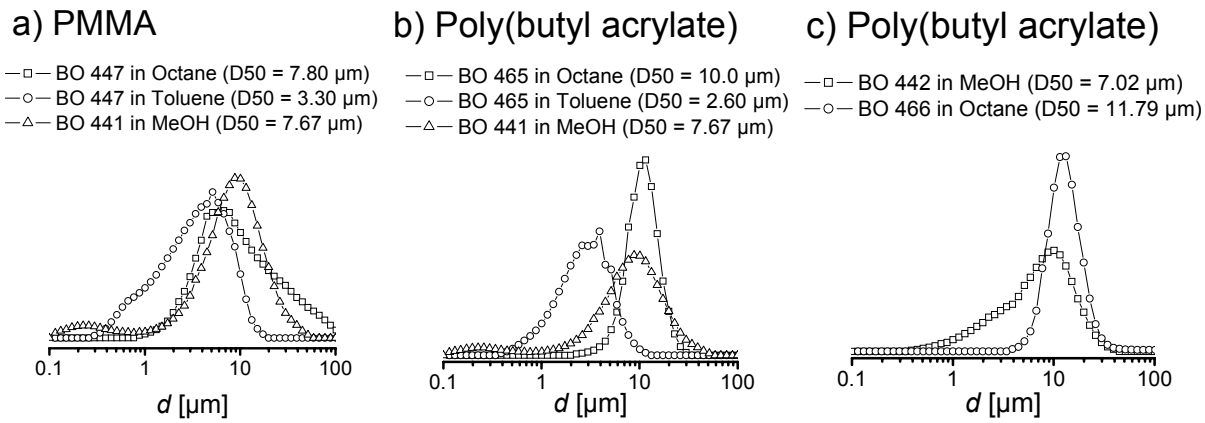

Figure 61. Juxtaposition of particle size distributions of TiO_2-particles prior to the grafting of polymers in MeOH and after grafting and redispersion of the reaction product in hydrophobic solvents. In a) and b) thiol- and carboxy-functionalized particles were used. The particles used for c) exclusively carried a thiol-functionality.

The particle size distribution of the dispersion of PMMA-grafted particles (Figure 61a) has a considerable fraction of larger particles, if dispersed in octane, which points to the fact that these particles are not readily dispersible in this solvent. The particle size distribution of the particles modified with PBA in octane (Figure 61b-c) are comparable to the one of the particles prior to modification in MeOH, which is consistent with the fact that these particles are dispersible in this solvent. Furthermore, dispersions of the grafted particles in toluene show a fraction of smaller particles, which was not present in the substrate particles BO 441 and BO 442. This fact is rather surprising.

Experiments carried out towards the dispersion of the TiO_2 particles synthesized in this work in dielectric media used for to electrophoretic ink revealed that the particles are due to their poor dispersability not suitable for this application.

9.6.5 Summarizing Discussion and Conclusion

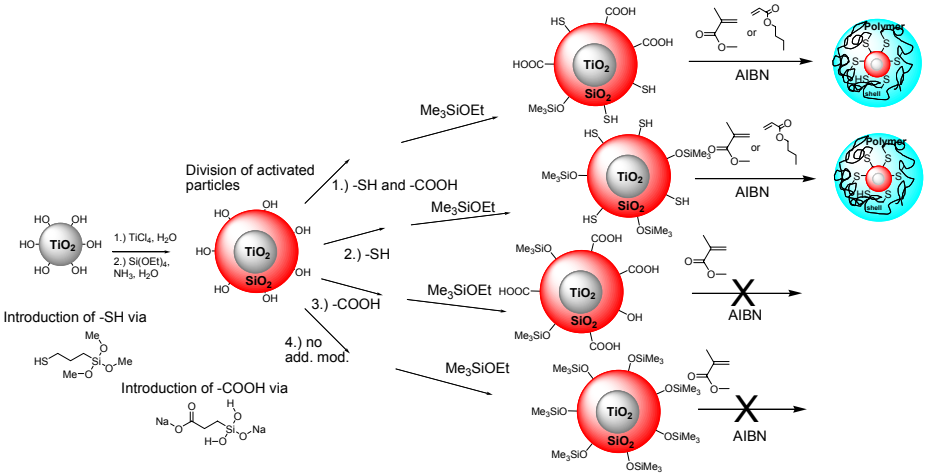

Scheme 25. Summary of experiments conducted towards the modification of TiO_2 leading to COOH- and SH-carrying particles *via* the hydrolytic cocondensation of functional silanes onto an activated particle surface (runs 8a – d, Table 28). Subsequent grafting experiments showed that grafting was only possible if a polymerizable group, e.g., thiol, was immobilized to the particle surface.

By the reaction sequence shown in Scheme 25, rutile particles, which were functionalized with the desired COOH-group and different polymers were acquired. The sequence consisted in particle activation *via* $TiCl_4$ in water, growth of a shell of small silica particles around the activated TiO_2 core using $Si(OEt)_4$ in a hydrolytic mixture containing MeOH, NH_3 and H_2O (see TEM micrographs in e.g., in Figure 54 on page 180). Addition of functional silanes **70**, **71** and **69** led to their incorporation into the SiO_2 shell. The coating with SiO_2 particles was frequently accompanied by a particle aggregation, however, the final particle size potentially still allows their use in electrophoretic displays. The functionalization of the TiO_2 was indirectly proven by elemental analysis and TGA-measurements. The incorporation of the functional silanes was directly proven for the thiol groups by elemental analysis and the photometric Ellman test. The presence of carboxy groups was shown by solid state NMR. Subjecting the functionalized particles to a radical dispersion polymerization in different monomers yielded polymer-functionalized particles, if a polymerizable group, namely, the thiol or methacryloylgroup, was present. The amount of incorporated polymer was typically between 20 and 30 wt%, as shown by elemental analysis and TGA. Although this is a higher polymer content than achieved by others[130] using a similar reaction strategy and grafting conditions, this amount of polymer is not large enough in order to effectively delay sedimentation within an electrophoretic pixel. If butyl acrylate was used for the grafting procedure, the particles were dispersible in octane. The reaction products of the grafting procedure were evaluated for their suitability as pigments in an electrophoretic display. However, they revealed poor dispersability in paraffin oil and were therefore not suitable.[131]

9.7 Experimental Procedures for TiO_2 Particles Modification

9.7.1 Particle Functionalization

The types and quantities of reagents that were used for surface activation and functionalization are summarized in Table 32. A typical procedure is described below.

Surface activation via $TiCl_4$: In a typical procedure a solution of $TiCl_4$ (1.9 g 10 mmol) in water (5 ml) is added to a dispersion of TiO_2 (6 g) in water (15 ml) at 60°C. After 30 min of stirring, a solution of NH_3 (2.24 g of a 25w% solution in water, 132 mmol) in MeOH (146 ml) was added to the dispersion, after which a solution of TEOS (2 g, 9.6 mmol) in MeOH (50 ml) is added dropwise to the alkaline TiO_2 dispersion. The reaction mixture is stirred overnight at 40°C. Then, $(MeO)_3Si(CH_2)_3$-SH (and possibly other compatible, functional silanes) is added dropwise to the reaction mixture. If a COOH-group should be incorporated into the particles, $NaOSi(OH)_2$-CH_2CH_2COONa (25w% in water) is added *via* an extra dropping funnel. The reaction mixture is stirred overnight and finally the particle dispersion is passivated by adding Me_3SiOEt (2 g, 16.9 mmol). Work-up consists of three centrifugation-redispersion-steps in MeOH or EtOH, which was acidified with HCl in order to prevent disulfide-formation of the surface-bound thiols.

Table 32. Experimental parameters during particle surface modification (see section 9.7.1).

Entry	Run	TiO_2	Disp. Media		$TiCl_4$-Treatment				Hydrolytic Mixture			
		m[a)]	Type	V	m_{TiCl4}	n_{TiCl4}	V_{H2O}[b)]	n_{H2O}	m_{NH3}[c)]	n_{NH3}	n_{H2O}[d)]	V[e)]
		[g]		[ml]	[g]	[mmol]	[g]	[mol]	[g]	[mol]	[mol]	[ml]
1	BO 375[g)]	2	EtOH	100					1.64	0.024	0.068	38
2	BO 385	2	Water	15	1.9	10	5	0.277	8.95	0.132	0.37	146
3	BO 386	2	Water	15	1.9	10	5	0.277	8.95	0.132	0.37	146
4	BO 389	6	Water	45	2	11	15	0.833	39	0.574	1.63	445
5	BO 412	6	Water	45	2	11	15	0.833	39	0.574	1.63	445
6	BO 416 [h)]	6	Water	45	2	11	15	0.833	39	0.574	1.63	445
7	BO 420	6	Water	45	2	11	15	0.833	39	0.574	1.63	445
8	BO 441	6	Water	45	2	11	15	0.833	39	0.574	1.63	445

a) mass of TiO_2 particles used for the modification (TIONA 568 from MILLENIUM). b) Volume of water added during the $TiCl_4$-treatment. c) Mass of NH_3-solution (25% in water) d) Moles of water added with the NH_3-solution. e) Volume of MeOH added to the hydrolytic mixture. f) Volume of EtOH used to dilute the respective reagent prior to its dropwise addition. g) An additional 5 ml of water was added to the hydrolytic mixture. h) $(MeO)_3Si(CH_2)_3O$-CO-CMe-$CH=CH_2$ (1.17g, 4.7 mmol) was added as functional silane in EtOH (40 ml).

Table 32. continued.

Entry	Run	$Si(OEt)_4$			$(MeO)_3Si(CH_2)_3SH$			$NaOSi(OH)_2Si(CH_2)_2COONa$			Me_3SiOEt		
		m	n	V[f)]	m	n	V[f)]	m	n	V[f)]	m	n	V[f)]
		[g]	[mmol]	[ml]	[g]	[mmol]	[ml]	[g]	[mmol]	[ml]	[g]	[mol]	[ml]
1	BO 375[g)]	2	9.6	50							2	16.9	30
2	BO 385	2	9.6	50							2	16.9	30
3	BO 386	2	9.6	50	0.308	1.6	27				2	16.91	30
4	BO 389	6	28.8	150	0.924	4.7	30				6	50.7	30
5	BO 412	6	28.8	150	0.924	4.7	30				6	50.7	30
6	BO 416 [h)]	6	28.8	150							6	50.7	30
7	BO 420	6	28.8	150	0.924	4.7	30				6	50.7	30
8	BO 441	6	28.8	150									
8a	BO 441				0.231	1.2	30	0.92	5.3	30	1.5	12.7	30
8b	BO 442				0.231	1.2					1.5	12.7	30
8c	BO 443							0.92	5.3	30	1.5	12.7	30
8d	BO 444										1.5	12.7	30

a) mass of TiO_2 particles used for the modification (TIONA 568 from MILLENIUM). b) Volume of water added during the $TiCl_4$-treatment. c) Mass of NH_3-solution (25% in water) d) Moles of water added with the NH_3-solution. e) Volume of MeOH added to the hydrolytic mixture. f) Volume of EtOH used to dilute the respective reagent prior to its dropwise addition. g) An additional 5 ml of water was added to the hydrolytic mixture. h) $(MeO)_3Si(CH_2)_3O$-CO-CMe-$CH=CH_2$ (1.17g, 4.7 mmol) was added as functional silane in EtOH (40 ml).

9.7.1.1 Photometric Determination of the Thiol Content

The photometric determination of the thiol content was based on the Ellman test.[110] Upon treatment of thiols with **80** in a slight basic medium the yellow color of **81** appears (Scheme 26).

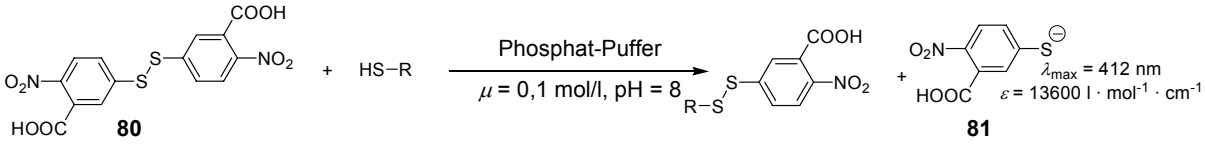

Scheme 26. Exchange reaction the Ellman test is based upon.

The absorbance at 412 nm may be used for the calculation of the initial thiol content according to Lambert-Beer's law. In this work, 3 – 10 mg of the modified TiO_2 particles were suspended in MeOH (5 ml) by means of ultrasound. Then 1 ml of a 0.1 M solution of **80** in water and 9 ml of phosphate buffer (pH = 8, μ = 0.1 M) were added. The suspension was treated in an ultrasound bath for 10 min, then the TiO_2 particles were removed by centrifugation. The supernatant was filtered through a 0.22μ syringe filter the absorbance was measured at 412 nm in 1 cm cuvettes.

9.7.1.2 Grafting of Polymers to Functional TiO_2 Particles

The precise composition of the reaction mixtures are summarized in Table 30 on page 186. The TiO_2 particles were dispersed in a solution of AIBN in the respective monomer. Oxygen was excluded from the reaction flask and the dispersion was heated to 65 °C (in some cases to 100 °C) under stirring with a magnetic stir bar. The mixture solidified within 30 min to 2 h. The work-up consisted in redispersion of the residue in THF (or toluene for PS) and three centrifugation-redispersion steps. The resulting products were dried under high vacuum.

10 References and Notes

[1] M. K. Nazeeruddin, A. Kay, I. Rodicio, R. Humpbry-Baker, E. Müller, P. Liska, N. Vlachopoulos, M. Grätzel, *J. Am. Chem. Soc.* **1993**, *115*, 6382.

[2] R. Amadelli, R. Argazzi, C. A. Bignozzi, F. Scandola, *J. Am. Chem. Soc.* **1990**, *112*, 7099.

[3] B. O'Regan, M. Grätzel, *Nature* **1991**, *353*, 737.

[4] M. Grätzel, *Nature* **2001**, *414*, 338.

[5] D. Cahen, G. Hodes, M. Grätzel, J. F. Guillemoles, I. Riess, *J. Phys. Chem. B* **2000**, *104*, 2053.

[6] U. Würfel, PhD thesis, Albert-Ludwigs-Universität (Freiburg), **2006**.

[7] U. Würfel, J. Wagner, A. Hinsch, *J. Phys. Chem. B* **2005**, *109*, 20444.

[8] T. Trupke, P. Würfel, I. Uhlendorf, *J. Phys. Chem. B* **2000**, *104*, 11484.

[9] M. K. Nazeeruddin, S. M. Zakeeruddin, R. Humphry-Baker, M. Jirousek, P. Liska, N. Vlachopoulos, V. Shklover, C.-H. Fischer, M. Grätzel, *Inorg. Chem.* **1999**, *38*, 6298.

[10] M. K. Nazeeruddin, P. Péchy, T. Renouard, S. M. Zakeeruddin, R. Humphry-Baker, P. Comte, P. Liska, L. Cevey, E. Costa, V. Shklover, L. Spiccia, G. B. Deacon, C. A. Bignozzi, M. Grätzel, *J. Am. Chem. Soc.* **2001**, *123*, 1613.

[11] P. Wang, S. M. Zakeeruddin, J. E. Moser, M. K. Nazeeruddin, T. Sekiguchi, M. Grätzel, *Nature Materials* **2003**, 1.

[12] M. Grätzel, *Inorganic Chemistry* **2005**, *44*, 6841.

[13] K. Hara, T. Horiguchi, T. Kinoshita, K. Sayama, H. Sugihara, H. Arakawa, *Solar Energy Materials and Solar Cells* **2000**, *64*, 115.

[14] K. Hara, Y. Tachibana, Y. Ohga, A. Shinpo, S. Suga, K. Sayama, H. Sugihara, H. Arakawa, *Solar Energy Materials and Solar Cells* **2003**, *77*, 89.

[15] K. Hara, M. Kurashige, S. Ito, A. Shinpo, S. Suga, K. Sayamaa, H. Arakawa, *Chem. Commun.* **2003**, 252.

[16] K. Hara, T. Sato, R. Katoh, A. Furube, T. Yoshihara, M. Murai, M. Kurashige, S. Ito, A. Shinpo, S. Suga, H. Arakawa, *Advanced Functional Materials* **2005**, *15*, 246.

[17] T. Horiuchi, H. Miura, K. Sumioka, S. Uchida, *Journal of the American Chemical Society* **2004**, *126*, 12218.

[18] K. Hara, M. Kurashige, Y. Dan-oh, C. Kasada, A. Shinpo, S. Suga, K. Sayama, H. Arakawa, *New Journal of Chemistry* **2003**, *27*, 783.

[19] S. Ferrere, B. A. Gregg, *New Journal of Chemistry* **2002**, *26*, 1155.

[20] S. Ferrere, A. Zaban, B. A. Gregg, *J. Phys. Chem. B* **1997**, *101*, 4490.

[21] K. Hara, K. Sayama, Y. Ohga, A. Shinpo, S. Sugab, H. Arakawa, *Chem. Comm.* **2001**, 569.

[22] C. Nasr, D. Liu, S. Hotchandani, P. V. Kamat, *J. Phys. Chem.* **1996**, *100*, 11054.

[23] K. Hara, T. Sato, R. Katoh, A. Furube, Y. Ohga, A. Shinpo, S. Suga, K. Sayama, H. Sugihara, H. Arakawa, *J. Phys. Chem. B* **2003**, *107*, 597.

[24] K. Hara, T. Sato, R. Katoh, A. Furube, T. Yoshihara, M. Murai, M. Kurashige, S. Ito, A. Shinpo, S. Suga, H. Arakawa, *Advanced Functional Materials* **2006**, *15*, 246.

[25] S. Ito, S. M. Zakeeruddin, R. Humphry-Baker, P. Liska, R. Charvet, P. Comte, M. K. Nazeeruddin, P. Pechy, M. Takata, H. Miura, S. Uchida, M. Gratzel, *Advanced Materials* **2006**, *18*, 1202.

[26] A. Burke, L. Schmidt-Mende, S. Ito, M. Gratzel, *Chemical Communications* **2007**, 234.

[27] S. Kim, J. K. Lee, S. O. Kang, J. Ko, J.-H. Yum, S. Fantacci, F. D. Angelis, D. D. Censo, M. K. Nazeeruddin, M. Grätzel, *J. Am. Chem. Soc.* **2006**, ASAP.

[28] J. R. Lakowicz, *Principles of Fluorescence Spectroscopy*, Kluwer Academic / Plenum Publishers, New York, **1999**.

[29] A. Adronov, J. M. J. Fréchet, *Chem. Comm.* **2000**, 1701.

[30] T. Förster, *Annalen Der Physik* **1948**, *2*, 55.

[31] T. Förster, *Zeitschrift Fur Naturforschung Section A - A Journal of Physical Sciences* **1949**, *4*, 321.

[32] X. Hu, A. Damjanovic, T. Ritz, K. Schulten, *Proc. Natl. Acad. Sci. USA* **1998**, *95*, 5935–5941.

[33] F. V. R. Neuwahl, R. Righini, A. Adronov, P. R. L. Malenfant, J. M. J. Fréchet, *J. Phys. Chem. B* **2001**, *105*, 1307.

[34] S. L. Gilat, A. Adronov, J. M. J. Fréchet, *J. Org. Chem.* **1999**, *64*, 7474.

[35] A. Adronov, P. R. L. Malenfant, J. M. J. Fréchet, *Chem. Mater.* **2000**, *12*, 1463.

[36] A. Adronov, S. L. Gilat, J. M. J. Fréchet, K. Ohta, F. V. R. Neuwahl, G. R. Fleming, *J. Am. Chem. Soc.* **2000**, *122*, 1175.

[37] A. P. H. J. Schenning, E. Peeters, E. W. Meijer, *J. Am. Chem. Soc.* **2000**, *122*, 4489.

[38] J. M. Serin, D. W. Brousmiche, J. M. J. Fréchet, *Chem. Comm.* **2002**, 2605.

[39] A. Adronov, D. R. Robello, J. M. J. Fréchet, *J. Polym. Sci. Part A: Polym Chem* **2001**, *39*, 1366.

[40] X. Schultze, J. Serin, A. Adronov, J. M. J. Fréchet, *Chem. Comm.* **2001**, 1160.

[41] J. Serin, X. Schultze, A. Adronov, J. M. J. Fréchet, *Macromolecules* **2002**, *35*, 5396.

[42] C. A. Bignozzi, R. Argazzi, C. J. Kleverlaan, *Chem. Soc. Rev.* **2000**, *29*, 87.

[43] F. Odobel, H. Zabri, *Inorg. Chem.* **2005**, *44*, 5600.

[44] L. Jullien, J. Canceill, B. Valeur, E. Bardez, J.-P. Lefèvre, J.-M. Lehn, V. Marchi-Artzner, R. Pansu, *J. Am. Chem. Soc.* **1996**, *118*, 5432.

[45] R. Argazzi, N. Y. Murakami, H. Zabri, F. Odobel, C. A. Bignozzi, *Coord. Chem. Rev.* **2004**, *248*, 1299–1316.

[46] M. K. Nazeeruddin, P. Liska, J. Moser, N. Vachopoulos, M. Grätzel, *Helvetica Chimica Acta* **1990**, *73*, 1788.

[47] W. M. Campbell, A. K. Burrell, D. L. Officer, K. W. Jolley, *Coord. Chem. Rev.* **2004**, *248*, 817–833.

[48] R. B. M. Koehorst, G. K. Boschloo, T. J. Savenije, A. Goossens, T. J. Schaafsma, *J. Phys. Chem. B* **2000**, *104*, 2371

[49] T. Hasobe, H. Imahori, H. Yamada, T. Sato, K. Ohkubo, S. Fukuzumi, *Nano Letters* **2003**, *3*, 409.

[50] J. He, J. Zhao, T. Shen, H. Hidaka, N. Serpone, *J. Phys. Chem. B* **1997**, *101*, 9027.

[51] Y. Takahashi, H. Arakawa, H. Sugihar, K. Hara, A. Islam, R. Katoh, Y. Tachibana, M. Yanagida, *Inorganica Chimica Acta* **2000**, *310*, 169.

[52] H. Sugihara, S. Sano, T. Yamaguchi, M. Yanagida, T. Sato, Y. Abe, Y. Nagao, H. Arakawa, *Journal of Photochemistry and Photobiology, A: Chemistry* **2004**, *166*, 81–90.

[53] A. M. Doherty, S. V. Ley, B. Lygo, D. J. Williams, *J. Chem. Soc. Perkin Trans. I* **1984**, 1371

[54] M. S. Alexiou, V. Tychopoulos, S. Ghorbanian, J. H. P. Tyman, R. G. Brown, P. I. Brittain, *J. Chem. Soc. Perkin Trans. II* **1990**, 837.

[55] S. Saha, A. Samanta, *J. Phys. Chem. A* **2002**, *106*, 4763.

[56] I. Grabtchev, T. Philipova, C. Méallier, S. Guittonneau, *Dyes and Pigments* **1996**, *31*, 31.

[57] I. Grabchev, I. Moneva, V. Bojinov, S. Guittonneau, *J. Mater. Chem.* **2000**, *10*, 1291.

[58] D. Rogez, H. Brandt, H. Finkelmann, P. Martinoty, *Macromolecular Chemistry and Physics* **2006**, *207*, 735.

[59] C. Bourgerette, B. Chen, H. Finkelmann, M. Mitov, J. Schmidtke, W. Stille, *Macromolecules* **2006**, *39*, 8163.

[60] B. Donnio, H. Wermter, H. Finkelmann, *Macromolecules* **2000**, *33*, 7724.

[61] A. Komp, H. Finkelmann, *Macromolecular Rapid Communications* **2007**, *28*, 55.

[62] H. C. Kolb, M. G. Finn, K. B. Sharpless, *Angew. Chem. Int. Ed.* **2001**, *40*, 2004.

[63] W. H. Binder, R. Sachsenhofer, *Macromol. Rapid Commun.* **2007**, *28*, 15.

[64] B. Helms, J. L. Mynar, C. J. Hawker, J. M. J. Fréchet, *J. Am. Chem. Soc.* **2004**, *126*, 15020.

[65] R. K. O'Reilly, M. J. Joralemon, K. L. Wooley, C. J. Hawker, *Chem. Mater.* **2005**, *17*, 5976.

[66] T. Cao, S. E. Webber, *Macromolecules* **1991**, *24*, 79.

[67] K. Y. Tornizaki, P. Thamyongkit, R. S. Loewe, J. S. Lindsey, *Tetrahedron* **2003**, *59*, 1191.

[68] H. Langhals, R. Ismael, O. Yürük, *Tetrahedron* **2000**, *56*, 5435.

[69] S. Krause, Diplom thesis, Universität Freiburg (Freiburg), **2002**.

[70] K. D. Bos, J. G. Kraaijkamp, J. G. Noltes, *Syn. Comm.* **1979**, *9*, 497.

[71] K. Nazeeruddin, K. Kalyanasundaram, M. Grätzel, in *Inorganic Synthesis, Vol. 32*, pp. 181.

[72] N. Garelli, P. Vierling, *J. Org. Chem.* **1992**, *57*, 3046.

[73] A. Ambroise, R. W. Wagner, P. D. Rao, J. A. Riggs, P. Hascoat, J. R. Diers, J. Seth, R. K. Lammi, D. F. Bocian, D. Holten, J. S. Lindsey, *Chem. Mater.* **2001**, *13*, 1023.

[74] Addition of NH4PF6 did not facilitate this separation.

[75] Using an NaCl gradient

[76] The results of the reaction in Run 1 of Table 9 suggest that the Ru-acac-bond is hypothetically acid sensitive

[77] A. Sunder, R. Mülhaupt, R. Haag, H. Frey, *Adv. Mater.* **2000**, *12*, 235.

[78] A. Sunder, H.Türk, R. Haag, H. Frey, *Macromolecules* **2000**, *33*, 7682.

[79] A. Sunder, R. Mülhaupt, R. Haag, H. Frey, *Macromolecules* **2000**, *33*, 253.

[80] M. Erberich, H. Keul, M. Möller, *Macromolecules* **2007**, ASAP.

[81] This polymer was initiated from tetramethylol propane (TMP)

[82] This polymer was synthesized via the polymerization of EEGE initiated from 2-(4-methoxybenzylthio)ethanol and acetal cleavage in THF/HCl

[83] S. Roller, H. Zhou, R. Haag, *Molecular Diversity* **2005**, 1.

[84] J. R. Thomas, X. Liu, P. J. Hergenrother, *J. Am. Chem. Soc.* **2005**, *127*, 12434.

[85] This is probably due to the rather hydrophobic backbone.

[86] D. A. Ossipov, J. Hilborn, *Macromolecules* **2006**, *39*, 1709.

[87] C. Girard, E. Önen, M. Aufort, S. Beauvière, E. Samson, J. Herscovici, *Organic Letters* **2006**, *8*, 1689.

[88] A 1,2,3-triazole derivative carrying a hydroxymethyl substituent in the 4-position and a 3-hydroxypropyl substituent in the 1-position has 13C NMR shifts at 122.8 and 148.9 ppm in CDCl3. A different water soluble triazole derivatives showed resonances at 123.2 and 147.7 ppm.

[89] T. Liebert, C. Hänsch, T. Heinze, *Macromol. Rapid Commun.* **2006**, *27*, 208

[90] Addition of reagents inhibiting the formation of hydrogen bonds (LiCl and urea) to the NMR sample did not lead to a change in the spectrum. From this behavior it was concluded, that the acceptor moieties within these polymers form a solution, while the donor moieties precipitate into the polymer core. Thus the solution may rather be a dispersion of polymeric donor precipitate which is electrostatically stabilized by the deprotonated acceptor groups leading to signals of the donor moiety being underrepresented in the 1H NMR spectrum. On dissolving the polymers 67c and 67b in alkaline DMSO, the donor unit is deprotonated on the amine nitrogen, as evident from the pronounced color change from yellow to bright pink. Under these conditions, both chromophoric units are prevalent in ionic forms, thus one would expect better 1H NMR spectra in this solvent system. Spectra of samples prepared using DMSO-d6:D2O (6:1) and NaOD showed signals of both chromophoric units but no satisfactory signal to noise ratio. The intensity ratio of the signals from donor and acceptor units was dependant on the temperature in the range 297 – 365 K.

[91] S. Roller, C. Siegers, R. Haag, *Tetrahedron* **2004**, *60*, 8711.

[92] C. Siegers, M. Biesalski, R. Haag, *Chem. Eur. J.* **2004**, *10*, 2831.

[93] R. Haag, A. Sunder, A. Hebel, S. Roller, *J. Comb. Chem.* **2002**, *4*, 112.

[94] In case of 67b a low ionic strength was a requirement for the solubility in water.

[95] J. Yang, R. S. Roller, M. A. Winnik, *J. Phys. Chem. B* **2006**, *110*, 11739.

[96] E. K. L. Yeow, K. P. Ghiggino, J. N. H. Reek, M. J. Crossley, A. W. Bosman, A. P. H. J. Schenning, E. W. Meijer, *J. Phys. Chem. B* **2000**, *104*, 2596.

[97] O. Varnavski, G. Menkir, T. G. III, P. L. Burn, *Applied Physics Letters* **2000**, *77*, 1120.

[98] M. Maus, S. Mitra, M. Lor, J. Hofkens, T. Weil, A. Herrmann, K. Müllen, F. C. D. Schryver, *J. Phys. Chem. A* **2001**, *105*, 3961.

[99] B. Zimmermann, personal communication.

[100] P. Bojarski, A. Matczuk, L. Kulak, C. Bojarski, *Asian Journal of Spectroscopy* **1999**, *3*, 1.

[101] It was observed that an increase in molar mass leads to a slight decrease the fluorescence lifetime tau for aminonaphthalimides.

[102] M. Späth, P. M. Sommeling, J. A. M. van Roosmalen, H. J. P. Smit, N. P. G. van der Burg, D. R. Mahieu, N. J. Bakker, J. M. Kroon, *Progress in Photovoltaics* **2003**, *11*, 207.

[103] A. Hinsch, J. M. Kroon, R. Kern, I. Uhlendorf, J. Holzbock, A. Meyer, J. Ferber, *Progress in Photovoltaics* **2001**, *9*, 425.

[104] P. M. Sommeling, H. C. Rieffe, J. A. M. van Roosmalen, A. Schonecker, J. M. Kroon, J. A. Wienke, A. Hinsch, *Solar Energy Materials and Solar Cells* **2000**, *62*, 399.

[105] Assuming a quantitative injection efficiency from the acceptor and also a quantitative collection efficiency, (k = 1).

[106] C. Siegers, J. Hohl-Ebinger, B. Zimmermann, U. Würfel, R. Mülhaupt, A. Hinsch, R. Haag, *ChemPhysChem* **2007**, Advanced online publication.

[107] C. Fik commenting the present work.

[108] H. Gerlach, H. Wetter, *Helvetica Chimica Acta* **1974**, *57*, 2306.

[109] J. W. Lee, S. I. Jun, K. Kim, *Tetrahedron Letters* **2001**, *42*, 2709–2711.

[110] G. L. Ellman, *Archives of Biochemistry and Biophysics* **1959**, *82*, 70.

[111] Changes in positions of the absorption maxima are due to a different pH.

[112] J. A. Castellano, K. J. Harrison, in *The Physics and Chemistry of Liquid Crystal Devices* (Ed.: G. J. Sprokel), Plenum, New York, **1980**, pp. 263.

[113] N. K. Sheridon, M. A. Berkovitz, *Proceedings of the Sid* **1977**, *18*, 289.

[114] B. Comiskey, J. D. Albert, H. Yoshizawa, J. Jacobson, *Nature* **1998**, *394*, 253.

[115] I. Ota, J. Ohnishi, Yoshiyam.M, *Proceedings of the Ieee* **1973**, *61*, 832.

[116] A. L. Dalisa, *Ieee Transactions on Electron Devices* **1977**, *24*, 827.

[117] B. Fitzhenryritz, *Ieee Transactions on Electron Devices* **1981**, *28*, 726.

[118] G. Hadziioannou, personal communication.

[119] C. H. M. Caris, R. P. M. Kuijpers, A. M. van Herk, A. L. German, *Makromol. Chem. Macromol. Symp.* **1990**, *35/36*, 535.

[120] R. D. Badley, W. T. Ford, F. J. McEnroe, R. A. Assinks, *Langmuir* **1990**, *6*, 792.

[121] E. Bourgeat-Lami, *J. Nanosci. Nanotech.* **2002**, *2*, 1.

[122] W. Yoshida, R. P. Castro, J.-D. Jou, Y. Cohen, *Langmuir* **2001**, *17*, 5882.

[123] A. V. Blaaderen, A. Vrij, *J. Coll. Int. Sci.* **1993**, *156*, 1.

[124] C. Beck, W. Härtl, R. Hempelmann, *Angew. Chem.* **1999**, *111*, 1380.

[125] see e.g. www.abcr.de

[126] W. Stöber, A. Fink, E. Bohn, *1968* **1968**, *26*, 62.

[127] P. Comte, personal communication.

[128] M. Wei, Y. Konishi, H. Zhou, M. Yanagida, H. Sugihara, H. Arakawa, *J. Mater. Chem.* **2006**, *16*, 1287.

[129] S. Ito, P. Liska, P. Comte, R. Charvet, P. Péchy, U. Bach, L. Schmidt-Mende, S. M. Zakeeruddin, A. Kay, M. K. Nazeeruddin, M. Grätzel, *Chem. Commun.* **2005**, 4351–4353.

[130] Y. Rong, H.-Z. Chen, H.-Y. Li, M. Wang, *Colloids and Surfaces A: Physicochem. Eng. Aspects* **2005**, *253*, 193.

[131] C. Brochon, personal communication.

11 Kurzzusammenfassung

In der vorliegenden Arbeit wurden Energie Donor-Akzeptor-Systeme (D-A-Systeme) konzipiert, synthetisch dargestellt und in der Farbstoffsolarzelle getestet. Unter monochromatischer Beleuchtung wurde mit den neu dargestellten D-A-Systemen eine Effizienzerhöhung im Vergleich zu Zellen, die lediglich mit der Akzeptor-Komponente sensibilisiert wurden, erzielt. Die folgende Vorgehensweise führte zu diesem Ergebnis: (i) Die auf der Förster-Theorie basierte Wahl geeigneter Chromophore als Energiedonor und –akzeptoreinheiten, (ii) die Darstellung verschiedener synthetischer D-A-Systeme, (iii) die Entwicklung einer Methode zur Charakterisierung des Energietransfers in der Farbstoffsolarzelle und (iv) die Auswertung der Zelldaten, die mit D-A-Systemen sensibilisiert wurden.

Die Akzeptor-Chromophore, die in dieser Arbeit verwendet wurde waren [Ru(dcbpy)$_2$acac]Cl Derivate (dcbpy = 4,4'-Dicarboxy-2,2'-bipyridin, acac = Acetylacetonato). [Ru(dcbpy)$_2$acac]Cl besitzt gute photoelektrochemische Eigenschaften. Weiterhin bot sich an letztgenanntem Komplex die Möglichkeit, den Acetylaceton-Liganden an den terminalen Methylgruppen zu modifizieren, ohne dadurch eine Änderung in seinem Verhalten als Sensibilisator zu bewirken.

Als Energiedonoren wurden alkylierten 4-Amino-1,8-naphthalimide (im Folgenden als Fluorole bezeichnet) eingesetzt. Diese Verbindungen erfüllen die Voraussetzungen für effizienten Energietransfer zu [Ru(dcbpy)$_2$acac]Cl, ihre komplementäre Absorption zu [Ru(dcbpy)$_2$acac]Cl war für die hier durchgeführten Arbeiten von Bedeutung.

Die kovalente Bindung zwischen Donor- und Akzeptorchromophoren wurde in der vorliegenden Arbeit über zwei verschiedene Konzepte erzielt. Zum einen wurde eine Dyade, die aus jeweils einer Donor- und Akzeptoreinheit bestand, in einer mehrstufigen Synthesesequenz dargestellt. Dazu wurde jeweils ein Olefin-funktionalisiertes Fluorol und Oct-7-en-2,4-dion nacheinander an das Dihydrosilan $HSiMe_2$-CH_2CH_2-$SiMe_2H$ gekuppelt. Das resultierende Derivat, das einen Donor-funktionalisierten Acetylaceton-Liganden darstellte, wurde weiterhin mit [Ru(di-Me-dcbpy)$_2$Cl$_2$] (di-Me-dcbpy = dcbpy-dimethylester) zu der Donor-Akzeptor-Dyade umgesetzt.

Ein weiteres Synthesekonzept ermöglichte die Darstellung von hyperverzweigten Polyglycerin-Derivaten, die mit Donor- und Akzeptoreinheiten funktionalisiert waren. Zunächst wurden Alkin-funktionalisierte Donor- und Akzeptoreinheiten sowie Polyglycerin-azid synthetisiert. Die kovalente Verknüpfung letztgenannter Bausteine erfolgte anschließend über eine 1,3-dipolare Cycloaddition der polymeren Azide mit den Alkin-Gruppen der Chromophore („Click-Chemie"). Es wurde eine Reihe von Polymeren mit verschiedenen Chromophordichten und Donor-Akzeptor-Verhältnissen dargestellt.

Die unterschiedlichen, hier dargestellten Donor-Akzeptor-Sensibilisatoren wurden in Farbstoffsolarzellen eingebracht. Außerdem wurden Zellen untersucht, die über Koadsorption mit einem Carboxy-funktionalisieten Donorchromophor und [Ru(dcbpy)$_2$(NCS)$_2$] als Akzeptorchromophor sensibilisiert waren. Folglich resultierten Solarzellen die (i) über die Dyade, (ii) über Polymere und (iii) über Koadsorption mit verschiedenen Donor-Akzeptor-Systemen funktionalisiert waren.

Die resultierenden Zellen wurden über Strom-Spanungs-, Transmissions- und EQE-Messungen charakterisiert (EQE = externe Quanteneffizienz). Daraus wurde unter anderem das Verhältnis der Kurzschlussströme (j_b/j_g^{-1}), die unter blauer und grüner Beleuchtung erzielt wurden, berechnet. j_b/j_g^{-1} besagt, um welches Ausmaß sich der Strom der Solarzelle infolge des Energietransfers steigern lässt.

Die Energietransfereffizienz wurde aus den spektralen Eigenschaften der Solarzellen bestinmmt. Es wurde gezeigt, dass in allen drei Fällen hohe Energietransfereffizienzen vorlagen. In einigen Fällen wurde auch eine absolute Zunahme der Zelleffizienz unter Beleuchtung bei 470 nm erzielt. Der Vergleich der verschiedenen, hier untersuchten Methoden zum Einbringen des Donor-Chromophors zeigte, dass sich durch Koadsorption bereits eine Zunahme der monochromatischen Zelleffizienz erzielen lässt, die jedoch stärker ausgeprägt ist wenn Donor- und Akzeptor-Einheit kovalent gebunden vorliegen. Der relative Energietransfer-vermittelte Stromgewinn (j_b/j_g^{-1}) in den Solarzellen betrug mittels Sensibilisierung über Koadsorption 21%, über die Dyade 24% und über Donor-Akzeptor-Polymere bis zu 179% (im Vergleich zum Strom, der erzielt wurde, wenn ausschließlich die Akzeptor-Komponente innerhalb der jeweiligen Zellen bestrahlt wurde). Diese Werte belegen das Potential, das Energietransfersensibilisatoren für die Farbstoffsolarzelle besitzen.

12 Lebenslauf

Name	Siegers
Vorname	Conrad
Titel	Dipl.-Chem.
Geburtsdatum	23.3.1976
Geburtsort	Recklinghausen
Nationalität	deutsch
Zivilstand	verheiratet seit 6.6.2003
Kinder	Andor, geb. 27.4.2004 Finn, geb. 23.10.2006
1995	**Allgemeine Hochschulreife (Abitur)** am *„Rhein-Maas-Gymnasium“*, Aachen
1995 – 1996	Zivildienst an der *„Rheinischen Schule für Körperbehinderte,“* Aachen
1996	Beginn des Studiums der Chemie an der Albert-Ludwigs-Universität, Freiburg
1998	**Vordiplom (Note: sehr gut)**
1998 – 1999	Studium der Chemie an der Queens University, Kingston, Ontario, Kanada im Rahmen des Ontario-Baden-Württemberg Programmes
2002	Diplomarbeit im Arbeitskreis von Prof. R. Mülhaupt; Betreuer: Prof. R. Haag: *„Evaluierung der proteinabweisenden Eigenschaften von Polyglycerin-derivaten an Oberflächen und Synthese difunktionalisieter Linkermoleküle zur Oberflächenmodifizierung“*
2002	**Diplom-Chemiker (Note: sehr gut)**
2003 – 2007	Promotion unter Prof. R. Mülhaupt und Prof. R. Haag, Freiburger Materialforschungszentrum (FMF): *“Light-harvesting via Energy Transfer in the Dye Solar Cell“*

Spectra

Butyl allyl fluorol **30a**

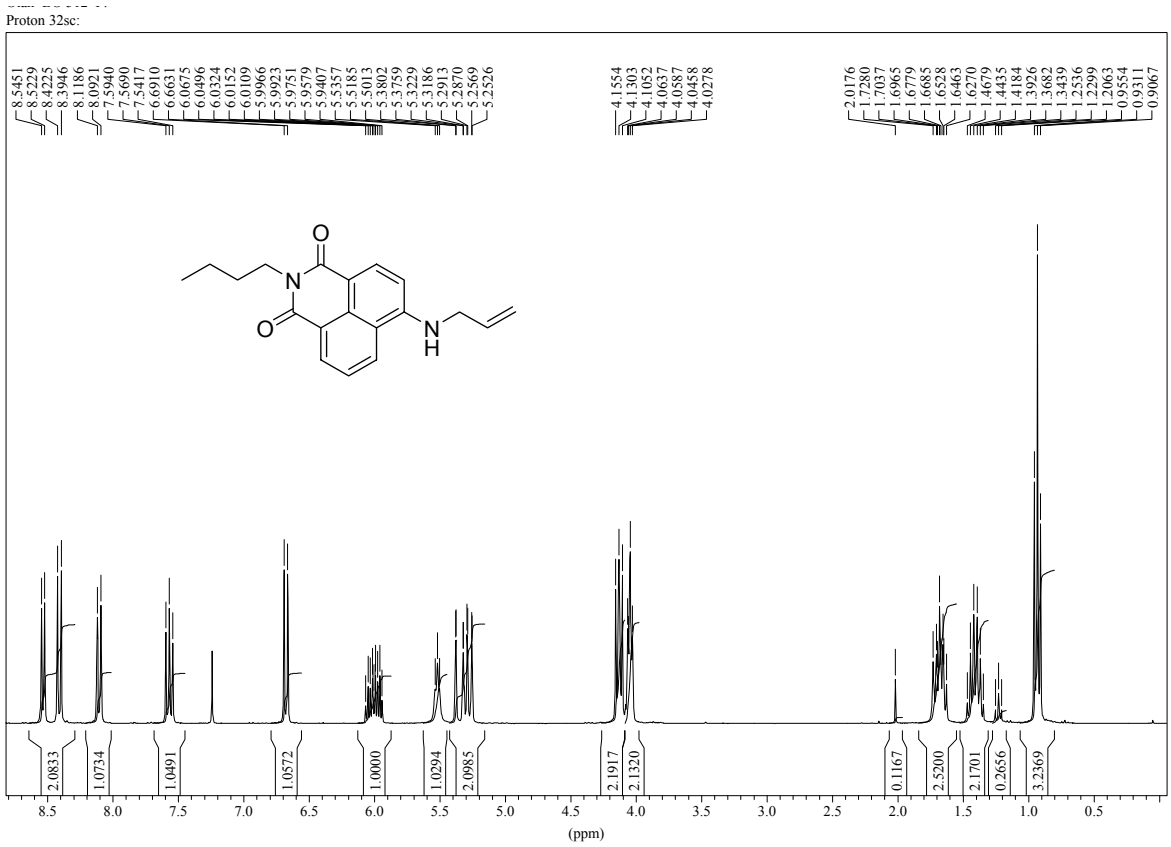

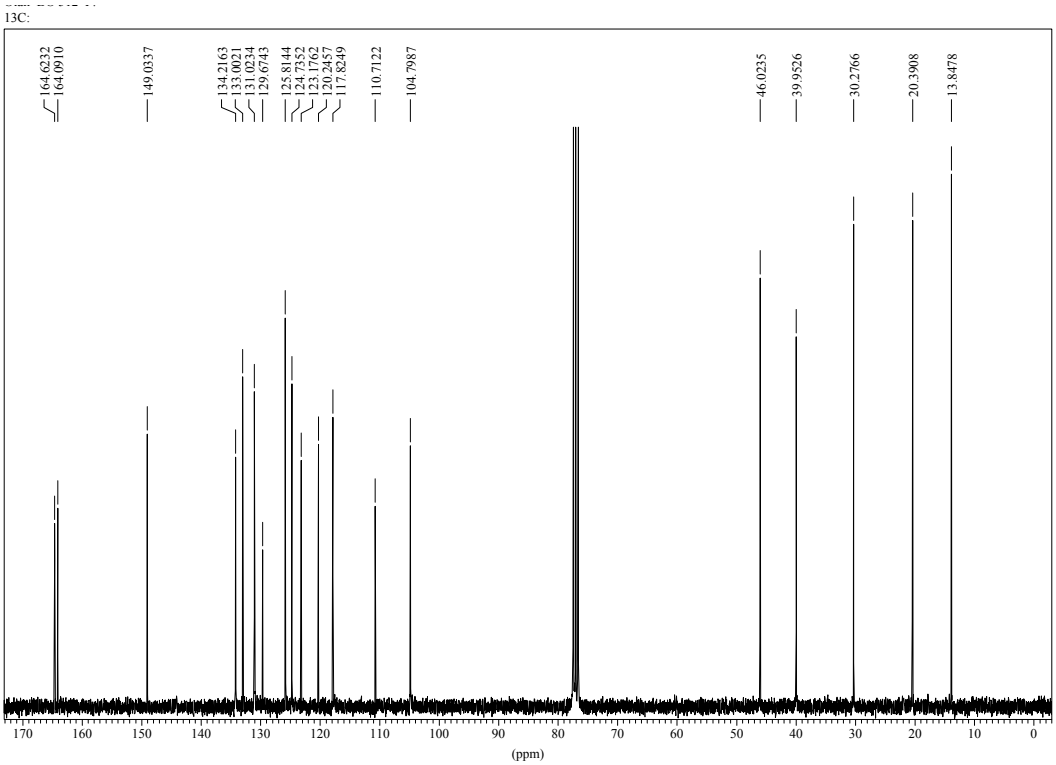

Dibutyl allyl Fluorol **30b**

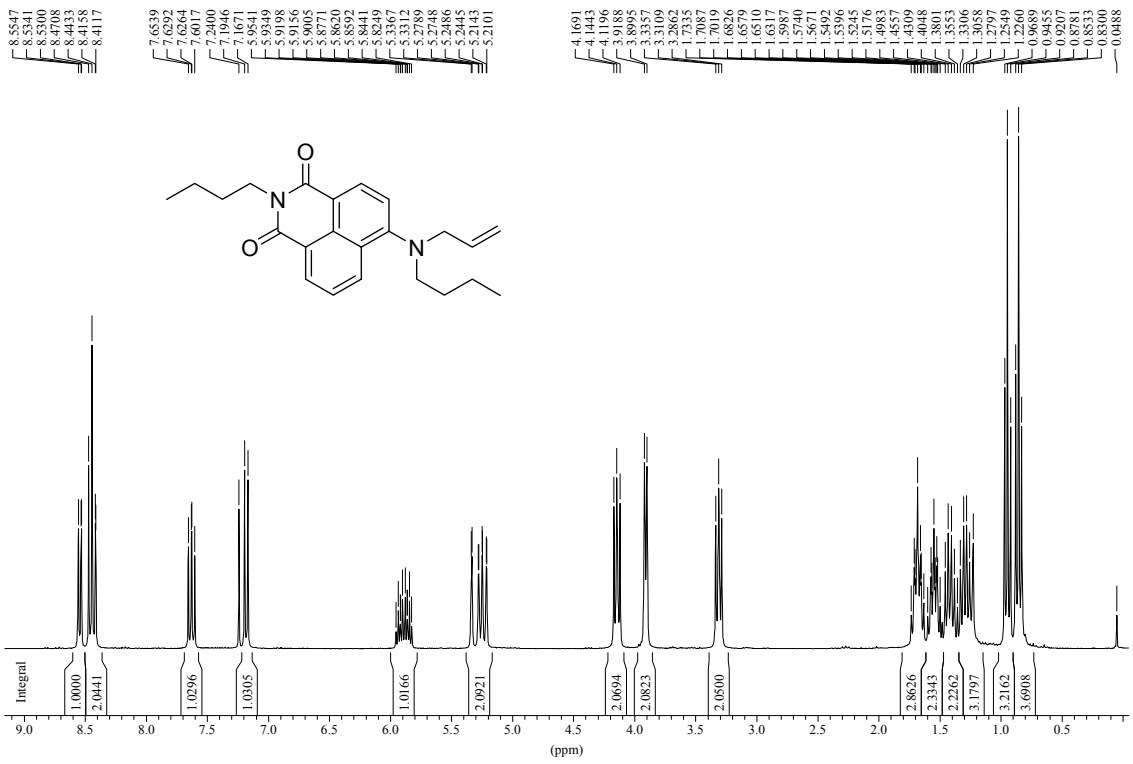

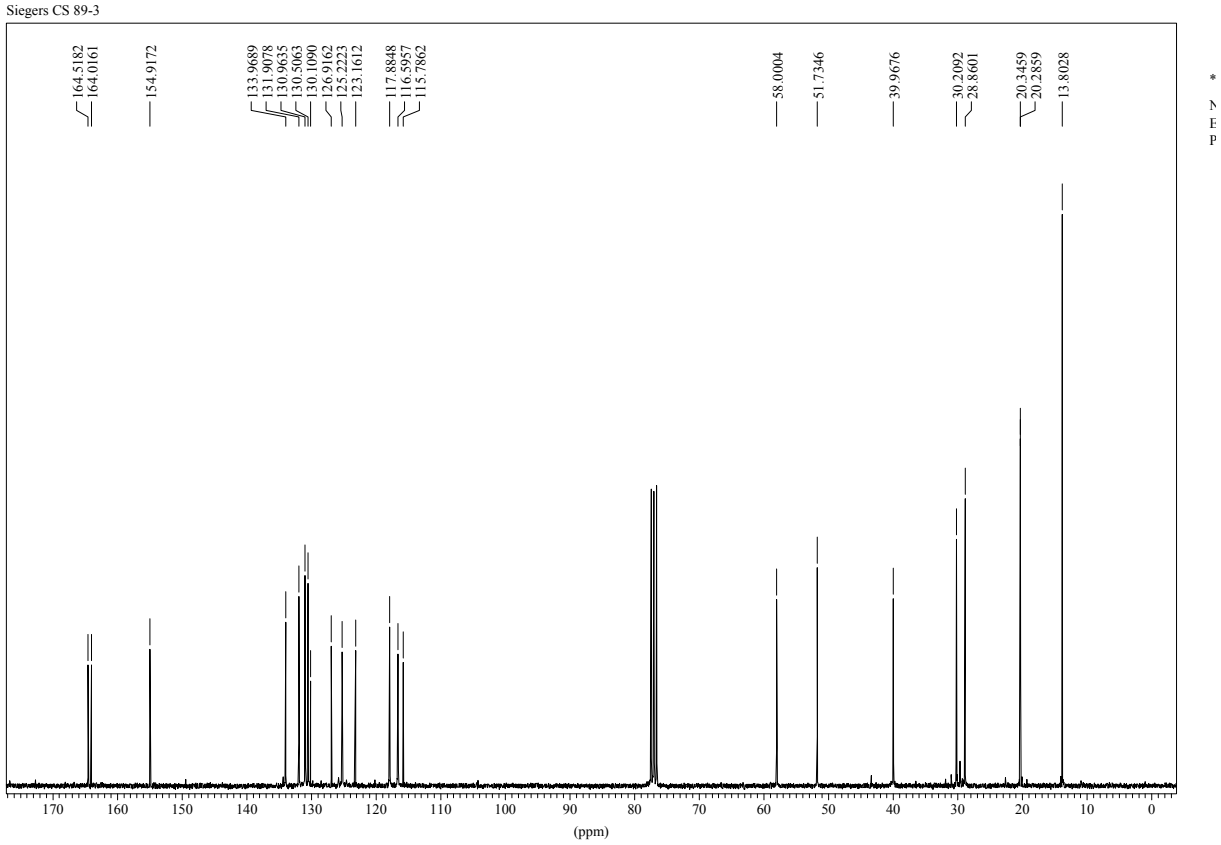

Propargyl butyl fluorol **31**

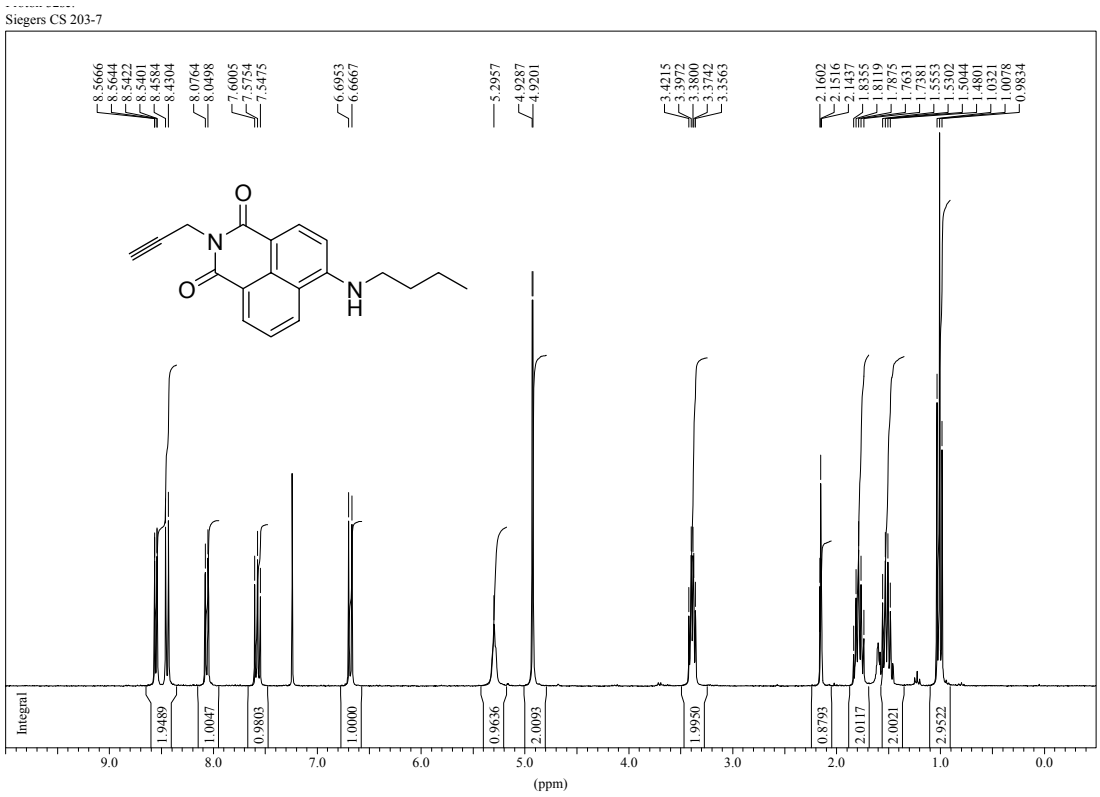

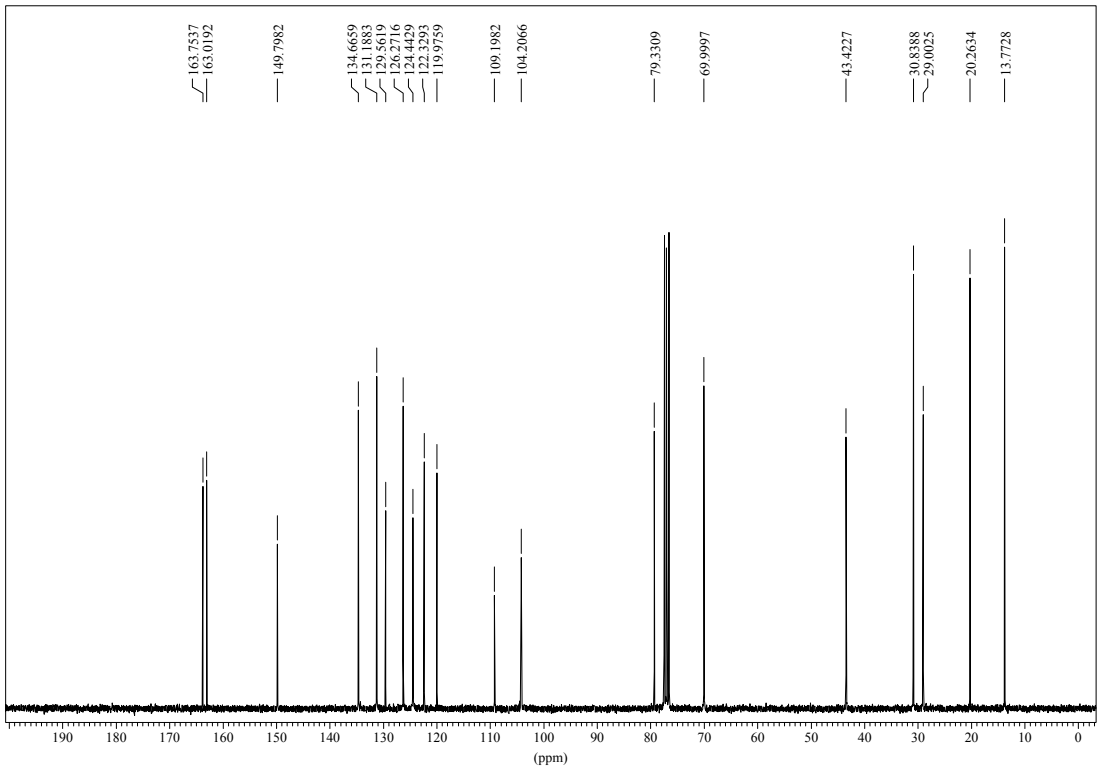

4-Carboxybutyl butyl fluorol **32**

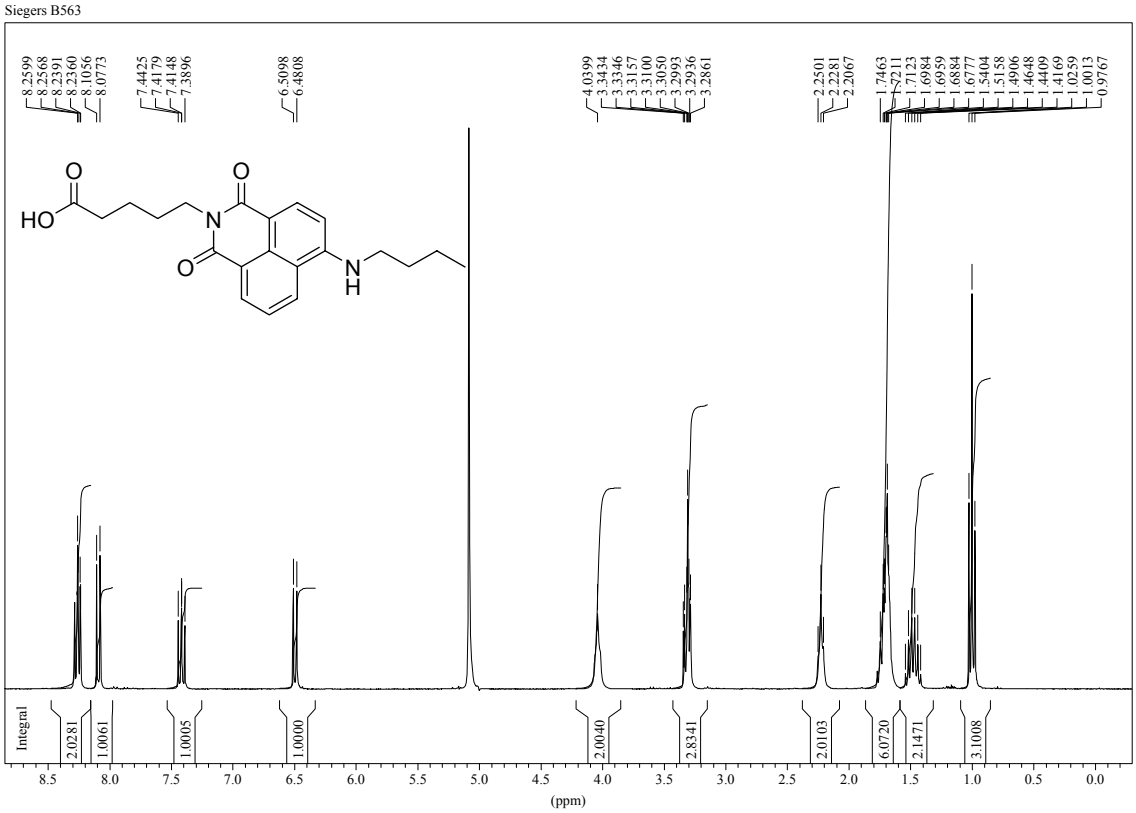

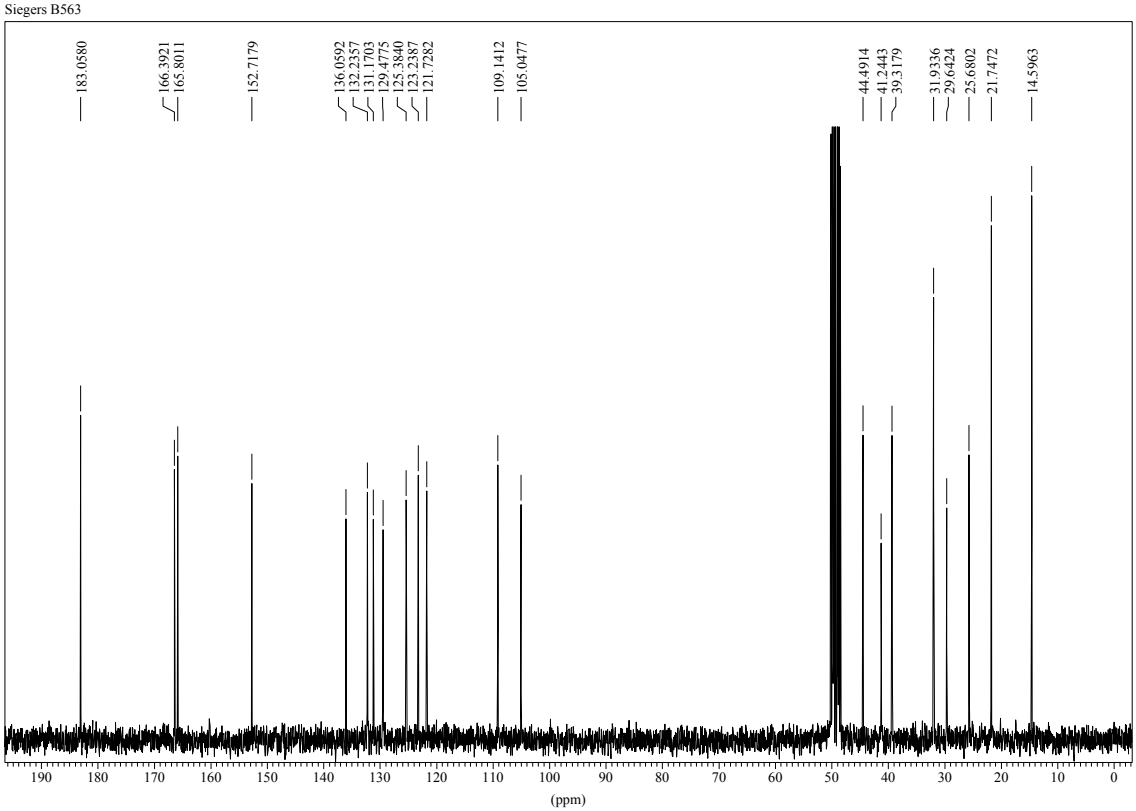

4-Azidobutyl butyl fluorol **33**

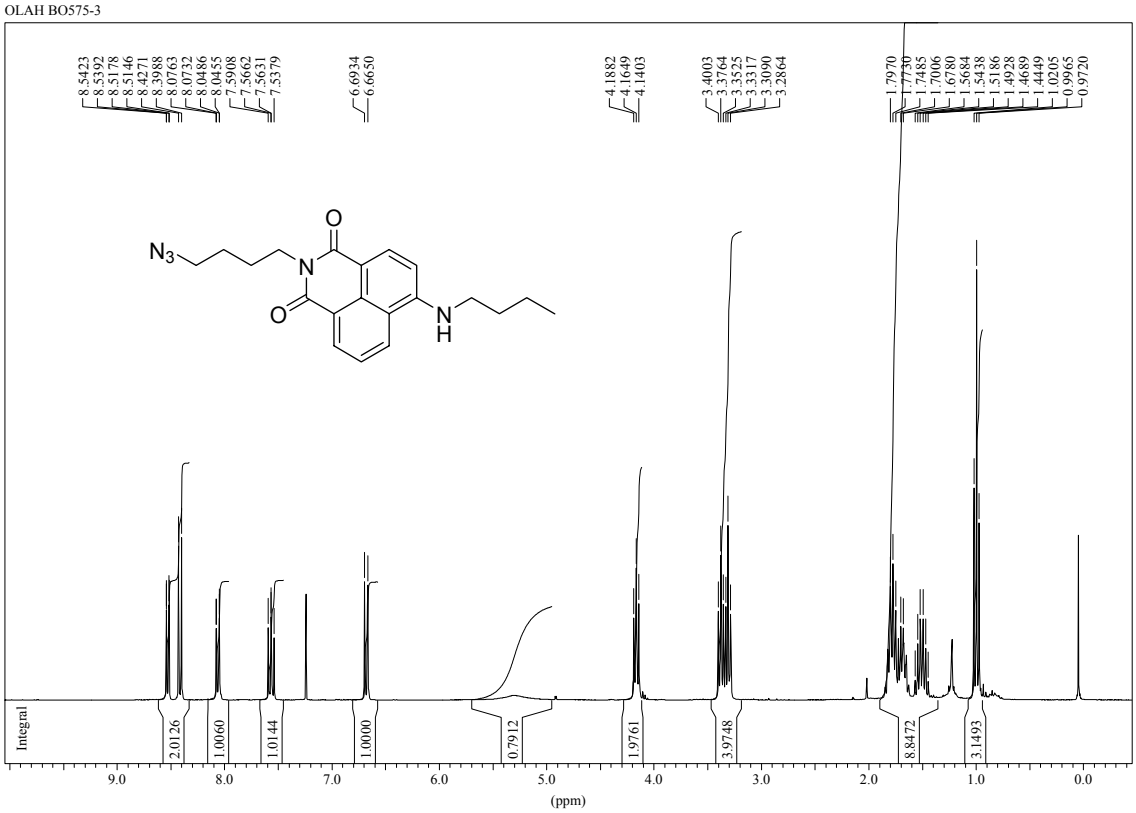

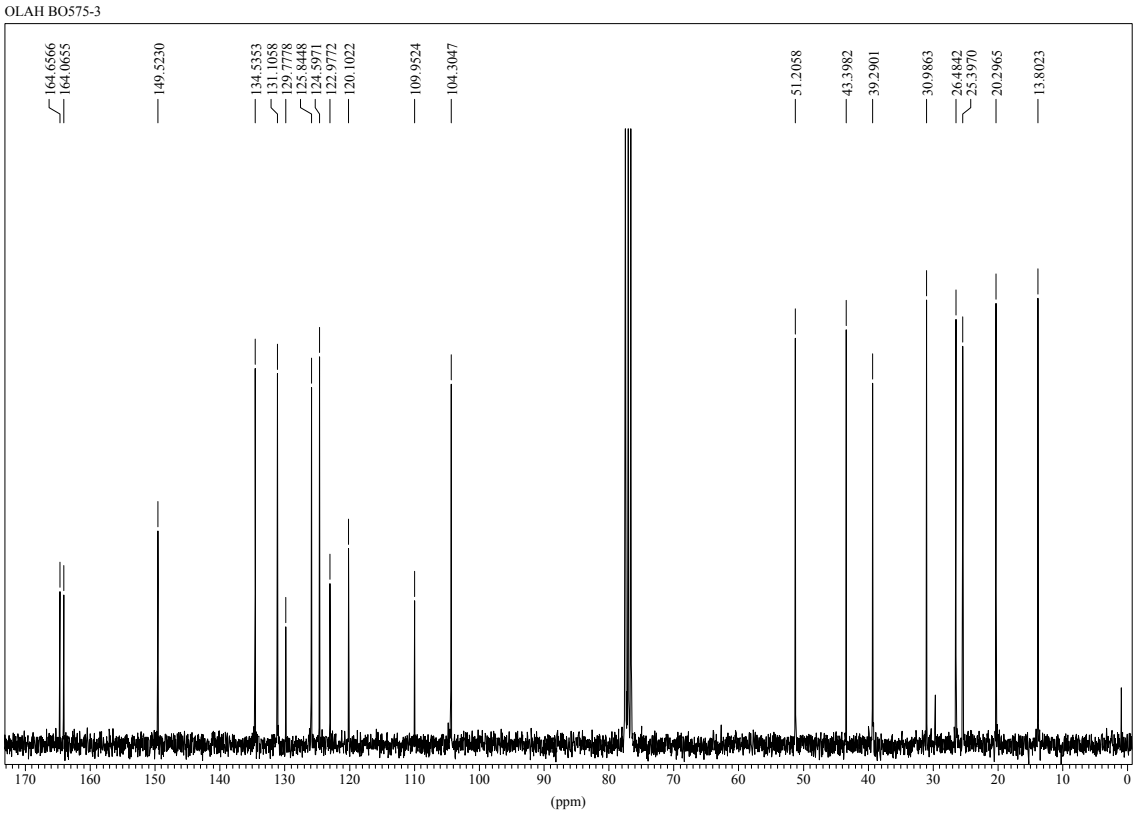

Butyl Hydrosilyl Fluorol **42a**

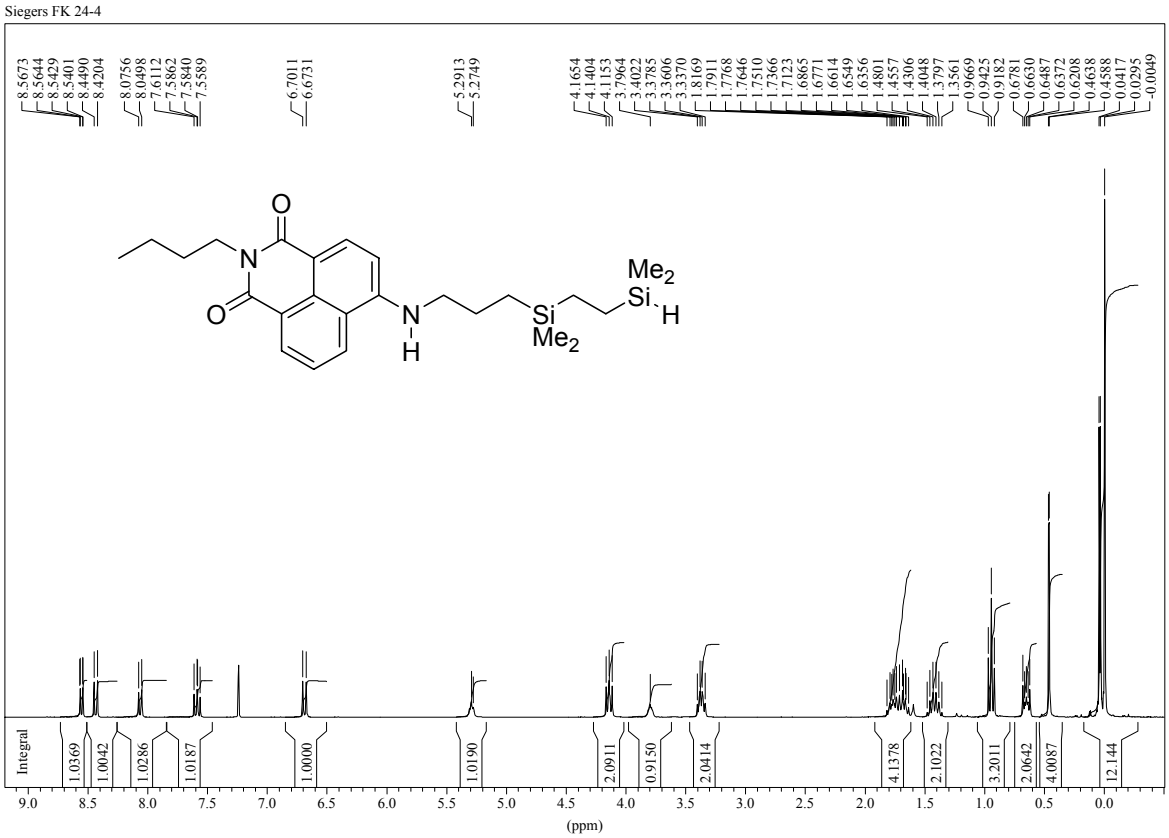

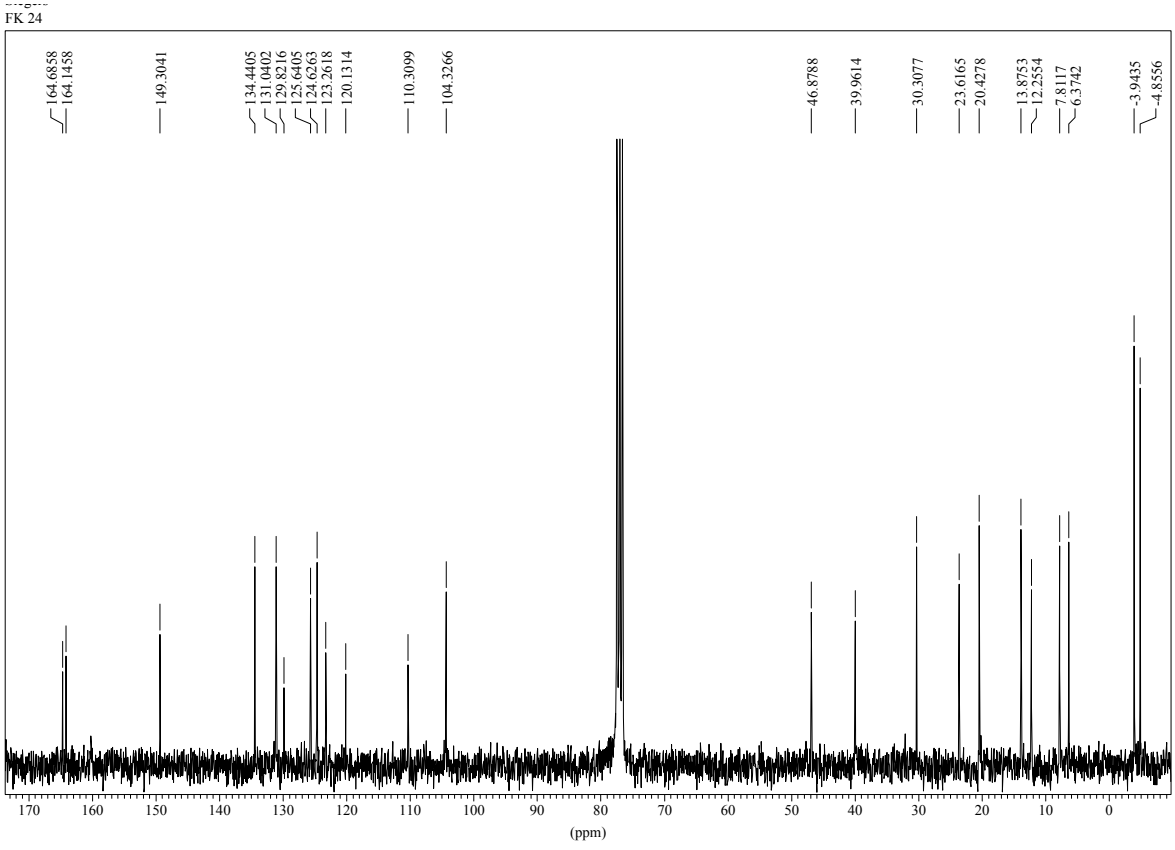

Dibutyl hydrosilyl fluorol **42b**

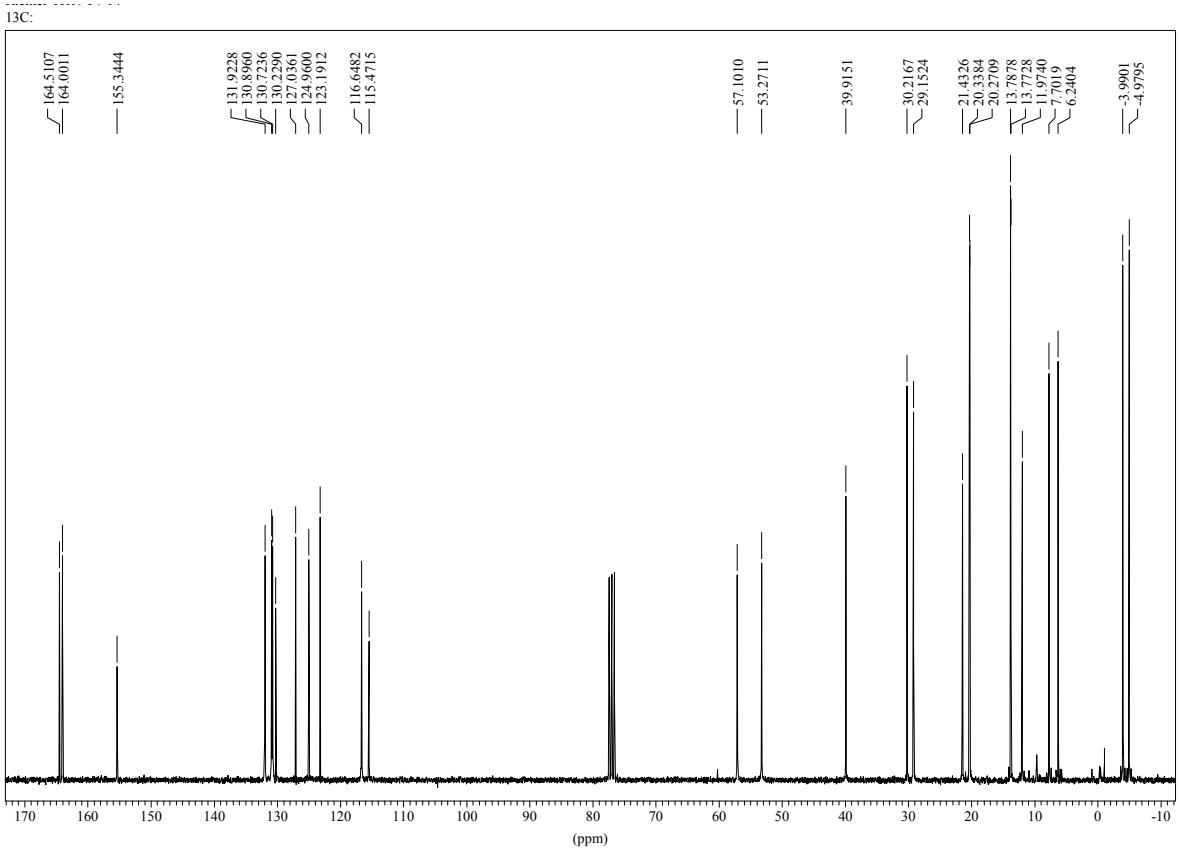

Butyl (diethylsilylpropyl) fluorol **43**

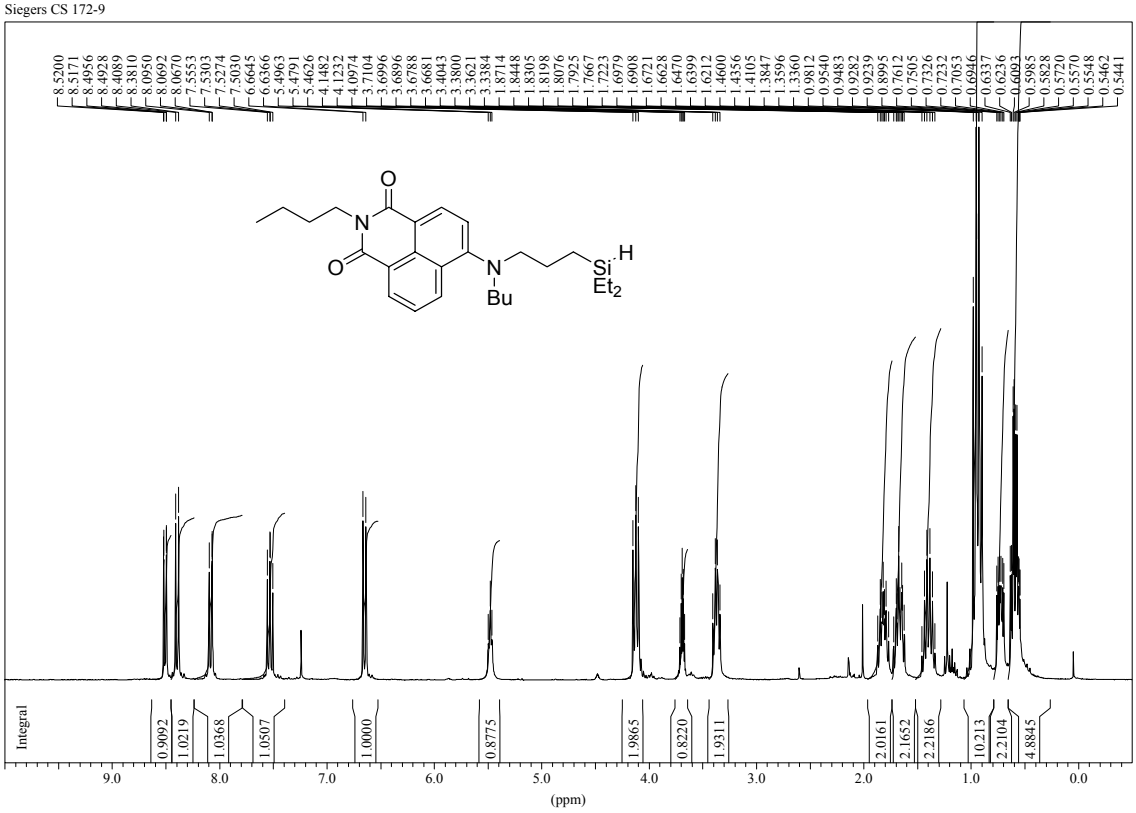

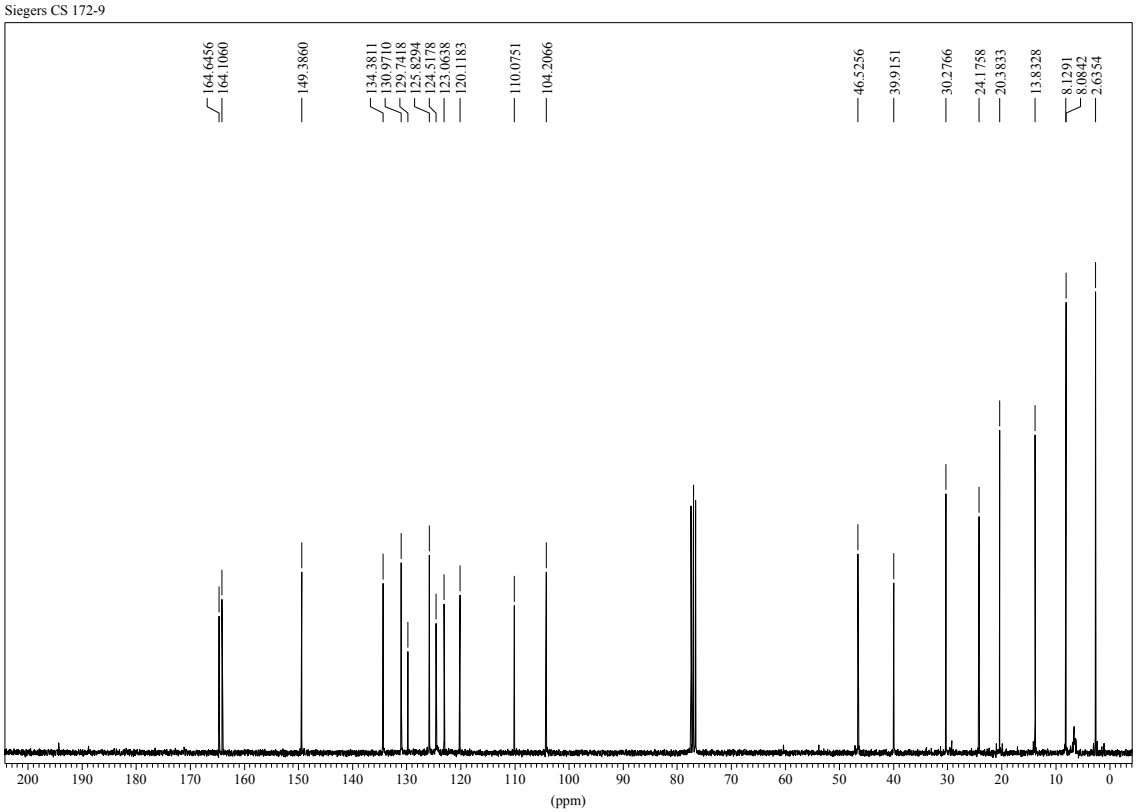

Butyl-acacH-Fluorol **44a**

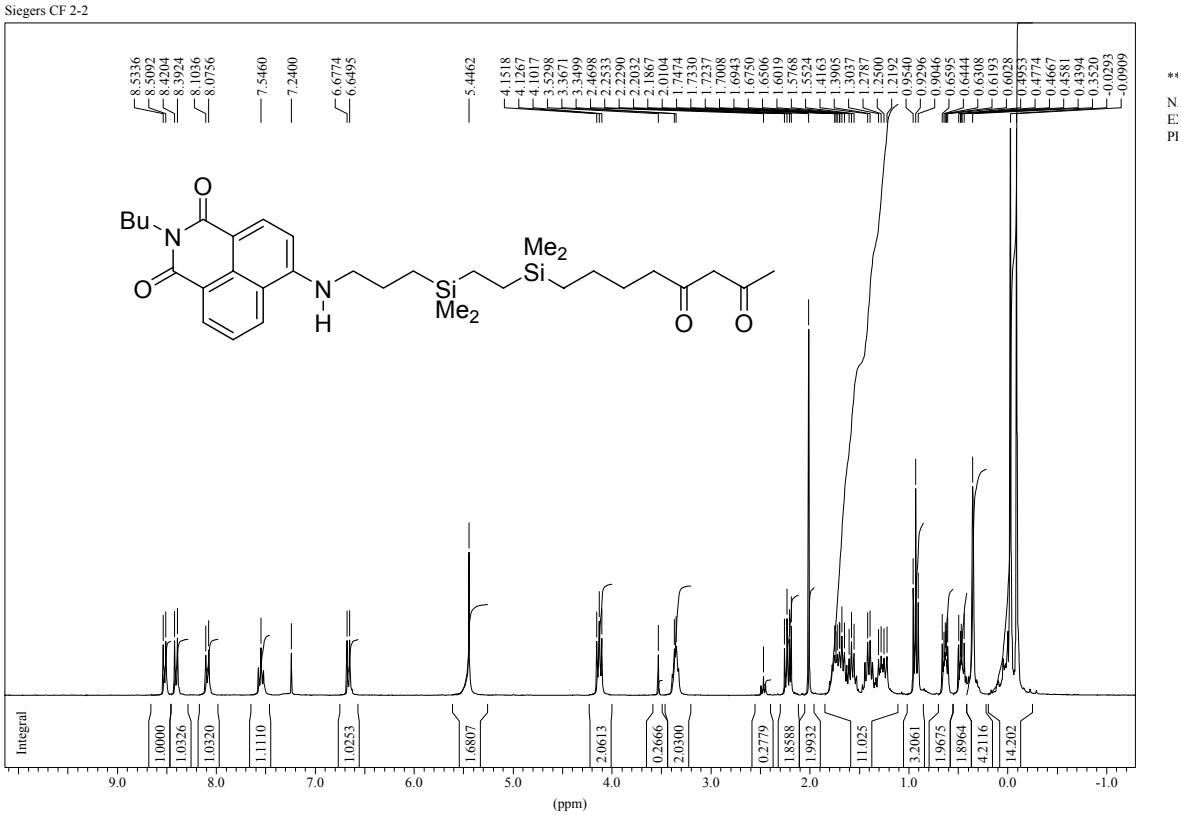

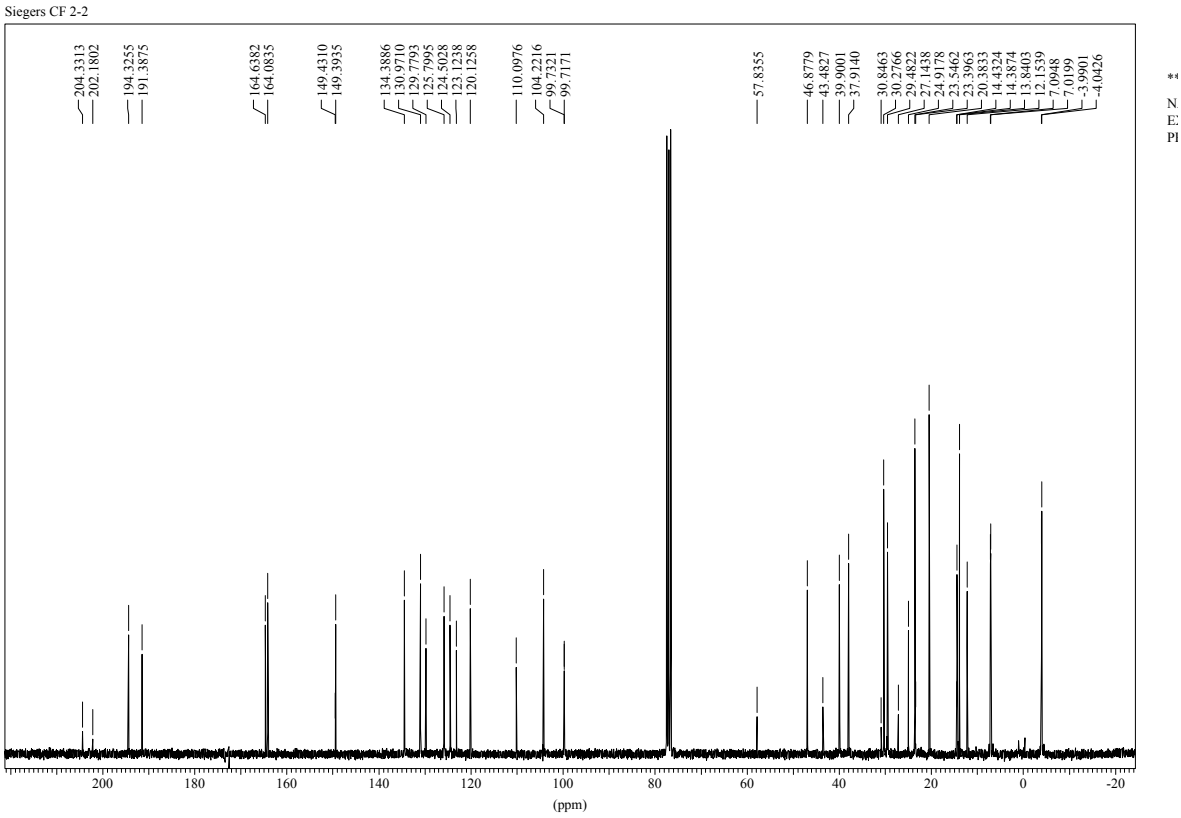

Dibutyl acacH fluorol **42b**

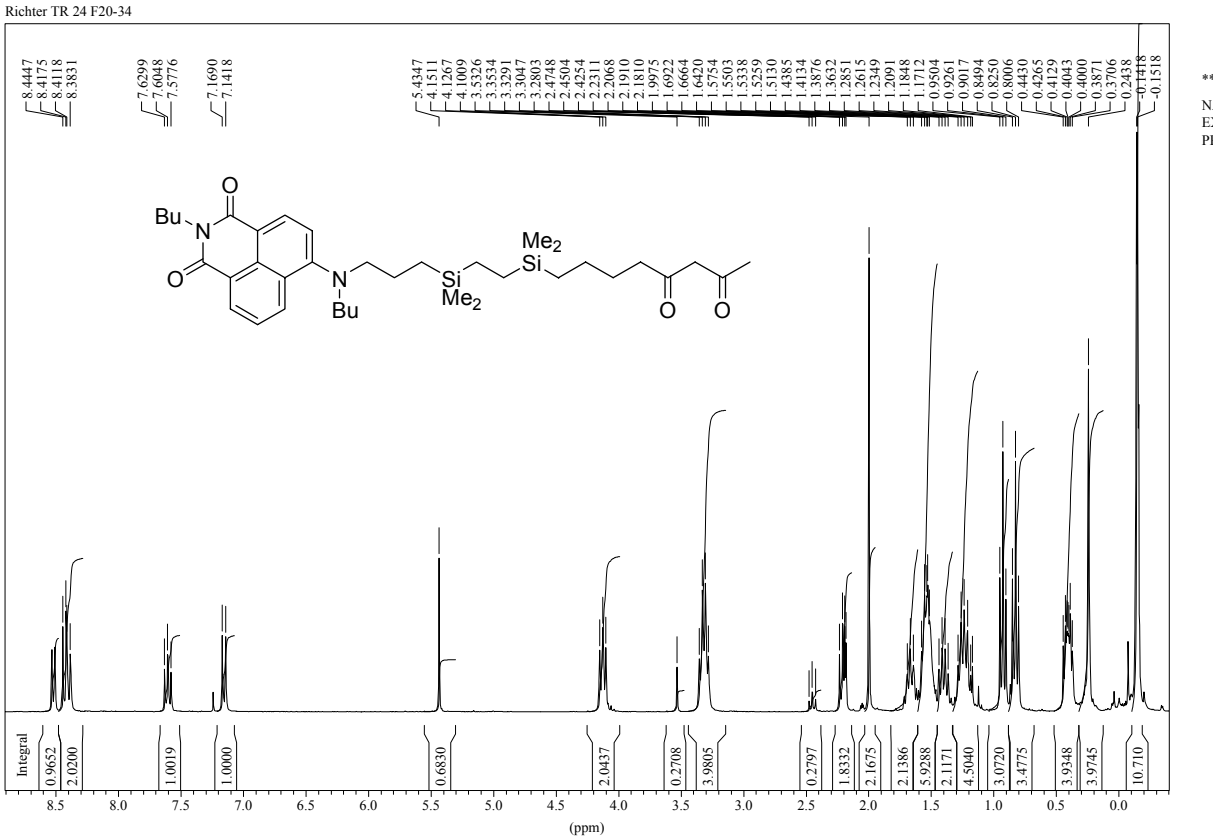

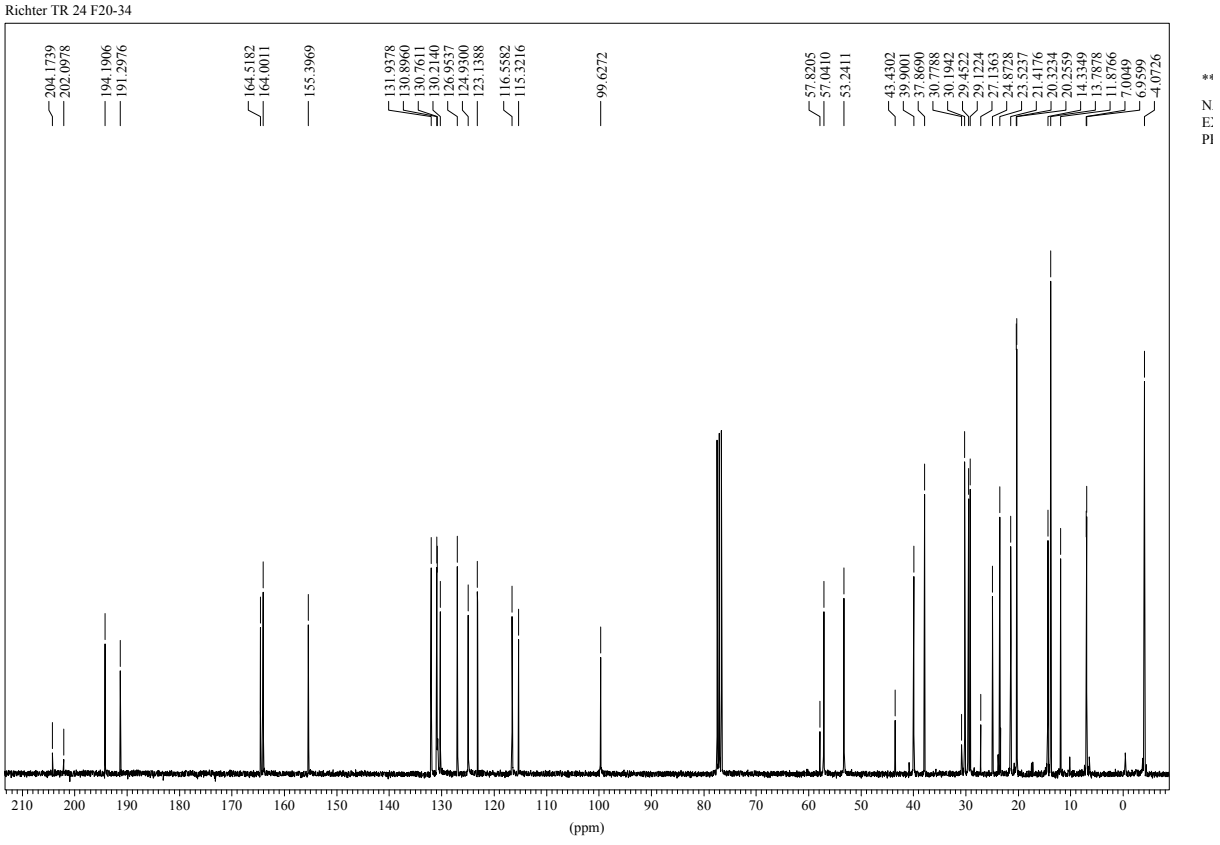

Tetra acacH dendrimer **46**

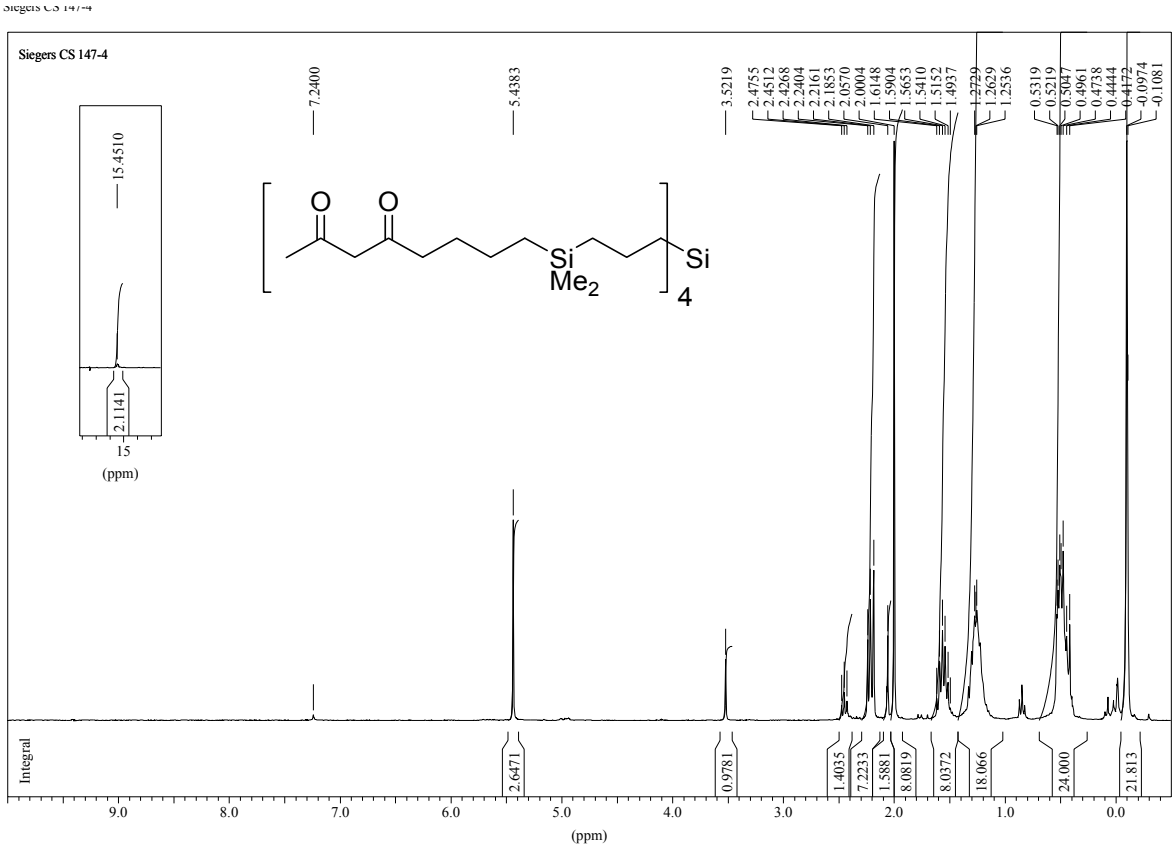

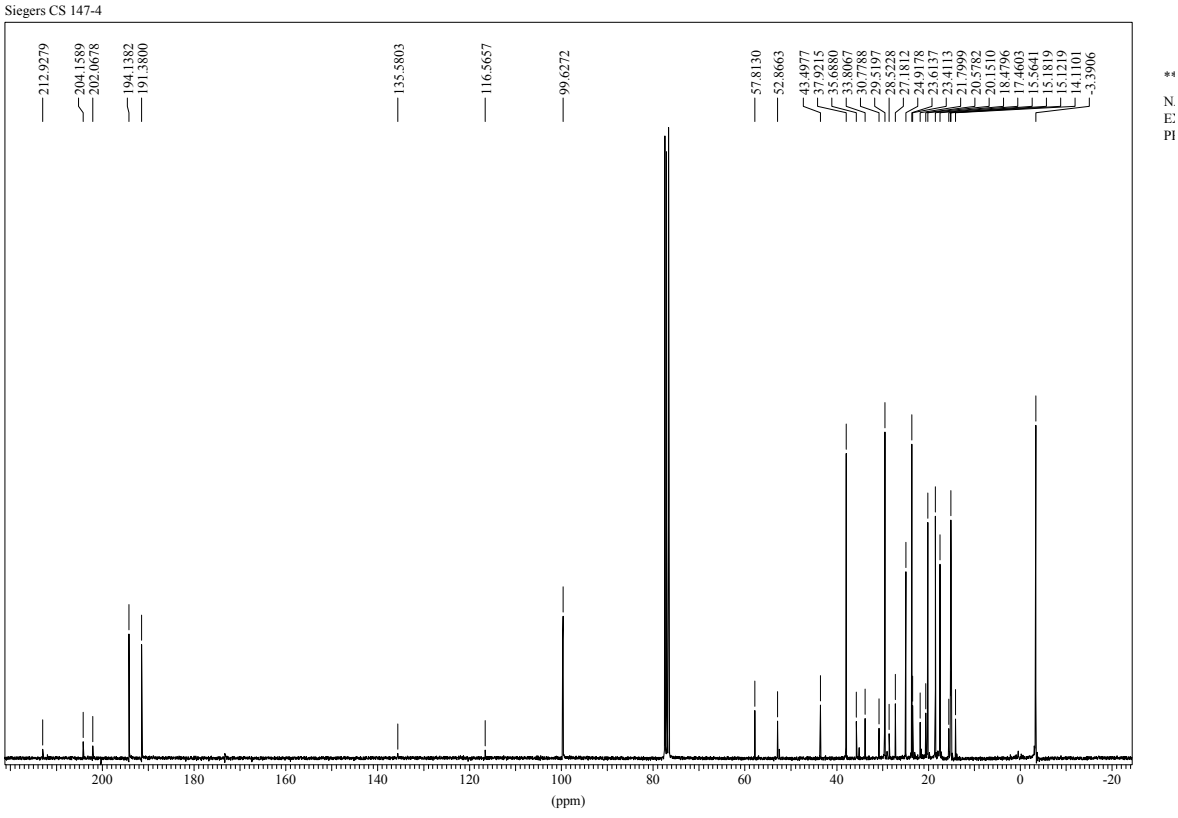

Donor acceptor dyad **45**

Siegers LB 89 Dy conc

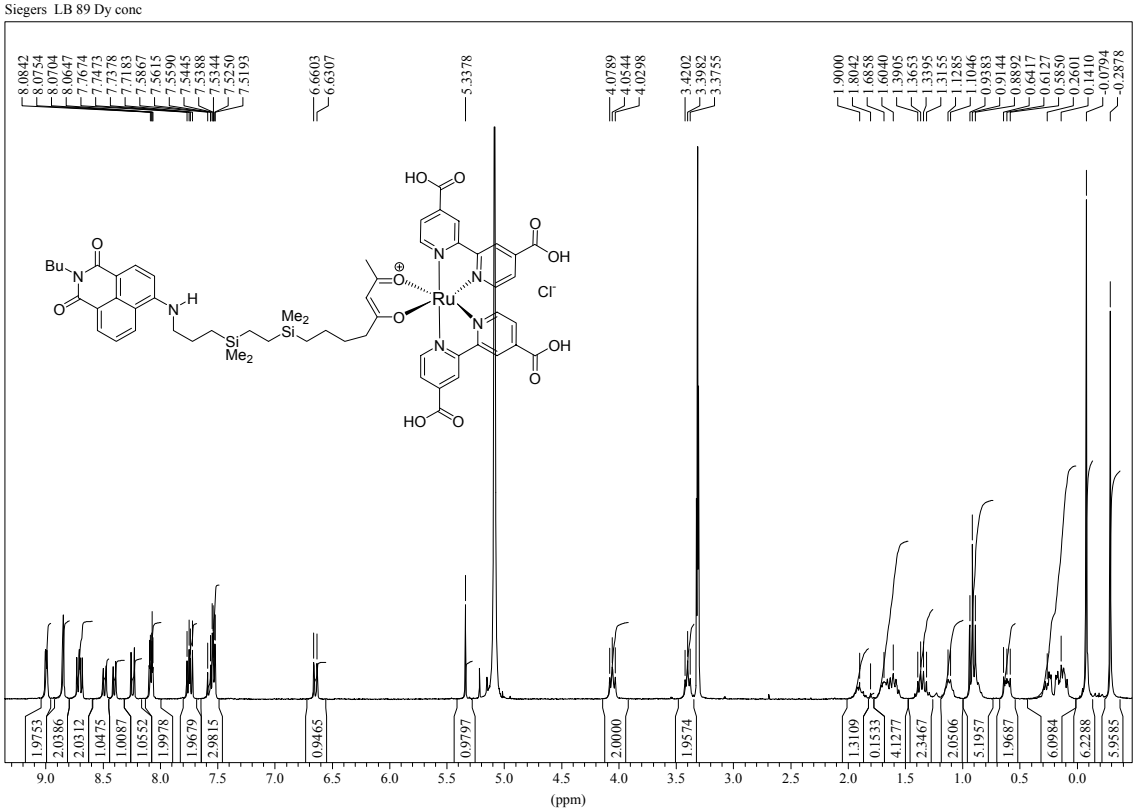

Siegers CS 171-18

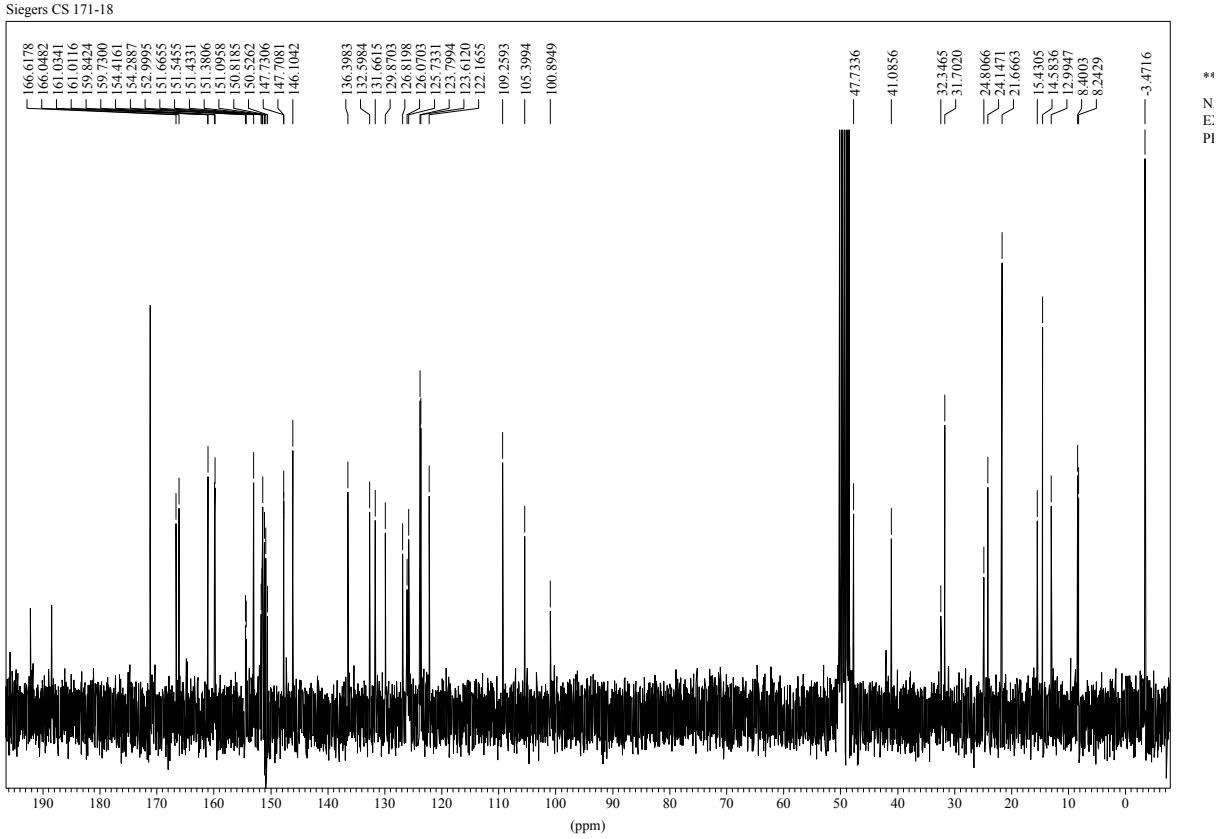

Butyl dyad **59**

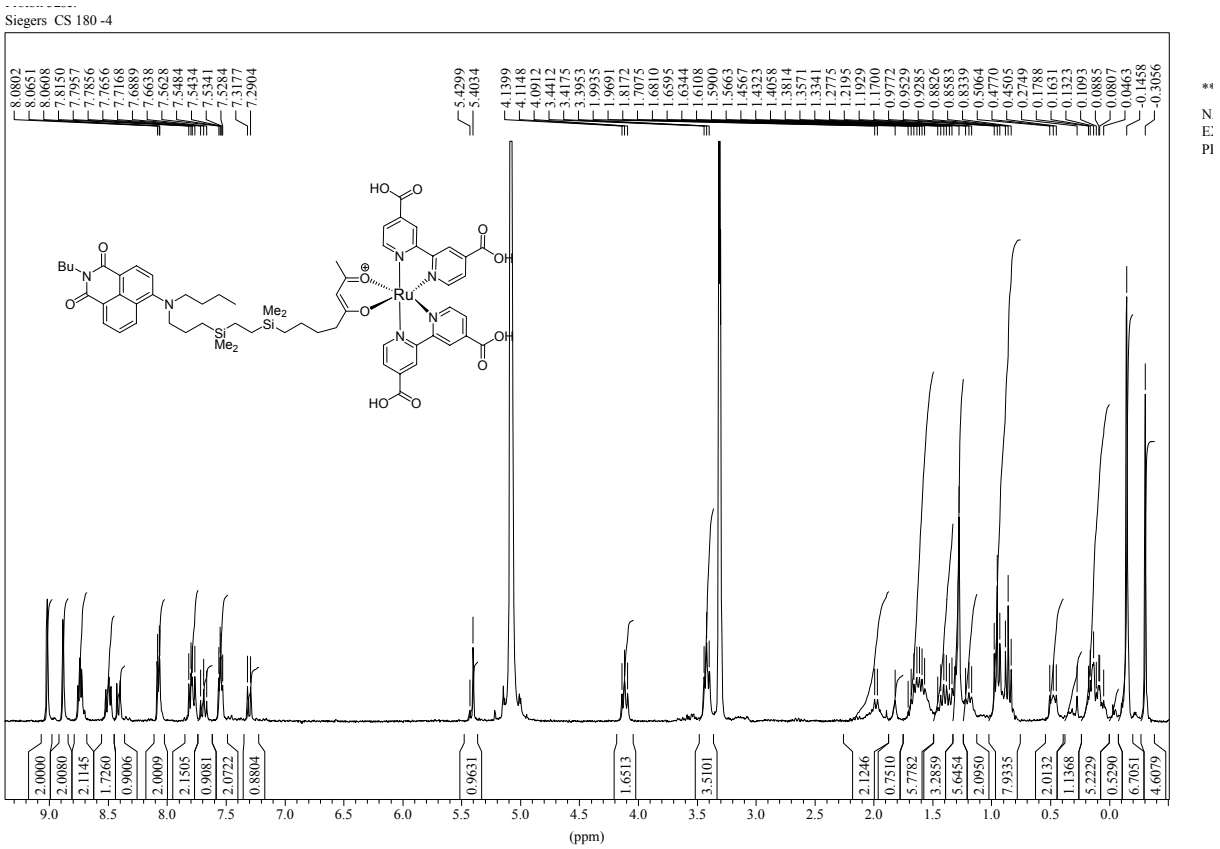

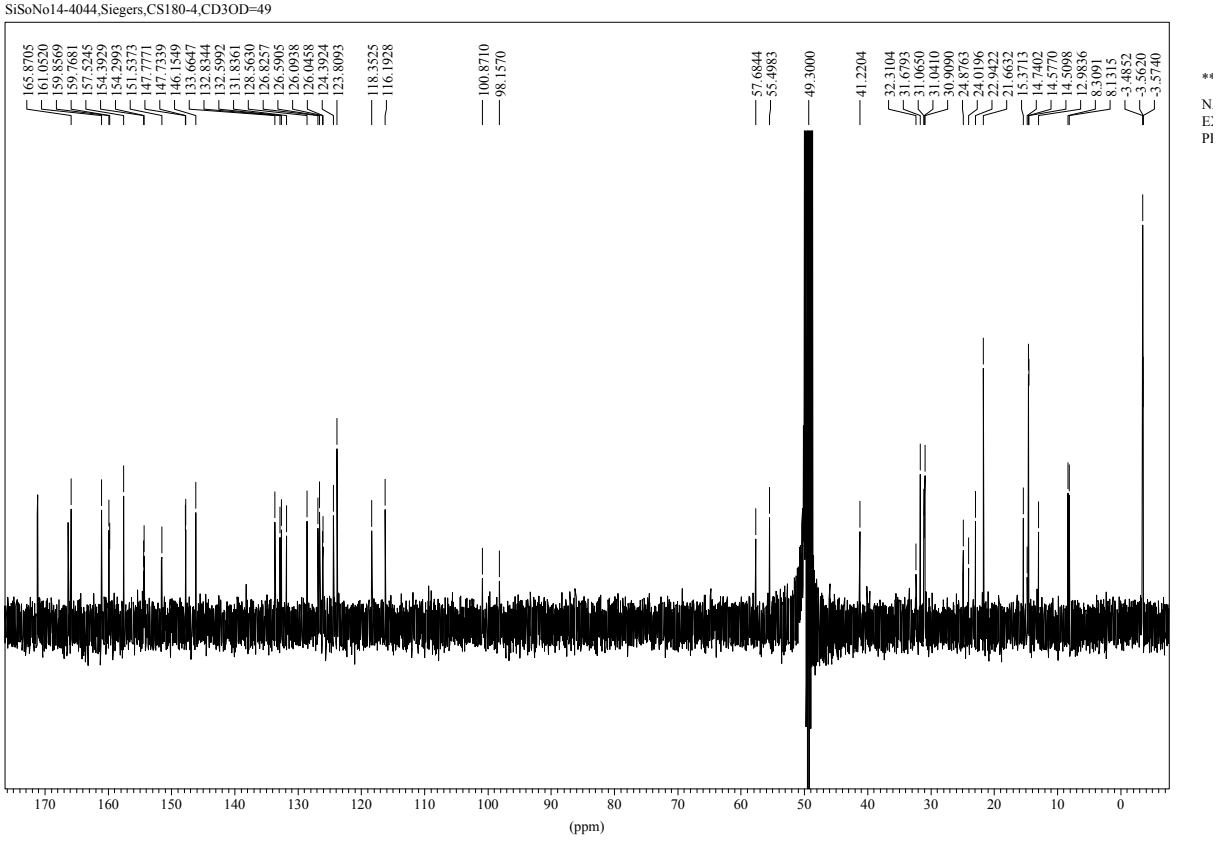

di-Me-dcbpy

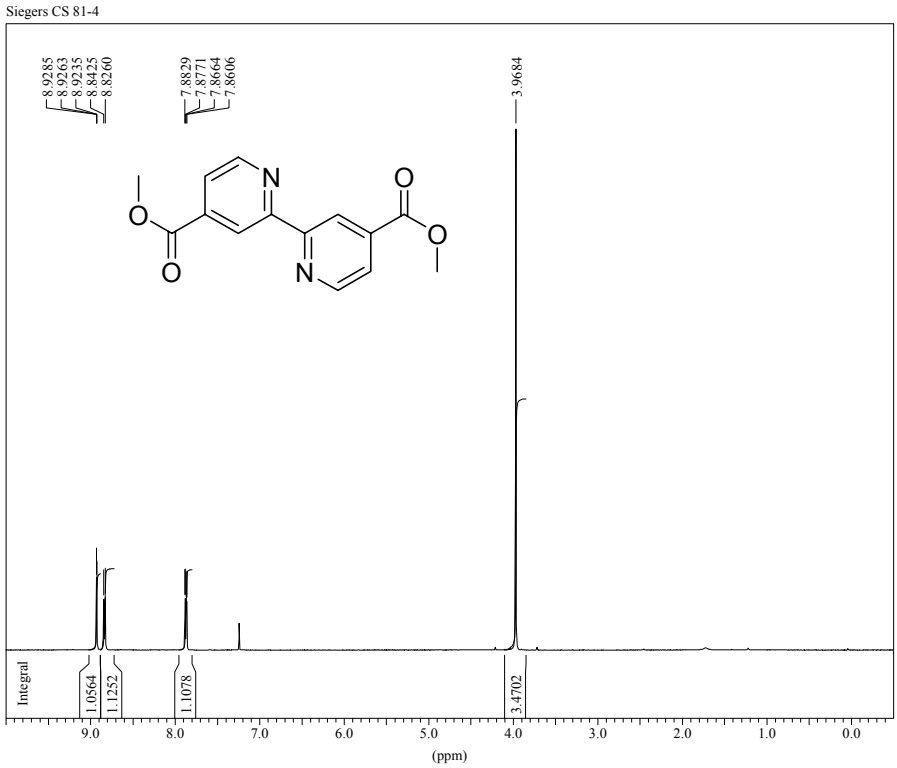
Siegers CS 81-4
8.9285
8.9263
8.9235
8.8425
8.8260
7.8829
7.8771
7.8664
7.8606
3.9684
Integral
1.0564
1.1252
1.1078
3.4702
9.0
8.0
7.0
6.0
5.0
4.0
3.0
2.0
1.0
0.0
(ppm)

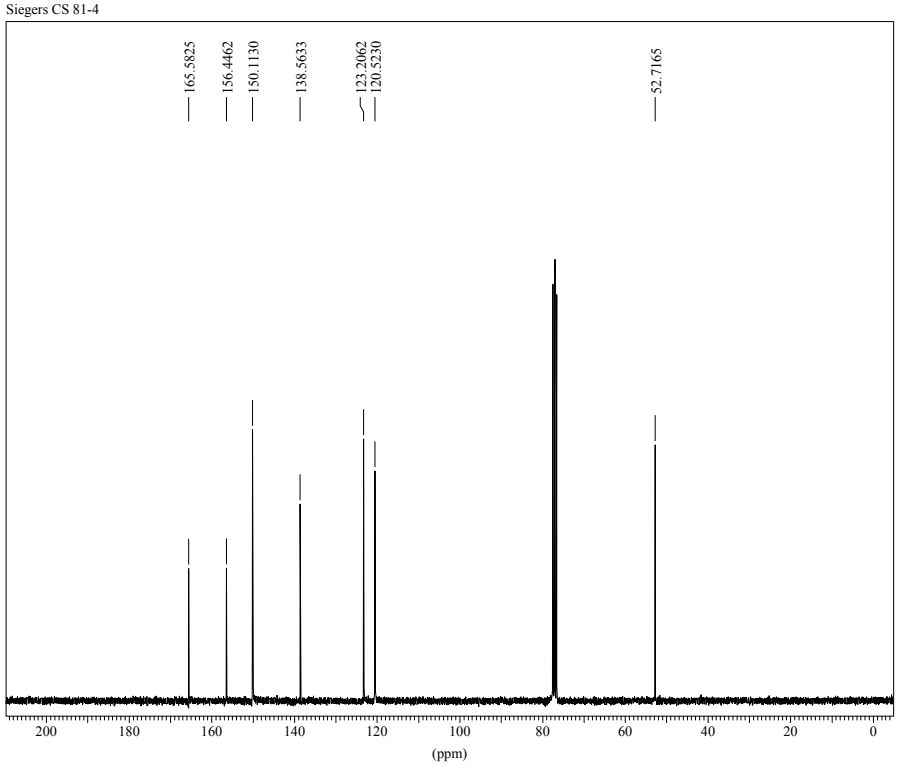
Siegers CS 81-4
165.5825
156.4462
150.1130
138.5633
123.2062
120.5230
52.7165
200
180
160
140
120
100
80
60
40
20
0
(ppm)

allyl-acacH **36**

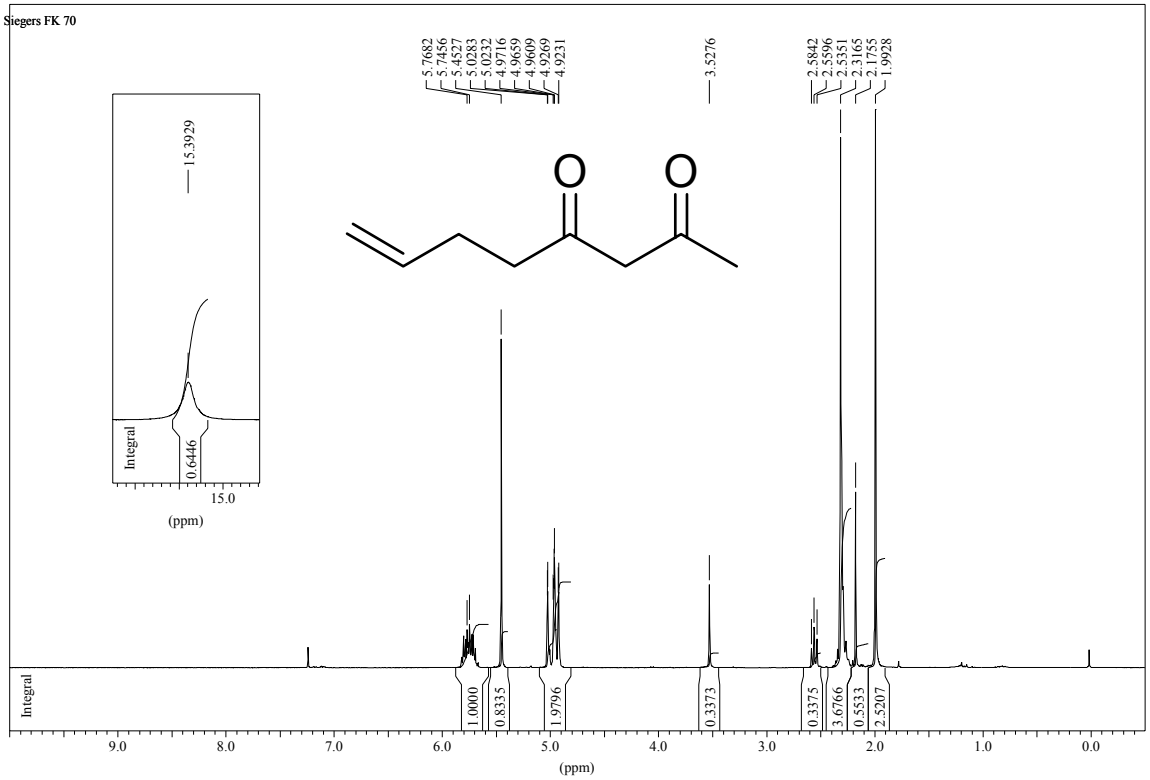

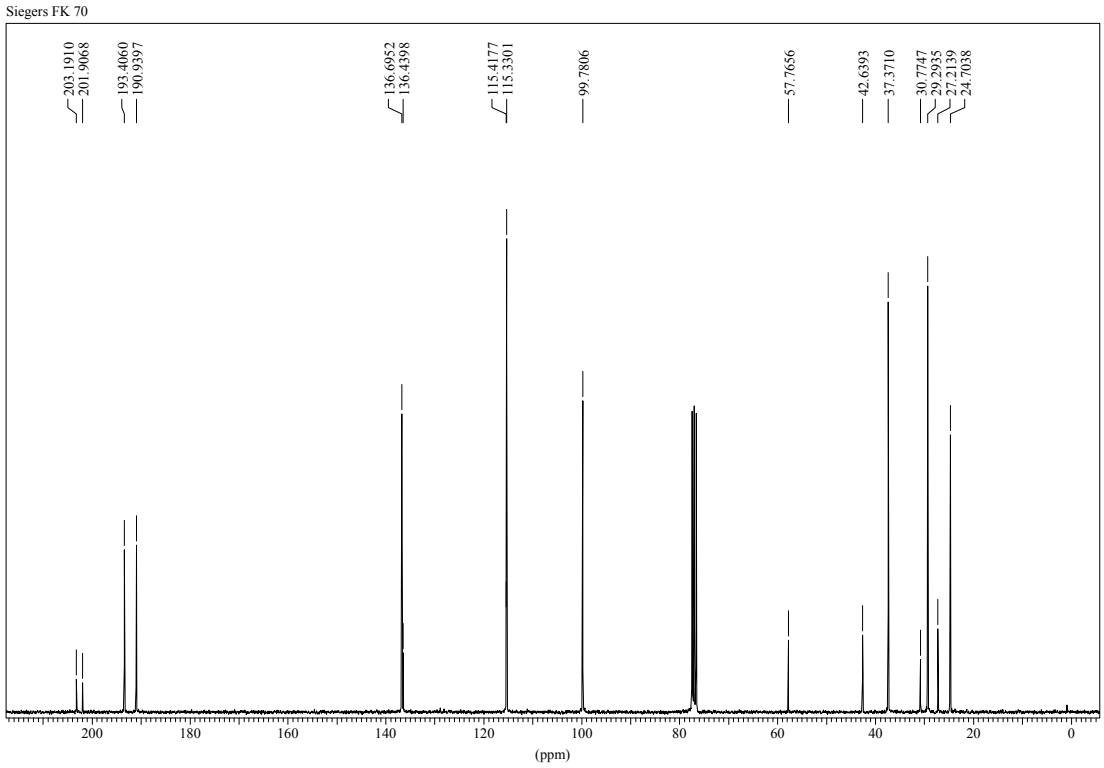

8-Trimethylsilyloct-7-yne-2,4-dione **55**

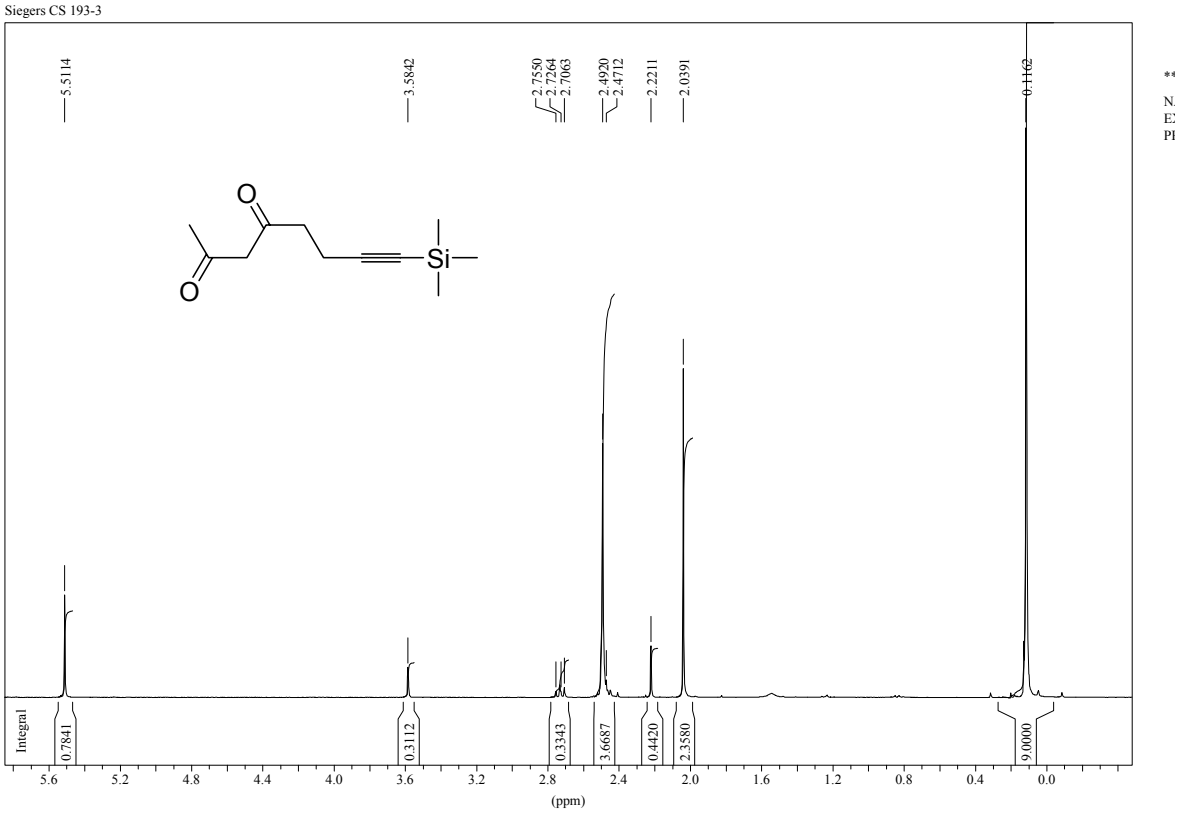

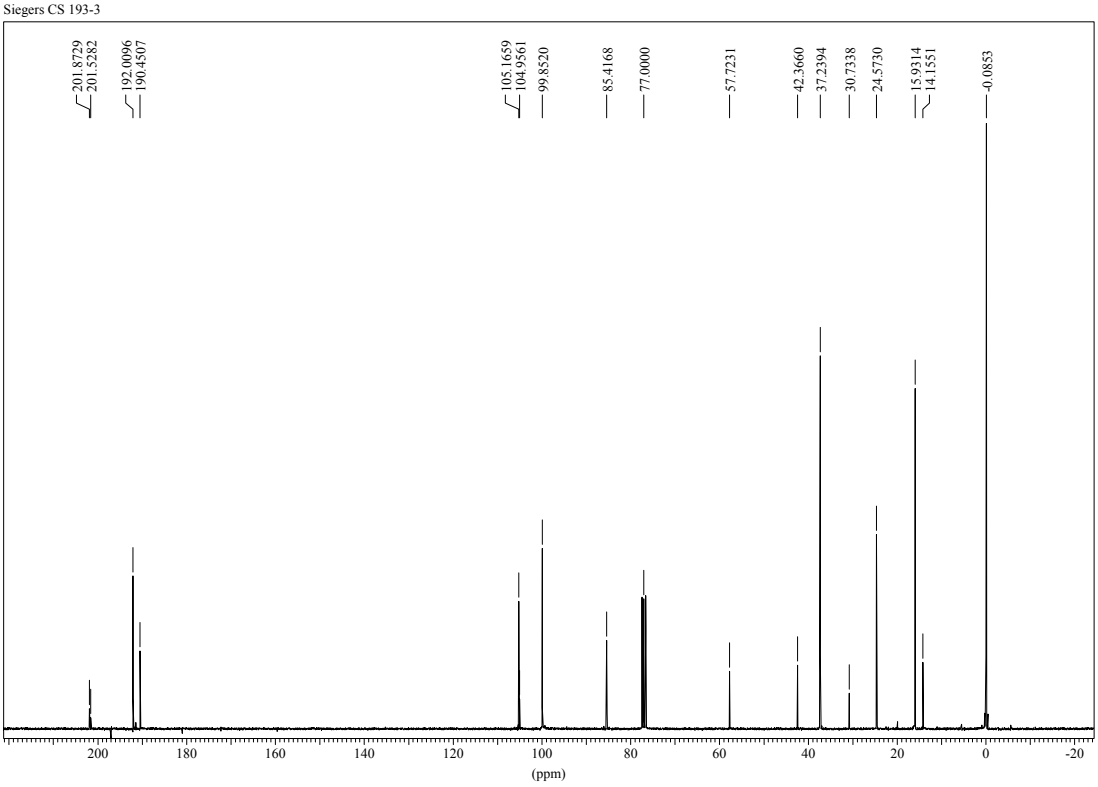

[Ru(dcbpy)$_2$acac]Cl **14**

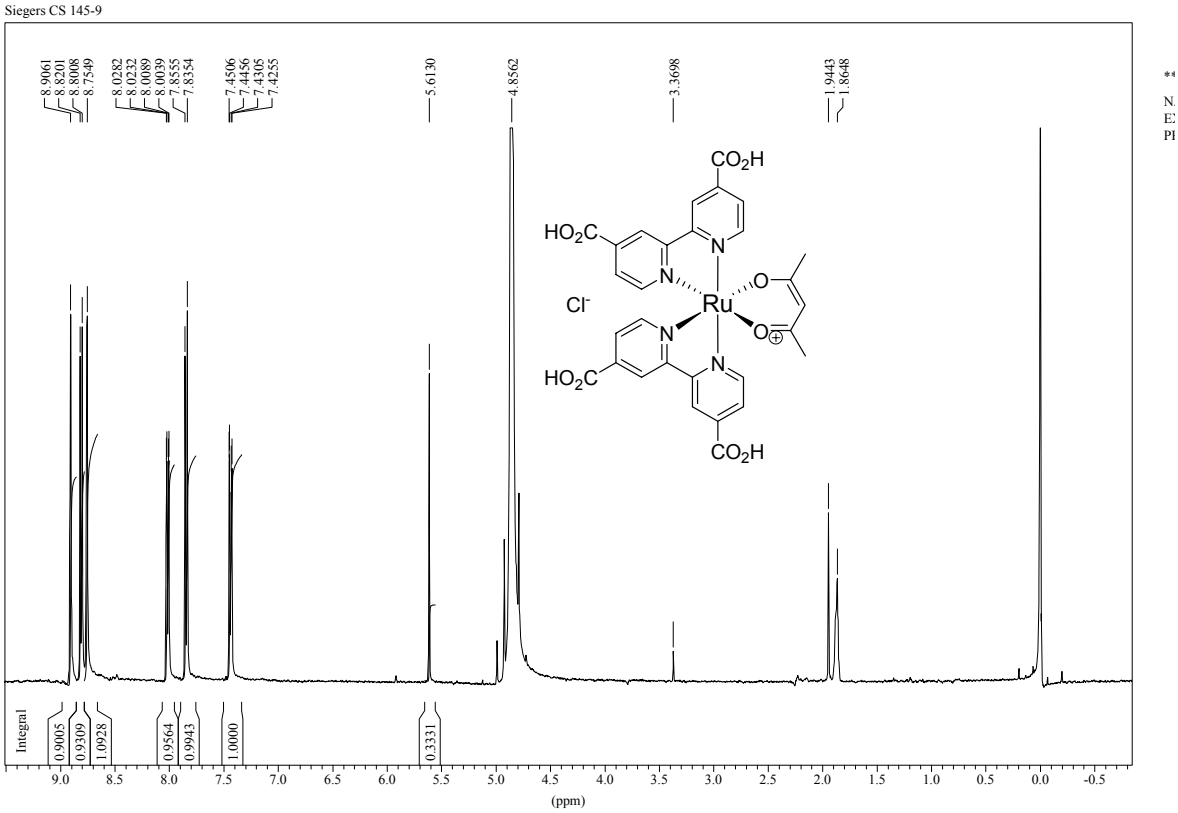

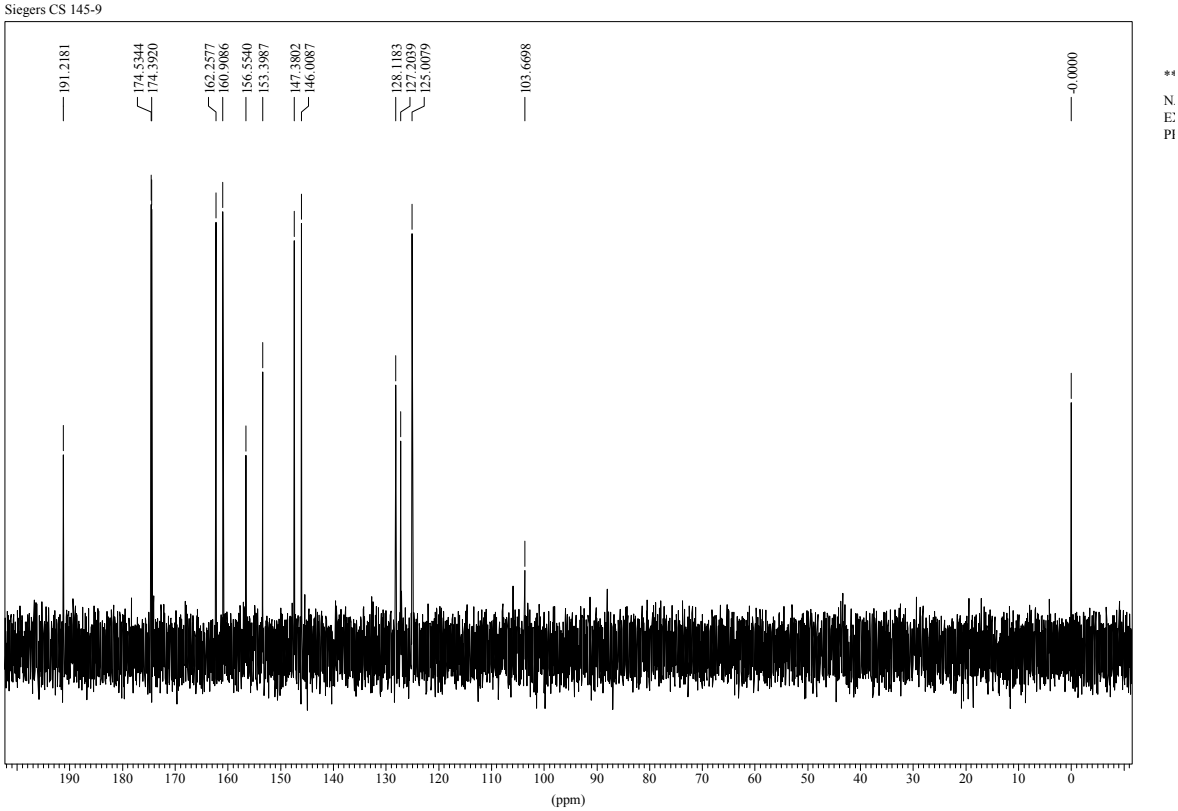

[Ru(dcbpy)$_2$allyl-acac]Cl **57**

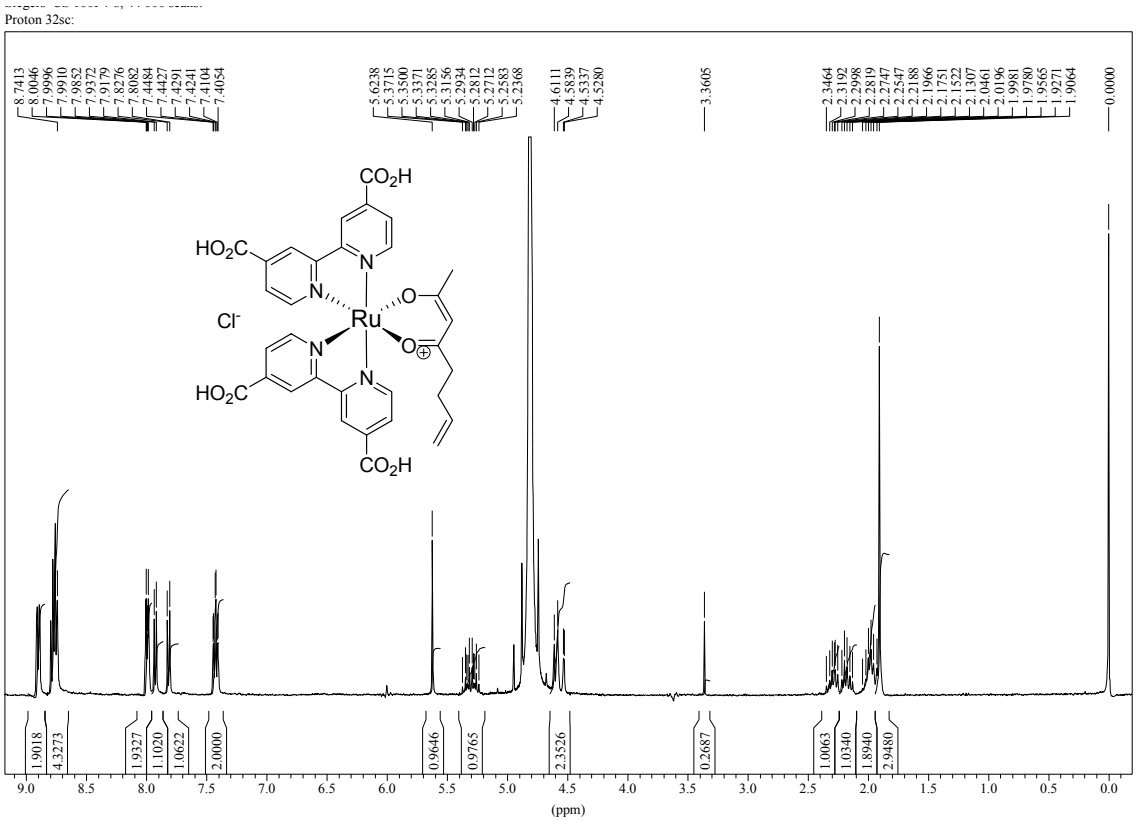

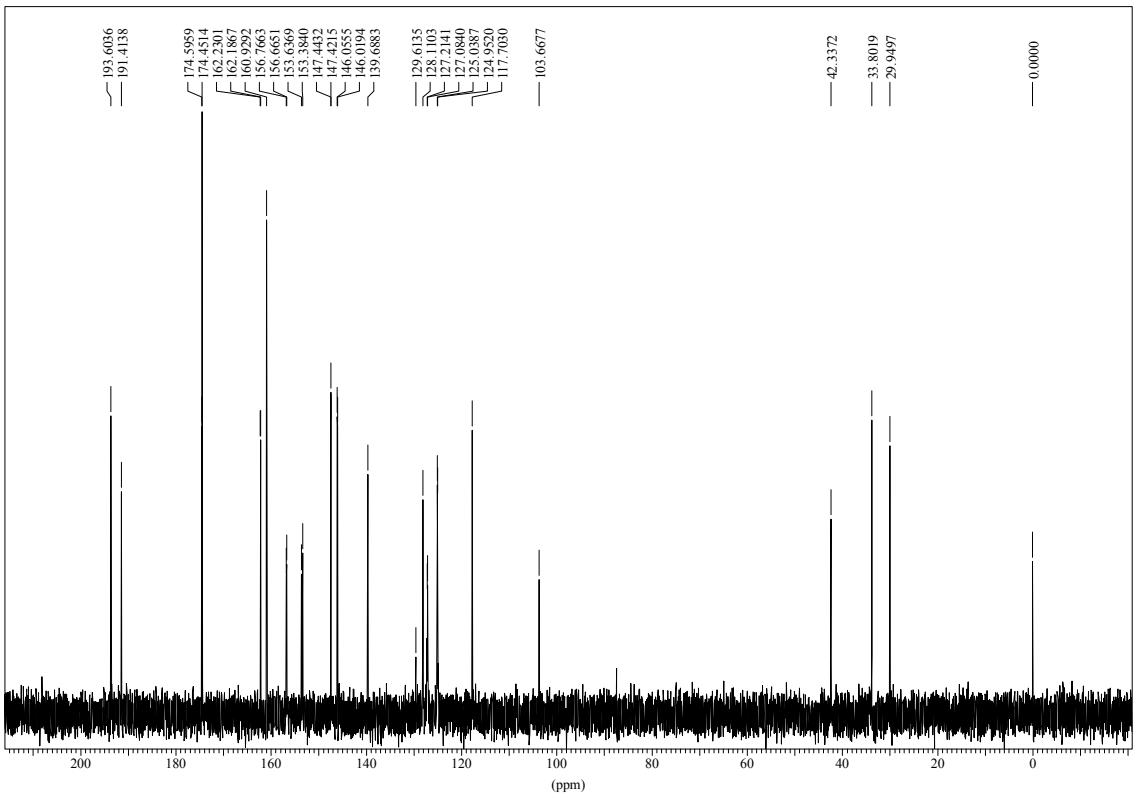

[Ru(dcbpy)$_2$propargyl-acac]Cl **58**

Siegers LB 19 F7-10

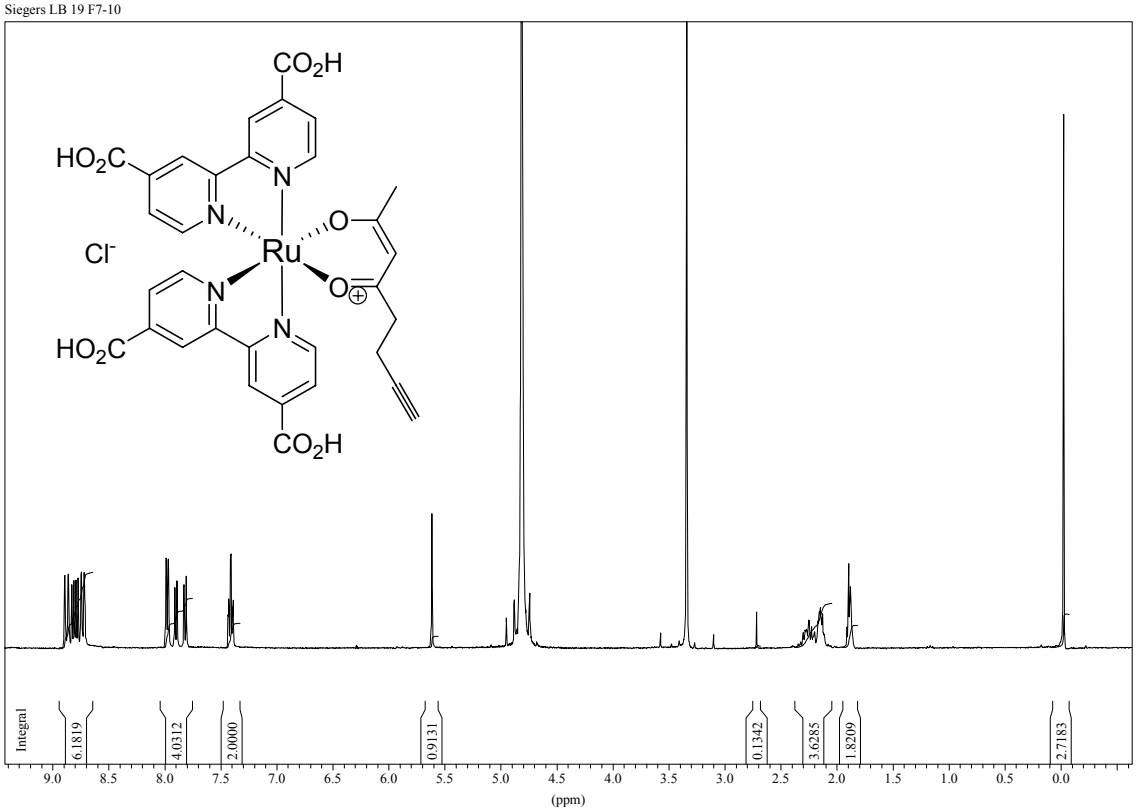

Siegers LB 19 F7-10

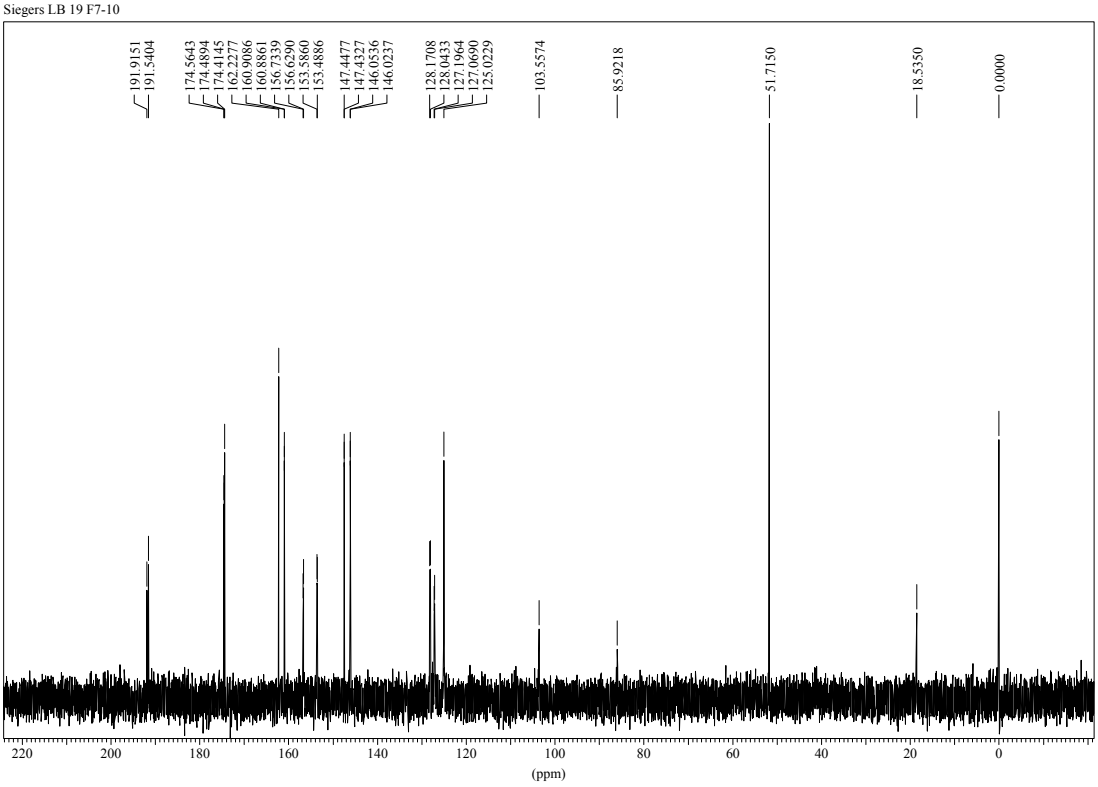

[Ru(di-Me-dcbpy)$_2$allyl-acacH]PF$_6$ **35b**

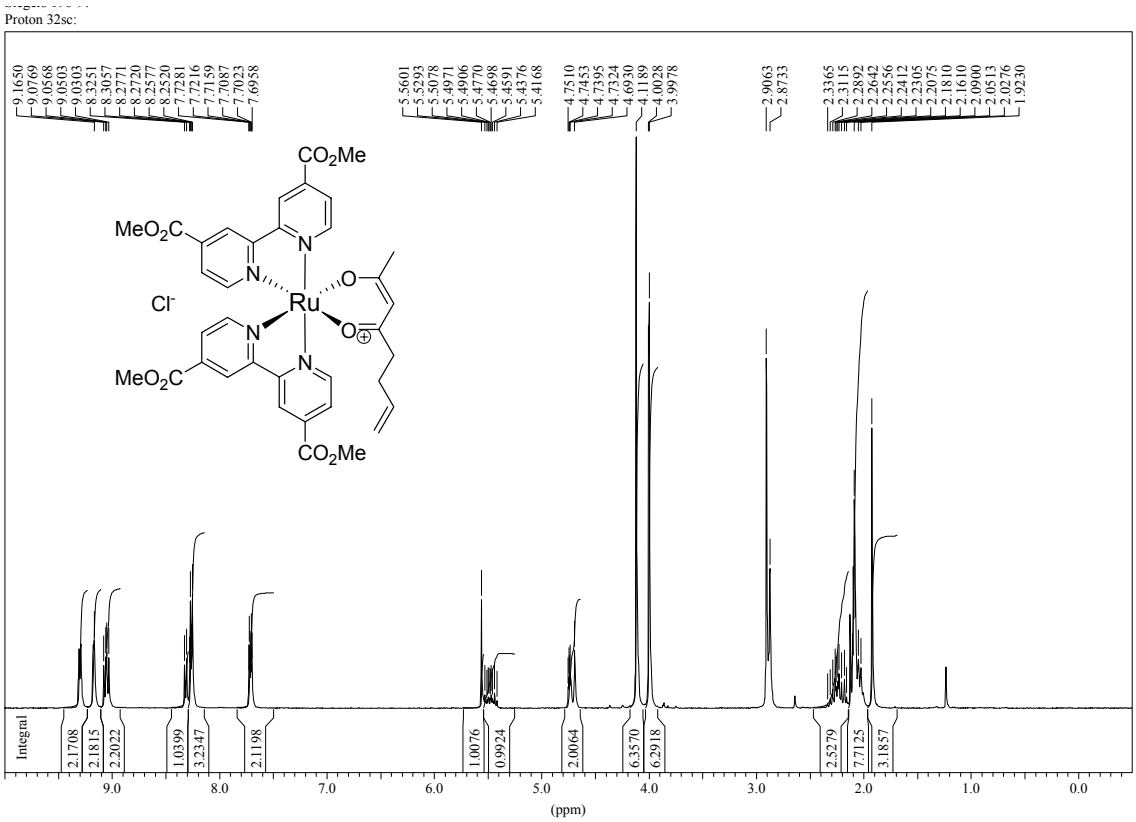

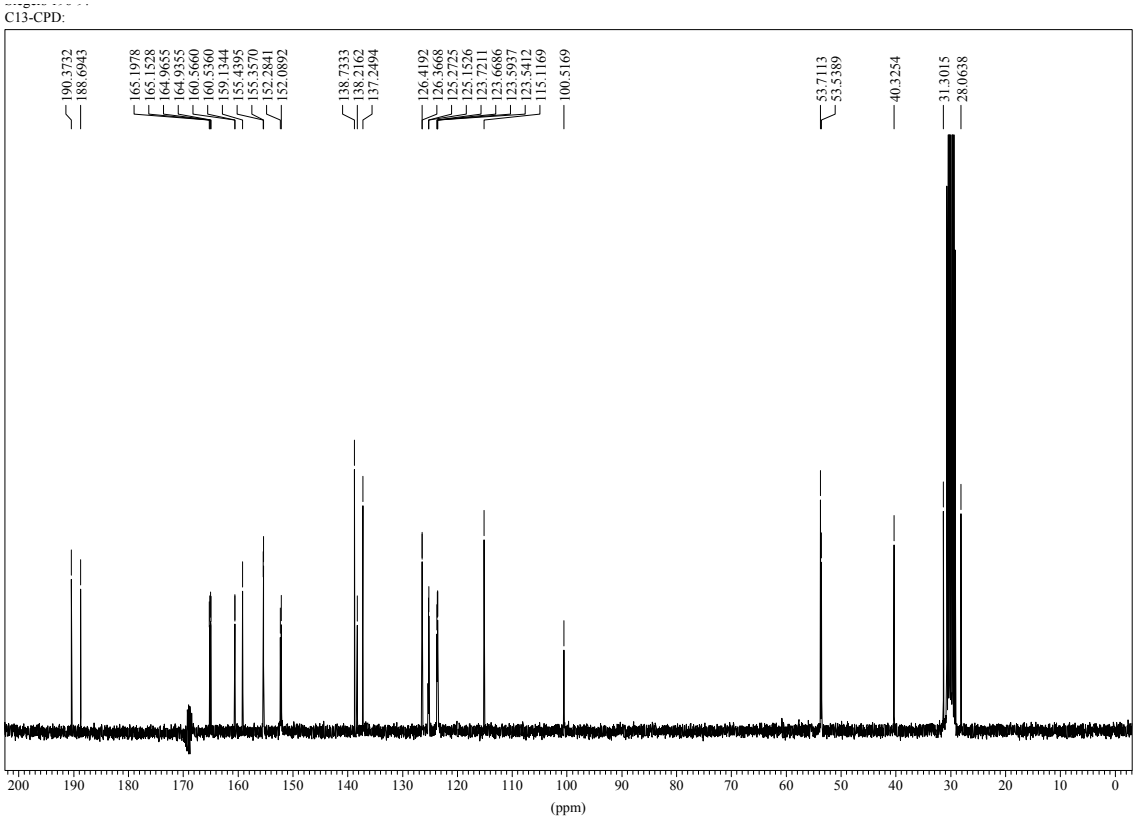

$A_{29\%}$-PG-$N_{3,\ 40\%}$ **66f**

Siegers FK76 F1-4

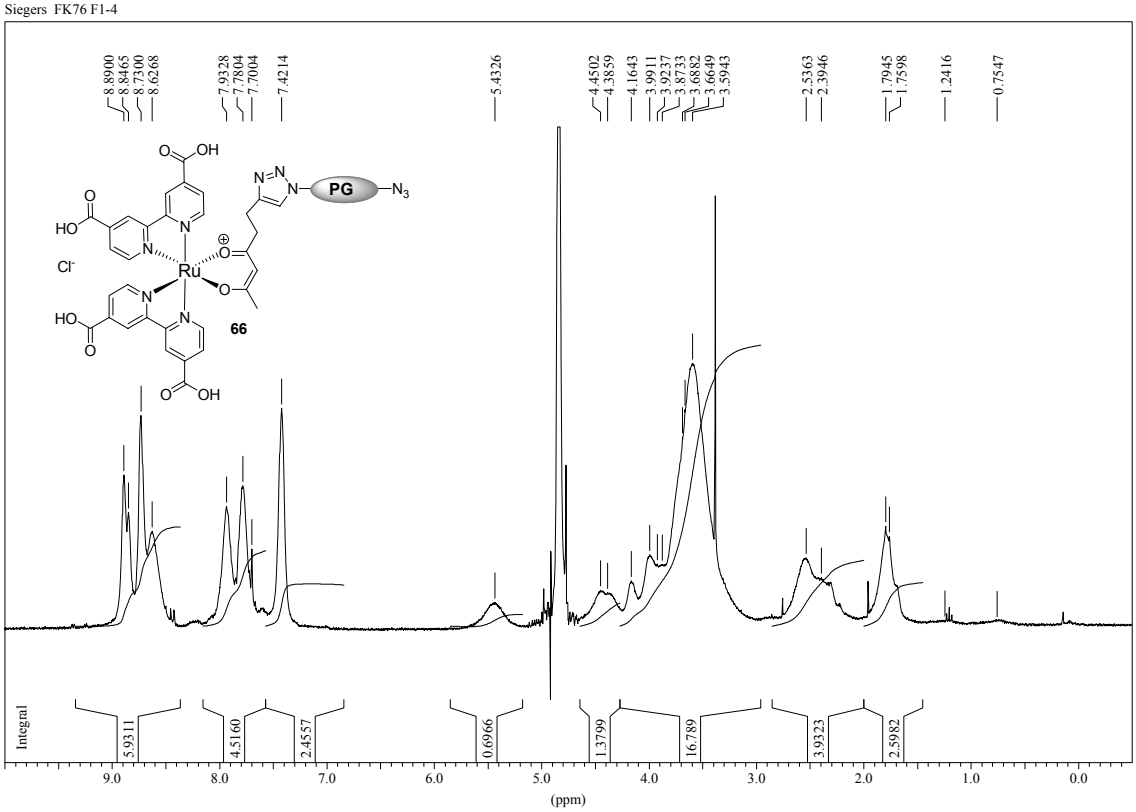

Siegers FK 76 F1-4

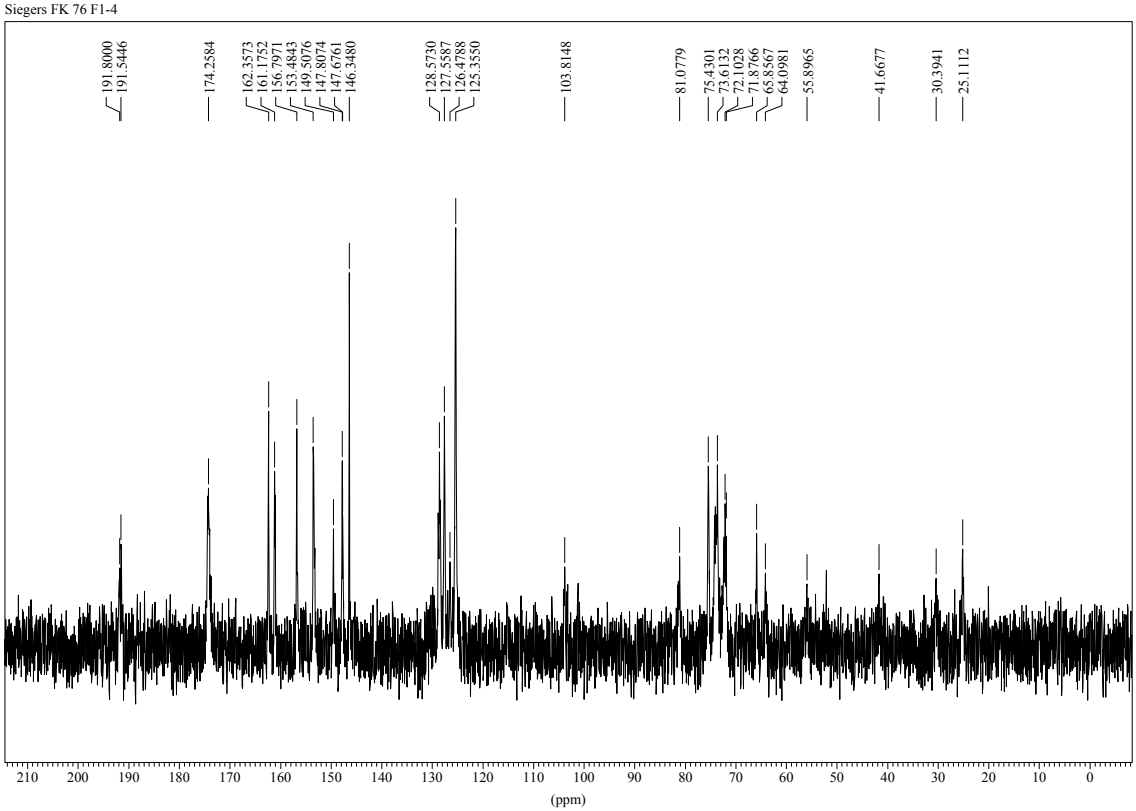

$A_{10\%}$-PG-$N_{3,\ 30\%}$ **66d**

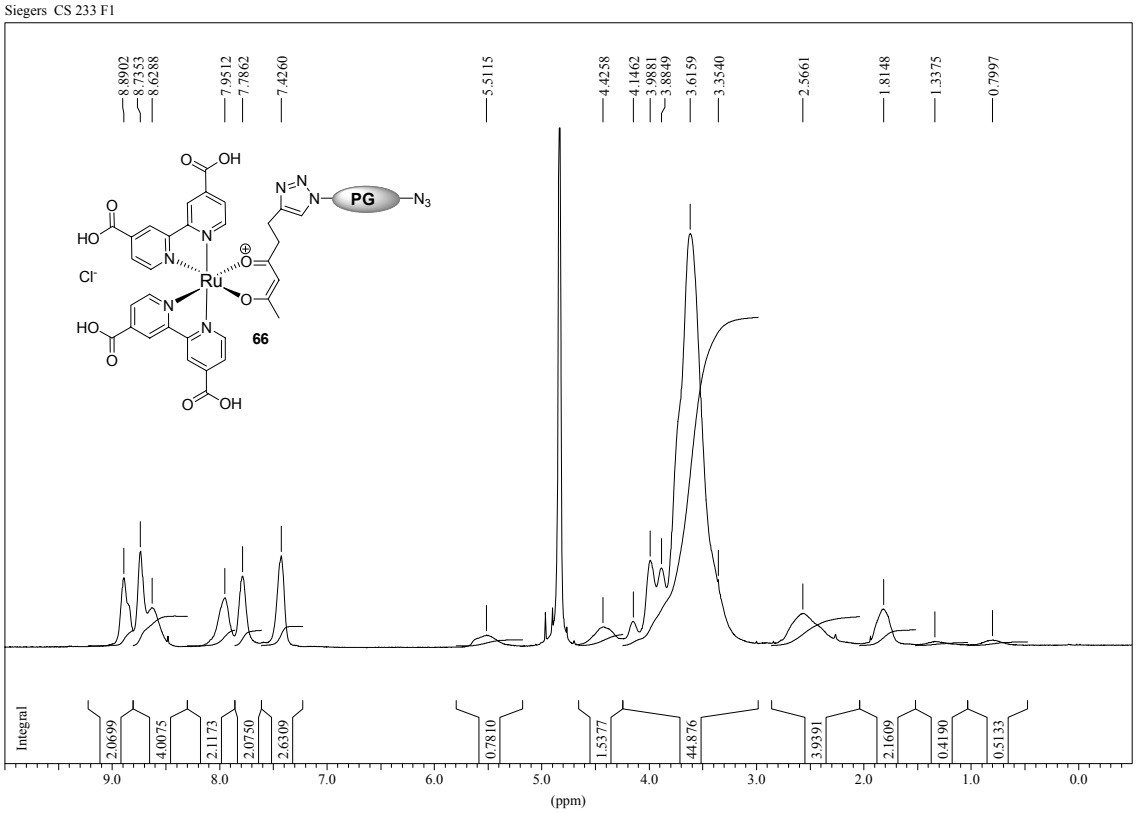

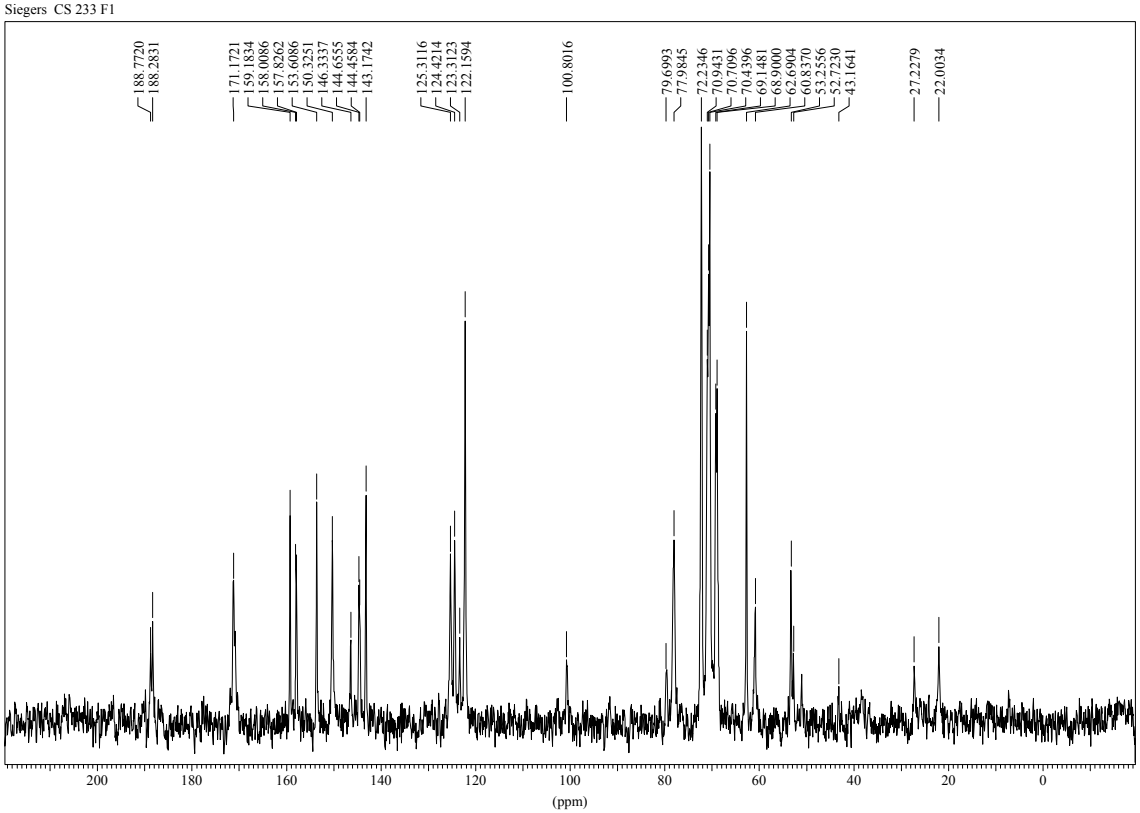

D_1-$A_{(20\%)}$-PG-$N_{3,\ 40\%}$ **64**

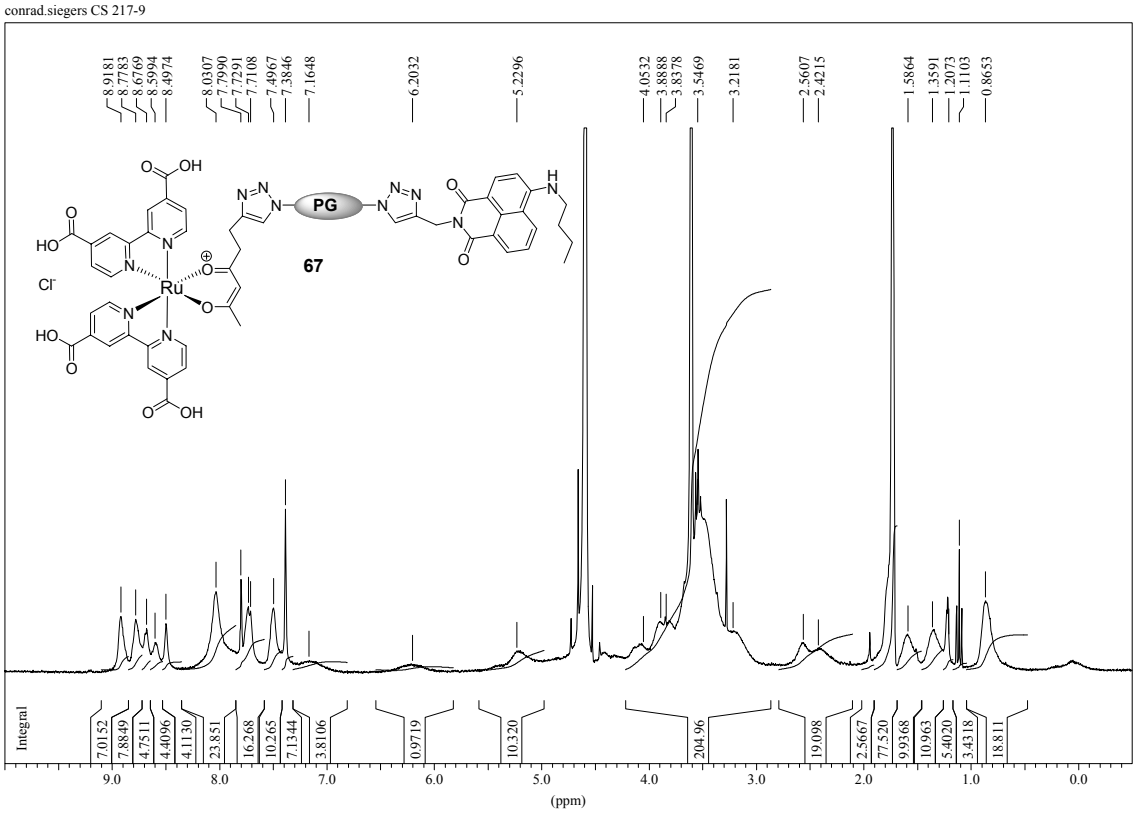

D_5-$A_{(10\%)}$-PG-$N_{3,\ 100\%}$ **65a**

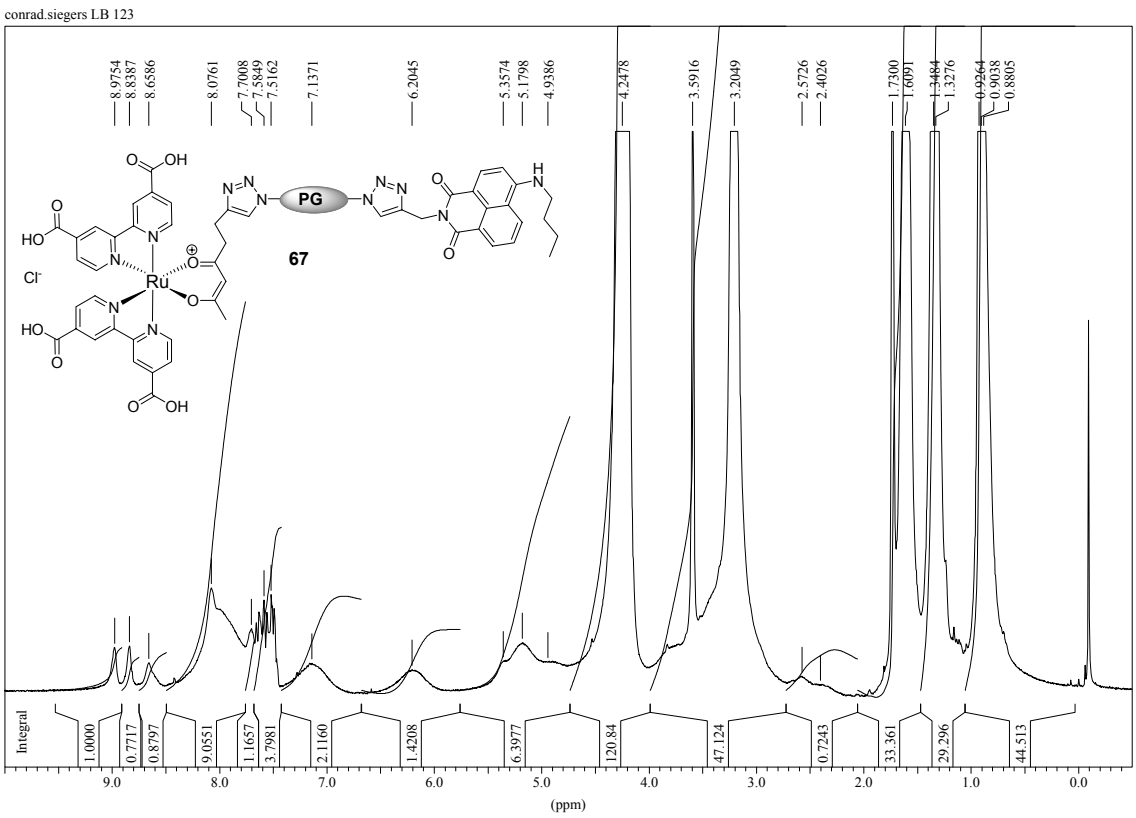

D_7-$A_{(10\%)}$-*l*PG-$N_{3,\ 85\%}$ **65b**

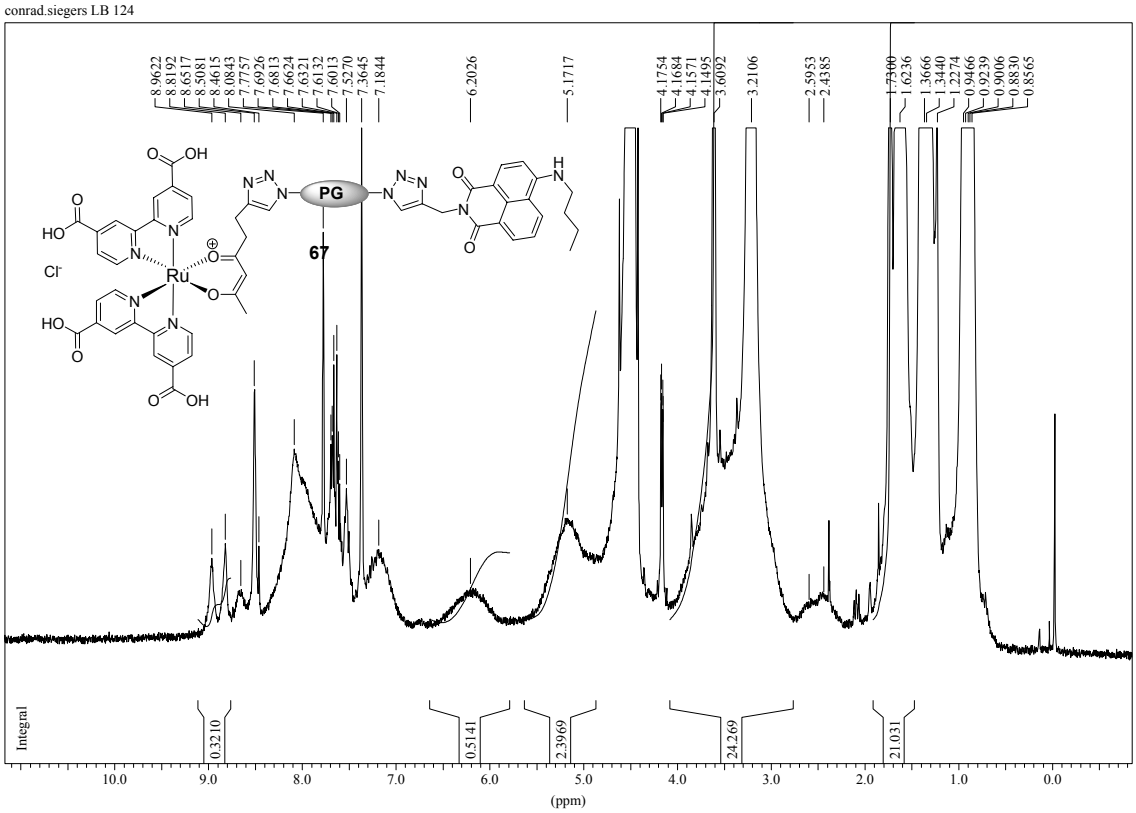

$D_{8.6}$-$A_{3\%}$-PG-$N_{3,\ 30\%}$ **67b**

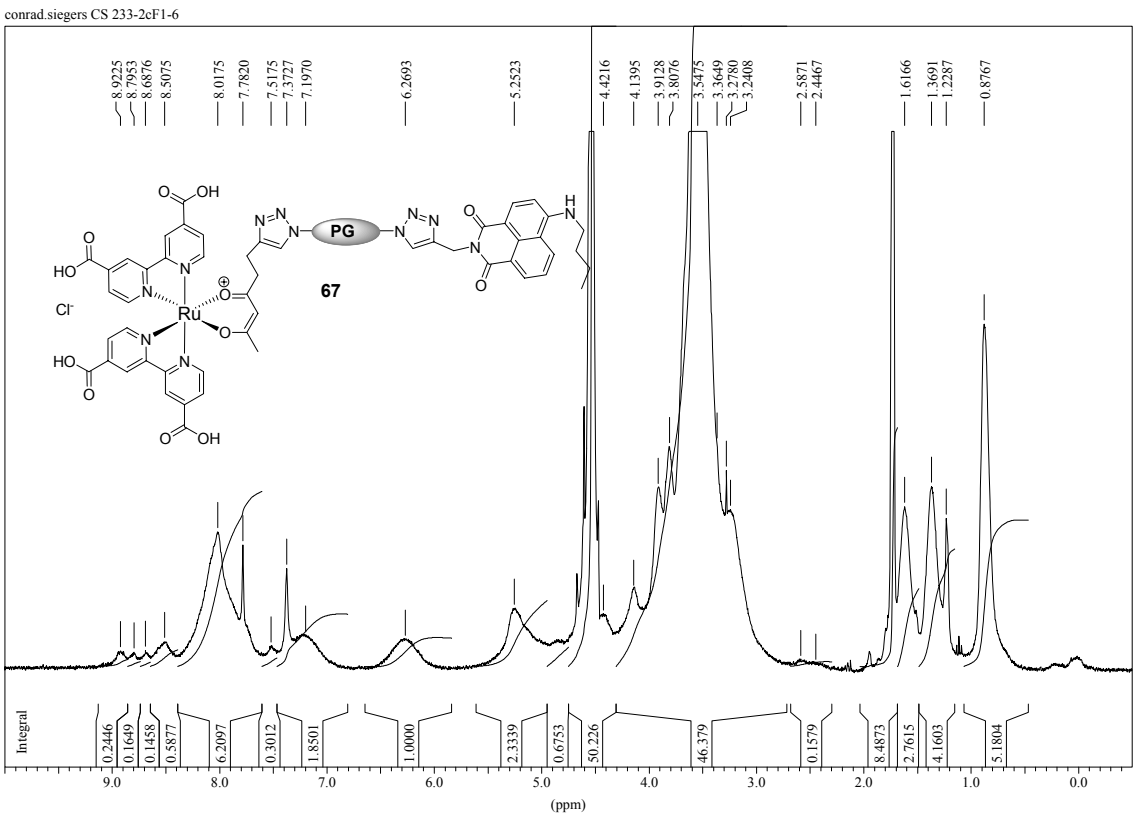

$D_{3.7}$-$A_{8\%}$-PG-$N_{3,\ 60\%}$ **67g**

conrad.siegers CS 227-2F1

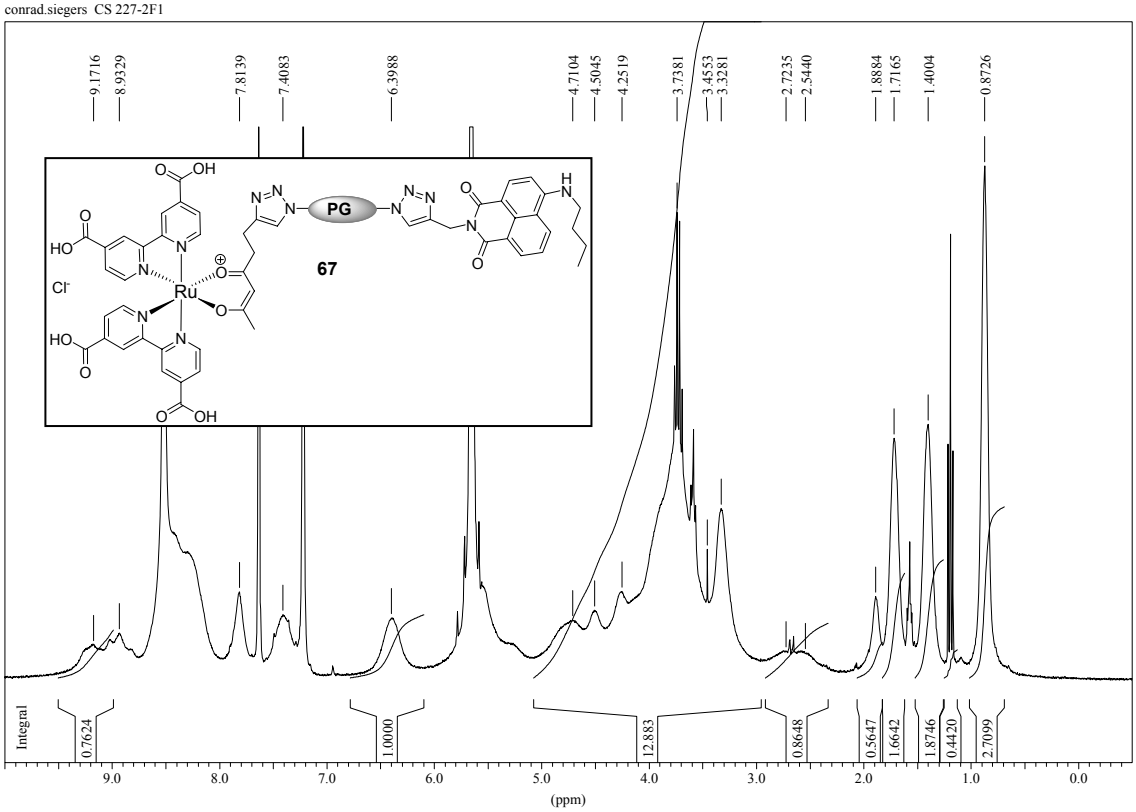

Summe Dept u. 13 C,expn.: 2 u. 6